Construction Of Artificial Skin Tissue With Placode-Like Structures In Well-Defined Patterns Using Dielectrophoresis

Rama Yusvana

B.Sc (Hons.), M.Sc.

Submitted for the degree of **Doctor of Philosophy**

Heriot-Watt University

School of Engineering and Physical Science

Department of Chemical Engineering

September 2010

ABSTRACT

During embryonic development of animal skin tissue, the skin cells form regular patterns of high cell density (placodes) where hair or feathers will be formed. These placodes are thought to be formed by the aggregation of dermal cells into condensates. The aggregation process is thought to be controlled by a reaction-diffusion mechanism of activator and inhibitor molecules, and involve mechanical forces between cells and cells with the matrix.

In this project, placode formation in chicken embryonic skin cells was used as a model system for the study of the mechanism by which the placodes are formed. Artificial aggregates of chicken embryonic skin cells were created by suspending them in a 300 mM low conductivity sorbitol solution and attracting them by positive dielectrophoresis to high field regions within microelectrode arrays by applying a 10 - 20 $V_{pk\text{-}pk}$ 1 MHz signal across the microelectrodes. It was demonstrated that using this method aggregates can be produced in a large variety of patterns and that the distance between the aggregates and aggregate size and shape within the pattern can be controlled effectively. Custom-built image analysis tools were developed in LabVIEW to analyze the patterns formed.

The formation of aggregates by dielectrophoresis was followed by an immobilization phase of the resulting patterns inside a gel matrix, forming an artificial skin. Nutrients and oxygen were supplied externally. Long-term incubation of the artificial skin shows that embryonic skin cells in the aggregates were viable and showed behavior similar to that of developing embryonic skin, including further aggregation of the cells and the formation of cell condensates. The domain size was shown to have an influence on the condensation process, with cells in small aggregates forming only one condensate near the centre of the aggregate, and several condensates in larger aggregates. Whilst the distribution of cell condensates within the aggregates in round large aggregates is predominantly random, some line formation could be observed in linear aggregations, indicating some self-organization may be occurring.

ACKNOWLEDGEMENT

First of all I would like to convey my utmost grateful to the Almighty God who has given me strength throughout my journey, as well as for the enormous blessings He has bestowed upon me during my research studies.

Secondly, I would like to thank the School of Chemical Engineering and Analytical Sciences at the University of Manchester and School of Engineering and Physical Science at Heriot-Watt University, Edinburgh for the funding / scholarships and all the supports towards my research studies.

I certainly would like to acknowledge with gratitude my supervisor Professor Gerard H. Markx, Professor of Bioprocessing, at Heriot-Watt University for all the countless help and wonderful support for the entire three years of my research studies, without which everything would have been impossible to achieve. I am heavily indebted and thankful to Gerard for firstly accepting me as one of his research students in his group, for the use of all facilities in the lab, for his skill in data interpretation and analysis that have led to several high quality publications, as well as his insights and dedication throughout my studies both in Manchester and Edinburgh. It is an honour to know him and his wonderful family.

I wholeheartedly would also like to offer my sincere thanks to a list of people who have been very supportive of my research needs. These are Professor Marc Desmulliez, Professor of Electrical, Electronic & Computer Engineering, School of Engineering & Physical Sciences, for his support and permission to the of use of the clean room laboratory at Heriot-Watt University, Dr. Denis Headon of Roslin Institute, Dr Kevin Painter of the Mathematics Department at Heriot-Watt University, Dr. Nicholas Willoughby of Chemical Engineering Department at Heriot-Watt University, Mark Leonard for technical assistance with electrode manufacture, Ms. Susan Slack (Research Technician, School of Life Science, the University of Manchester) and last but not least Mr. Aftab Aziz for all my IT needs and technical support at the Heriot-Watt University.

In addition, there are also a list of very talented people and wonderful friends

throughout my journey. I would like to thank you all for very helpful discussions and inspirational thoughts. These people include Ms. Ankita Singal of Life Science Department - the University of Manchester, Researchers at the Micro Structures and Micro Environments Research Group at Heriot-Watt University; Ms. Sneha Agarwal, Mr. Manuel Garcia-Albornoz, and Mr. Supavej Maniyom. Other very wonderful colleagues of mine are Dr. Anil Sebastian and Dr. Louise Carney (Research Associates, School of Chemical Engineering and Analytical Science, the University of Manchester), Dr. Pareshkumar Patel (Research Scientist, UCB-Celltech, Slough), Ms. Marzieh Bayati, Mr. Mike Littlefair, and Dr. Ke Zhu. I also would like to thank my fellow friends in my office for general discussions; Mr. Daniel Rylat, Mohammad, Yifan Liu and all other colleagues whose name are not mentioned in this thesis acknowledgement.

Finally, it is a pleasure to acknowledge all the assistance and patience of my loving wife Ita Lutfiana, and my wonderful family, as well as my parents for all the everlasting support, prayer and love they have given me. Without this, it is almost impossible to achieve anything or to tackle all difficulties that may still come ahead of us. May God be with us all, both in this world and in the hereafter. I love you all.

Thank you.

RESEARCH THESIS SUBMISSION AND DECLARATION

TABLE OF CONTENTS

CONTENTS

LIST OF TABLES

LIST OF FIGURES

LIST OF ABBREVIATIONS

2-D	Two Dimensional
3-D	Three Dimensional
µm	Micrometer
µL	Microliter
AC	Alternating Current
BMP	Bone Morphogenetic Protein
$CaCl_2$	Calcium chloride
CO_2	Carbon Dioxide
DC	Direct Current
DEP	Dielectrophoresis
DKK	Dickkopf (genes)
DMEM	Dulbecco's Modified Eagle Medium
DP	Dermal Papillae
ECM	Extra Cellular Matrix
Eda	Ectodysplasin A
EdaR	Ectodysplasin A Receptor
EDTA	Ethylene Diamine-Tetraacetic acid
EGF	Epidermal Growth Factor
EHD	Electrohydrodynamic (force)
FCS	Fetal Calf Serum
FGF	Fibroblast Growth Factor
GFP	Green Fluorescent Protein
IL	Interleukin
IRS	Inner Root Sheath
ITO	Indium Tin Oxide
Kg	Kilogram
M	Molar
mL	Mililiter
mM	Milimolar
MRM	Multi Regions Masking
NCAM	Neural Cell Adhesion Molecules

ORS	Outer Root Sheath
PBS	Phosphate Buffered Saline
P-ERK	Phosphorylated Extracellular-signal Regulated Kinases
r	radius
RCAS	Replication Competent Avian Sarcoma
ROI	Region of Interest
RPMI	Roswell Park Memorial Institute
SG	Sebaceous Gland
SHH	Sonic Hedgehog Homolog
TE	Tissue Engineering
TGF	Tumor Growth Factor
TNF	Tumor Necrosis Factor
TNFR	Tumor Necrosis Factor Receptor
$V_{pk\text{-}pk}$	Voltage Peak to peak
WNT	Wingless and Int (genes)

LIST OF PUBLICATIONS

Peer-reviewed journal publications:

Yusvana R., Headon D.J., Markx G.H. *Isolation and measurement of the features of arrays of cell aggregates formed by dielectrophoresis using the user-specified Multi Regions Masking (MRM) technique*. Journal of Physics: Conference Series 183 (2009) 012022.

Yusvana R., Headon D.J., Markx G.H. *Creation of Arrays of Cell Aggregates in Defined Patterns for Developmental Studies Using Dielectrophoresis*. Biotechnology and Bioengineering, Vol. 105 (2010), No.5, Page 945-954.

Yusvana R., Headon D.J., Painter K.J., Singal A. and Markx G.H. *Engineering embryonic skin with artificial follicle precursor patterns*. (Status: Under review for publication).

Oral presentations given at seminars (conference) around the UK:

Yusvana R., Headon D.J., Markx G.H. *Development of Virtual Instrument For The Isolation And Automatic Measurements of Distinct Features in Bio-Dielectric Patterns of Cell Aggregates Using User-Specified Multi Regions Masking (MRM) Technique*. Institute of Physics (IOP) Dielectrics Conference (15-17 April 2009), University of Reading, UK.

Yusvana R., Headon D.J., Markx G.H. *Bioengineering of Artificial Skin Tissue with Defined Geometrical Patterns of Placode-Like 3D Structures Using Dielectrophoresis*. IchemE Biochemical Engineering Subject Group – Young Researchers Meeting (13 January 2009), University of Sheffield, UK.

Scientific image competitions:

Yusvana R. Second (2^{nd}) prize in the Annual EPS Technical Photo Competition 2009

as well as several runner up prizes. Image entitled *Cell Aggregation* can be viewed online at http://www.eps.hw.ac.uk /~ryf1/EPS%20photocompetition-winner-new.htm, and is attached at Appendix section of this thesis.

Yusvana R. Runner Up prize in the SELEX Galileo EPS Scientific Photo Competition 2010. Image entitled *Fibroblast Cell Morphology* can be viewed online at: http://www.eps.hw.ac.uk/~ryf1/Main%20page%202010%20EPS%20photocompetition.htm, and is attached at Appendix section of this thesis.

Poster / online presentations:

Yusvana R., Headon D.J., Markx G.H. *Creation of Defined Arrays of Cell Aggregates Using Dielectrophoresis for The Study of Developmental Processes in Embryonic Skin*. This poster was presented in two events: (1). Edinburgh Research Partnership (ERP)-Institute of Integrated System (IIS) Advisory Group Meeting held on the 22nd January 2009. (2). MicroTech 2009 Conference: Bio-Sensors and MEMS Packaging (2-3 March 2009). Organized by I-MAPS, Edinburgh, UK.

Yusvana R, Headon D.J., Markx G.H. *Artificial Skin Tissue With Cell Arrays Created Using Dielectrophoresis: A Novel Tool For the Study of The Interactions Between Cells and Between Cells and Their Environment*. BioSysBio Conference 2009 on Synthetic Biology, Systems Biology and Bioinformatics (23 - 25 March, 2009), the University of Cambridge, UK (Status: abstract used for online presentation). Link can be seen at https://theiet.conference-services.net/resources/299/1441/pdf/BioSys2009_0122.pdf.

Yusvana R, and Markx G.H. *3D Aggregation and Patterning of Cells for Artificial Tissue: Bioengineering, Modeling and Image Analysis*. 2008 Postgraduate Research Conference on Information, Communication and Modeling at Edinburgh Business School, Heriot-Watt University on 12 June 2008.

THE AUTHOR

The author, ***Mr. Rama Yusvana***, currently works as a Biomedical Engineering Research Assistant in the Bioelectronics Research group under the leadership of Professor Jon Cooper of the University of Glasgow, UK. A biotechnology graduate from the University of Nottingham, UK and the University of New South Wales Australia, he has now expanded his interests to the field of biosensors using microfluidic devices and electrochemistry. He also has an interest in the use and application of computer programming language for science, and is a National Instrument (NI) Certified LabVIEW Associate Developer (2008). In his current role at the University of Glasgow he is involved in teaching LabVIEW for scientific applications and image analysis.

CHAPTER 1

A Preface To The Thesis

1.1 Introduction

Embryonic pattern formation is the process by which the adult form is generated by the growing embryo. The adult form of an embryo includes the formation of organs such as hairs and feathers. Pattern formation is necessary to split initially homogeneous fields of cells into cells with two or more distinct fates in a spatially organised manner, thus generating complexity.

One of the most widely studied systems of pattern formation is the exquisite arrangement of feather bud primordia in chicken in a regularly-spaced hexagonal pattern (Jiang *et al.*, 1999; Jiang *et al.*, 2004). Feather follicle formation starts on the dorsum (back) of a chicken embryo on the 6^{th} day of incubation with a linear aggregation of cells along the neural tube. Following this, the line breaks up into individual spots, and further lines and spots are formed in a wave-like mechanism, finally giving rise to a pattern of feather buds in a hexagonal pattern. Different areas of the chicken skin produce placodes with different sizes, which then develop into different appendages. For example, small circular placodes tend to develop into downy feathers, whilst large rectangular placodes develop into scales. The shape of the placode also affects the final shape of the appendage formed. To obtain full control over all these parameters, it will therefore be necessary to control not only the distribution of the aggregates in a well-defined pattern, including the distance and relative position between the aggregates, but also the aggregate size and shape.

Skin consists of two layers, the epidermis, which is the top layer, and the dermis. During the early stages of development the skin has no follicles, and although the cells in the epidermis and dermis themselves are different, within the dermis and epidermis they are thought to be all the same. At a certain stage of their development follicles form, and to be able to do that the cells must at some stage have decided to choose to become part of a follicle, or interfollicular skin. From recombination studies of embryonic skin of various organisms at different times of their development it is well-known no external signals are needed for the decision process, and that both epidermis and dermis are needed for follicles to be formed. The signal that starts follicle formation comes from the epidermis (Sengel, 1975).

The fact that the pattern *in vivo* started from a mid-line above the neural tubes which then subsequently breaks up bi-directionally along the lateral side in wave-like fashion, into individual placodes, has intrigued many scientists to propose various models to explain their formation. One of the earliest models of feather follicle formation suggested that new feather primordia are formed through sequential propagation (Sengel, 1975). Pre-existing primordial patterns were thought to work as a template for the subsequent emerging primordia. This however leaves questions such as what set up the initial template pattern. If it is positional information as suggested by Wolpert (Wolpert, 1971), then the question remains what determines the spacing between the foci. If it is differential adhesiveness as suggested by Steinberg and Takeichi (Steinberg and Takeichi, 1994), then the question remains what factor sets up the initial difference in the adhesion.

Other researchers have proposed that, rather than using a prepattern, the cells use their self-organizing capabilities to gradually emerge as periodic pattern from an initially homogeneous state (Kopan and Turner, 1996). One of the most compelling paradigms to explain the emergence of ordered heterogeneity from homogeneity has been the Reaction-Diffusion model. This idea, originating from the work of Alan Turing (Turing, 1952) and Gierer and Meinhardt (Gierer and Meinhardt, 1972), in its simplest form relies on the production of two kinds of chemical signaling molecules: an Activator, which catalyses its own production as well as its own inhibiting molecules, and an Inhibitor, which acts as antagonist of the action of the Activator. If the Inhibitor diffuses more rapidly than the Activator then foci with high Activator and Inhibitor production will emerge from an essentially homogeneous initial distribution of each compound. The Inhibitor produced by these foci will diffuse away to inhibit the reaction in the surrounds, while the Activator remains locally to maintain the reaction. This mechanism amplifies small, perhaps stochastic, deviations from absolute homogeneity to generate a spatial pattern. The actual pattern that emerges, whether large or small spots, or stripes, depends on the domain size, the kinetics of the reaction and the diffusion characteristics of the Activator and Inhibitor (Turing, 1952; Gierer and Meinhardt, 1972; Dulos *et al.*, 1996). Application of the reaction diffusion theory to the initiation and development of follicles was first proposed by Nagorcka and Mooney, without knowledge of the molecules involved (Nagorcka and Mooney, 1982; Nagorcka and Mooney, 1985).

The molecular interactions and processes involved in hair formation and feather formation are thought to be similar. Various attempts have been made to unravel the molecular processes involved in hair and feather pattern formation. The approaches used and the model animals under study varied from one group to another.

Mou *et al.* (Mou *et al.*, 2006) studied the generation of primary hair follicle patterns in mice using wild-type and mutant-type of embryonic mouse skin cultures as model system. They came up with a model for the generation of primary hair follicle pattern formation which is analogous to a Turing reaction-diffusion system (Figure 1.1-1).

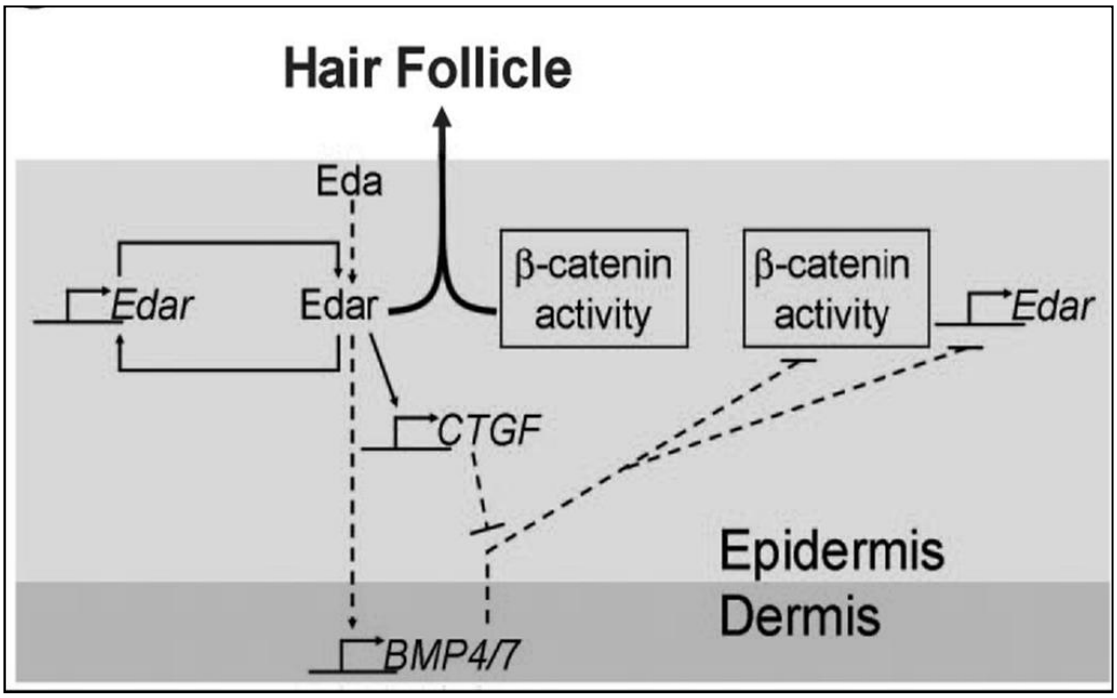

Figure 1.1-1. A model for the generation of primary hair follicle pattern showing molecular interactions that are involved in the process. Solid lines indicate local interactions, and dotted lines indicate action at a distance. Image taken from Proceeding National Academy of Science USA, June 13, 2006, volume: 103, issue number: 24, page: 9075–9080.

They proposed that the signal that starts follicle formation is ectodysplasin (Eda). Eda is an extracellular ligand which is produced by the epidermal cells and diffuses freely in the tissue. Eda binds to its receptor Edar (ectodysplasin receptor), which is bound to the cell membrane of the cells in the epidermis, and cannot diffuse through the tissue. Eda also induces the production of bone morphogenetic proteins or BMPs (BMP4 and 7) in the dermal cells.

The binding of Eda to Edar has two effects: it enhances further production of Edar by a positive feedback mechanism, and induces the production of CTGF (connective tissue growth factor). CTGF is free to diffuse; it also inhibits BMP action. High concentrations of Eda-Edar interaction in the cell are necessary for the cell to assume a follicular fate; this is linked with β-catenin production. BMP molecules are small proteins which can diffuse rapidly. BMPs inhibit β-catenin, and hence the assumption of a follicular fate.

The molecular model proposed by Mou *et al*. (2006) is similar to a Turing reaction-diffusion system. The Eda/Edar/CTGF complex forms the Activator in the reaction-diffusion system. Eda is evenly produced, and does not itself lead to pattern formation. Edar upregulates its own production (one of the prerequisites of an Activator), but does not diffuse. CTGF however does, and therefore fulfills the 2nd role of the Activator. The BMPs are the Inhibitors in the reaction-diffusion system (Mou *et al.*, 2006).

Although the molecular model of Mou *et al*. (2006) describes follicle formation in skin adequately, in reality, many other signaling molecules are also involved in follicle formation in skin including Shh, Wnt, Dkk, FGF, TGFβ2, Notch, Delta, noggin, and follistatin (Lin *et al.*, 2006a). Molecular signaling in feather and hair morphogenesis is therefore complex. Alternative models, which are also based on Turing-type reaction diffusion systems, but different signaling molecules play the roles of Activator and Inhibitor, can be found in the literature (Sick *et al.*, 2006), in which WNT/β-catenin played the role of Activator, and Dkk was the Inhibitor).

As the cells are induced to acquire a follicular fate by the gradients of signaling molecules set up in the skin, they adhere to each other and form micro aggregates. At first the adhesive forces between cells are not strong and the micro aggregates are unstable, but as the time progresses the adhesive forces between cells increase. The micro aggregates stabilize and transform to stable condensations.

Jiang (Jiang *et al*., 1999), used a feather reconstitution assay to trace back the processes involved in the formations of dermal condensations. They isolated dissociated feather mesenchymal (dermal) cells and allowed various quantities to settle on top of intact epidermal tissue, where they would receive signaling molecules and be able to reform

the periodic pattern. Different numbers (or concentrations) of dissociated mesenchymal cells resulted in feather primordia of the same fixed size when placed on the same area of epithelium. The number of inter bud spaces however varied with the mesenchymal cell concentration. This suggested that the dissociated cells were able to determine the size of the follicles, and that determination of follicle size is an intrinsic property of dissociated cells. Addition of exogenous Bone Morphogenetic Proteins (BMP) decreased the size of the follicle primordia. Addition of an inhibitor of the BMP pathway, such as Noggin, reversed the action of BMP and increased the size of primordia. The authors also suggested that adhesion molecules such as Neural Cells Adhesion Molecules (NCAM) may play a crucial role in pattern formation. They proposed that a certain number of mesenchymal cells was needed for the number of adhesion molecules to be sufficient to trigger the patterning process, which itself is modulated by morphogen ligands and receptors in the system. These studies suggest that one of the major functions of cell adhesion molecule is to mediate cell-cell contact or adhesion between the cell population in order to increase the chance that this molecule serves a key role in morphogenesis of the tissues.

Adhesion forces are mechanical forces. Some alternative models for the reaction-diffusion models for follicle pattern formation have been proposed in which mechanical forces play dominant roles. These include the mechanical and mechano-chemical models of Oster, Murray and Maini (Oster *et al.*, 1983; Oster *et al.*, 1985; Murray, 1989), which were proposed as alternatives of a Turing-type reaction diffusion system as a model for pattern formation in skin. In the Oster-Murray mechanical model the mesenchymal cells exert traction forces on the extracellular matrix (ECM), which deform the tissue. Tissue deformation leads to long-range forces in the tissues, creating local areas of tensions and compression. The mesenchymal cells in the dermis use these mechanical force gradients as guidance for the movement in the tissue, accumulating at areas of high compression.

Clearly, follicle pattern formation is complex. To date, however, the majority of experiments have involved investigations of the molecular aspects of follicle pattern formation, often by modulating certain components involved in the system (e.g. studying the effect of addition of certain exogenous morphogens and analyzing the expression of molecular transcripts related to a certain phenotype such as the size and

spacing of hair or feather primordia). Most researchers have studied follicle pattern formation in intact skin, and not reconstituted skin. The roles of parameters such as cell density, cell migration and mechanical forces are much less studied because to date they have been less amenable to experimentation. Novel methods for controlling these parameters are needed.

1.2 Aims and Objectives

The aim of this project is to construct artificial embryonic skin tissue containing placode-like 3D structures of well-defined shapes and sizes and arranged in well-defined patterns, using cells dissociated from chicken embryonic skin tissue, as a new tool for developmental biology studies. The research project will primarily focus on physical phenomena occurring during and shortly after aggregate formation of embryonic (artificial) skin tissue, rather than on the molecular processes happening in the tissue.

To achieve this aim the project will use a tissue engineering approach to create artificial skin from dissociated embryonic chicken skin cells isolated by enzymatic digestion from the dorsal part of chicken embryo (E7-E8). The project will use positive dielectrophoresis inside a miniaturized open-ended chamber for the construction of the arrays of cell aggregates as artificial placodes, followed by embedding the re-constructed tissue within a peptide hydrogel matrix. Although the use of negative dielectrophoresis for the formation of cell aggregates is also possible (Matsue *et al*, 1997), the work in this project will only use positive dielectrophoresis because the trapping forces are higher, making it more easy to hold cells against a flow through a chamber. The higher inter-particle forces also encourage cells to be in strong contact with each other for the duration of experiments, and enhance the exchange of signals between cells by direct cell-cell contact. In addition, the more natural distribution of cells in the 3-dimensional aggregates creates a more natural distribution of oxygen, nutrients, diffusible signals and other factors in the artificial tissue.

The resulting artificial tissue can be expected to have properties that are close to that of the original skin, in the sense that the reconstructed tissue also contains regions of

highly packed cells similar to placodes in the skin which are essentially aggregates of dermal and epidermal cells. The primary variables involved are aggregate size (analogous to placode size), aggregate shape (analogous to spots or stripes formation in the skin) and pattern (e.g. hexagonal or line).

Once the skin has been constructed this project will then look at the short-term behavior of the pre-patterned cells as a result of the interactions between cells and their microenvironment. It will be assumed that prior to pattern formation by dielectrophoresis the dissociated cells are equal and therefore have equal opportunities of becoming feather bud primordia or inter-bud regions. After dielectrophoresis cells in the aggregate and the inter-aggregate regions can be expected to have unequal opportunities in terms of their developmental fate. Those forming part of cell aggregates can be expected to have a greater chance of becoming feather bud primordia, and those making up the inter-aggregate regions have a greater chance of becoming inter-bud tissue.

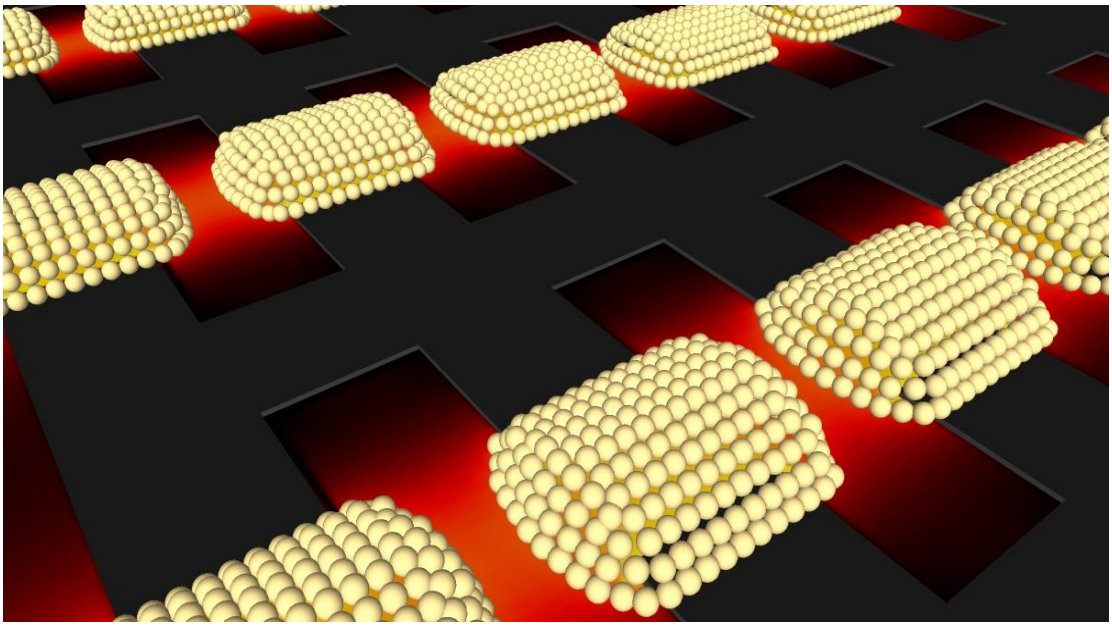

Figure 1.2-1. Stylised image of cells aggregating at high-electric field regions between electrode castellations.

Figure 1.2-1 illustrates a stylized version of cells aggregating at regions of high electric fields between the microelectrode castellations, in 3D shape with defined geometry and pattern. As illustrated in the figure, the work in this project relies on the use of microelectrode with defined geometry. Finding the best optimum process parameters involved in the chip (microelectrode) fabrication processes, used for the construction of

array of cell aggregates with defined geometry, is therefore part of the list of objectives that are aimed to be achieved in this project and attached in this thesis as a technical note in an appendix (Appendix A). Some of the primary objectives that are expected to be achieved in this project are listed in the following diagram.

1. To find the optimum process parameters for the construction of microelectrodes used for pattern formation.
2. To demonstrate the formation of 3D aggregates of skin cells with defined geometries in various patterns using dielectrophoresis, from cells dissociated from embryonic skin tissue, containing a mixture of dermal and epidermal cells.
3. To compare and study electric field simulation models with the actual data on the shape of the aggregates that were constructed during experiments with dielectrophoresis.
4. To develop a computer image analysis tool which allow the simultaneous analysis of the biodielectric pattern, using LabVIEW Vision Development Module.
5. To use LabVIEW 3D facility to assess the resulting images of cell aggregates in relation to the distribution of cells in the aggregate for a certain electrode geometry.
6. To study the response of the embryonic skin cells and their patterning with dielectrophoresis.
7. To determine factors that may play a key role in the *in vivo* pattern formation, based on on-chips observations.

1.3 Thesis Outline

The outline of the thesis is shown in the following diagram. There are a total of eight (8) chapters and a few appendices at the end of this thesis containing technical notes, poster displays, and an image gallery from a scientific image competition.

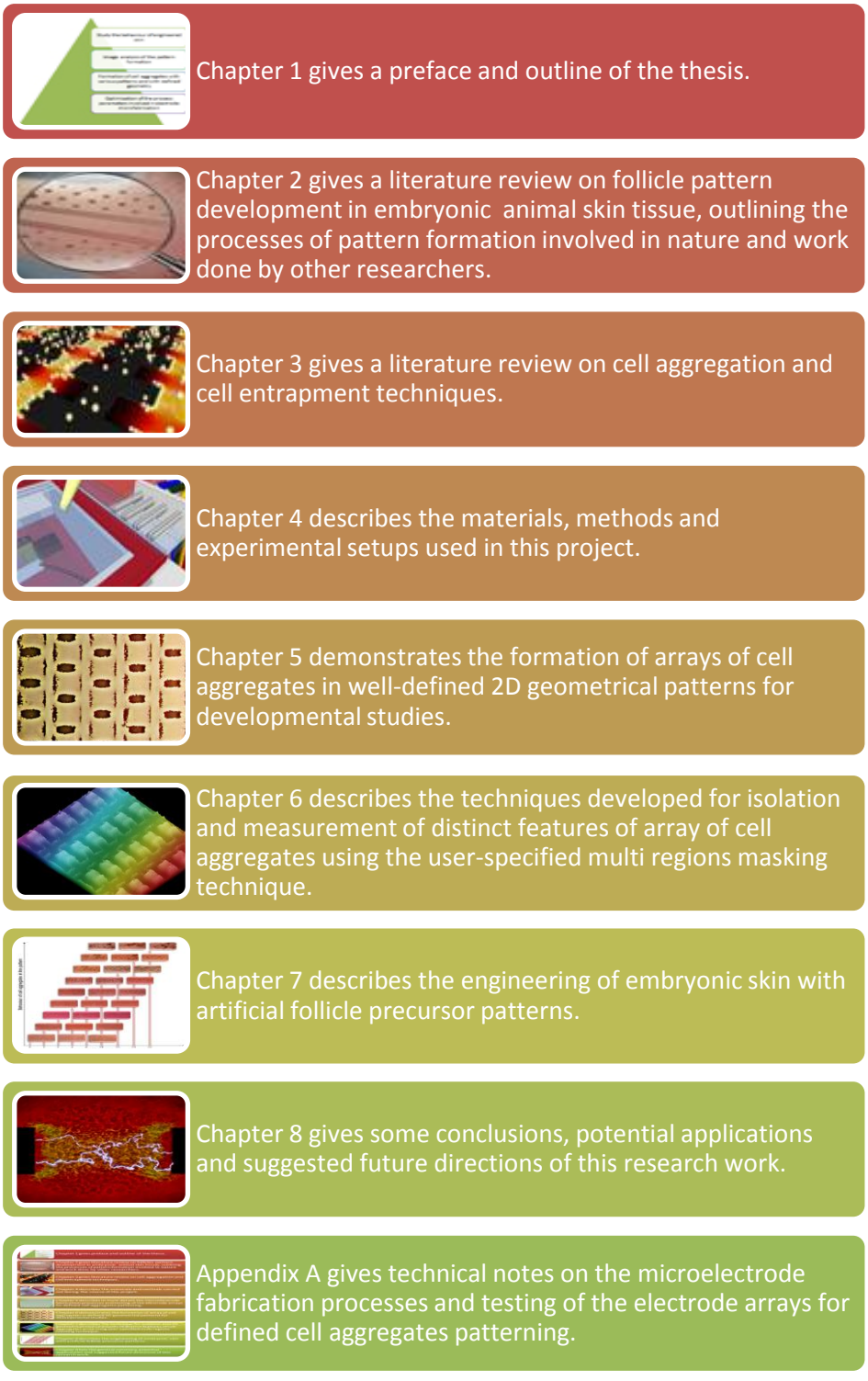

Based on the main contents of the research activities in this project, the thesis can be alternatively viewed using the following pyramid diagram, where at the base of the pyramid, we started off with general pattern formation and then focus the work more on the application side of the previously studied aggregate formation.

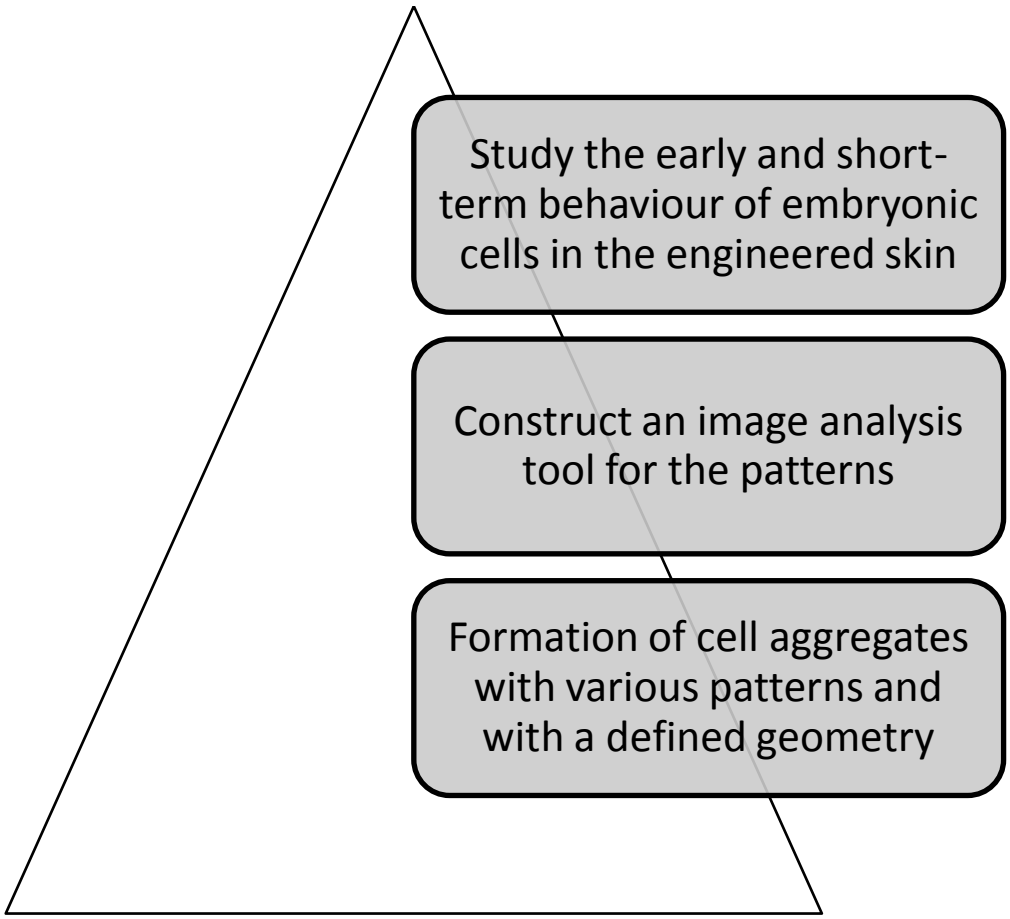

After the introductory chapters the author will explore the use of dielectrophoresis for the creation of array of 3D cell aggregates in a defined pattern mimicking the feather follicle patterns found in developing chicken embryonic skin tissue. The author will show how variations of this pattern can be produced, and demonstrate that the cells remain viable and active. In a later section, the author will show custom-built image analysis tools which can be used to extract features from biodielectric patterns for measurement purposes. The changes that occur in the aggregates after their formation will be explored and it will be discussed how artificial tissues with controlled properties could be used to test models of regular pattern formation that exist in nature.

CHAPTER 2

Literature Review on Follicle Pattern Development in Embryonic Animal Skin Tissue

2.1 Introduction

The aim of this chapter is to review the processes of natural pattern formation occurring in embryonic animal skin tissue. The chapter begins with a description of (mammalian) skin - the main layers, structures and functions. The discussion then continues with an overview of major events involved in feather / hair follicle morphogenesis and the molecular signaling involved in the processes. Fibroblast cells and their importance in the formation of feather / hair follicles are also briefly described. The review continues with a discussion of the importance of positional information with regards to the subsequent pattern development (i.e. 'the fate') of the embryonic cells. The next section reviews the mechanisms that lead to the formation of periodic patterns, in particular the reaction-diffusion mechanism. A brief review on current interests in skin tissue engineering as well as its limitations is covered in the last section.

2.2 Skin Tissue: Structures and Functions

Skin is the largest organ in the body and essential for survival. The skin is a bilayer structure that is derived from the ectoderm (epidermis) and mesoderm (dermis) of the embryo. Within these layers are specialized appendages which are also derived from the ectoderm and/or mesoderm. These include sensory nerves, sweat glands and hair follicles. Underneath mature skin is subcutaneous tissue (the hypodermis) that is composed of a loose mesh of collagen fibers, fat (adipose) cells and muscle tissue.

2.2.1 Functions

The skin has a diverse range of functions. In acts as a cover for underlying tissues and provides physical support. It helps in maintaining a constant body temperature through its blood supply, sweat glands and hairs. Protection against heat loss can be altered by adjustment of hair density through contraction of the arrector pili muscle attached to each hair follicle. Melanin pigments in the skin protect the organism against excess ultra violet rays. The epidermis, particularly the stratum corneum (the outer most keratinized skin layer) is relatively impermeable and provides a barrier against entry of

opportunistic infecting organisms. It also prevents absorption of unwanted or potentially dangerous materials, and protects the organism against desiccation. It contains an extensive network of sensory nerve receptors which enable the organism to sense pressure, texture, temperature and pain.

2.2.2 Overall structure

The top layer of skin is the epidermis. The epidermis is also called the outer avascular epithelial layer. Within the epidermal layer, there are several distinct sub layers (shown in Figure 2.2-1).

The basement membrane or basal lamina is a thin membrane that lies between the epidermis and the dermis. The stratum basale (stratum germinativum) consists of single layer of cuboidal cells with sparse, basophilic cytoplasm and a variable amount of melanin which are connected to adjacent cells by desmosomes and to the basal lamina by hemidesmosomes. Their role is to continually divide and produce new skin cells. Above the stratum basale is the stratum spinosum, which is typically several cells thick, followed by the stratum granulosum which is usually 1-3 cell layers thick, flattened, and has nucleated cells with basophilic keratohyalin granules. The stratum lucidum is usually found only in thick skin, and consists of a thin layer of very flat, eosinophilic, enucleated cells. The stratum corneum is the uppermost layer. This layer is comprised of non-living, highly keratinized (cornified) cells.

Keratinocytes make up about 90 % of the epidermal layer. As keratinocytes leave the germinal layer (stratum germinativum) the epidermal cells undergo a specialized form of cell death known as anoikis. As they progress towards the top of the skin, the skin cells desquamate: they produce keratin, flatten and lose their nuclei and other internal organelles. When they reach the stratum corneum the skin cells are dead, filled with keratin and devoid of nuclei and organelles.

The dermis is a dense inner connective tissue layer. Its main function is to provide mechanical support and strength. The sweat glands and hair follicles mostly reside in this layer. The dermis is of mesodermal origin and consists mainly of two sub layers. The papillary layer forms dermal papillae (DP) and ridges, and also contains type I

collagen and reticular fibers. This sub layer contains lots of blood vessels and nerve endings. It is more cellular in appearance. The second main component of the dermis is the reticular layer which is typically thicker and less cellular than papillary layer. It contains larger diameter type I collagen and elastic fibers. Cells within it are mainly fibroblasts, lymphocytes, macrophages and mast cells Figure 2.2-1.

The hypodermis or subcutaneous layer is a loose connective tissue between dermis and underlying structures which permits movement between the two. It is not considered to be part of skin proper. It is also sometimes called the superficial fascia. The hypodermis is the principal area of fat storage, providing energy reserves and insulation. Cell types in this layer are mainly adipocytes, fibroblasts, lymphocytes, macrophages, and mast cells.

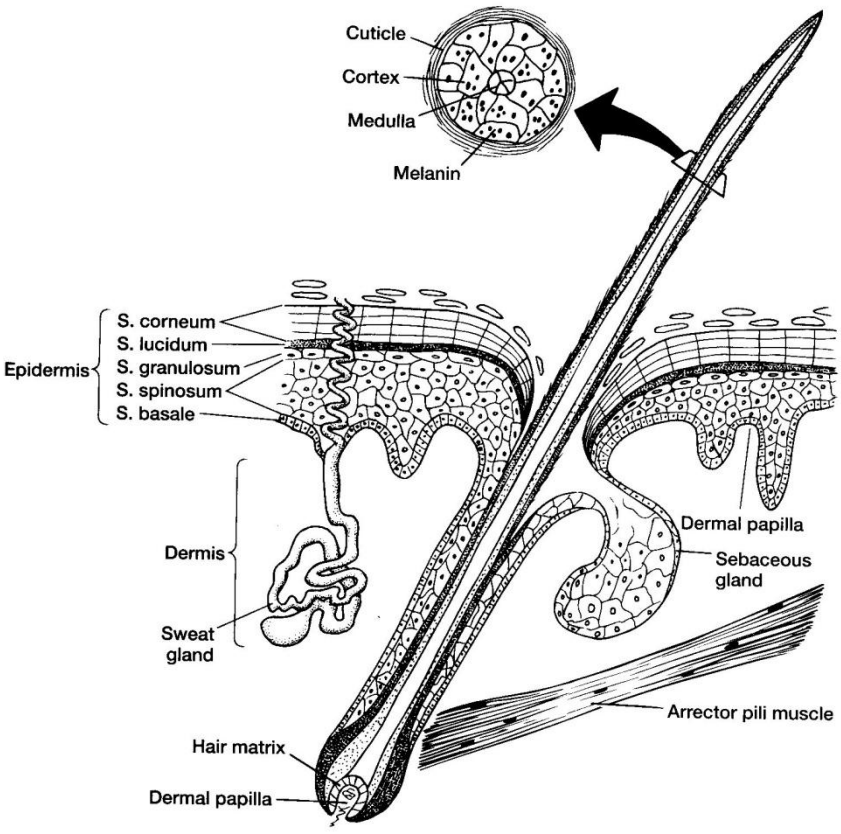

Figure 2.2-1. Hair follicle morphology showing the major layers and structures of the skin. Image taken from www.anatomy.iupui.edu.

Fibroblasts play an important role in synthesizing and maintaining the extra-cellular matrix of many animal tissues and have a critical role in wound healing. The main bulk of the skin consists of fibroblasts and related connective tissues. Unlike the epithelial

cells lining body structures, fibroblasts do not form flat mono-layers. There are two main types of fibroblasts – active fibroblasts and inactive fibroblasts (fibrocytes). Active fibroblasts contain abundant rough endoplasmic reticulum. On the other hand, the inactive fibroblasts are smaller and spindle-shaped, and have a reduced amount of rough endoplasmic reticulum. The cells usually have a branched cytoplasm, speckled nuclei and contain one or two nucleoli.

Fibroblasts are derived from the primitive mesenchyme (Doljanski, 2004). These cells play a vital role in extra cellular matrix (ECM) production and deposition. This enables them to shape the ECM and push or pull other cells. These cells continuously secrete precursors of the ECM, a variety of fibres and thus maintain the structural integrity of connective tissue. Much research has been carried on the role of fibroblasts in the formation of hair follicles (Hardy, 1992; Reynolds, 1999).

2.2.3 Structures within the skin

The sebaceous gland and the sweat gland are the two major glands in the skin. The sebaceous glands form part of the hair follicle. The sweat glands help in maintaining body temperature and assist in the secretion of waste metabolites. The structure of sweat glands is relatively simple and consists of coiled tubules.

The other major structures in mammalian skin are hair follicles. Hair follicles are responsible for the production and growth of hair. Their formation and maintenance are based on the interaction between dermal and epidermal components. During fetal development the follicles develop by down-growth of epidermal cells into the underlying mesenchyme. They have the same basic structure but vary in size and shape (Millar, 2002). They are composed of several concentric cylinders of epithelial cells called the root sheaths, which surround the hair shaft. In addition, the structure at the base contains specialized dermal cells forming the dermal papilla (Figure 2.2-1). These dermal cells play a vital role in the regulation of successive cycles of postnatal hair growth. Apart from producing hair, the hair follicles are also capable of restoring the epidermis and are considered to play a role in wound healing. Extensive researches have been carried out on investigating hair follicles in animals such as mice (Hardy, 1992), and sheep (Jiang *et al.*, 1999).

2.3 Hair Follicle Development

Hair follicle formation has mainly been studied in mice. In mice the larger primary guard hairs are formed first, and the bulk of the hair coat follicles follow a few days later. Hair follicle morphogenesis in mice commences at approximately embryonic day (E) 14.5. The process starts when the dermal cell population receives signals from the epithelium and are induced to form dermal condensates. Continuous interaction between the mesenchymal (dermal) and the epithelial (epidermal) part of the skin results in the formation of placodes, which are aggregates of tightly packed dermal cells beneath the epithelium and appear at a cross-section view as small epidermal penetration into the dermis area (Figure 2.3-1). The dermal condensates subsequently develop into dermal papillae (DP), which form the permanent mesenchymal component of the hair follicle.

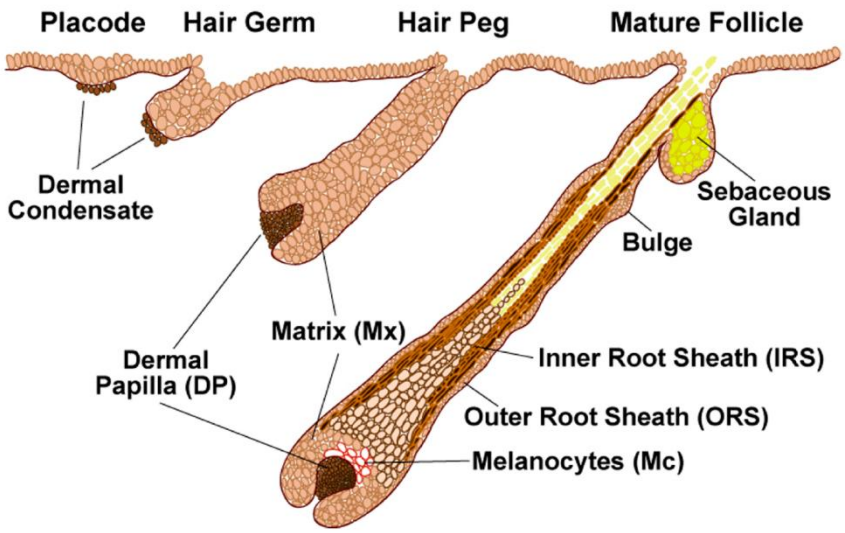

Figure 2.3-1. Embryonic stages of hair follicle morphogenesis in mouse (Image from: Fuch. E, J. Cell Biol., Volume: 180, No: 2, January 28, 2008 273–284).

Within the next 24 hours , around day (E) 15.5 of embryogenesis, the placodes undergo a marked downward proliferation to produce the first wave of the hair germs as shown in Figure 2.3-1, followed by subsequent hair peg formation at around E-16.5 to E-17.5. At this stage cell condensates within the dermal papillae have increased in size. The matrix cells at the front end remain actively growing. Through cell-cell contact with the enclosed cell condensate (DP) they activate a cascade of gene expression that differs from that of the root sheath. Through contact with the basement membrane, the outer root sheath (ORS) continues to grow while at around E-18.5, the inner part of the root

sheath provides the channel for the budding hair follicle. On the day the embryo is born, the most fully developed hairs begin to penetrate the skin surface, and at around the same time, sebaceous gland (SG) precursor cells begin to develop in the upper part regions of the shooting root. The hair follicle continues to become mature throughout the first week after birth (Fuchs, 2007).

Hairs are formed by continuous proliferation of the cells in the dermal papilla. As these cells are pushed up the central canal of the hair shaft they become filled with keratin.

2.4 Feather Follicle Development

Feathers are much more complex than hairs. Feathers have three levels of branching, firstly from shaft (rachis) to barbs (ramus), then from barbs to barbules and finally from barbules to cilia or hooklets, also called barbucelles. Feathers can eventually develop into a variety of forms, including downy feathers, contour feathers, or flight feathers (Figure 2.4-1).

Feather follicle development occurs in the embryo, forming a long bud. Actively proliferating cells continue to divide to produce new daughter cells at the base of feather follicle and push the more differentiated portion of the feather filament upwards to the distal end. Immediately above this zone, the epithelial cells start to form the rachidial ridge and the barb ridges or ramogenic zone as shown in Figure 2.4-1 and Figure 2.4-2.

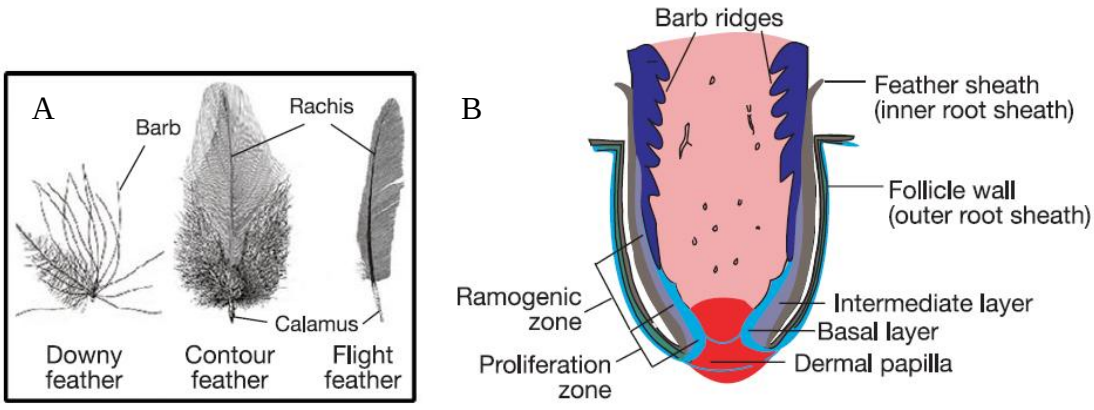

Figure 2.4-1. Feather morphogenesis. A. Different types of feather. B. Diagram of feather follicle structure (Image from: Yu e*t al*, Nature, Volume 420, 21 November 2002, page 308-312).

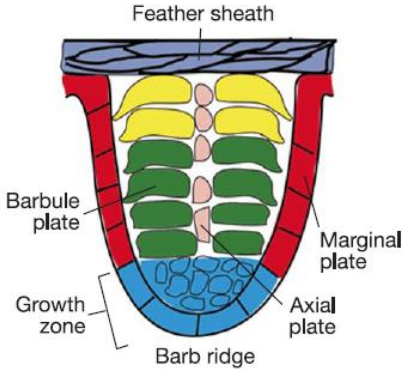

Figure 2.4-2. Diagram of feather barb ridge (Image from: Yu *et al*, Nature, Volume 420, 21 November 2002, page 308-312).

Feathers are formed in the feather follicles by a series of invagination and evagenation activities leading to the three levels of branching. In a more distal position along the follicle, the barb ridge epithelia experience active cell division and differentiate to form the marginal plates, barbule plates and axial plates (Figure 2.4-2). The barb ridges proliferate to form barbs, whereas the marginal and axial plate cells proceed to apoptosis (cell death) to become the intervening space (Chang *et al.*, 2004). The central pulp can also undergo apoptosis, allowing the feathers to unfold and assume a flat shape (i.e. from 3D cylindrical back to 2D plane). The individual barbule plate cells undergo further cell shape changes to form the cilia. The barb ridges fuse at the proximal end to form the rachidial ridge, which eventually becomes the rachis.

There are five distinct phases during feather follicle morphogenesis (Figure 2.4-3). The macro-patterning phase is an active proliferation phase during which the dermal cells start to build up a high population cell density. The formation of competent feather tract fields (specification of the areas where the feathers will be formed) also occurs during this phase. In the micro-patterning stage placodes are formed. This can first be seen by the formation of elongated epithelial cells (epidermal collar) followed by dermal condensation (Wu *et al.*, 2004). The formation of placodes in periodic patterns is thought to involve a molecular reaction-diffusion mechanism which sets up gradients of follicle-promoting Activator molecules such as Edar and Shh, and a follicle-inhibiting group of Inhibitor molecules such as BMP, leading to the formation of placodes in periodic patterns. The next phase is the intra-bud morphogenesis phase during which short buds develop an asymmetry along the anterior-posterior axis and elongate along the proximal-distal axis to form long buds (Chuong and Edelman, 1985b). The fourth phase is the feather follicle morphogenesis stage which involves changes in the

topobiology of the follicle, including follicle invagination and the formation of barb plates and marginal plates. During this stage the locations of epithelial stem cells, transiently amplifying cells and differentiating cells are specified. The fifth stage involves cycles of feather loss and regeneration, whilst lasts the bird's whole lifetime.

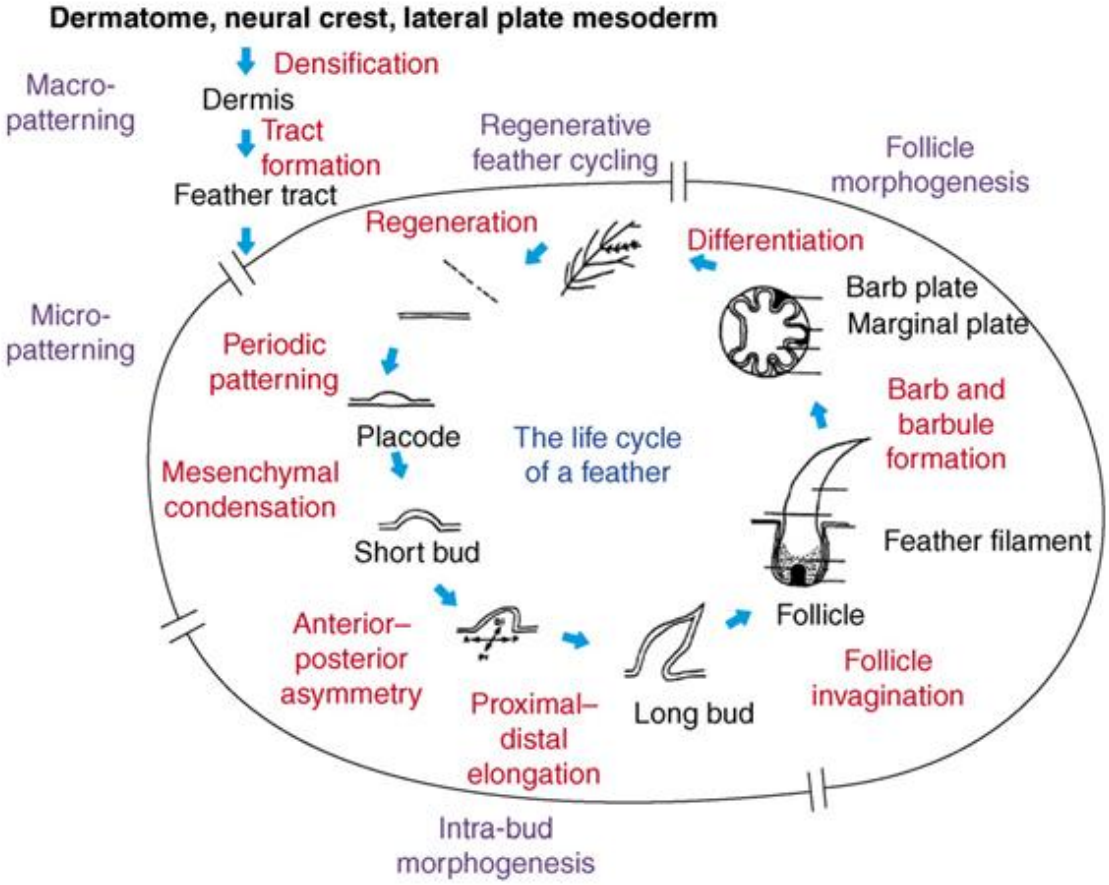

Figure 2.4-3. Overview of feather morphogenesis showing the life cycle of a feather. The five phases of feather morphogenesis are shown in blue. Major morphological events are in red. Image taken from Lin *et al*. (2006).

2.5 Molecular Signaling During Morphogenesis

2.5.1 Molecular signaling during feather follicle morphogenesis

Whilst the molecular signaling that leads to the formation of periodic densification of dermal cells (macro-patterning phase) and ultimately placode formation (micro-patterning phase by a reaction-diffusion mechanism) in hairs and feathers are generally similar, feather undergoes a more complex morphogenesis that eventually leads to various feather types (downy, contour and flight feathers). There are three additional distinct phases after placode formation in feather. These are intra-bud morphogenesis

phase, feather follicle morphogenesis phase, and regenerative feather cycling phase.

There have been quite a few studies into the molecular signaling that occurs during feather formation. Results of *in situ hybridization* experiments against RNA transcripts expressed during feather morphogenesis have suggested that the expression of the genes involved in the process is dynamic. For example, during the formation of flight feathers of 15-day-old chicken embryos (E15) - BMP4 transcripts were present in the dermal papilla and overlying pulp area, but at a later time, BMP4 was also expressed in barbule plate cells. Similarly, BMP2 was present in the marginal plate epithelia in early ramogenesis (Harris *et al.*, 2002), but quickly transferred to barbule plate epithelia. Noggin transcripts were detected in the pulp cells, overlapping with BMP4 transcripts. Noggin was not expressed in the dermal papilla, but was expressed in the pulp regions adjacent to the epidermis (Yu *et al.*, 2002).

Genetic recombination experiments are often conducted by either over expressing exogenous genes in the organism, repressing the expression of specific genes by a known inhibitor or using mutants of specific phenotypes and restoring the function of the genes using molecular vectors. A commonly used vector in this is the Replication Competent Avian Sarcoma (RCAS) retrovirus. Because remige feathers can regenerate relatively quickly at a rate of approximately 0.5 cm day^{-1} (after plucking), the organs are excellent recipients transgenic constructs of RCAS-mediated gene expression, which only transduces cells undergoing active proliferation (Morgan and Fekete, 1996). The control usually use feathers injected with RCAS–LacZ virus and show no changes in the formation of ectopic rachis or barbs.

For example, to test the role of Noggin in feather morphogenesis, a construct containing RCAS–Noggin was injected into the feather follicles to perturb the BMP pathway (sample number, n = 36). Many of the regenerated feathers were severely dwarfed, forming few barbs (33%) and split rachis (i.e. transformed into two or four mini-rachides (44%). These smaller rachides gradually converged at the proximal end. Barbs of the regenerated feathers expressing exogenous Noggin were inhibited (50%) and some barbs (11%) were branched into two. This indicates that Noggin plays a role by inhibiting the BMP pathway. Repression of the BMP pathway disturbs the balance of follicular morphogenesis and results in over-expression on the follicle formation side

and consequently leads to ectopic feather morphogenesis.

Similarly, in order to investigate the role of Shh in feather follicle morphogenesis (branching), Shh could be suppressed using cyclopamine (Cooper *et al.*, 1998) or RCAS – antisense Shh in plucked and actively proliferating feathers. The two independent reagents gave similar results that showed regions where barbs were fused by means of a web-like membrane, thus forming continuous feather vanes, which indicated that barb ridges failed to separate because the marginal plate cells failed to disappear.

The result of this study suggested that feather morphogenesis involve the transformation of epidermis into epidermal ridges by modulation of Activators (such as Noggin) and Inhibitors (such as, BMP4) in the adjacent dermal cells. The balance between these two molecules determines the number, size and spacing of barb ridges. At the tip of highly mitotic zone, the level of BMP4 is much higher than that of Noggin, thus the epithelial cells form a cylindrical structure. Above this zone (ramogenic area), the level of Noggin in the pulp nearby to epithelia gradually exceeds that of BMP4, resulting in the epithelial cells starting to form multiple barb ridges. Subsequently, the basal layer becomes regularly arranged into Shh positive/BMP2 transiently positive marginal plate cells that undergo apoptosis and Shh negative cells from the barb ridge growth zone that actively divides. The death of marginal plate cells ensures the formation of spaces between barb ridges and has also been reported by other researchers (Chuong and Edelman, 1985a). The cells in the barb ridge express BMP2 and BMP4, line up, and become two rows of barbule cells that eventually differentiate to form the barbule plate cells which upon signaling by BMP2 and BMP4 change shape to form the cilia and hooklets. Towards the end of feather follicle morphogenesis, Noggin activity is finally decreased and the situation reverts back to the beginning, forming the calamus without branches at the proximal end of the feather shaft. If the ratio of Noggin:BMP becomes polarized in the anterior – posterior axis, the site with higher BMP activity eventually becomes the rachis, that results in symmetric feather formation (Yu *et al.*, 2002).

2.5.2 Molecular signaling during hair follicle morphogenesis

Similar to molecular signaling involved in feather morphogenesis, one signaling molecules that appears to be important in hair follicle development and maturation is

Noggin, a BMP inhibiting protein. The removal of this molecule affects hair follicle morphogenesis severely, and gives rise to an abnormal (probably ectopic) morphology (Botchkarev *et al.*, 1999). Wnt signaling molecules derived from ectodermal tissue, such as Wnt10b, are believed to work in conjunction with mesenchyme signaling molecules leading to downgrowth proliferation of the epidermal cells (Botchkarev *et al.*, 1999; DasGupta and Fuchs, 1999; Reddy *et al.*, 2001; Andl *et al.*, 2002).

Complex transcriptional factor LEF1 and stabilized β-catenin molecules are essential during hair follicle morphogenesis (Van Genderen *et al.*, 1994; Zhou *et al.*, 1995; Gat *et al.*, 1998). Inhibition of BMP pathway allows expression of LEF1 gene and stabilize the β-catenin pathway (Jamora *et al.*, 2003; Kobielak *et al.*, 2003; Andl *et al.*, 2004; Zhang *et al.*, 2006). The large primary guard hairs rely on a complex of TNF-like ligand and its receptor made up of Ectodysplasin A (Eda) and Eda receptor (Edar). This complex promotes two different inhibitors - BMP4 and BMP7. Wnt signaling acts on Ectodysplasin A (Laurikkala *et al.*, 2001). When follicle morphogenesis begins and LEF1/ β-catenin pathway are initiated (by E14.5), Wnt reporter gene activity can be used as molecular marker for the process (DasGupta and Fuchs, 1999; Pummila *et al.*, 2007).

The results of research activities in the past few years indicate that β-catenin pathway is the key to hair follicle morphogenesis. The presence at unnatural location of hair follicles formation in between the bud regions can be derived when surplus production of β-catenin is alleviated in the epithelium of transgenic mice, resulting in the formation of super-hairy mice (Gat *et al.*, 1998). Conversely, if Dickoff 1 (Dkk1) – a repressor of Wnt signaling is expressed ectopically or when the pathway of β-catenin is repressed, the formation of hair follicle is stopped (Huelsken and Birchmeier, 2001; Andl *et al.*, 2002). The finding emphasizes the critical function of stabilized β-catenin in determining the decision of becoming either bud or inter bud regions. At the onset of placode development a cascade of transcriptional activation further down the pathway of Wnts/BMPs transduction forces the downward proliferation and development of newly formed hair follicles (Fuchs, 2008).

Expression of Sonic hedgehog (Shh) genes commences further down of the Wnt/BMP receptor pathway (or Eda/Eda receptor pathway for hair) during placode formation

(Dahmane *et al.*, 1997; Oro *et al.*, 1997; Gat *et al.*, 1998; Morgan *et al.*, 1998; St-Jacques *et al.*, 1998). It is well known by many researchers in the field that Shh is involved in the transformation of dermal cells into condensates which are subsequently transformed into dermal papillae (Hardy, 1992; St-Jacques *et al.*, 1998; Oro and Higgins, 2003; Levy *et al.*, 2007).

In addition to genes expressed in the early stages above, the activation of other transcriptional factors such as Lhx2 and Sox9 also play a critical role (Vidal *et al.*, 2005; Rhee *et al.*, 2006). The ablation of transcripts of these gene results in the failure of the stem cells to maintain hair follicles in mice. Additional modulation involved in hair follicle morphogenesis may also include attenuation of some adhesion proteins such as NCAM and cadherin and increased expression of other genes (Jamora *et al.*, 2003).

2.6 The Role of Positional Information in Pattern Development

Having reviewed the main components and structures of the skin, the next question is to find out how nature controls the relative size and location of the organs such as hair follicles, in a precise pattern and proportional manner. The molecular processes that lead to these periodic patterns, including the black and white stripes in zebra skin and hexagonal patterns of feather buds in chicken, are of great interest to developmental biologists.

Cells in early embryonic stages exist in developmentally uniform or homogeneous conditions. These cells can generate any cell type in the mature animal (toti- or multi-potency). This uniformity then breaks down to ultimately produce different and often complex organ structures. The transition from a uniform state to a non-uniform state requires the ability of the cells to sense the external environment. According to Headon and Painter (2009), a degree of positional information could be gained even in a passive mode. For example, cells could detect asymmetries due to external stimuli (e.g. at the point of entry of sperm cells into the egg cells during fertilization) or it can also be due to aspects of intrinsic non-uniformity resulting from the embryo's own geometry (e.g. differentiated cells at the embryo periphery compared to those at the inside of the embryo). The extent of positional information gained from this method is however

inadequate to trigger more complex and yet organised structures such as placode primordia (Headon and Painter, 2009).

Further development of the cells in the embryo to their ultimate fate is often mediated via the production of diffusible signaling molecules, known as the morphogens. Morphogens are macro molecules (such as proteins) that are capable of eliciting one or more of a number of possible effects via extra- or intra- cellular signal transduction pathways that ultimately affect the cell's fate according to the morphogen's local concentration. As a result, a morphogen gradient present in one cell population can further subdivide the population and produce large distinct regions in the surrounding cells, leading the cells to various developmental states according to their relative distance or proximity to the morphogen's original source (Headon and Painter, 2009).

These main conceptual modes of pattern formations have been very successful in explaining major aspects of development related to structures exist in mainly periodic manner. The morphogen gradient theory as a means to generate embryonic cell positional information has received strong experimental evidence from systems such as segmentation in insects and digit patterning of the hands and feet (Vincent and Briscoe, 2001; Gilbert, 2006; Wolpert, 2006).

There are two main distinct types of positional information that are used to explain the widespread occurrence in nature of the periodic structures such as hair follicles, feather buds, renal glomeruli, intestinal villi or pulmonary alveoli. They are termed absolute and relative cell positional information.

2.6.1 Absolute cell positional information

The absolute cell positional information theory has been used to explain the 14 segmented patterns that occur in the fruit fly *Drosophila melanogaster*, which consist of 7 striped elements and 7 intervals. In this system, it is thought that there is no single patterning mechanism to lay out all the 7 striped segments as a whole simultaneously (Akam, 1989). The pre-pattern however, already exists prior to egg fertilization and emanates from molecular asymmetries of morphogen gradients. As a result, a set of genes transcriptional regulatory apparatus, called pair-rule genes, are expressed in an alternating pattern encoding the periodic pattern of parasegments of the seven striped

elements and seven intervals in the fruit fly body segments. The process triggers a complex cascade of molecular interactions and a large number of genes to place each of the 14 parasegment stripes in a regular pattern (Wolpert, 2006). It has been proposed that each stripe of pair-rule gene expression is regulated independently of the others (Harding *et al.,* 1989). When a genetic perturbation experiment was conducted in which development of one of the parasegments in the fruit fly was disturbed, the position of the other parasegment was not affected in the pattern. Thus, it was concluded that each cell in the parasegments acquires its location and identity information independently of the other elements in the pattern and acquires absolute information about its position in the embryo.

2.6.2 Relative cell positional information

The relative cell positional information theory is mainly used to explain the occurrence of periodic patterns of a structure that exists in numerous quantities such as hair and feather follicles in skin. The absolute positional information model would be unsuitable as it is difficult to imagine such regulatory system being able to determine the position of every one of the total approximately 2×10^6 hair follicles in a human skin (Paus and Cotsarelis, 1999). Therefore, an alternative approach has been proposed in which a single rule determines the position of each follicle relative to its immediate neighbors, rather than giving each hair a definite coordinate of its anatomical position. Such a relative positional model could cover any area of skin with a given hair density. The relative cell positional information theory can easily adapt to changes in size and growth of the organism and provides a regulatory efficiency compared with the absolute positional model. This system will be discussed further in the following section.

2.7 Molecular Reaction-Diffusion Mechanism for Generating Periodicity in Follicle Patterns

This section reviews and discuss the mechanisms of pattern formation that give rise to many steady state patterns in a biologically oriented activator–inhibitor model system. The review will begin from the most basic concept of mechanistic models of biological pattern formation.

2.7.1 Basic mechanisms for biological pattern formation

A wide variety of mechanistic models have been proposed by scientists in the field of developmental biology with regards to *de novo* pattern formation in the cells of embryonic animal systems (skin follicle patterns, digits formation, etc). However, there are two major types that are commonly believed to be most successful in explaining the phenomenon of pattern formation. The first type is the chemical pre-pattern model and the second is the cell/mechanical interaction model. There are however, inevitably grey areas between the two, in that a chemical pre-pattern model often involves a certain degree of mechanical contact between the cells, and *vice versa*.

The chemical pre-pattern model, as the name implies, begins with a certain pre-existing molecular pattern derived from the amplification of an essentially uniform system in the cell's own environment. The cells in this case are essentially passive and pattern formation relies heavily on the chemicals involved (often termed the morphogens) to drive further, subsequent organization of the cells (often termed chemotaxis – the movement of cells to the source of chemo-attractant or areas with higher morphogen concentration). Such mechanisms have received a significant amount of experimental evidence explaining the existence of spatially periodic embryonic structures, such as hair follicles, pigment patterns, as well as the process of somitogenesis.

The cell/mechanical interaction models are best exemplified by chemotaxis as occurs in the life cycle of the cellular slime mold *Dictyostelium* where cells play a fundamental role in driving pattern formation (Keller and Segel., 1970). In this process, the formation of patterned cell aggregates of slime mold *Dictyostelium* is the result of the migration of the cells up a chemical gradients generated by the cell's own population. Armstrong *et al.* (2006) proposed a continuum approach to modeling spatial cells patterning based on adhesion molecules expressed by the cell's own population (Armstrong *et al.*, 2006). Murray *et al.* have suggested that reciprocal forces between the cells and the surrounding extracellular matrix are required for biological pattern formation in a mechanochemical model (Murray, 2003).

2.7.2 Reaction-diffusion mechanism

All of the cell-based models for biological patterning described above are capable of generating periodic structures from an essentially homogeneous initial condition. The mathematical illustration of this concept originates from the work of the mathematician Alan Turing who first proposed the idea of a reaction-diffusion mechanism in the beginning of 1950s. Important further work was done by Gierer and Meinhardt in 1972. It is also often termed the diffusion-driven instability (DDI) mechanism, which at its simplest form involves the existence of two reacting and diffusing substances or morphogens. The 'reaction' part of the component involves an Activator, which catalyses its own production as well as stimulating the production of its own Inhibitor. The 'diffusion' part of the system refers to the diffusion of an Inhibitor at relatively faster speed than the Activator. It does not necessarily mean that the physical properties of Inhibitors include a lower molecular weight than the Activator, because most extracellular proteins are subjected to post-translational modification once secreted from the cells. It is therefore better explained that the Inhibitor has greater range of action than the Activator. As a consequence, local signal intensification surrounded by attenuation of the activating signatory molecules in the periphery results in the formation of periodicity, which in the case of feather morphogenesis in chicken embryonic skin gives rise to a periodicity of bud and inter-bud regions. Foci of high Activator production surrounded by an inhibited zone can emerge from near homogeneous initial concentrations through a process of short-range activation and long-range inhibition (Turing, 1952; Gierer and Meinhardt, 1972). This is one of the most convincing models to explain the emergence of periodic patterns from an initially uniform condition.

Similar to an 'Activation-Inhibition' type of reaction-diffusion model is the 'Substrate Depletion' model. In this model however, there is no Inhibitor. Periodic patterns are the result of a limiting amount of a diffusible Activating factor. Competition for this substance eventually leads to a similar result of foci with high intensity surrounded by inhibition of the signal in the surrounding, in the form of local sequestration of the ligand and reduction of the signal in the periphery regions of activated cells. One of the best examples utilizing this model is the work on Trichome patterning in *Arabidopsis*,

where patterning is governed by the removal of the trichome-promoting factor *Transparent Testa Glabra1* (TTG1) from non-trichome cells (Bouyer *et al.*, 2008).

In order to give rise to anatomical structures such as placodes or hair follicles in an embryonic skin, the cells in the activated zone must be able to perceive the signaling molecules and respond according to the type and concentration of the morphogens. This is the beginning of the generation of complexity by resolving the essentially homogeneous field of cells into two or more distinct types in a spatially organised and periodic manner, using relative models of cells positional information.

Scientists have suggested that the appearance of spots (large or small) or stripes (long or short, straight or bent) in a 2-dimensional field depends on both the kinetics of the reaction and the diffusion characteristics of the Activator and Inhibitor (Jiang *et al.*, 2004; Meinhardt, 2004). The intrinsic properties of the field within which the mechanism operates can significantly affect the pattern outcome. For example, the existence of a controlled growing domain in the underlying field may determine a precise patterning sequence (Crampin *et al.*, 1999). In addition, the boundary conditions also play a role in the resulting pattern formation (Dillon *et al.*, 1994). Researchers have also given a detailed analysis in one or two spatial dimensions, and explored the pattern formation mechanisms and their dependence on the initial conditions. The existence of pre-patterning within the field may provide regional heterogeneity prior to the onset of pattern formation (Yochelis *et al.*, 2008).

There are quite a few examples of experiments which have been conducted worldwide in order to verify and conform that the molecular interactions are in agreement with the predictions of reaction-diffusion models (Jiang *et al.*, 1999; Harris *et al.*, 2005; Mou *et al.*, 2006; Sick *et al.*, 2006). Many of these experiments have been carried out using embryonic skin from various animals as it provides an excellent experimental system for exploring periodic patterning in development. In addition, simple experiments that have ablated pigment pattern elements (stripes) in zebra fish (Yamaguchi *et al.*, 2007) or perturbed patterning fields experiments of hair follicles in mouse (Mou *et al.*, 2006) have indicated that the cells have acquired relative positional information to their neighbouring pattern elements and not according to an absolute positional coordinate system, consistent with the operation of a reaction-diffusion mechanism.

In addition to being theoretically well developed and successful at explaining biological patterning, the reaction-diffusion simulations are also able to generate organic-looking patterns and textures in computer modeling, mimicking those found in biological patterns (Turk, 1991). Such simulations provide a convenient tool to study naturalistic, non-repeating patterns in skin images, and could make such systems useful during studies of embryonic development.

2.8 Pattern Development in Hair and Feather Follicle

As mentioned above, the formation of hair and feather follicles pattern can be explained using a Turing reaction-diffusion mechanism. There are several key characteristics of this model. The core molecular interactions of the system consist of an Activator that promotes its own activity as well as indirectly impairs its own production via the activation of its Inhibitors. Activator and Inhibitor production must be restricted or confined to the same spatial location, in this case the sites of placode formation. The range of action of the Inhibitor must be higher than that of the Activator in order to suppress the surrounding of cells with high Activator concentration. The diffusion characteristics of these two components must be determined empirically as extra-cellular proteins are subjected to further modification such as lipid addition or glycosilation (Cui *et al.*, 2001; Teleman *et al.*, 2001; Eaton, 2006). The timing of the interactions, i.e. upregulation of the Activator, initiation of Inhibitor production, diffusion of the Inhibitor, and downregulation of the Activator by the Inhibitor at a distance must all occur just before pattern formation.

For the purpose of literature review, we will start the review by identifying the major components of the interaction and then briefly the molecular processes that lead to follicular or inter-follicular fate.

2.8.1 Major components of reaction diffusion system that control follicle fate

Identification of the molecules that play a role in hair follicle (Schmidt-Ullrich and Paus, 2005) and feather (Yu *et al.*, 2004a) placode development has come mainly from the study of inherited skin abnormalities during development and the advanced molecular analyses of candidate genes known to play a role in the development of many

organs. In addition, computer numerical analysis has long been able to mimick the periodic patterns formed using a reaction-diffusion mechanism (Mooney and Nagorcka, 1985; Nagorcka and Mooney, 1985). Skin has also been a good source of raw material for the identification of the major components of the reaction-diffusion mechanism from practical point of view considerations. The availability of large amount of embryonic skin tissue for conducting the experiments, analysis, and observation, as well as the non-essential nature of follicle formation and manipulation for the organism's viability have driven researches in this area to use skin as a primary source of raw materials. In addition, the method to culture dissected embryonic skin in order to observe and manipulate pattern formation has long been established.

Several groups of Activators and Inhibitors of placode formation have been identified. Known activators of placode fate are Wingless/Int (Wnts) family members (Noramly *et al.*, 1999; Andl *et al.*, 2002; Narhi *et al.*, 2008), Ectodysplasin or Eda for short (Laurikkala *et al.*, 2002) and Fibroblast Growth Factors, FGFs (Song *et al.*, 1996; Mandler and Neubuser, 2004). As the name implies, downregulation of the function of any of these molecules diminishes placode formation, and conversely their experimental enhancement leads to placode overproduction.

Inhibitors of placode formation are characterized by their ability to inhibit placode formation when activated, and placode overproduction when repressed. Known inhibitors of placode formation are the Bone Morphogenetic Proteins, BMPs (Jung *et al.*, 1998; Noramly and Morgan, 1998), Dickoff proteins, Dkks (Andl *et al.*, 2002) and Epidermal Growth Factor, EGF (Kashiwagi *et al.*, 1997; Atit *et al.*, 2003). There are also groups of molecules classified as inhibitors of Inhibitors, Noggin and CTGF (Connective Tissue Growth Factors). These are macro molecules that bind to and inhibit the function of the BMPs in the extracellular space (Abreu *et al.*, 2002; Balemans and Hul, 2002).

All of the above Activators and Inhibitors are secreted proteins that act as intercellular signals and, as mentioned earlier, may be subjected to various post translational modifications. Because the plasma membrane is relatively impermeable for the relatively large molecular weight Activators and Inhibitors, the perception of the signal involves signal transduction pathways that typically end with altered gene expression in

the cell nucleus as a primary signal outcome that either leads to initiation of follicle fate or inter-follicular state of the cells. There are certainly other molecules involved in follicle development that remain to be discovered and may contribute a significant role.

With regards to the animal system used, BMPs were first investigated as inhibitors of placode formation using chicken as the model animal under study (Jung *et al.*, 1998; Noramly and Morgan, 1998). The placode activating functions of the FGFs (Mandler and Neubuser, 2004) and Wnt/β-catenin (Noramly *et al.*, 1999; Widelitz *et al.*, 2000) were also identified in embryonic skin tissue from chicken. However, compared to chicken, mouse provides spontaneous mutations that allow scientists to study the effects of gene regulation in a relatively less time for the outcome of gene modulation. The technology for engineering specific genetic manipulations in this species is also well developed. This poses distinct advantages over chicken for patterning studies.

2.8.2 Molecular interactions that lead to follicle pattern development

Having identified the major components involved in the reaction diffusion mechanism that leads to pattern formation, the next challenge now is to put the pieces together and identify the key molecular interactions that guide spatial organization of the skin.

Recombination experiments using epidermis and dermis have indicated that all cells of the embryonic skin are capable of contributing to follicle development, but the patterning processes ensures that only some actually do assume the follicular fate (Sengel, 1976). The cells that are destined to a follicular fate must activate expression of specific genes, form micro aggregates (due to the presence of adhesion molecules), followed by aggregation of the micro aggregates to larger and stable cell condensates, and to ultimately form a structure known as a placode, and proliferate rapidly to drive downgrowth into the underlying dermis. Further cell differentiation allows production of a complete hair fibre, sebum from a sebaceous gland, and specialized areas for the maintenance of stem cells that continuously supply new and differentiated cells (Schmidt-Ullrich and Paus, 2005).

The use of mutant animals such as mice that lack certain organs such as hair follicles, helps scientists to identify key regulatory elements involves in the reaction-diffusion

mechanism. Cultured skin tissue from Eda-deficient mouse embryos was used to analyze regulatory interactions during the generation of primary hair follicle patterning (Mou *et al.*, 2006). The application of exogenous proteins, such as Eda itself, to the cultured skin enabled the synchronization of hair placode formation. By doing this, researchers have successfully identified alterations in gene expression and control placode arrangement at defined time points in the patterning process. The study led to the conclusion that Eda and its transmembrane receptor – Edar, played an Activatory function in the signal transduction pathway. The BMPs on the other hand, acted as Inhibitors. Eda and its transmembrane receptor Edar expressions were initially homogeneously present in the early development of the embryo. At a later stage however, the ligand - receptor pairs are confined mainly to specific regions at periodic pattern (i.e. the placode), where in the surrounding placode area, the interaction of Eda and Eda receptor is inhibited by BMP. This is often called a restrictive mode of expression. The study concluded that BMPs were rapidly acting inhibitors of Edar gene expression, and Edar was found to induce upregulation of BMP gene expression. As Edar is located only in the membrane, its direct effects are limited to the cells that produce it. As mentioned earlier, BMP responses were found outside the activated placode regions. The result suggests that in a developing skin embryo, BMPs act at a distance from their site of synthesis and has therefore been proposed to have a larger range of action than Edar (Headon and Painter, 2009). The absence of BMP responses at their site of synthesis in the placode itself was due to the presence of CTGF (Connective Tissue Growth Factor), up regulated by Edar, which inhibits the BMPs by binding to them in the extracellular space (Yoshida and Munakata, 2007). This model requires that the range of action of CTGF be less than that of BMP family members.

2.9 Tissue Engineering of Skin

A commonly applied definition of tissue engineering is that it is "an interdisciplinary field that applies the principles of engineering and life sciences toward the development of biological substitutes that restore, maintain, or improve tissue function or a whole organ" (Langer and Vacanti, 1993). Tissue engineering has also been defined as "the employment of natural biology of the system that will allow for greater success in developing therapeutic strategies aimed at the replacement, repair, maintenance, and/or enhancement of tissue function" (MacArthur and Oreffo, 2005).

Tissue engineered skin is especially useful when wounds are not healing well, or too much skin has been lost. Such loss can for example occur through, burns, accidents, chronic wounds (e.g. diabetics), and cancer.

2.9.1 Applications and limitations of organ or tissue implantation

The use of organ / tissue implantation approach for the treatment of tissue-related problems such as accidents and end-stage organ failures, have traditionally been employed. These include transplantation of tissues and organs known as homo-(or allo-) graft (from the same species, e.g. human heart transplant), autograft (from different part of the same individual), and hetero-(or xeno-)graft (from different species). In some cases mechanically assisted devices are used (Fuchs *et al.*, 2001).

There are however limitations to the application of the techniques. In the autograft technique, autologous cells or tissue are used from the same person or individual that the cells or tissue shall be implanted. Autologous cells therefore have the least risks or issues with incompatibilities and transmission of diseases. However sometimes the cells or tissues are not available for immediate use and need some culturing. It can take considerable amount of time to culture the cells together with its associated risk of failure due to contamination. Adequate quantities of autologous cells may be required for establishing useable cell lines. Auto grafting may not be suitable for persons suffering from genetically inherited diseases or exceedingly ill or aged persons, and people having very severe burns. Alternative approaches to using autologous cells may therefore be required.

In the hetero-(xeno-)graft method of transplantation, the tissue or organ is isolated from a different species as the patient. These transplantation methods are associated with an increased risk of immuno-incompatibilty which requires the patient to undergo immuno-supression treatment for life. Moreover, viral disease transmission, tumor development and increased risk of infection are some more risks that pose serious issues with these methods.

In the past, homo-(allo-)grafts were often of low quality and carried a considerable risk of disease transfer. With the advance of technology however, allograft approaches have

improved noticeably, and the risks have been minimized. Tissue storage and availability is still a problem. The risk of disease transmission is almost certainly unavoidable and cannot be eliminated completely.

Tissue and organ transplantations, in general involve significant amount of costs and a complex surgery. Furthermore, shortage of donors and limited preservation time of the organs outside the body are few other factors that limit the applicability of such techniques for treatments.

2.9.2 Advances in skin tissue engineering

Through continuous research and development, tissue engineering is leading to the creation of a variety of new tissue replacement parts or components. Improved understanding and knowledge of biomaterials, stem cells, growth and differentiation factors, as well as the physiological conditions required to successfully grow tissue in artificial environments have made it possible for mankind to manufacture (artificial) tissues in the laboratory using engineered extracellular matrices acting as scaffolds, constituent (feeder) cells, or other molecules that are biologically active. Many challenges are, however, still faced by researchers in the field of tissue engineering. Amongst these are the need for more complex tissues, as well as the stability and compatibility of the tissues used for transplantation. Before the ultimate off-the-shelf human replacement parts are available, more technological developments is needed in manufacturing techniques and sterilization techniques, including the handling of tissues in a super clean room environment.

A functional organ in living system normally possesses many different cell types organized into tissues of a unique 3D architecture or structure in order to successfully exert physiological roles. An organ’s physiological function demands a specific organization of the cells and tissues in the form of cell sheets or tubes-type structure, as well as accurate cell-to-cell interactions, including intercellular communication through soluble or surface-bound molecules and specific micro environmental conditions such as pH, conductivity, osmolarity, extra cellular matrix (ECM) production or degradation of metabolites.

Cultured skin substitutes, which were initially created to serve as models for *in vitro* studies, are nowadays used to treat victims of deep and extensive burns by transplanting them on patients (Horch *et al.*, 2001). In general, two cell types have been used in the tissue engineered skin substitutes, i.e. epithelial cells or keratinocytes, and dermal fibroblasts (Auger *et al.*, 2000).

Advanced and commercially available products for replacement or repair of human skin are Apligraf™, Dermagraft™ and Transcyte™. Apligraf™ is an artificial skin tissue that consists of a layer of dermal cells (fibroblasts) in a collagen gel, with a layer of epidermal cells (keratinocytes) on top. Transcyte consists of a nylon polymer mesh in which dermal fibroblast cells are seeded and grown. Once the cells have proliferated and filled the gaps in the mesh, a less permeable layer is added and the end product is frozen. In Dermagraft™ the cells are grown on a polyglycolic / polylactic acid mesh. Fibroblasts derived from newborn foreskin tissue are grown on the mesh. Dermagraft™ is frozen at low temperature, but the cells in it are still alive.

Tissue engineered skin is therefore, a product that is made up of cells, extracellular matrix and also growth factors (Lanza *et al.*, 2000). Extracellular matrix and growth factors are often not added as pure compounds during the fabrication process, but formed by the cells during culture. For example, the end product Dermagraft™ contains many molecules that aid in wound healing that are produced by the cells during culture. These include matrix proteins (e.g. collagen type I, III, V, VI, VII as structural proteins), fibronectin and tenascin (high molecular weight ECM glycoproteins that bind to membrane-spanning receptor proteins such as integrins), involved in cell adhesion and migration. In addition, it also contains glycosaminoglycans (versacin, decorin, betaglycan, syndecan); their main roles are as structural molecules. They are also involved in the binding of growth factors. Various growth factors, for example, the mitogens IGF (stimulate the division of fibroblasts and keratinocytes), interleukin (IL) - 6 and IL-8 (stimulate cell division, in particular of white blood cells), compounds that stimulate matrix deposition such as TGF-β1 and TGF-β3, are all part of engineered skin products such as Dermagraft™.

Several critical factors need to be controlled whilst engineered skin is being produced. These factors include but are not limited to the quality of the cells. Features such as cell

morphology, proliferative capacity and expression of tissue specific functions must be retained when cells are included in reconstructed skin substitutes. Therefore, it is of paramount importance that the culture conditions (the media, additives, matrix, the pH, temperature and three dimensional environment) must be close to their natural physiological conditions (Horch *et al.*, 2001).

At present tissue engineering only allows the development of skin without any other structures. Real skin, however, contains many other structures like blood vessels, sweat pores, hair shafts and follicles, glands, and nerve fibers (some are shown in Figure 2.2-1). In order to develop an artificial skin tissue similar to real human skin it is necessary to introduce such features. This project will show the use of dielectrophoresis for creating artificial tissues containing 3D placode-like structures, mimicking those found during early embryonic skin tissue development.

CHAPTER 3

Literature Review on Cell Aggregation and Entrapment Techniques

3.1 Introduction

The primary aim of this chapter is to review techniques for the formation of artificial patterns of cells commonly used by researchers around the world, and their associated potential applications and limitations. The review will concentrate on methods for physically manipulating cells at the micro scale. A brief review on cell immobilization techniques which can be used in combination with cell patterning techniques is also included.

3.2 Techniques for Cell Aggregations, Patterning and Entrapment

It is widely appreciated that having the ability to control the relative position and arrangement of cells or cell aggregates *in vitro* is highly useful in many areas, and often used by scientists in an attempt to mimick the *in vivo* environment. Ideally, the technology for doing this should allow patterning of multiple cell types with high accuracy in a three-dimensional field. If possible, the technology would also offer a way to change the patterns with time. The fact that the cell diameter is only a few micrometers makes this challenging. Despite this, scientists are increasingly gaining the skills and capabilities to make patterns of more than one cell type, to produce dynamic cell patterns and build tissues in 3D.

There are in general two types of cell patterning - passive and active. The difference between passive and active patterning is the force that drives the patterning. The passive types are based on adhering forces that drive the interaction between the cells and the substrate; often this involves surface modification for cellular attachment. The active types of cell patterning involve the use of (physical) forces (usually mechanical or electromagnetic forces, or combination of them) to actively direct cells to desired locations. This section will review some of literature in each of these areas.

Unlike passive techniques, active methods of patterning tend to be quite general and non-specific, which makes these approaches attractive (Desai *et al.*, 2007). The techniques of dielectrophoresis and electrophoresis for example, only oblige cells to be

polarizable and charged, respectively (Voldman, 2006). Most cells are charged, and all intact cells are polarizable (Mehrishi and Bauer, 2002). These techniques are therefore applicable to many different types of cells. Approaches based on magnetic manipulation however require the cells to be magnetisable. Some cells have natural magnetic capabilities (for example red blood cells). If they do not, the cells have to be made magnetisable. For example, Tanase *et al*. (Tanase *et al.*, 2005) put magnetic nano-wires as magnetic labels into cells for the construction of cell micro arrays.

3.2.1 Surface modification

Surface modification is an example of a passive technique used for creating 2D patterns of cells. It involves alteration of the chemical and sometimes physical properties of a surface so that cells preferentially bind to some areas and not others. Depending on the interaction between the occupying cells and the surface, the resulting pattern can have a high or low specificity. The key to having successful cell patterns based on surface modification lies in the design of materials and the interfaces. It is however, possible to change the cells. For example, in order to improve the specificity of their system Kato and Mrksich (2004) utilized cells that expressed specific trans-membrane proteins which bind selectively to adhesive regions on a surface. Therefore, using a library of cells expressing unique trans-membrane molecules on their surface it is also feasible to guide several cell types onto different regions of a substrate (Kato and Mrksich, 2004).

If control over the timing of the adsorption behavior of cells or molecules and the interface involved could be realized then this would give added advantages to the system, especially if it is reversible and can be repeated many times. Such systems are relevant to many areas including biosensors (e.g. adsorption of glucose oxidase on electrode surface), biomaterials, regenerative medicine, and drug delivery (Lee *et al.*, 1997; McArthur *et al.*, 2000; Sung and Bae, 2003). This however, would be more complex as it requires that the surface of a material can be activated in real time from an interactive state (i.e. a state that adsorbs proteins in a cell membrane) to a non-interacting phase (or a state that repels proteins) and *vice versa*. The factors that trigger the interaction between the cells to be patterned, either directly on to the surface or mediated by adhesion molecules, are varied. They can either be physical- or energy-based triggers (such as light, temperature, electric- or magnetic field, ultra sonic

radiation., and pressure (Kwok *et al.*, 2001; Ainslie *et al.*, 2005) or chemical-based stimuli such as pH, solvents (Hyun *et al.*, 2004), ionic strength, metal ions or biomolecules (Zhu *et al.*, 2004; Edahiro *et al.*, 2005; Panayiotou and Freitag, 2005).

Kaji *et al*. utilized a controllable platinum probe to oxidize a surface coated with albumin around the vicinity of the probe (Kaji *et al.*, 2004a; Kaji *et al.*, 2005). Within 24 hours, HeLa cells had migrated to the new unoccupied and uncoated regions. The dynamic surfaces allowed the creation of patterns of multiple cell types (Kaji *et al.*, 2004b).

Yousaf *et al*. did pioneering work on the use of electro active substrates which are capable of switching their adhesive properties. They showed that a self-assembled monolayer of alkanethiolates on gold could be repeatedly changed from a state that promotes cells attachment to a state that prevents cells attachment (Yousaf *et al.*, 2001). Jiang *et al.* also developed a relatively easy and straightforward technique that make use of the principle of electron transfer in a redox reaction to desorb monolayers and to control the substrate's adhesiveness towards cells (Jiang *et al.*, 2003).

3.2.2 Flow-based techniques

Most of the micro patterning technique discussed until now are restricted to making 2D patterns of cells on a surface. Most if not all cells *in vivo*, however, live in a 3D environment. To mimic the cells' natural microenvironments, it is therefore necessary to use techniques that make 3D structures. A set of techniques that can be used to make 3D-structures are flow-based techniques. They can be divided into methods based on the use of moulds, and mould less techniques.

The mould-based techniques involved the use of microfluidic channels to control the formation of cell aggregates. A typical examples is the work in Desai's laboratory (Tan and Desai, 2004), which used pressure-driven microfluidics to move cell-matrix mixtures with controlled flow rates into micro channels. Contraction of the biopolymer matrices creates space in the channels which can be used to create layer-by-layer tissue constructs inside a microchannel with different cell types one on top of each other in three dimensions. The thickness of each layer can be controlled down to micro scale

dimensions.

A typical example of a mould-less technique is the use of inkjet printing technology. The use of inkjet printing has in the past few years been expanded to various applications in the field of biotechnology (Lemmo *et al.*, 2005). Inkjet printing is a relatively low cost and high throughput technique. Commercially available equipment can be been customized to print bio-molecules onto a surface with minor or no changes in their native properties. Researchers have used them to develop DNA chips (Okamoto *et al.*, 2000), make arrays of embedded proteins (Roda *et al.*, 2000) and also to make arrays of cell aggregates (Roth *et al.*, 2004).

Xu *et al.* patterned *Chinese Hamster Ovary* (CHO) cells and motor-neuron cells using an inkjet printing technique. The cells were put down onto a paper-like surface that was gel-based and with special adherence characteristics to form pre-defined patterns. More than 90% of cells remained intact (viable) during the bio printing (Xu *et al.*, 2005). In addition, Xu and coworkers have also made use of inkjet printing to pattern mammalian cells onto a surface (Xu *et al.*, 2005). Nevertheless, the spatial resolution attained by the group is currently low. Other researchers have successfully adapted this technique into the 3D construction of cell aggregates for tissue engineering application with high-throughput (Roth *et al.*, 2004).

Gao and co-workers have designed a laser cell deposition system that employs the phenomenon of laser guidance to place single cells at specific points in a variety of *in vitro* environments (Pirlo *et al.*, 2006). The patterning system was accurate within one micrometer. The patterning was done repeatedly using polymer microspheres and then measuring their position. The group claimed that the laser guidance cell patterning system did not affect the cell's viability or morphology as demonstrated by the neurite outgrowth after 8 hour of culture for over a week long period.

3.2.3 Ultrasound

Ultrasound can be described as sound waves with a frequency which is too high for the human ear to hear (Nyborg, 2002). The highest frequency a human can hear is about 20 kHz.

Longitudinal ultrasound standing waves create periodic patterns of low (node) and high / maximum (antinode) pressure amplitude. Particles in a longitudinal standing wave field are subjected to two generic effects, radiation pressure and convective drag due to acoustic streaming (Spengler and Coakley, 2003). In areas where the acoustic streaming is small, particles in the fluid will accumulate according to the local radiation pressure only. Depending on the density and compressibility values of both the suspended particles and the medium, the particles can move either to the node regions (if the acoustic contrast factor, , is positive) or *vice versa* (Laurell *et al.*, 2007; Shi *et al.*, 2008). The patterning effect of acoustic radiation forces acting on suspended particles occurs if the particle size is relatively small compared to the acoustic wavelength used in the suspending fluid (Yosioka and Kawasima, 1955), and can be quantified as shown in the following equation:

F_r = - ([1]

[2]

where p_0, λ, V_c are the acoustic pressure, wavelength, and volume of the object (e.g. cell) respectively and ρ_c, ρ_w, β_c, β_w represent the density of the object (e.g. cell), density of the medium (e.g. water), compressibility of the object, and compressibility of the medium respectively, and represents the acoustic contrast factor and determines the balanced positions of the objects. Index *c* and *w* represents cell and water respectively.

Longitudinal standing waves can be produced by reflecting sound from a surface; the reflected sound wave then interferes with the incident sound to form a standing wave. The other way standing waves can be produced is by interference of sound produced by two or more transducers (Coakley *et al.*, 2004). Ultrasound standing waves have been used for the concentration and separation of cells, for enhancing immunological reactions, and for the formation of tissue-like materials.

Due to non-contact nature of the technique, ultrasound is often considered as a non-invasive technique. One of the limitations of this approach is however, that the high intensity ultrasonic waves can potentially break cells and denature enzymes. This effect is particularly strong at low frequencies (below 1 MHz), and is thought to be caused by

cavitation (i.e. the rapid contraction and expansion of air bubbles). For example, Vargas and co-workers demonstrated that ultrasound can be used to release invertase from *Aspergillus niger* cultivated in a medium containing sucrose and peptone growth medium (Vargas *et al.*, 2004). Irradiation was conducted for periods of 2 –10 minutes ultrasound with a frequency of 20 kHz. It was found that ultrasound irradiation caused cell disruption, releasing invertase from the cells. However, inactivation of the enzyme was already observed after 4 minutes incubation. High frequency ultrasound (above 1 MHz), however, does not induce cavitation, and does relatively little harm to cells. The research group of Wiklund investigated the growth profile and the percentage of live and death of adherent cells constructed using ultrasound in a microfluidic chip (Hultström *et al.*, 2007). The cells were held in the trap for a duration ranging between 30 and 75 minutes and 0.85 MPa acoustic pressure and a frequency greater than 1 MHz. The cells formed 2D aggregates inside the chip maintained against a destabilizing flow of cell culture medium. The group found no significant variation in the doubling time of COS-7 cell line from the expected values (24 to 48 h).

In addition to patterning of cells and micro particles using longitudinal standing waves, ordering of cells can also be achieved using standing surface acoustic waves. For example, Shi *et al*. (2009) made use of standing surface acoustic wave (SSAW) to manipulate and pattern cells and bead micro particles. The power intensity used was approximately 5 x 10^5 times lower than that of optical tweezers (Jinjie *et al.*, 2009).

It is possible to immobilize cells after a pattern has been created using ultrasound. For example, Gherardini *et al*. (2005) have developed gel-based cell immobilization technique that permits positioning and patterning of cells (yeast and human red blood cells) and particles (fluorescent latex beads) for long periods of time, within a confinement of various non-toxic gel matrices such as agar and alginate (Lisa *et al.*, 2005). The group demonstrated, using the Live/Death assay, that the yeast cell viability, patterned by an ultrasound standing wave followed by semi solid phase-immobilization, remains high and that the cells continue to proliferate up to 4 days after the experiment.

3.2.4 Optical tweezers

There are two types of laser-based devices that researchers commonly use for particle

movement. The first one involves the use of a strongly divergent laser beam to form tweezers to entrap particles. The second type involves the use of a weakly divergent laser beam; the optical radiation pressure of the beam is used to move small objects such as cells along the path of the laser beam. The second type utilizes much simpler optics.

Using strongly-focused beams of light allows movement of small objects (such as cells) ranging in size from few nanometers to tens of micrometer in diameter. Laser traps can exert forces exceeding 100 pN (Litvinov *et al.*, 2002). An extensive review on the application of optical tweezers in biological and macromolecular systems has been written by Svoboda et al. (Svoboda *et al.*, 1994). Optical manipulation of cells requires a discrepancy in the refractive index between the suspended cell and the suspending medium. This is usually true for undamaged cells (Gaugiran *et al.*, 2005) as the cell membrane or cell wall components (lipids / carbohydrates respectively) have different physical properties than the suspending medium. Therefore, the technique can be used for most (but intact) cell types. Optical tweezers used for cell manipulation normally work in the near-infrared (NIR) regions (0.75 - 1.4 μm in wavelength) to avoid absorption which can cause thermal and chemical deterioration that occur at lower wavelengths (e.g. UV photo-damage). Some cell types, however, such as pigmented cells (e.g. skin melanocytes) are still comparatively absorbent in the near infra red regions (Jacques and McAuliffe, 1991), and NIR cannot be used with these cells.

A common application of laser tweezers is sorting of cells. For example, Wang *et al.* utilized a laser beam to deflect HeLa cells across the center of a microfluidic channel (Wang *et al.*, 2005) for cell sorting purposes. With high power (~10 W) and at relatively short on-times (2-4 ms), the group was able to accomplish practical sorting rates (tens of cells/sec) with minimal or no stress on the cells (as determined by HSPA6 and FOS expression as indicators of cellular stress).

Optical tweezers are usually used to manipulate a single or very few particles or cells at a given time, as opposed to simultaneously manipulating multiple cells. However, other researchers have used optical tweezers with multiple optics system which can control larger amounts of particles at the same time. They can be achieved by a laser array (Flynn *et al.*, 2002), beam splitters (Fallman and Axner, 1997), and spatial light

modulator (Curtis *et al.*, 2002). For example, Robert *et al*. (2004) demonstrated that entrapment and organization of micron-sized objects such as cells or beads is possible within microfluidic systems by utilizing a diode laser bar (Robert *et al.*, 2004). The approach used by the group overcomes the scaling limitations of conventional scanned laser traps, and avoids the computational and optical complexity commonly found in a holographic optical trapping mechanism. The diode laser bar enabled the group to control a large trapping zone, 1 μm by 100 μm, without the need for scanning or altering the phase of the beam.

3.2.5 Electrophoresis

Cells are usually negatively charged, as a consequence this can be used for cell trapping and manipulation. When a suspension of (negatively charged) cells are subjected to DC electric field, the cells are readily moved by electrophoresis to positively charged electrode region and applying suitable voltages to the area (Ozkan *et al.*, 2001; Ozkan *et al.*, 2003). The electric field strength that is needed to electrophorese cells is however quite large (typically 10 V/mm). The thickness of the membrane is only around 5 nm, and the structure of the cells cause the external electrical field to be amplified across the cells membrane. The high electric field strength across the cell membrane can potentially have an adverse effect on cell viability. In addition, electro-osmotic flow of the medium and heating effects give rise to flows near the electrode regions making it difficult to stabilize and control cell movement. Decreasing the medium conductivity by replacing salt components by iso-osmotic solutions containing sugars such as sorbitol can attenuate or lessen these problems. Toriello and co-researchers used the electrophoretic force to move cells to oppositely charged gold electrodes (Toriello *et al.*, 2005). The researchers showed patterning of two cell types, but the group claimed that the approach could be extended to additional (more than two) populations.

3.3 The Use Of AC Electrokinetics For Cell Trapping And Patterning

Electrophoresis uses the net charge on a particle to move it in a DC field. However, it is also possible to move neutral particles in AC fields. The term ‘dielectrophoresis’ refers to the induced movement of particles in non-uniform electric fields. The force on a particle can be described by equation 3 as:

[3]

where ε_m is the medium permittivity, r is the equivalent radius of the cell and *Re* stands for 'the real part of'. The term '∇E^2_{rms}' defines the time-average of the divergence of the square of the field strength, and is dependent on the applied voltage and the electrode geometry and size. K^* is the complex Clausius–Mossotti factor, which is defined in equation 4 as:

——— [4]

–, in which $j = \sqrt{-1}$; ε is the permittivity, σ is the conductivity and ω is the radial frequency. The subscripts refer to the particle (p) and the medium (m). The real part of the Clausius - Mossotti factor, varies with the radial frequency (ω) and depends on the comparative difference in permittivity (ε) and conductivity (σ) between the particle and the medium. The Clausius - Mossotti factor may vary in value between -0.5 and +1.0, characteristic of the properties of the suspended particles, the medium, and the applied frequency in the field. If $Re(K^*) > 0$ (positive), the particle is more polarizable than the medium and is attracted toward the large electric field gradient regions of the electrode. This phenomenon is known as positive DEP or p-DEP. In the contrary, if the medium is more polarizable than the particle, then $Re(K^*) < 0$ (negative). A negative DEP (n-DEP) force repels the particle toward the local electric-field minimum region. When at a particular frequency the value of the complex component $Re(K^*) = 0$, then the particle will not experience any dielectrophoretic force. This frequency is called the cross-over frequency. The use of media with modified (increased) permittivity makes it possible to increase field-induced forces (Arnold, 2008).

Cells are particles which have frequency-dependent electrical properties. Cells can have several cross-over frequencies, and the same cell can show positive and negative DEP at different frequencies. Dielectrophoretic spectra of different cell types are very similar (Pethig and Markx, 1997). All cells when suspended in a low conductivity osmoticum show positive DEP at a frequency around 1 MHz. Negative DEP can be induced using a frequency below the lower cross-over frequency of the cells (typically 50 kHz),

provided the medium conductivity is higher than the particle conductivity; n-DEP also occurs at higher frequencies, typically 20-50 MHz. The p-DEP force is an attractive-type force, actively holding the particles (or cells) together in areas where the field gradient is high (maximal). These are regions in between electrode castellations as well as along the edges of the electrodes (Figure 3.3-1). The n-DEP force pushes the particles (cells) away from the high field regions. As a result of n-DEP forces the particles (or cells) eventually end up in the low field regions, such as the gap between adjacent electrodes, or if the repelling force is strong enough, above the electrode plane. The net forces holding cells down when using n-DEP are usually less strong than the net forces when using p-DEP.

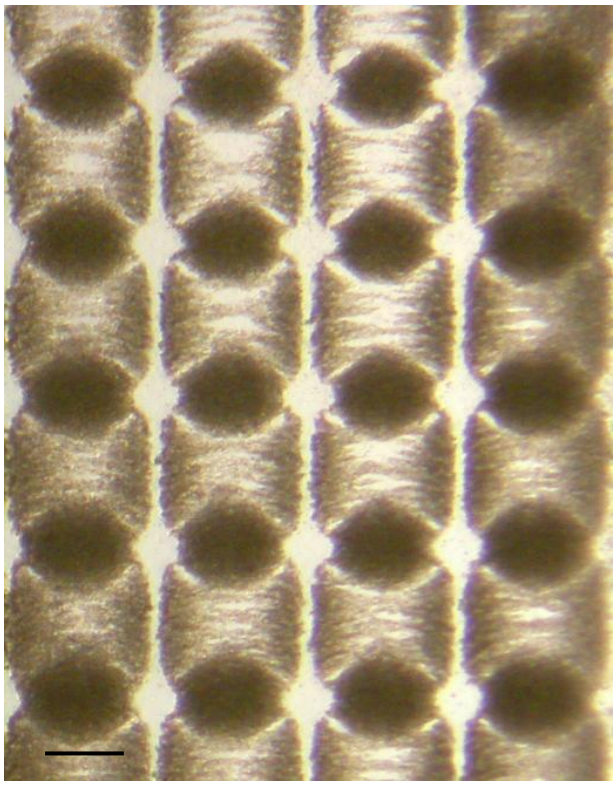

Figure 3.3-1. Positive DEP of yeast (*Saccharomyces cerevisiae*) cells showing aggregate formation between electrode castellation and the pearl-chain phenomenon (scale bar = 250 μm).

3.4 Electrode Design

Early experiments on DEP used simple wires, razor blades and other relatively large objects, and relatively large voltages (kV) (Pohl, 1978). Advances in microfabrication have made it possible to fabricate microelectrodes with high fidelity and specificity according to the design of the template mask, allowing DEP to be studied using much

lower voltages (typically 2-20 V_{pk-pk}). Even though these microelectrodes are usually much thinner (typically 100 nm) than the diameter of the entrapped particles (e.g. mammalian cells ~ 10 µm), the electric field gradient created in the surrounding electrode area extends into the 3D space above the electrodes. An example of the analysis of a vertical cross section of the electric field between castellated electrodes using modeling software is shown in Figure 3.4-1.

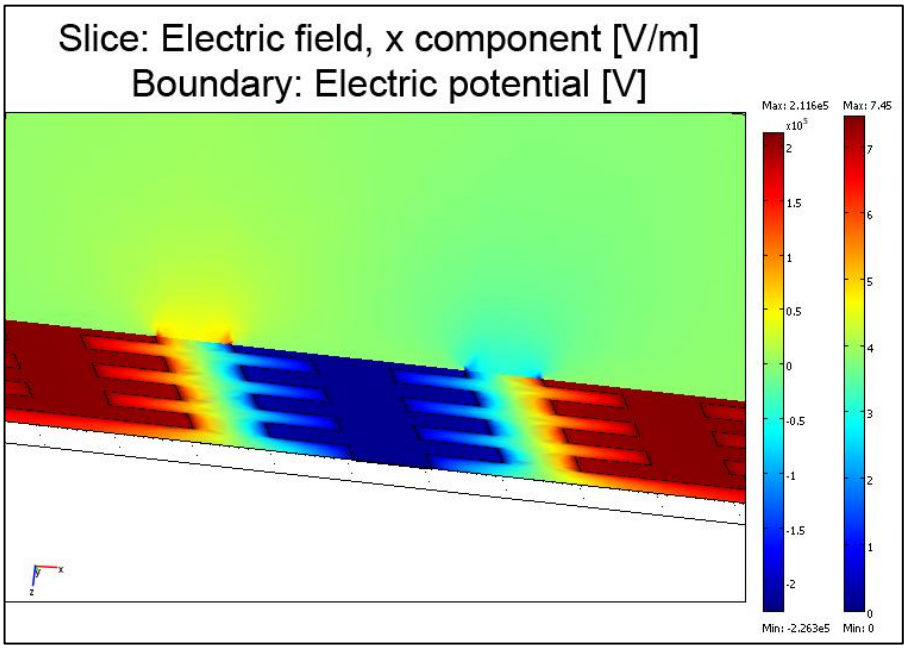

Figure 3.4-1. Modelling electric field gradient showing a vertical cross section (a slice) perpendicular to electrode plane, between a castellated electrode, using COMSOL Multiphysics 3.4.

Progress in microchip design and technology have made it possible to make various custom-made microelectrode patterns various DEP applications. Simple geometries include, interdigitated electrode with or without castellations (Wang *et al.*, 1996); Sebastian *et al.*, 2006), and the quadrupole electrode (Huang and Pethig, 1991; Green *et al.*, 1997). The latter is a commonly used electrode configuration where four electrodes point towards a central enclosed region (Huang and Pethig, 1991), and has been used to characterize the DEP phenomenon and achieve simple cell patterning.

Various novel geometries developed to enhance the effect of dielectrophoresis approach include a parallel array of triangular-shape electrodes created by Lin and Yeow (Lin and Yeow, 2007). They showed that this design could be used to generate bands of increasing horizontal electric field which in turn could be used to force micro beads to

form a straight horizontal line at specified regions around the electrodes.

The theoretical background to determine DEP patterning efficiency according to electrode geometry is quite well established (Albrecht *et al.*, 2004). At low electric field strength and low particles concentrations, colloidal particles trapped by DEP typically form a monolayer on the electrode plane. On the other hand, at higher electric field strength and high or denser particle concentration, DEP typically results in multilayer aggregates (Docoslis and Alexandridis, 2002).

3.4.1 Application of DEP for cell separation

DEP has been used extensively as cell sorting technique, in particular viable (live) and non-viable (dead) cells (Markx and Davey, 1999; Gascoyne and Vykoukal, 2002; Hughes, 2002). In viable cells the lipid membrane bilayer is intact and acts like a capacitor in an electronic circuit that functions as a resistive barrier for the electric field to access the cell cytoplasm. When suspended in a low conductivity medium and applied electric field with high frequency (at or more than 1 MHz), the cells become more highly polarizable than the surrounding medium. If the applied electric field is non-uniform, the intact cells move to high-field regions by positive dielectrophoresis. The membrane of dead or non-viable cells however, is generally damaged and allow ions (such as Na^+, K^+, Ca^{2+}) to pass through, equilibrating themselves with the suspending medium (with a relatively low conductivity). The low internal conductivity and high membrane permeability cause cells to experience negative dielectrophoresis at the higher frequency end of the DEP spectrum (typically around 10 MHz) and move away to low field regions, creating separation. For example, by utilizing the difference of dielectric properties between live and dead cells Li and Bashir (2002) separated live and dead *Listeria* cells.

3.4.2 Application of DEP for cell trapping and the creation of biofilms/tissues

Pohl (1978) was the first scientist to show the use of AC electrokinetics for the creation of tissue-like materials from cell suspensions. It took almost a decade before scientists again looked seriously at the use of dielectrophoresis for the construction of 3D cell aggregates using yeast cells, bacteria, blood cells and other cells (Pethig and Kell, 1987;

Price *et al.*, 1988; Fuhr *et al.*, 1992a; Markx *et al.*, 1994a; Markx *et al.*, 1994b). A review on the use of electric fields of various methods for the formation of artificial biofilms / in tissue engineering has recently been given (Markx, 2008).

Cell patterning can be done with both positive or negative dielectrophoresis (Wang *et al.*, 1993) using any cell type (microbial, animal or plant), and even non-living materials can be patterned (Pethig *et al.*, 1992; Velev and Bhatt, 2006). The size of the aggregates can range from single cells (5 – 10 microns) to hundreds of microns (Albrecht *et al.*, 2004; Albrecht *et al.*, 2005; Sebastian *et al.*, 2006; Sebastian *et al.*, 2007b). Microelectrode arrays with well-defined geometries can be relatively easily fabricated by standard photolithography. Cells of different cell types can then be manipulated at different times using signals of different voltages and frequencies, creating complex two- and three-dimensional patterns.

The formation of cell aggregates begins with the formation of short pearl chains of few cells (Sebastian *et al.*, 2007b), followed by gradual extension and thickening of the chain by the mutual attraction during dielectrophoresis. This is ultimately followed by the movement of the pearl chains to high field regions (p-DEP) or low field regions (n-DEP). An example of pearl chain formation by p-DEP is shown in Figure 3.4-2. A stylized version is shown in Figure 3.4-3. Pearl-chain effects have been used for the formation of straight cell chains in a radial direction in ring-shaped electrode arrays to mimic liver structure (Ho *et al.*, 2006).

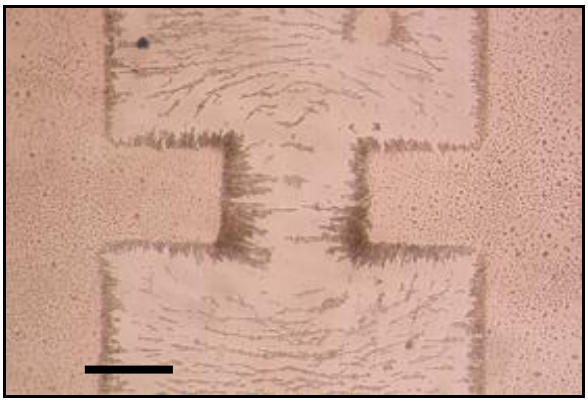

Figure 3.4-2. Positive DEP of mammalian cells showing the phenomenon of pearl-chain formation (scale bar = 250 μm)

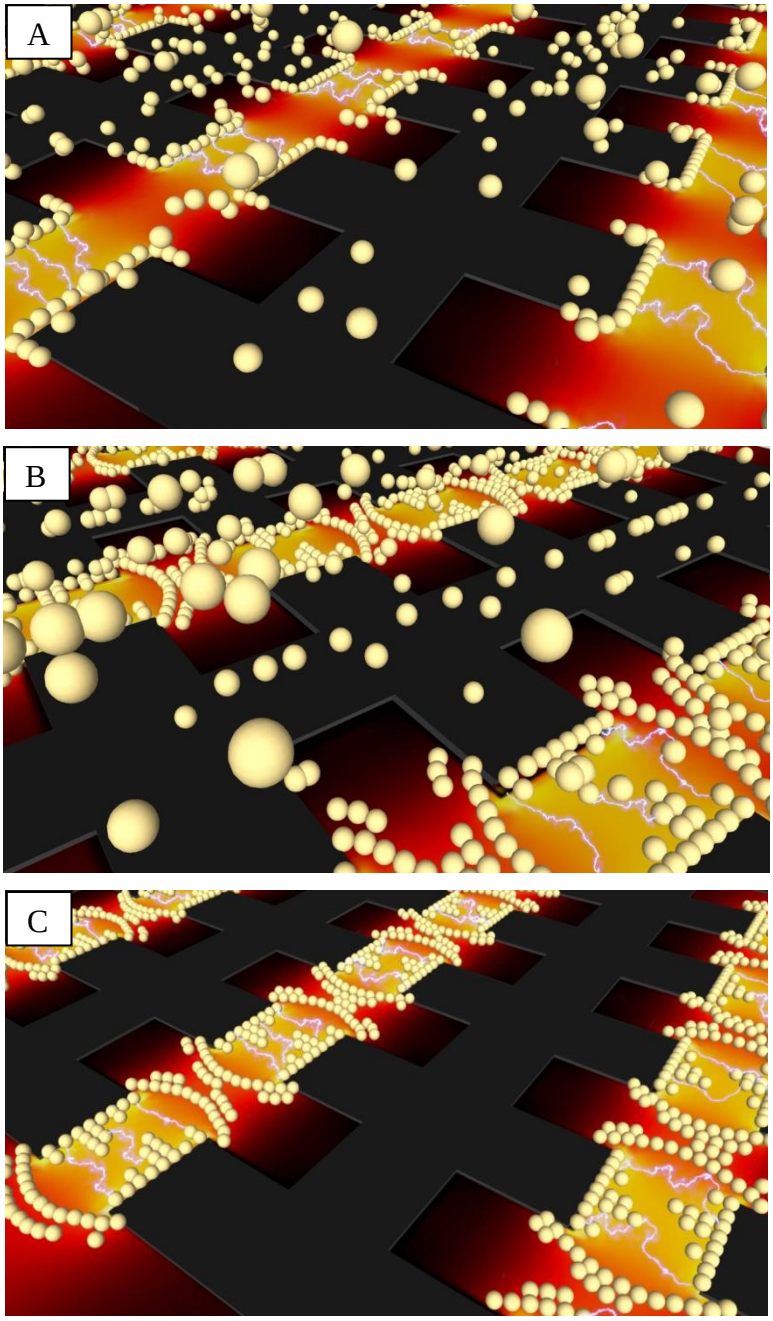

Figure 3.4-3. Stylised illustration of pearl chain formation by positive DEP between interdigitated castellated electrodes. A. Cells in suspension initially attracted to regions on the electrode edges where the field strength is highest in positive dielectrophoresis. B. Several cells align into chains oriented along electric field lines, forming a short pearl-chain of few cells. C. Two nearby cells are polarized in the same way such that the negative end of the first cell lies close to the positive side of the second cell forming a longer chain.

Aggregates of cells have been made of both micro-organisms and mammalian cells. Microbial biofilms containing artificially structured microbial consortia with defined internal microstructure consisting of various different cell types of different species were constructed by Markx's research group at the University of Manchester (Alp *et al.*, 2002; Alp *et al.*, 2003; Verduzco-Luque *et al.*, 2003).The group used positive DEP to

trap cells of different microbial species at planar microelectrodes. At first microbial cells such as *Saccharomyces cerevisiae*, *Escherichia coli* and *Micrococcus luteus* were deposited between the castellated microelectrodes sequentially to form 3D cell aggregates with distinct layers and defined internal structures. The position of the different microorganisms on the surface and within the cell layers were controlled by varying the electrode geometry and by introducing the different microorganisms at different times, as well as having the control over different parts of the electrode structure at different times for AC electric field supply. Cells were initially immobilized in an acrylamide gel, but later cross linking techniques were used, and the range of microorganism studied extended (Verduzco-Luque *et al.*, 2003). The method was subsequently used to study various interactions in microbial biofilms (Markx *et al.*, 2004; Mason *et al.*, 2005; Andrews *et al.*, 2006). The formation of microbial biofilms at large scales has been shown to be possible (Abidin *et al.*, 2007).

Work on mammalian cells has concentrated on the formation of artificial tissues. Often these experiments were aimed at increasing our understanding of the roles of multicellular organization and interaction in three-dimensional microenvironment of the same or different cell types (Albrecht *et al.*, 2006). Some examples of artificial constructs made of mammalian cells in aggregates using dielectrophoresis created in the lab include the assembly of artificial neural networks (Heida *et al.*, 2001a; Heida *et al.*, 2001b; Yu *et al.*, 2004b), artificial liver constructs (Ho *et al.*, 2006) and artificial stem cell niches (Sebastian *et al.*, 2007a; Markx *et al.*, 2009).

Suzuki *et al*. showed that it is possible to use n-DEP to pattern two different cell types on the glass slide without any special pre-treatment (Suzuki *et al.*, 2008). An interdigitated microelectrode array with four independent microelectrode subunits was fabricated with indium tin oxide (ITO), and placed above a culture slide without electrodes. A suspension of C2C12 cells was introduced into the chamber between the upper microelectrode slide and the bottom culture slide. Negative DEP forces were induced by applying an AC voltage (typically $12V_{pk\text{-}pk}$, 1 MHz) to direct cells toward regions of lower electric field strength on the lower slide. The cells aligned on the lower slide within 1 min. The continued application of the AC voltage for a further 5 minutes ensured the cells adsorbed onto the bottom culture slide. It was possible to pattern a second cell type using the same method as with the first set of cells; the total time taken

for patterning two cell types was less than 15 min.

In addition to trapping cells in aggregates, DEP can also be used to trap thousands of single mammalian cells individually (Gray *et al.*, 2004; Rosenthal and Voldman, 2005; Mittal *et al.*, 2007). For example, Gray *et al*. (2004) used very high fidelity micro fabrication techniques to create electrode arrays for trapping of thousands of single individual cells between electrode castellations with a characteristic size of 3 μm (Gray *et al.*, 2004). The dielectrophoretic force was capable of holding each cell against a destabilizing fluid flow generated within the chamber. The group claimed that each electrode trapped only one cell.

In a smaller scale, DEP has also been successfully used for trapping particles smaller than cells including biomacromolecules such as DNA (Yamamoto *et al.*, 2000; Sung and Burns, 2006), proteins (Asokan *et al.*, 2003; Holzel *et al.*, 2005) and viruses (Hughes *et al.*, 1998). Arnold (2008) recently explored the use of DEP with nano-particles such as nano tubes and nano wires. The study was aimed to assess the suitability of the techniques for the formation of structured nano-composites.

3.5 The Use of DC DEP for Cell Trapping and Patterning

DC-Dielectrophoresis (DC-DEP) is similar to AC dielectrophoresis. DC-Dielectrophoresis (DC-DEP) is the induced movement of the dielectric particles in a spatially non-uniform DC field, and like AC –DEP can also be used for trapping or separating biological cells. The method involves the application of very high voltage electric fields. However, the contact between the field and the medium can be physically far from the region of interest for DEP. The static DC electric field can be made non-uniform in a microchannel with heterogeneous structures, such as a channel with varying cross-sectional area or arrays of insulating posts (made by glass or polymers) (Cummings, 2003; Lapizco-Encinas *et al.*, 2004b;a; Lapizco-Encinas *et al.*, 2005; Ozuna-Chaco´n *et al.*, 2008). This method is sometimes referred to as insulator-based dielectrophoresis (iDEP) or electrodeless DEP. The dielectrophoretic forces created within the strong non-uniform electric fields within the constriction regions dominates over the diffusion, electro-osmotic force, and electrostatic repulsion among the particles and thus particles are trapped and concentrated. Compared with the AC-

based dielectrophoresis with embedded electrodes as introduced in the previous section, DC-DEP has a few major advantages. Firstly, fouling can generally be minimized by the use of insulators retaining their function despite surface changes. Secondly, the structure is physically robust and chemically inert, and hence is more biologically compatible. Fabrication is generally more simple as no metal components are involved. Techniques used for fabrication include glass etching and plastic stamping. Disadvantages are mainly related to use of a relatively high voltage DC electric field, causing similar problems as encountered with electrophoresis of cells.

3.6 The Influence of Other Forces During Dielectrophoresis

During dielectrophoresis, the particles subjected to non-uniform AC electric fields are also subjected to other forces. These other forces may play a significant role in the final morphology of 3D biodielectric patterns. These forces include, but are not limited to, electro-hydrodynamic forces, electro-osmotic forces, viscous drag, buoyancy effects, gravity and Brownian motion. Some of these forces will be discussed briefly in the following section.

3.6.1 Electro-hydrodynamic forces

Electrohydrodynamic (EHD) motion of fluids can become significant in a relatively small electrode regions and volumes. In particular at lower frequency ranges (100 Hz to 500 kHz) electrohydrodynamic motion of the fluid may prevent the accumulation of particles by DEP as these two forces (i.e. DEP and EHD) may act in opposite directions (Ramos *et al.*, 1999; Gonzalez *et al.*, 2000; Green *et al.*, 2000). Ramos *et al*. have given an in-depth study on this subject (Ramos *et al.*, 1998), which has been summarized by Green *et al*. (Green *et al.*, 1999). The two major components of electro-hydrodynamic forces are the electro-thermal and the electro-osmotic force.

The localized high electric field strength used in dielectrophoresis experiments often results in Joule heating effects, that subsequently lead to volume forces in the liquid. The high temperatures create gradients in the conductivity and permittivity of the particles and the suspending medium, ultimately giving rise to electro-thermal effects (Fuhr *et al.*, 1992b; Castellanos *et al.*, 2003). The resulting fluid motion (Hughes, 2003)

in turn gives rise to a viscous drag on the particles. Localized heating effects may not only come from the use of high electric fields, but also from illuminating light on the microscope, or ambient temperature of the surrounding.

The electric fields used for DEP induce forces on charges in the diffuse double layer at the electrode – suspension interface. This subsequently induces motion of the liquid. This flow is called AC electro-osmosis because of its similarity to electro-osmosis in a DC field (Ramos *et al*., 1999). The electric field and the double layer charge are time-varying and give rise to a steady oscillating fluid motion. AC electro-osmosis dominates fluid motion at low frequencies and small system sizes; electro-thermal flow dominates at high frequencies and voltages (Castellanos *et al*., 2003).

3.6.2 Gravity, buoyancy and Brownian motion

Buoyancy and gravity are forces which act in opposite directions. Using electrodes fabricated in the bottom of the DEP chamber, the gravitational force aids positive dielectrophoresis because particles are actively pulled downwards towards the high field regions in between the castellation of the electrodes. On the other hand, buoyancy aids the levitation of particles in the case of negative dielectrophoresis (Flores-Rodriguez and Markx, 2004). If the electrodes are built on top of the DEP chamber, the buoyancy force favors positive DEP. Levitation is achieved by balancing the gravitational force and negative DEP forces on particles, using electrodes on the bottom.

The effects of Brownian motion become greater as the size of the particles become smaller, but gravity could play significant role if the particle size become larger due to the associated mass (Pethig, 1996).

3.7 The Effect of Dielectrophoresis on Cell Viability

During dielectrophoresis, particles or cells were subjected to non-uniform AC electric fields whilst at the same time suspended in non-growth medium solution of a much lower than normal ionic conductivity. To some extent this creates stress on the cell, some of which will be discussed briefly in the following section

3.7.1 The effect of electric field exposure

Long-term exposure to low frequency electric fields below 100 Hz leads to a significant change in membrane potential and permeability (Djuzenova *et al.*, 1996), negative effects on cell homeostasis like growth arrest and cytoskeleton reorganization (Cho *et al.*, 1996), and apoptotic cell death (Hofmann *et al.*, 1999). No prominent damage or permanent effects were found in cells exposed at high-frequency AC electric fields (for short-term), regardless of the diversity in proliferation (Docoslis *et al.*, 1999)

According to Gray *et al.*, exposure to high-frequency electric fields in DEP for only a short time, avoids harmful effects and limits cell damage (Gray *et al.*, 2004). The researchers worked on dielectrophoretic registration of living cells (bovine pulmonary arterial endothelial and fibroblasts cells) to a microelectrode array. By powering the device with different voltages, the group showed that the trapped cells could be killed by stronger electric fields. However, with weaker fields, cells were not damaged during trapping, as indicated by the similar morphologies and proliferation rates of trapped cells versus controls. The research also aimed to study the effect of DEP on cell proliferation capability based on viability assay using propidium iodide after certain period of time (24 – 48 hours post DEP). The group however concluded that cell viability was reduced to only around 10%, if the cells experienced dielectrophoretic force under $10V_{pk\text{-}pk}$ and 2 MHz electric field exposure for 30 minutes of DEP. The result of work conducted by Sebastian *et al*. by using the same assay reagent (propidium iodide) however, showed that for 100 mm electrodes used, a decline in the cell viability of only around 8% has occurred during cell aggregation, with a further 8% in the 10 min period of additional field exposure. The cells appear to survive the aggregation process, including the electric field exposure (Sebastian *et al.*, 2007a).

Similarly, Gascoyne *et al*. noticed that high cell viability above 95% was obtained and DS19 murine erythroleukemia cells were able to proliferate after applying 1-kHz to 10-MHz, 7 $V_{pk\text{-}pk}$ voltage in DEP for up to 40 minutes in planar microelectrodes with a 100-μm gap (Wang *et al.*, 1999). The lag in cell growth as a result of decreasing field frequency or increasing voltage, medium conductivity and exposure time, presumably resulted from damage caused by hydrogen peroxide produced electrochemically in a sugar-containing media. Optimization of the composition of the suspending medium, for

example by the inclusion of some calcium or dextrose can reduce cell death even further (Rintoul *et al.*, 2001; Gascoyne and Vykoukal, 2004; Chen *et al.*, 2006).

Heida *et al.* observed that rat neural cells showed no difference in cell morphology, adhesion, or growth compared to control cells in negative DEP cell trapping experiments (Heida *et al.*, 2001a; Heida *et al.*, 2001b). In addition, Archer *et al.* concluded there were no significant effects on cell morphology, proliferation, and oxidative respiration of mitochondria when fibroblast-like BHK21 C13 cells were exposed to a 5 MHz, 21 $V_{pk\text{-}pk}$ electric field with a similar DEP electrode setup (Archer *et al.*, 1999). The research group also performed further molecular analysis using Western blot and RT-PCR and revealed that gene expression (in *fos* gene) was differentially expressed between control cells and exposed cells. Differential gene expression observed between control and exposed cells was thought not relate to thermally induced heat shock response because only a minimal fluctuation of DEP buffer temperature was observed between the two cells.

3.7.2 The effect of low conductivity buffer

Low conductivity buffer is required for efficient DEP cell manipulation to make the particles more polarizable than the medium in (+)DEP. However, cells require certain ionic compounds to maintain their physiological state. In fact, if used over a prolonged period of time (over 2 h) low conductivity DEP buffer can bring about negative effects on cell viability and is thought to be the major cause of cell death during DEP manipulation. The use of low conductivity buffer however, reduces certain undesired effects during DEP operation. These effects include induction of trans membrane potential (Sukhorukov *et al.*, 1998), increased temperature due to electric currents (Docoslis *et al*.,1999) and the electrolytic processes accompanied by bubble formation and pH fluctuations (Pucihar *et al.*, 2001).

A common DEP iso-osmotic solution used is sorbitol 300 - 400 mM in deionized water. Alternatively, 8.5 % (w/v) sucrose and 0.3 % (w/v) dextrose in pure water, could achieve the same function of low conductivity and isotonicity compatible for mammalian cells. Low ionic conditions are undoubtedly critical to cell physiology. Alberts suggested that ion leakage from cells disturbs cell ionic homeostasis and

disrupts cell physiology due to diffusional pressures that drive intracellular ions passing through plasma membranes into the DEP buffer (Alberts, 2001). Tzagoloff suggested that prolonged exposure of cells to low-ionic conditions ultimately leads to loss of mitochondrial potential and irreversible cell damage (Tzagoloff, 1982).

All the above information suggests that the time during which the cells are manipulated, exposed to alternating currents and patterned must be kept to a minimum. Even so, cell viability after a short period of exposure to DEP (less than 30 min) in an iso-osmotic buffer is usually still above 85% (Sebastian *et al*., 2006; Yusvana *et al*., 2009). Therefore, rapid cell patterning can be achieved with DEP whilst maintaining cell viability (Gray *et al*., 2004).

3.8 Immobilization of Previously Patterned Cells

When active force fields are used to pattern cells, the patterns formed are only temporary, and cells will spread once the field has been removed. Maintenance of the force field however, is not always possible. For example, during the process of pattern formation with p-DEP cells must be maintained in a low conductivity osmoticum, such as sorbitol, which needs replacing by a regular growth medium as soon as possible, to maintain the cell viability. To stop disintegration of the resulting 3D structures, cells have to be immobilized. Typical approaches involve cross linking of the cells and immobilization in a gel. Various issues need to be considered, one of them being the compatibility of the immobilizing agent with the living cells. The following section gives a review of various immobilizing agents that are successfully used for immobilizing cell patterns formed with DEP.

Gray et al. (2004) combined substrate patterning lithography (passive cell adhesion) and DEP (active cell aggregation) to efficiently arrange ~20 000 cells on a 1 cm^2 chip into a high fidelity array. Before DEP manipulation, the cell adhesion region was first coated with fibronectin using a membrane mask to define the pattern. The remaining areas outside the electrode region adsorbed a highly hydrophobic Pluronic™ gel to prevent nonspecific cell binding. After applying the field, cells were trapped on the electrodes and selectively immobilized on the substrate containing adhesive regions. The fibronectin boundaries restricted cells from spreading, resulting in a sharp cell arrays

with an average of two cells in a single spot. In this combined approach, DEP does not form the pattern itself, but assists cell aggregation onto an adhesive region to enhance effective cell adhesion and patterning.

Lin *et al*. proposed that increasing the Ca^{2+} and Mg^{2+} ion concentration to around 1 – 5 mM in medium can enhance adhesion between cells and the ECM substrate by cadherin and integrin activation (Lin *et al.*, 2006b). By gradually substituting a DEP buffer with a Ca^{2+} and Mg^{2+} containing buffer in a stepwise manner, strong cell adhesion was established between cells and a poly-L-lysine-coated glass surface. A normal culture medium for the growth and maintaining cell viability then replaced the Ca^{2+} and Mg^{2+} containing buffer to allow the establishment of primary adhesion. The flow rate of this buffer needed to be optimized to balance the effects of the divalent ions enhancing cell adhesion and the flow disrupting the DEP force.

Verduzco-Luque *et al.* (2003) showed that it was possible to crosslink microbial cells aggregated by DEP using polyethylenimine and form biofilms.

Sebastian *et al.* (Sebastian *et al.*, 2007) found that mammalian cells could be immobilized by simply extending the exposure of cell aggregates to electric field during DEP for another 10-15 minutes. It was proposed that was due to the enhanced and prolonged physical contact between the cells whilst the electric field was on, which subsequently led to non-specific binding (ionic / hydrophilic) of membrane components.

Other researchers have used gel immobilization to stabilize patterns. Factors that initiate polymerization of the gel have included UV-based curing, temperature changes, enzymatic reactions (e.g. fibrin gels), pH changes and cross linking with divalent ions (e.g. in the collagen / PuraMatrix system). Some of these techniques are described below.

Markx's group reported the use of cell arrays stabilized using UV photo-polymerized acrylamide-based hydrogels containing acrylamide and N,N′-methylene-bis acrylamide in the ratio of 15 / 2.2 (w/w), and at a concentration of 5% (Alp *et al.*, 2002). Although the viability of yeast strain *S. cerevisiae* was only slightly affected after incubation in the monomer solution for 30 min, cells immobilized in the polymerized hydrogel

exhibited reduced rates of glucose consumption and ethanol production compared with freely suspended cells, possibly due to diffusion limitation in the relatively thick hydrogels used. The gel-stabilized, structured consortia were reported to be capable of either remaining on the microelectrode arrays as a structured biofilm for several days, or being removed from the electrodes and used in a suspended form.

Bhatia and co-workers used a photo cross-linking PEG-based pre-hydrogel solution that was mixed with DEP buffer without lowering fidelity of pattern formation (Albrecht *et al.*, 2005). In addition, Koh and colleagues also suggested that after DEP patterning, PEG-diacrylate polymers can be set to solidify in the presence UV exposure and photo initiators such as Irgacure 2959 or 2,2-dimethoxy-2-phenylacetophenone, by initiating free-radical polymerization into a biocompatible, transparent, and elastic hydrogel (Revzin *et al.*, 2001). Selective UV exposure using a mask makes it possible to combine photo- and electro-patterning (Albrecht *et al*., 2005).

It is, however, not always necessary to remove the electric field after patterning cells. Arnold and Franich (2006), for example, demonstrated it is possible to pattern cells using n-DEP and maintain the pattern by maintaining the electric field. They showed that after the cells were collected above the electrode surface in a raft-like manner it was possible to trap them at a reduced voltage of 0.6 – 0.9 V at 0.3 MHz. During an experiment in which dielectrophoresis was continuously maintained they showed that the growth and division of fission yeast cells (*Saccharomyces cerevisiae*) continued through several generations, resulting in the formation of a small colony within each minimum field trap (Arnold and Franich, 2006). Live cells were held in defined electric-field-induced traps suspended slightly above a horizontal array of planar, micron-sized electrodes by repulsion force of negative dielectrophoresis, away from regions of high electric-field strength. A thermal convection cell was also created around 20 µm above the planar electrode array in response to heating of the liquid close to the electrode surface. This convection cell helped in keeping the cells levitated and maintaining the temperature of the culture fluid.

CHAPTER 4

Materials, Methods and Experimental Setup

4.1 Introduction

This chapter describes the materials, methods and experimental setups that were used during the experiments and illustrates the relevant techniques or approaches used. All of the cell aggregates produced in this study were constructed using the dielectrophoresis technique. The resulting size, shape or pattern of the aggregates were dependent on the electrode geometry and designs. This chapter also explains how the electrodes were made from the indium tin oxide (ITO) glass wafers. Further information for specific experiments are available in the subsequent chapters.

4.2 Construction of the Dielectrophoresis Chamber

Two types of DEP chamber were used in this project, the open-ended chamber and the closed chamber system. Both types of DEP chamber have advantages and disadvantages. The open-ended chamber is relatively simple and easy to use. It is good for testing the quality of the electrodes or looking at pattern development. The open-ended chamber allows fresh medium and oxygen to diffuse passively from either ends. However, liquid flows inside the chamber are difficult to control. For this, closed chambers were constructed.

4.2.1 The open-ended DEP chamber

An open-ended DEP chamber is shown in Figure 4.2-1. It was made from a microscope glass slide with electrode arrays connected at both ends with electrical fingers to the AC signal / frequency generator. The open-ended chamber was made by placing a microscope cover slip on top of microelectrode arrays, using insulating tape as a spacer. Cells were pumped from the source container into the chamber using a peristaltic pump fitted with 0.25 mm hole diameter tubing and needles. The unbound cells left the other end of the slightly inclined glass slide setup. The whole system was mounted into a plastic petri dish under the microscope.

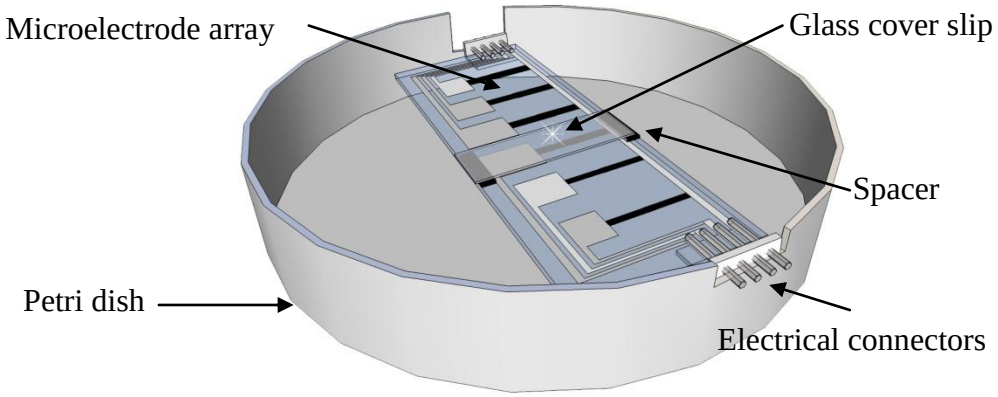

Figure 4.2-1. The final setup of open-ended DEP chamber.

The open-ended DEP chamber was used mainly for creating arrays of cell aggregates with defined geometries and patterns as shown in Chapter 5. Oxygenation was more efficient and cells spent a minimum amount of time suspended in buffer solution without nutrients. One of the advantages is that it was easy to use and setup the experiment.

4.2.2 The closed DEP chamber

A closed DEP chamber was constructed on top of the microelectrode slide using insulating silicone sheet as a spacer (560 μm thick), cut in the form of a square as shown in Figure 4.2-2, and a microscope glass slide (60 mm × 20 mm x 1mm) on top, covering the entire length of fabricated ITO glass slide. This chamber covers all the microelectrode array regions. The height of the chamber with the insulating sheet was around 560 μm, its length 75 mm and its width 25 mm. At both ends of the closed chamber, pipette tips were embedded for cell input / output using a peristaltic pump.

An alternative design of the chamber was the "mini" version. Instead of the full-length DEP chamber, by resizing the size of the cover glass slide and silicone sheets, a smaller chamber was created. The mini cover glass slide was also fitted with pipette tips and tubings, used as inlet and outlet. The mini size version of the closed DEP chamber was used if the aim of the experiment was to look at cell aggregate pattern formation with controlled liquid flow rates on any other factors (such as cell concentration) using a minimum amount of cells at a particular region of the electrode array.

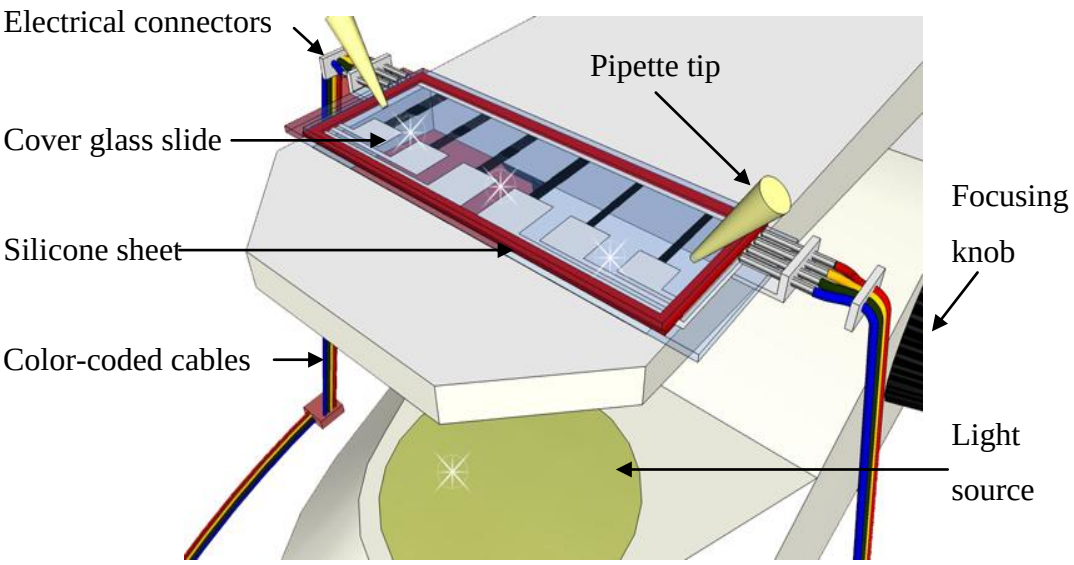

Figure 4.2-2. The final setup of closed-ended DEP chamber

A closer look of the sealed DEP chamber, showing one of the electrode arrays and electrical connectors, is shown in Figure 4.2-3. The clip-on electrical fingers were inserted in alignment with the fabricated ITO electrode array regions. Colour coded cables connected to different regions of the electrode array.

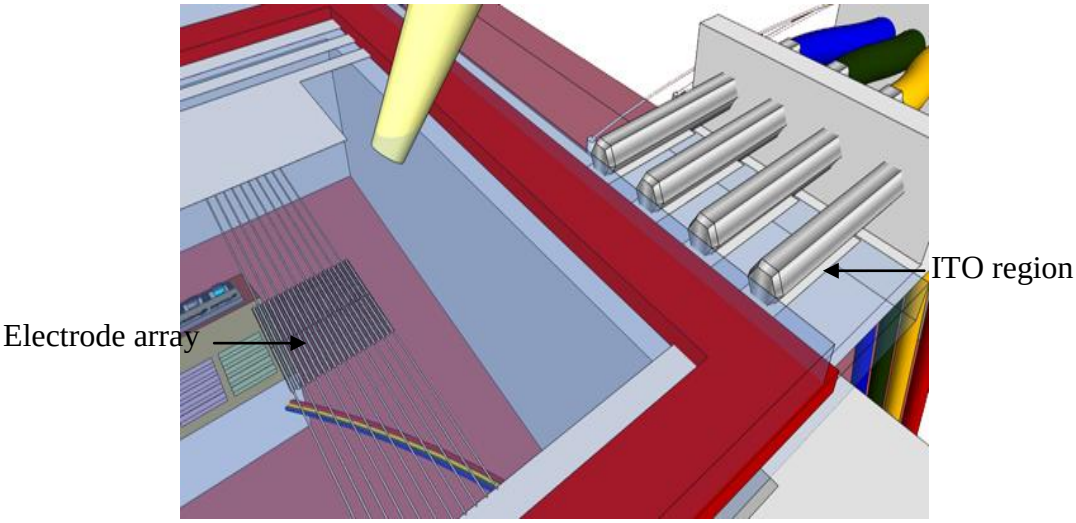

Figure 4.2-3. Closer look of the sealed DEP chamber, showing one of the electrode arrays and electrical connector.

An alternative closed DEP chamber was constructed using micro channels made of negative photoresist SU8-50 polymer. The final design of this chamber is shown in Figure 4.2-4. One of the advantages of using SU8 is the ability to control the height of the chamber during photolithography as described in the technical notes (Appendix A of this thesis). The disadvantages of using a closed DEP chamber made of SU8 are the associated cost of the chemicals and complex additional microfabrication steps. In

addition, possible leaks of liquid coming from the inside of the chamber to the surface of the device created unnecessary loss of cells. The SU8 microchannel enclosure system was therefore primarily used for prototyping and device comparison purposes.

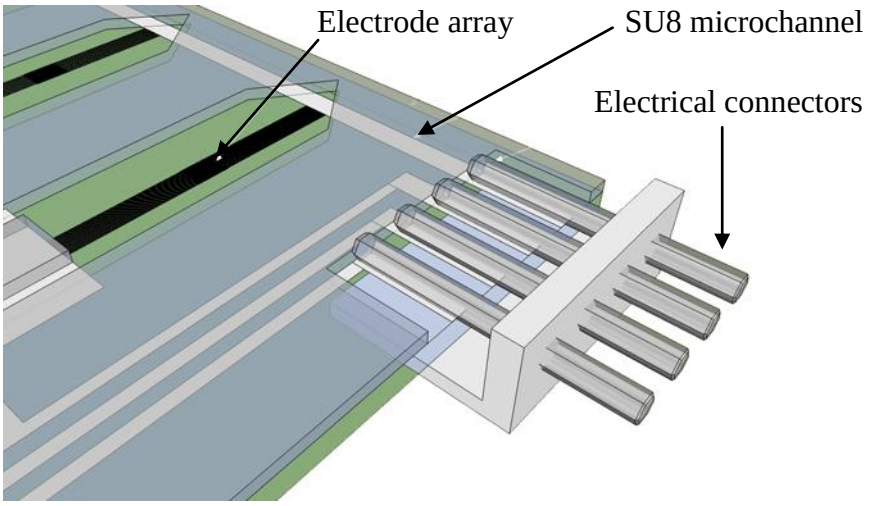

Figure 4.2-4. Closer look of the sealed DEP chamber made of Microposit SU8 polymer, showing the electrode arrays and electrical connector aligned with the ITO conductive regions.

4.3 Various Microelectrode Designs

Drawing of microelectrodes was done using industry-standard Protel Design Explorer 99 SE software. The CAD file containing the drawing was then sent to JD Photo Tools (Oldham, UK) for ultra-high resolution printing on acetate film. The film was subsequently used as the mask in the photolithography process described in the following section. Some of the full drawings of the electrode designs used for the creation of cell aggregates array with repeated (characteristic) feature size are shown from Figure 4.3-1 to Figure 4.3-7. Each ITO glass slide contains duplicate designs of electrodes of five (5) different characteristic sizes (50 to 250 µm) mirrored around the middle of the glass slide.

There were three main types of microelectrode design that were used in this project. Type 1 consists of parallel bars with a variable gap-width (from 50 to 250 µm) without any castellation. Type 2 contains castellated side bars, and type 3 also contains castellations but with pointed microelectrode edges. Type 1 allows the formation of 3D cell aggregates in a line pattern in between and along the side bars of microelectrode. The castellations of type 2 allows the formation of distinct and separate 3D cell

aggregates. Type 3 gives more elongated cell aggregates. All of the microelectrode arrays have characteristic sizes between 50 – 250 micron feature size (in 50 μm increments).

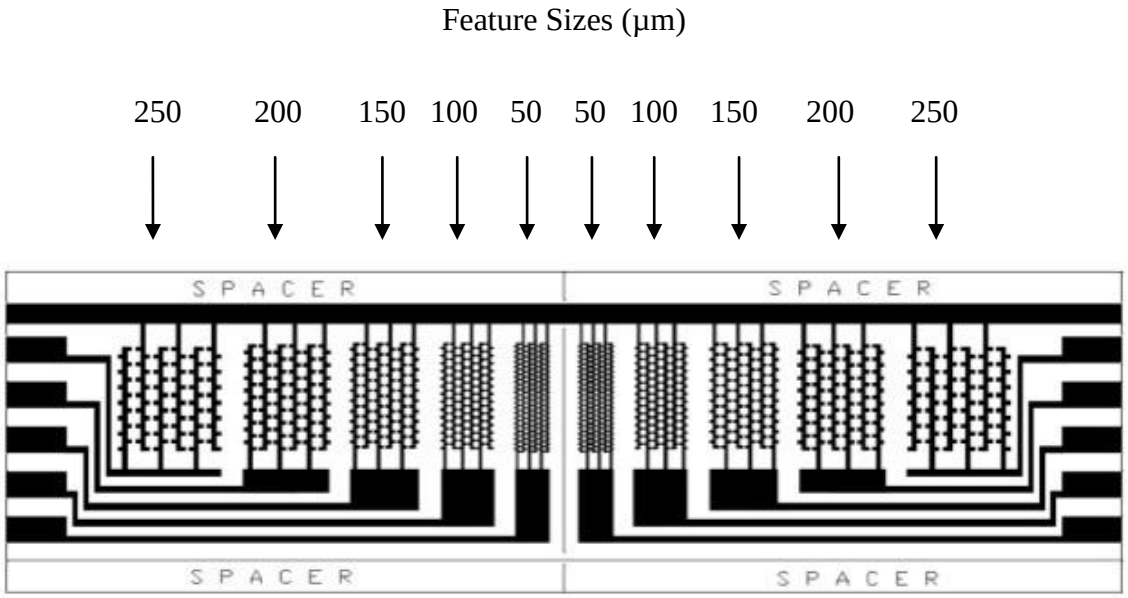

Figure 4.3-1. Microelectrode with hexagonal pattern designs, used for cell patterning with characteristic feature sizes from 50 to 250 μm, arranged in a mirror image.

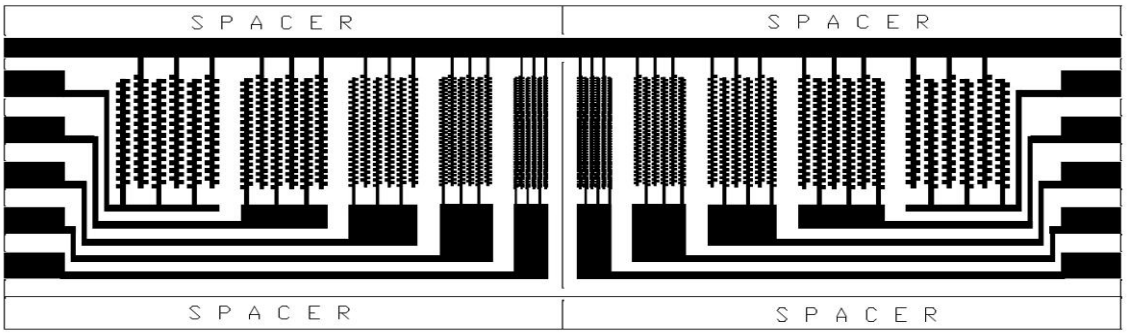

Figure 4.3-2. Microelectrode with 'W' or Zig-Zag pattern designs, used for cell patterning with characteristic feature sizes from 50 to 250 μm, arranged in a mirror image.

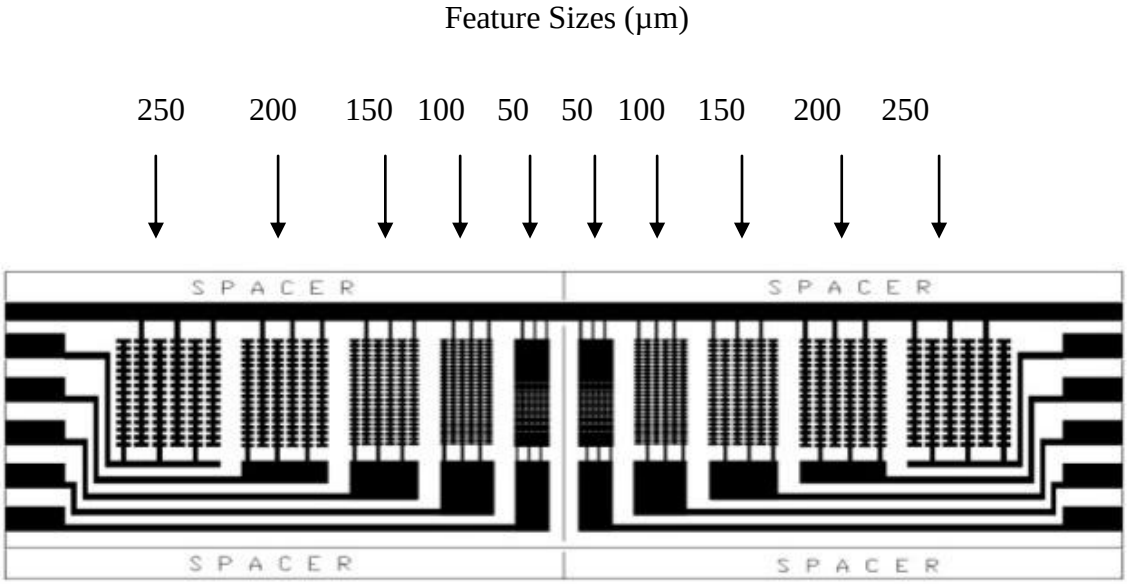

Figure 4.3-3. Microelectrode with square (4 x 2) pattern designs, used for cell patterning with characteristic feature sizes from 50 to 250 µm, arranged in a mirror image.

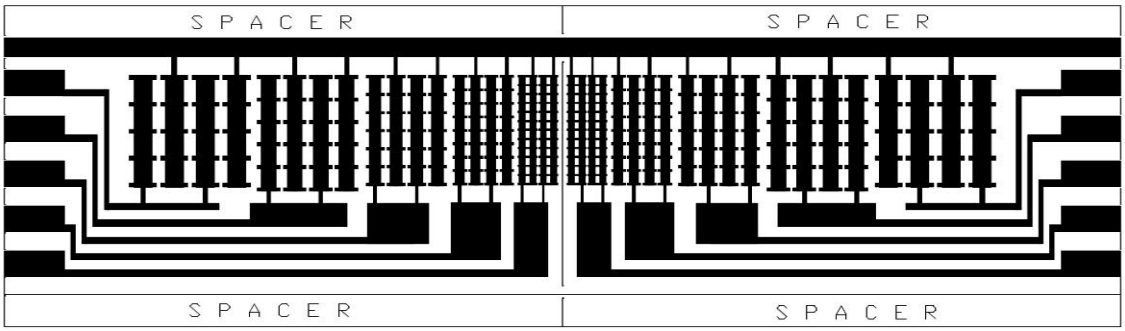

Figure 4.3-4. Microelectrode with square (7 x 7) pattern designs, used for cell patterning with characteristic feature sizes from 50 to 250 µm, arranged in a mirror image.

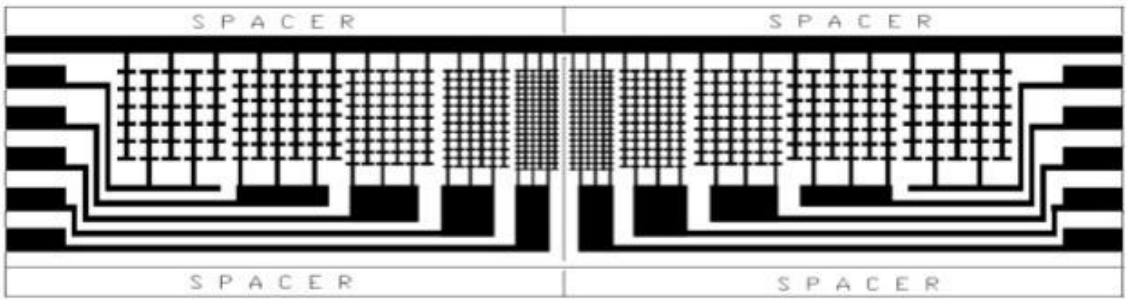

Figure 4.3-5. Microelectrode with square (5 x 5) pattern designs, used for cell patterning with characteristic feature sizes from 50 to 250 µm, arranged in a mirror image.

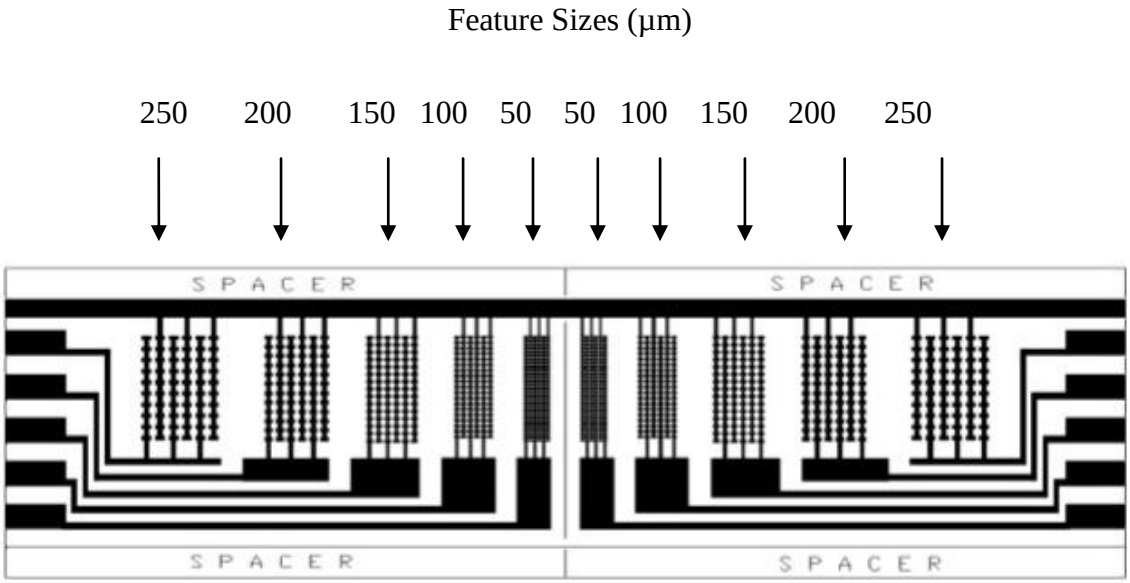

Figure 4.3-6. Microelectrode with square (3 x 3) pattern designs, used for cell patterning with characteristic feature sizes from 50 to 250 µm, arranged in a mirror image.

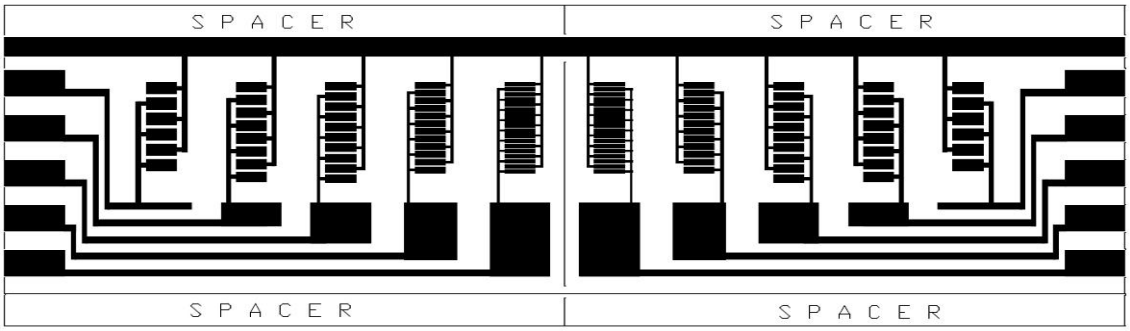

Figure 4.3-7. Microelectrode with line pattern designs, used for cell patterning with characteristic feature sizes from 50 to 250 µm, arranged in a mirror image.

The designs on the left hand side of the electrode are mirror images of the designs on the right-hand side. This is a useful feature as this allows them to be used as sandwich-type dual microelectrodes, as done by Bhatia's research group (Albrecht, 2005).

4.4 Microfabrication of Electrodes by Photolithography

Microelectrodes with characteristic sizes between 50 and 250 µm were fabricated in a clean room laboratory in Heriot-Watt University in Edinburgh and the University of Manchester in Manchester, using photolithography as shown in Figure 4.4-1. The starting material was an Indium Tin Oxide (ITO) - coated wafer (with dimensional size 75 mm x 25 mm x 11 mm) of Delta Technologies, with 100-nm thick ITO (Figure 4.4-1 part I). The resistivity of ITO is between 5-15 ohms. A layer of photo resist (Microposit

1813, Shipley) was spin-coated onto the wafer for 60 seconds at 3000 rpm (Figure 4.4-1 part II). A photomask containing a specific pattern was placed on top of the wafer (Figure 4.4-1 part III) and subsequently exposed to UV (365 nm) for 30 seconds, in an automatic mask aligner machine (Tamarack). As a result, some regions of photoresist were exposed to UV light, whilst mask-protected photoresist regions remain unexposed, according to the pattern design on the mask (Figure 4.4-1 part IV). After development of the wafer using fresh (Microposit) MF26 developer buffer for 60 seconds, the UV-exposed photoresist layer dissolved in the buffer leaving behind the mask-protected photoresist patterned regions (Figure 4.4-1 part V). ITO layers underneath the photoresist chemical were protected by the photoresist layer, whilst unprotected regions could be etched away using a fresh solution of hydrochloric acid (38% v/v) isotropic etching solution (Sigma) at room temperature for around 45 to 60 minutes leaving behind the glass substrate (Figure 4.4-1 part VI). It is important to note that smaller feature sizes below 50 µm may need less time to fully etch. The wet-chemical etching rate can increase at higher temperature. After the ITO microelectrodes were fully etched (Figure 4.4-1 part VII), the unexposed photoresist was easily removed using acetone leaving behind the ITO electrode pattern on the glass substrate (Figure 4.4-1 part VIII).

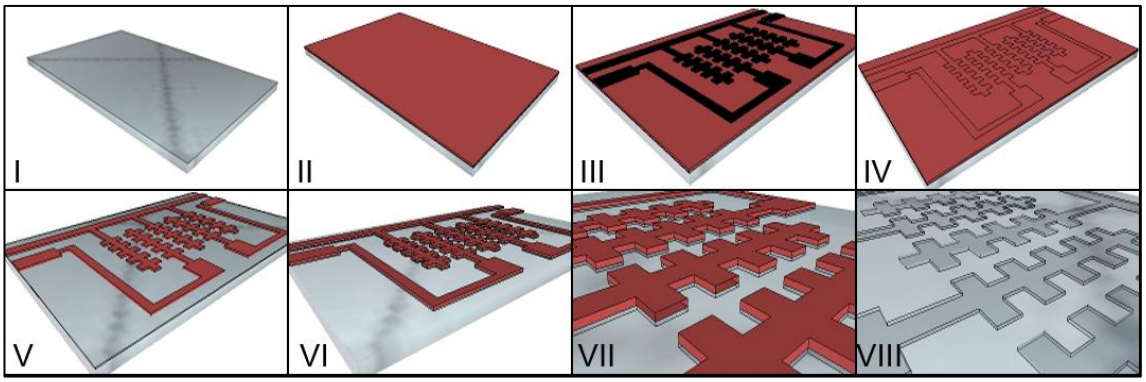

Figure 4.4-1. Fabrication of microelectrode by photolithography.

4.5 Setup Used for Dielectrophoresis Experiments

The setup shown in Figure.4.5-1 and Figure 4.5-2 was used to form 3D cell aggregates by dielectrophoresis. Liquid flow rates at the inlet / outlet were controlled and maintained using a peristaltic pump (Dynamax – Rainin), fitted with silicone tubes with an inner diameter of 0.25 mm. The chamber was filled with filter-sterilized low conductivity D-sorbitol (300 mM) solution prior to the application of any electric current. AC electric fields were supplied using at 1 MHz signal frequency and voltages between 10 - 20 V_{pk-pk} (depending on feature size used) generated using a Thurlby-Thandar TG120 function generator. Two types of microscopes were used. The first one is wide field stereomicroscope (CELSI) as shown in Figure.4.5-1, the second one is a phase contrast NIKON E600 microscope as shown in Figure 4.5-2.

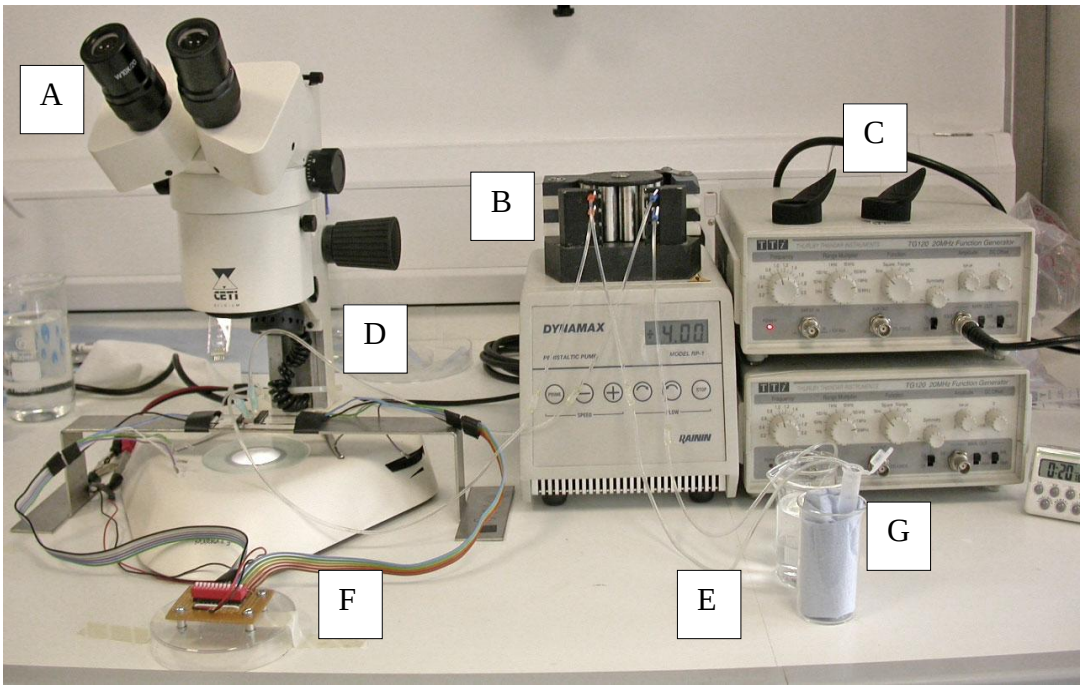

Figure.4.5-1. Setup used for the construction of patterned cell aggregates. A. Wide field stereo microscope, B. Peristaltic pump, C. AC signal frequency generator, D. Inlet / outlet, E. Silicone tubing connected to the peristaltic pump (ensuring equal rates of inflow and outflow), F. Electrical switch / controls and connections, and G. Cells contained in Eppendorf tubes.

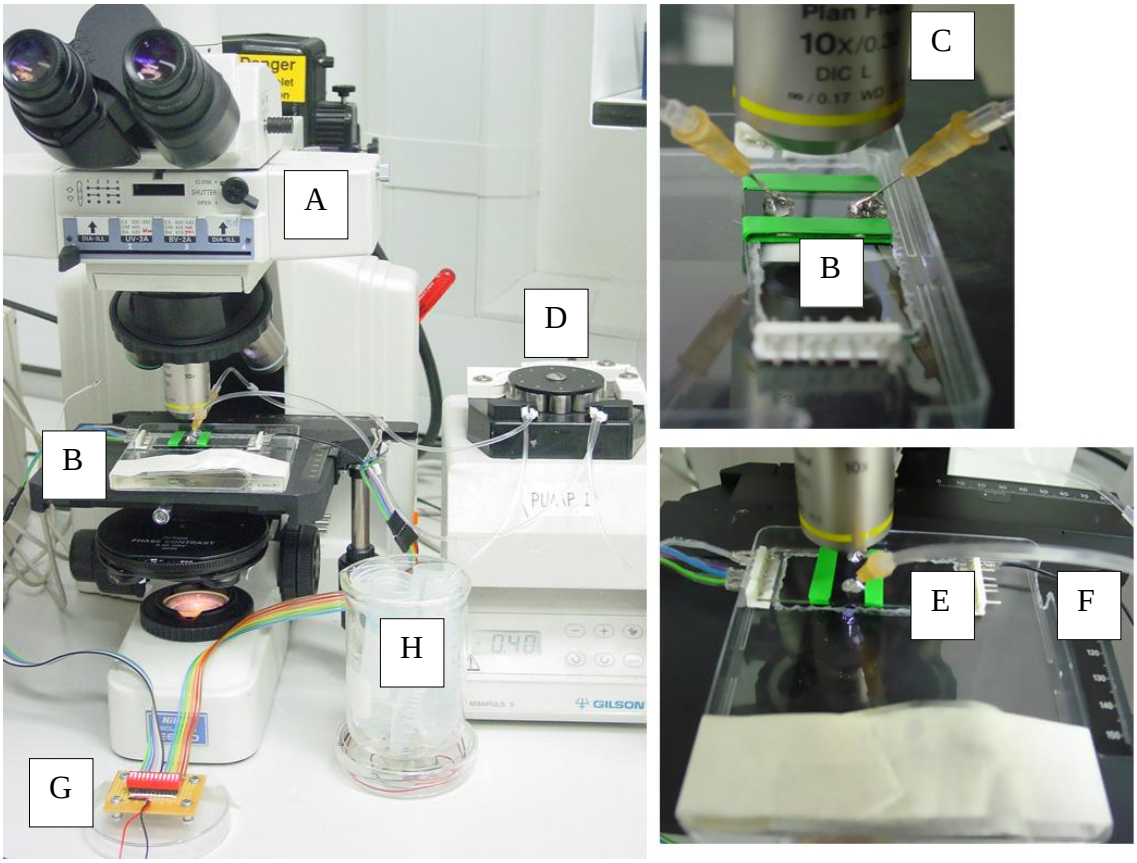

Figure 4.5-2. Setup used for the construction of cell aggregates / artificial tissue formation. The photo shows: (A) NIKON E600 phase-contrast microscope. (B) Closed "mini" chamber, (C), microscope lenses with 10X magnification, (D) peristaltic pump, (E) inlet – outlet, (F), silicone tubes connected to the peristaltic pump (ensuring equal rates of inflow and outflow, (G) Electrical switch / connections. (H) Cells contained in tubes.

4.6 Electric Field Calculation (Modeling) With Finite Element Analysis

Electric field calculations were performed using COMSOL Multiphysics 3.4 as described previously (Sebastian *et al*., 2007b). The Electromagnetic - Electrostatics module was used to simulate the experiments in 2D only (due to high computational demand of working with 3D field calculations). The work aims to see overall pattern of high field regions between electrode castellation in a larger area. Various microelectrode array designs were drawn to scale. A DC voltage equivalent to the experimentally applied AC voltage was assigned by dividing the AC $V_{pk\text{-}pk}$ value by $2\sqrt{2}$. Each object forming the microelectrode array was alternately assigned an electric potential of 3.55 V DC (after the original 10 $V_{pk\text{-}pk}$ AC) as the boundary condition. The electrodes adjacent to the ones that were energized were grounded (V = 0). An extra fine meshing parameter was applied prior to solving the equation using the default

stationary linear solver. After solving the problem, a surface plot of the electric field was displayed.

4.7 Tissue and Cell Preparation

4.7.1 Yeast Saccharomyces cerevisiae

Yeast (*Saccharomyces cerevisiae*) was used for preliminary experiments. It was also used to test the quality of newly microfabricated electrodes. Yeast cells were derived from commercially available baker's powder and suspended in filter-sterilized distilled water by repeated (four to five times) vortexing and centrifugation (also known as washing step). This ensures that the cells were suspended in a low conductivity medium. Prior to injecting them into the dielectrophoresis chamber, the cells were passed through a fine needle to maximize individual cellular detachment.

4.7.2 Chicken embryonic skin cells

To create artificial skin with artificial feather placodes, embryonic skin tissue was isolated (using autoclaved-sterilized fine tools) from the dorsal part of 8-days old embryos of fertilized eggs harvested from white leghorn chickens. The cells from the skin, which were a mixture of dermal and epidermal cells, were isolated by treating the freshly dissected skin tissue with a solution of 0.5 (v/v) % trypsin-EDTA for 60-90 minutes. Following this, the cells were washed 4 times with a 300 mM sorbitol solution by repeated centrifugation and decanting of the supernatant. After 4 washes the cells were diluted in 300 mM sorbitol at a final cell concentration of 3.75×10^6 cells ml^{-1}. In some experiments epidermis and dermis were separated prior to their dissociation in order to obtain epidermal and dermal cells separately.

DMEM was used as growth medium or to store cells when not in used in DEP. The medium was supplemented with 10% fetal calf serum (FCS), 2 mM glutamine, 100 units ml^{-1} penicillin and 100 µg ml^{-1} streptomycin. Cells were cultured in a humidified chamber with 5% CO_2 at 37°C. Medium was exchanged every 3 days. When the cells were ready to be used, the cells were harvested using filter sterilized 0.5% trypsin and 0.5% Ethylene Diamine Tetra Acetic acid (EDTA) dissolved in 1 x PBS pH 7.4 and

then harvested by centrifugation at 1700 rpm for 5 minutes. Prior to their use in dielectrophoretic experiments, harvested cells were washed 3 – 4 times by refrigerated centrifugation with 300 mM D-Sorbitol. The cells were then resuspended in 300 mM D-sorbitol solution at an approximate concentration of 3×10^6 cells ml^{-1}.

4.8 Formation of Cell Aggregates by (+)Dielectrophoresis and Monitoring

Freshly prepared (washed / centrifuged) skin cells (at approximately 3 x 10^6 cells.ml^{-1} concentration) were introduced into the chamber at a speed of 40 μL.$minute^{-1}$ and allowed to be attracted to the high field regions between the electrode castellations whilst maintaining a small flow of fresh sorbitol solution through the chamber to redistribute the cells, remove non-attracted cells and maintain a low conductivity buffer inside the chamber. The conductivity was maintained close to that of fresh sorbitol (σ = 6.1 x 10^{-4} S.m^{-1}) determined using JENWAY 4010 conductivity meter. The settings of the conductivity meter were as follows: cell constant, 1.00 cm^{-1}; coefficient, 1.910; medium temperature, 25 ºC; TDS effect, 0.5 and the band, 9600.

The chamber was filled with a filter sterilized low conductivity (6.1 μS cm^{-1}) D-sorbitol solution at 300 mM concentration prior to the application of any electric current. Electric fields of 1 MHz frequency were generated using a Thurlby-Thandar TG120 function generator using voltages of 10 - 20 $V_{pk\text{-}pk}$. Cells were introduced into the chamber with a peristaltic pump (Dynamax - Rainin) at a concentration of 40 μL per minute and attracted to the high electric field regions on the electrode.

The formation of distinct cell aggregates with defined geometry is illustrated in Figure 4.8-1. A high electric field gradient was set up between the electrode castellations (part I) as indicated by the yellow gradient color. Cells entered the chamber at a small flow rate (part II). A continuous and small flow of fresh sorbitol solution was maintained in the chamber in order to redistribute the cells, remove non-attracted cells and keep the medium conductivity around the cells low. Initially, cells were aggregated on the electrode edges (part III). As more and more cells were added (part IV), some cells formed pearl-chains (part V). Cells were continuously introduced into the chamber (part VI and VII) until full aggregates were formed in most of the electrode (part VIII). Typical total time needed to form multi layered 3D cell aggregates was 15-20 minutes

(depending on cell concentration, liquid flow rates, voltage and electrode characteristic size). The aggregates formed between the electrodes were observed using either a phase contrast NIKON E600 microscope or a wide field stereo microscope (CELSI). Pictures were taken using a Nikon Coolpix 4500 digital camera.

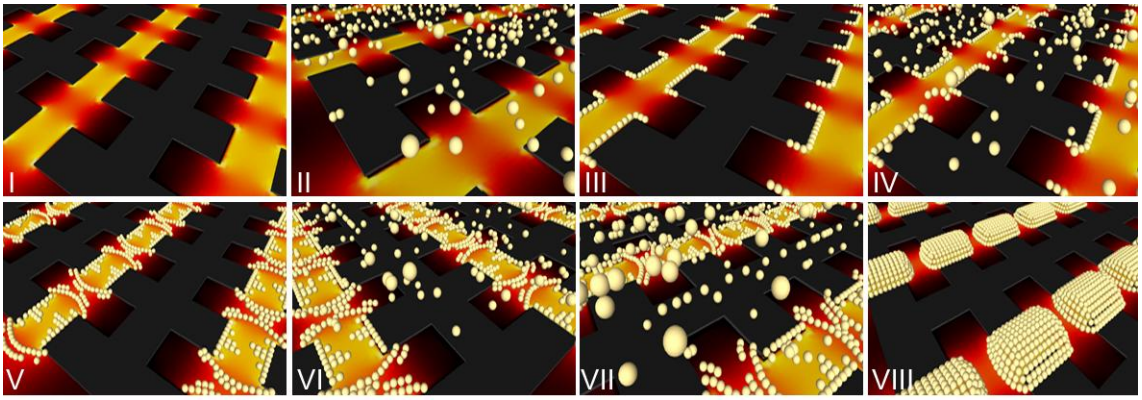

Figure 4.8-1. Formation of cell aggregates by dielectrophoresis (refer to text for illustration).

4.9 Cell Viability Assay

In some of the experiments, a cell viability assay was also carried out to determine the effects of the electric field on cell viability. The viability of the skin cells was determined using the TrypanBlue™ exclusion dye, by adding an equal volume of a dye solution containing 0.4 gram TrypanBlue in 100 mL PBS pH 7.4 directly to the buffer medium. The intact cell membrane is impermeable to the dye, which can, however, enter dead or dying cells. The cell viability was assayed within 5 minutes of exposure to the dye solution prior to live / death cell counting in a hemocytometer chamber with at least 100 cells in each quadrant.

4.10 Further Cell Immobilization in Gel Media

Immobilization of the cells in the aggregates was initially performed as described previously by Sebastian et al., 2007a. The cells were first attracted to the electrodes and forced to adhere to each other by keeping the electric field applied for a further 10 minutes. Following this, a 9:1 v/v mixture of a fibrinogen (10 mg ml^{-1} in DMEM medium) and thrombin solution (10 units ml^{-1} in a 4 μM $CaCl_2$ solution) was introduced into the chamber at a flow rate of 5 μL min^{-1} to further immobilize the cells and create

an artificial skin-like material with cell aggregates embedded within the structure in a defined pattern.

In most of the later DEP experiments however, PuraMatrix™ hydrogel was the preferred choice for immobilizing the patterned cell aggregates using the open-ended DEP chamber as disturbance of the cell aggregates during the immobilization step was less with Puramatrix than with fibrin gels. For the formation of artificial skin with artificial placodes, skin cell aggregates were made as described previously. PuraMatrix™ peptide hydrogel precursor was introduced into the chamber (at 50% concentration in 300 mM sorbitol). To solidify the gel and form an artificial skin-like material, DMEM medium (containing the ions needed to induce gel formation) was added at both ends of the open-ended chamber.

4.11 Image Analysis of Cell Aggregates

Investigation of the resulting biodielectric patterns were carried out using LabVIEW VISION Development Module, a graphical image analysis tool. To analyze the patterns produced and to study their development after their formation a Virtual Instrument (VI) system was developed using the LabVIEW IMAQ Vision Development Modules. This section is described in more detailed in Chapter 6.

CHAPTER 5

Creating Arrays of Cell Aggregates in Well-Defined 2D Geometrical Patterns for Developmental Studies

5.1 Abstract

It is shown that dielectrophoresis- the movement of particles in non-uniform electric fields- can be used to create engineered skin with artificial placodes of different sizes and shapes, in different patterns. Modeling of the electric field distribution and image analysis of the cell aggregates produced showed that the aggregation is highly predictable. The system developed could be of considerable use for the *in vitro* study of developmental processes where local variations in cell density and direct cell-cell contacts are important.

5.2 Introduction

It has long been noted that the sites of vertebrate organ rudiments can first be morphologically identified by changes in cell packing densities, which are easily observed on stained tissue sections. For example, the sites at which sensory organs of the head (McCabe and Bronner-Fraser, 2009) and the appendages of the skin (such as hair follicles, feather follicles, glands and teeth) will develop are first identifiable as placodes of tightly packed cells within the ectodermal epithelium and underlying mesenchyme (Hardy, 1992; Jiang *et al.*, 1999; Jiang *et al.*, 2004; Mou *et al.*, 2006). The cells that constitute the placode have a different developmental fate to that of the surrounding, non-placode, cells and develop into a discrete structure in the adult, such as an ear, lens, nose, tooth, feather or hair follicle.

In recent decades it has become possible to identify organ initiation sites using *in situ* hybridization to detect specific marker gene expression that is distinct from the surrounding cells. The technical ability to modulate gene function in model species (Nagy *et al.*, 2003) has meant that some, though by no means all, marker genes expressed during early organ development have been conclusively demonstrated to have key functional roles in organ development. The developmental roles of the long noted focal packing of cells, and the forces that draw them together, have remained relatively unexplored due to the difficulties in experimentally manipulating these processes at the small scales involved. This imbalance in technical ability has contributed to the

perception that molecular signaling phenomena play a decisive role in vertebrate development, with morphological changes in cell density representing secondary consequence of prior molecular signals. To enable studies aimed at dissecting the role of heterogeneous cell densities on developmental processes, this chapter will show the work on designing a method that allows the construction of tissues with defined cell density patterns.

One of the best examples of pattern formation is the formation of feather buds in chicken (Jiang *et al.*, 1999; Jiang *et al.*, 2004). During embryonic development chicken skin of embryos 6 or less days old do not show any follicle patterns, indicating that the cells in the embryonic skin have not committed whether they are going to form part of the feather follicle or part of the interfollicular skin. In the next two days, the development of placodes can be seen starting at a line above the neural tube, which subsequently breaks up into individual placodes. From this line a regular hexagonal follicle pattern then emerges in a wave-like pattern. A variety of models have been proposed which explain the emergence of these patterns (Murray *et al.*, 1983; Harris *et al.*, 1984; Murray, 1989). However, limited experimental evidence for these models is available, and there is a need for more experimental approaches to explain pattern formation. One of these approaches could be to create artificial patterns in the cell density. Study of the chemical and physical gradients subsequently produced by the cells, and the redistribution of the cells that follows, could give important information about the processes involved.

A variety of methods can be used for artificially creating patterns of cells density *in vitro*. Of the methods available, methods based on surface attachment are relatively unsuitable because of the 3-dimensional and layered structure of many patterns in nature. Various other approaches are available which can create 3-dimensional distributions in the cell density. These include fluidic, ultrasonic, optical and electrical approaches (Birkbeck *et al.*, 2003; Mironov, 2003; Tan and Desai, 2004; Tsang and Bhatia, 2004; Albrecht *et al.*, 2005; Gherardini *et al.*, 2005; Abidin *et al.*, 2007; Markx, 2008). Of those techniques, electrical, and in particular dielectrophoretic approaches, are some of the most useful (Markx and Buckle, 2005; Markx, 2008) because of the relative simplicity of the experiments, the ease of control, and the relatively high spatial resolution that can be achieved. In addition to this, many cells can be manipulated

simultaneously in different areas (Yusvana *et al.*, 2010).

Dielectrophoresis (DEP) is the induced movement of particles in non-uniform electric fields (Pohl, 1978; Hughes, 2003; Morgan and Green, 2003). To experience a dielectrophoretic force, the electrical properties of the particle need to be different from that of the surrounding medium. In an applied electric field the particle then attains a net dipole, and when the applied electric field is non-uniform this results in a net force on the particle. Dielectrophoresis can be observed in DC as well as AC electric fields, and positive (towards regions of high electric field) as well as negative (away from regions of high electric field) dielectrophoresis are possible (Pethig *et al.*, 1992). Cells have frequency-dependent electrical properties, which make it possible for a given cell to show both positive and negative dielectrophoresis, depending on the frequency of the applied electric field. Dielectrophoresis has been used for characterizing, separating, manipulating and trapping cells. The creation of tissue-like materials from suspended cells with dielectrophoresis was first demonstrated by Pohl (1972), using bacterial cells. Later work has used both micro-organisms (Alp *et al.*, 2002; Verduzco-Luque *et al.*, 2003; Abidin *et al.*, 2007) and animal cells (Matsue *et al.*, 1997; Albrecht *et al.*, 2005; Albrecht *et al.*, 2006; Ho *et al.*, 2006; Albrecht *et al.*, 2007; Sebastian *et al.*, 2007a; Markx *et al.*, 2009). In recent years the method has attracted increased attention because of its ability to controllably pattern different cell types in a 2D and 3D (micro) environment (Albrecht *et al.*, 2005; Albrecht *et al.*, 2006; Albrecht *et al.*, 2007; Sebastian *et al.*, 2007a; Markx *et al.*, 2009). Reviews of the use of dielectrophoresis - and more generally electrical fields - in tissue engineering have been given previously (Markx and Buckle, 2005; Markx, 2008).

This chapter will discuss how dielectrophoresis was used to create patterns in the cell density in artificial skin, mimicking feather follicle patterns during development in the skin of embryonic chicken. In addition, it will also show how variations of this pattern can be produced. Although the use of negative dielectrophoresis for the formation of cell aggregates is also possible (Matsue *et al.*, 1997), this project will only use positive dielectrophoresis because the trapping forces are higher. A major advantage of positive dielectrophoresis is also that the electric field used strongly forces the cells within the aggregates in direct contact with each other, encouraging exchange of signals between cells by direct cell-cell contact. In addition, the more natural distribution of cells

(mimicking the actual 3D structures of placode *in vivo*) encourages the formation of more natural distributions of oxygen, nutrients, diffusible signals and other factors in the artificial tissues, in the sense that cells on the surface of the 3D structure get more access to oxygen from the environment than the cells on the inside of the aggregate.

5.3 Materials and Methods

5.3.1 Microelectrodes

Microelectrodes were fabricated from ITO-coated microscope glass slides (Delta Technologies Ltd, USA) using photolithography technique as described in more details previously in Chapter 4 (Materials, Methods and Experimental Setup), and with reference to other works (Albrecht *et al.*, 2005; Markx and Buckle, 2005; Flores-Rodriguez and Markx, 2006). Electrodes were of the interdigitated form, parallel or castellated, and designed and fabricated to make aggregates in the form of straight or wavy ("W") lines or spots in hexagonal or square patterns. Each slide contained only electrodes of the same design, but electrodes with different characteristic sizes were fabricated on the same slide. Electrodes within the arrays had characteristic sizes between 50 and 250 micron (in some slides, the array is up to 300 μm), increasing with a step size of 50 micron. To separate the arrays of electrodes with different sizes on a given slide, a simple removable chamber was made from silicone sheet on top of the microelectrode arrays as shown in Figure 5.3-1, using a thin microscope slide as a cover. The height of the chamber was 560 μm, its width 20 mm and length 25 mm. Connections to the signal generator (Thurlby-Thandar TG120) were made using clip-on PCB connectors.

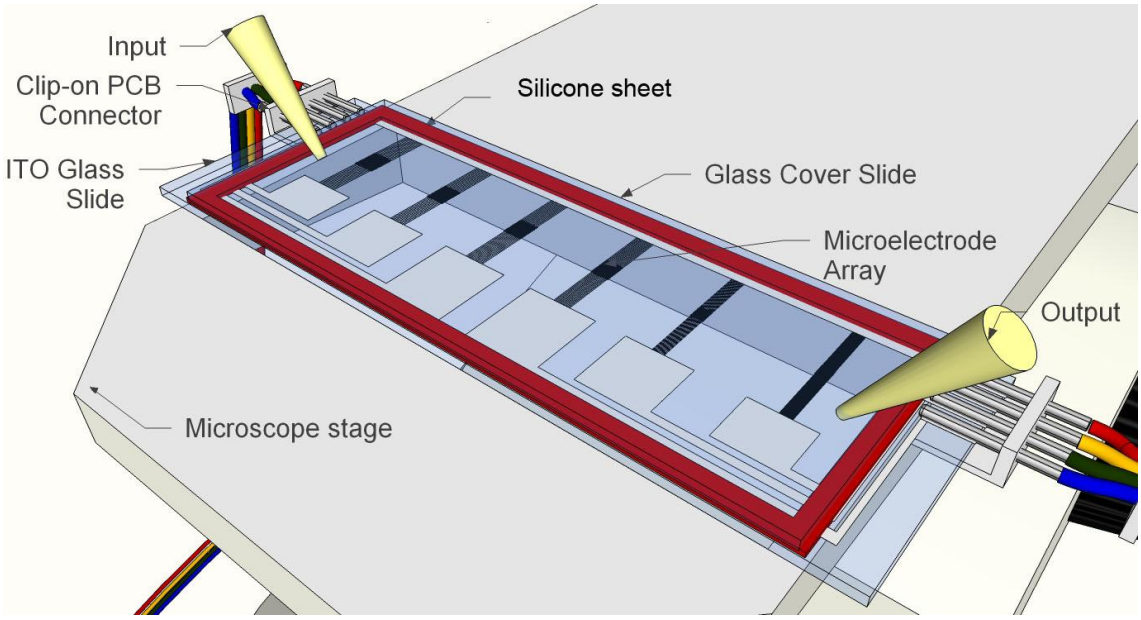

Figure 5.3-1.Diagram of dielectrophoresis chamber setup used in the experiments.

5.3.2 Electric field simulations

Electric field simulations were performed using COMSOL Multiphysics 3.4 as described previously (Sebastian *et al.*, 2007b). The Electromagnetic - Electrostatics module was used to simulate the experiment in 2D only. Various microelectrode array designs were drawn to scale, using a characteristic size of 100 µm as the model for electric field simulation. A DC voltage equivalent to the experimentally applied AC voltage was assigned by dividing the AC $V_{pk\text{-}pk}$ value by $2\sqrt{2}$. Each object forming the microelectrode array was alternately assigned an electric potential of 3.55 V DC (after the original 10 $V_{pk\text{-}pk}$ AC) as the boundary condition. The electrodes adjacent to the ones that were energized were grounded (V = 0). An extra fine meshing parameter was applied prior to solving the equation using the default stationary linear solver. Under static conditions the electric potential, V, is defined by the equation 5:

[5]

The electric field, E, is tangential to the *xy*-plane. After solving the equation, a surface plot of the electric field (normE) was displayed, where the expression of normE is given by (Refer to COMSOL Multiphysics 3.4 manual for the electrostatic application mode, embedded with the package).

5.3.3 Formation of cell aggregates

To create artificial skin with artificial feather placodes, embryonic skin tissue was isolated from 8-days old embryos from fertilized eggs of white leghorn chickens. The cells from the skin, which were a mixture of dermal and epidermal cells, were isolated by treating the skin with a solution of 0.5 (v/v) % EDTA/trypsin for 90 minutes. Following this, the cells were washed 4 times with a 300 mM sorbitol solution by repeated centrifugation (1800 rpm in a refrigerated centrifuge at 4º C) and decanting of the supernatant. After 4 washes the cells were diluted in 300 mM sorbitol at a final cell concentration of 3.75×10^6 cells ml^{-1}. Cell suspension was pumped continuously into a chamber above one of the electrode arrays using a Rainin peristaltic pump. Fresh sorbitol was also pumped in to keep the medium conductivity in the chamber as close as possible to that of fresh sorbitol solution ($\sigma = 6.1 \times 10^{-4}$ S m^{-1}). Aggregates were made of the cells by applying a 10 $V_{pk\text{-}pk}$ 1 MHz signal to the electrodes in the array using a TG120 Thurlby-Thandar frequency generator. Aggregate formation was continuously observed using a Celsi stereomicroscope, and pictures were taken of the aggregates using a Nikon Coolpix 4500 digital camera. Images taken were analyzed using LabVIEW Vision Development Module and Vision Assistant 8.5 using the user-specified Multi Regions Masking (MRM) technique as described in the following chapter.

Viability of the skin cells was determined using TrypanBlue™ exclusion dye, by adding an equal volume of a dye solution containing 0.4 gram TrypanBlue in 100 mL PBS pH 7.4 directly to the sample medium. The intact cell membrane is impermeable to the dye. However, the dye is capable to enter the dead or dying cells. The cell viability was assayed within 5 minutes of exposure to the dye solution.

Immobilization of the cells in the aggregates was performed as described previously (Sebastian *et al.*, 2007a). The cells were first attracted to the electrodes and forced to adhere to each other by keeping the electric field applied for a further 10 minutes. Following this, a 9:1 v/v mixture of a fibrinogen (10 mg ml^{-1} in RPMI medium) and thrombin solution (10 units ml^{-1} in a 4 μM $CaCl_2$ solution) was introduced into the chamber at a flow rate of 5 μL min^{-1} to further immobilize the cells and create an artificial skin-like material with cell aggregates embedded within the structure in a

defined pattern. The flow was stopped when the gel has covered and immobilized the DEP-patterned cell aggregates.

5.4 Results and Discussion

5.4.1 Optimization of the conditions for aggregate formation

Although negative dielectrophoresis can also be used for aggregate formation (Matsue *et al.*, 1997), because the forces holding the cells are stronger when using positive dielectrophoresis it was decided from the start to use positive dielectrophoresis only. The optimum conditions for obtaining positive dielectrophoresis of cells are relatively constant (1 MHz; medium conductivity as low as possible to maximize the DEP force), and the electric field strength that could be used was determined by ability of the cell to maintain its viability (Menachery and Pethig, 2005). Therefore, the major factor that could be optimized was the flow rate.

Figure 5.4-1 shows the formation of aggregates of chicken embryonic skin cells at electrodes of the interdigitated oppositely castellated design at different flow rates as a function of time.

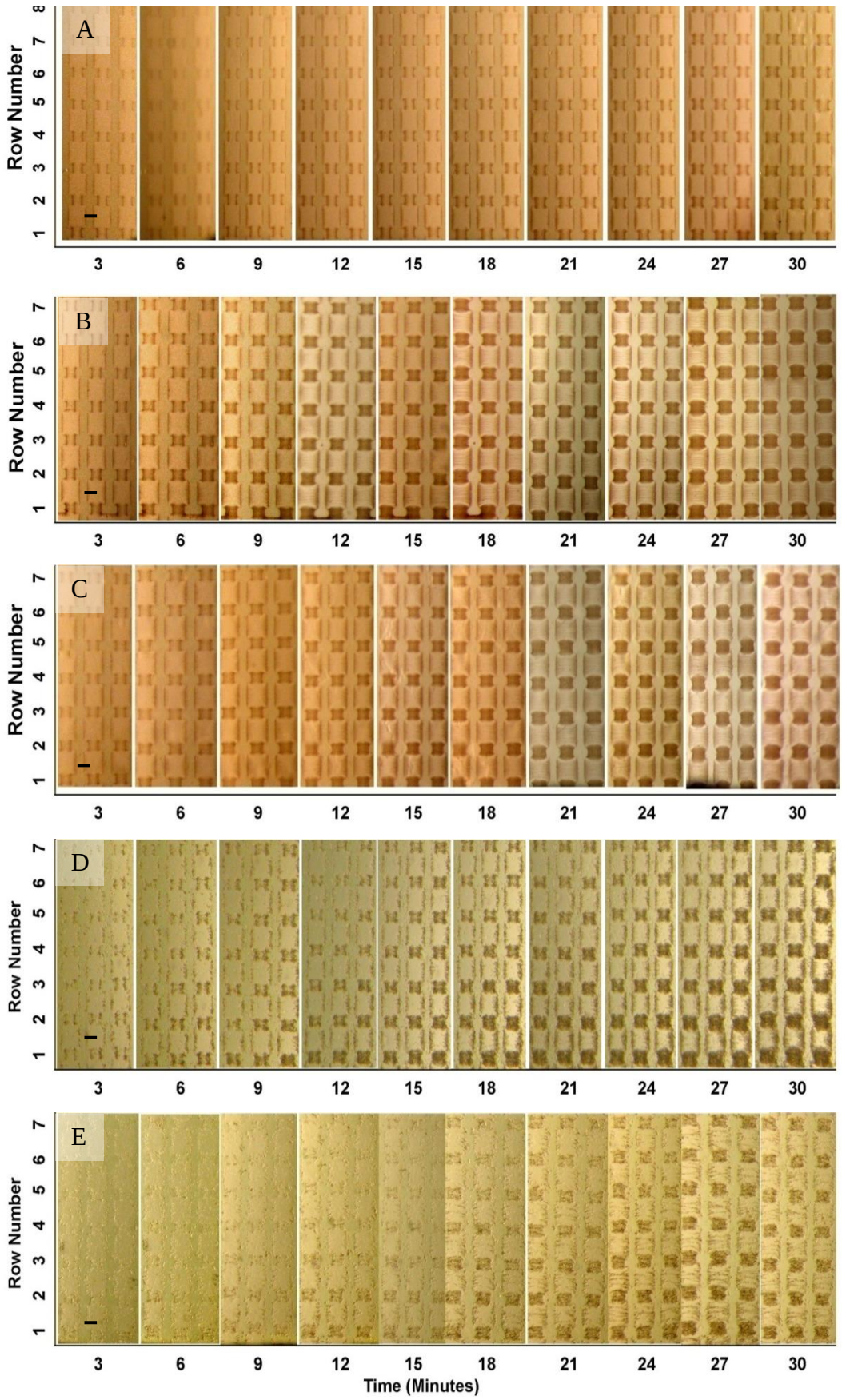

Figure 5.4-1. Aggregates formation at electrodes of the interdigitated oppositely castellated design (square pattern). The distance between aggregates is 3 times the characteristic size (100 μm). In the images shown the cells enter the chamber at a flow rate of A. 20 μL min^{-1}; B. 40 μL min^{-1}; C. 60 μL min^{-1}; D. 80 μL min^{-1}; E. 100 μL min^{-1}.

A flow rate of 100 μL.min^{-1} corresponded to an average fluid velocity of 150 μm. s^{-1}. Scale bar is 100 μm

Whether a cell in the fluid is captured by dielectrophoresis depends on the balance of the forces on the cell, which includes hydrodynamic forces, electrical forces, and gravitational forces (Ramos *et al.*, 1998). The electric field strengths are highest at the tips of the castellations, and the aggregates can be seen to first form there in the first few minutes. In time the aggregates grow, filling the space between the castellations. When 20 μL min^{-1} is used the full space between the castellations is not used because the supply of cells to the aggregates is too slow. Fully formed aggregates were obtained at 40 and 60 μL min^{-1}. Aggregate height appears to reduce again at flow rates of 80 μL min^{-1} and higher as the drag forces induced by the flow through the chamber remove cells from the top layers of the aggregates. Some aggregation can be seen at regions of high electric field gradient that form at the electrode edges between the aggregates. Some limited non-evenness can be seen in the pattern formation across the chamber; this is mainly caused by the pattern of the flow through the chamber, as cells are more likely to be captured by the first set of electrodes they encounter. This problem reduces in time and is less at higher flow rates and higher cell concentrations (data not shown). All further experiments were performed at a rate of 40 μL min^{-1}.

It is possible that at a slower flow rate (e.g. 20 μL.min^{-1}), some of the cells adhere (passively) to the wall regions in the chamber or of the inlet tubings more readily than at a faster flow rates and did not flow through the trapping microelectrode array regions, resulting in less aggregate being formed within a specified time frame. For example After 15 minutes at 40μL min^{-1}, many more cells are collected than after 30 minutes at 20 μL min^{-1} (Figure 5.4-1).

5.4.2 Formation of 3D cell aggregate in a pattern using dielectrophoresis

Figure 5.4-2 and Figure 5.4-3 show the formation of 3D skin cell aggregates in various patterns, at specific time intervals and at a constant microelectrode characteristic size (100 μm), using approximately the same cell concentration and constant optimum flow rate as determined previously (40 μl. min^{-1}). Time 0 was determined to be the time at which the first few cells started to accumulate at the electrode edges. The images indicate that cell aggregates were not fully developed in the first 7 minutes of DEP. The

cell aggregates continued to develop and partially fill the regions where electric field is the strongest until around 14 minutes. Cells tended to have filled up the areas between the castellations region after around 21 minutes.

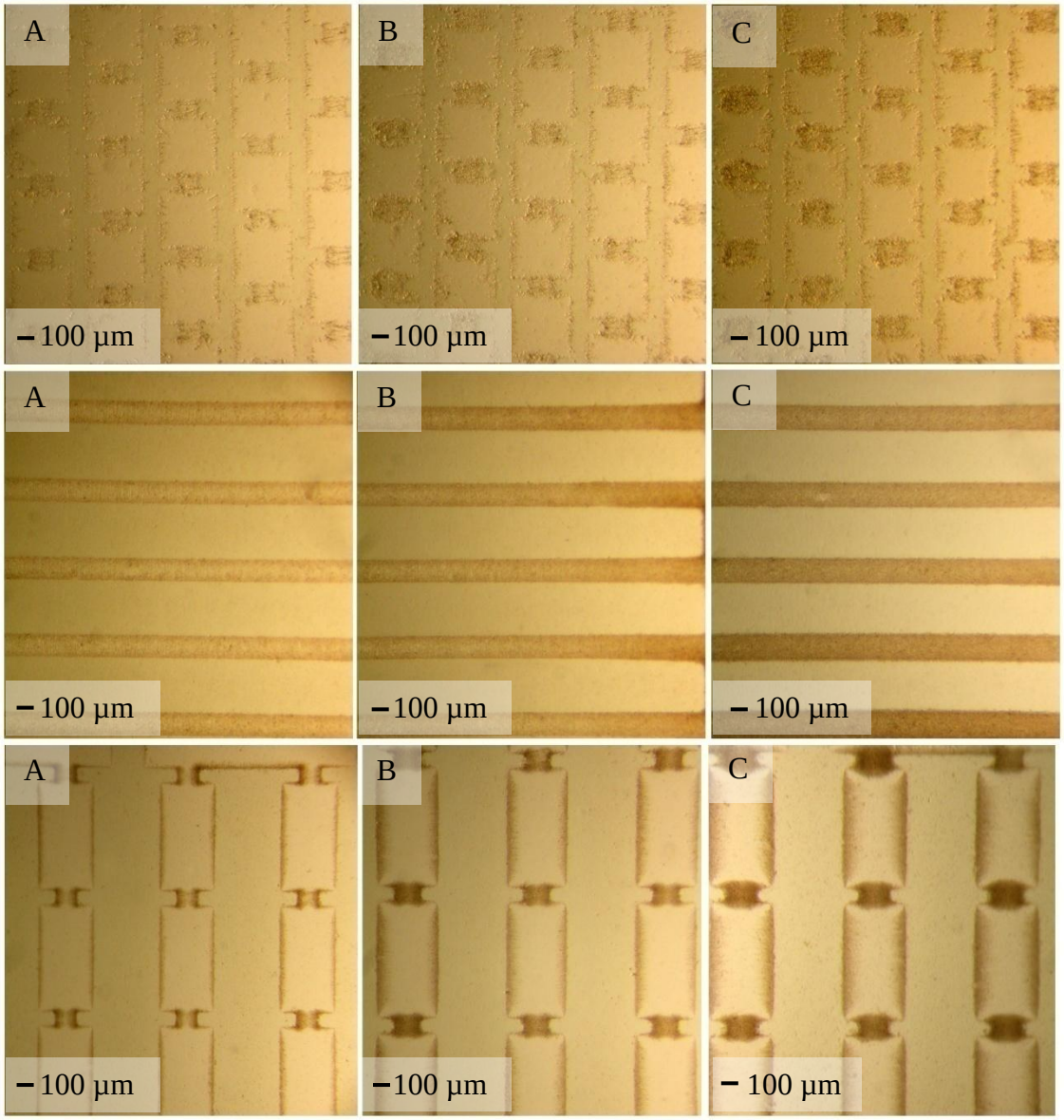

Figure 5.4-2. 3D cell aggregate development at a fixed liquid flow rate (40 µL min^{-1}) after: (A) 7, (B) 14, (C) 21 minutes of DEP. Average cell concentration used was 3.75 x 10^6 cells mL^{-1}. Microelectrode designs used were hexagonal pattern (upper row), line pattern (middle row) and square pattern where the distance between aggregates is 7x the aggregate characteristic size (lower row). Each pattern has an electrode characteristic size of 100 µm.

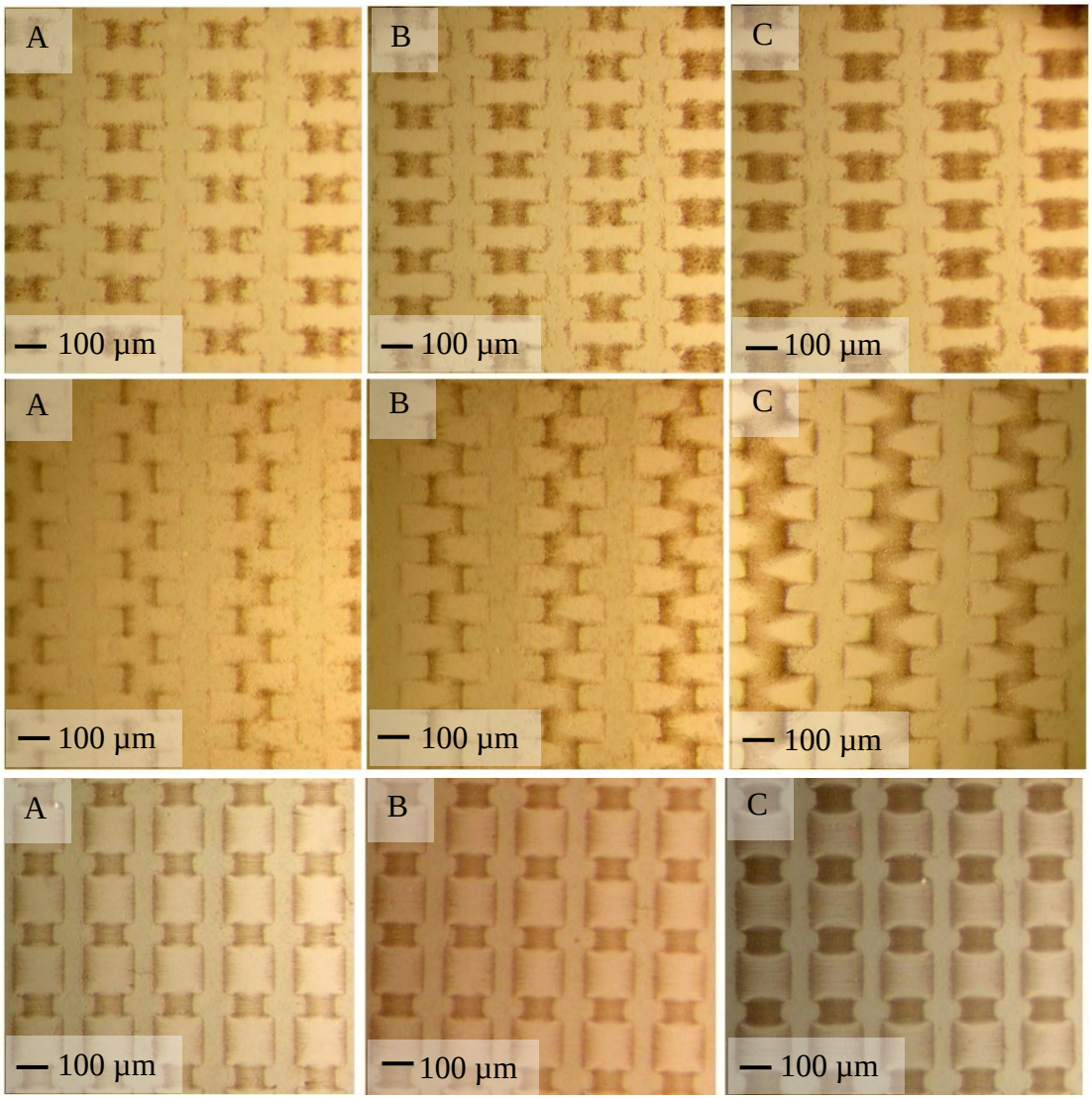

Figure 5.4-3. 3D cell aggregate development at a fixed liquid flow rate (40 µL. min^{-1}) after: (A) 7, (B) 14, (C) 21 minutes of DEP. Average cell concentration used was 3.75 x 10^6 cells mL^{-1}. Microelectrode designs used were rectangular square pattern (upper row), 'W' pattern (middle row) and square pattern where distance between aggregates 3x the electrode characteristic size (lower row). Each pattern has an electrode characteristic size of 100 µm.

5.4.3 Effect of electrode design

Aggregates of chicken embryonic skin cells formed by dielectrophoresis at electrode arrays of different designs are shown in Figure 5.4-4 until Figure 5.4-15. Also included in the figures are electric field calculations and 3D representations of the cell aggregates. Cell aggregation by DEP has been used previously in attempts to create artificial tissue-like aggregates such as artificial (hematopoietic) stem cell niches (Markx *et al.*, 2009). However, in these experiments the interest was in the (architecture of) the aggregates themselves, and not the way in which the individual aggregates were

distributed relative to each other.

Figure 5.4-4 and Figure 5.4-5 show the now standard interdigitated alternating and oppositely castellated electrodes arrays which have been used extensively in dielectrophoresis-based research (Albrecht *et al.*, 2006; Sebastian *et al.*, 2006; Abidin *et al.*, 2007; Albrecht *et al.*, 2007; Markx *et al.*, 2009). The interdigitated alternately castellated electrode arrays produce high field regions over a larger area of the microelectrode array. The "W" pattern (Figure 5.4-4) does not occur in nature. The oppositely castellated arrays produce aggregates in a rectangular pattern (Figure 5.4-5). However, rectangular patterns are also uncommon in nature, and the pattern is therefore biologically irrelevant.

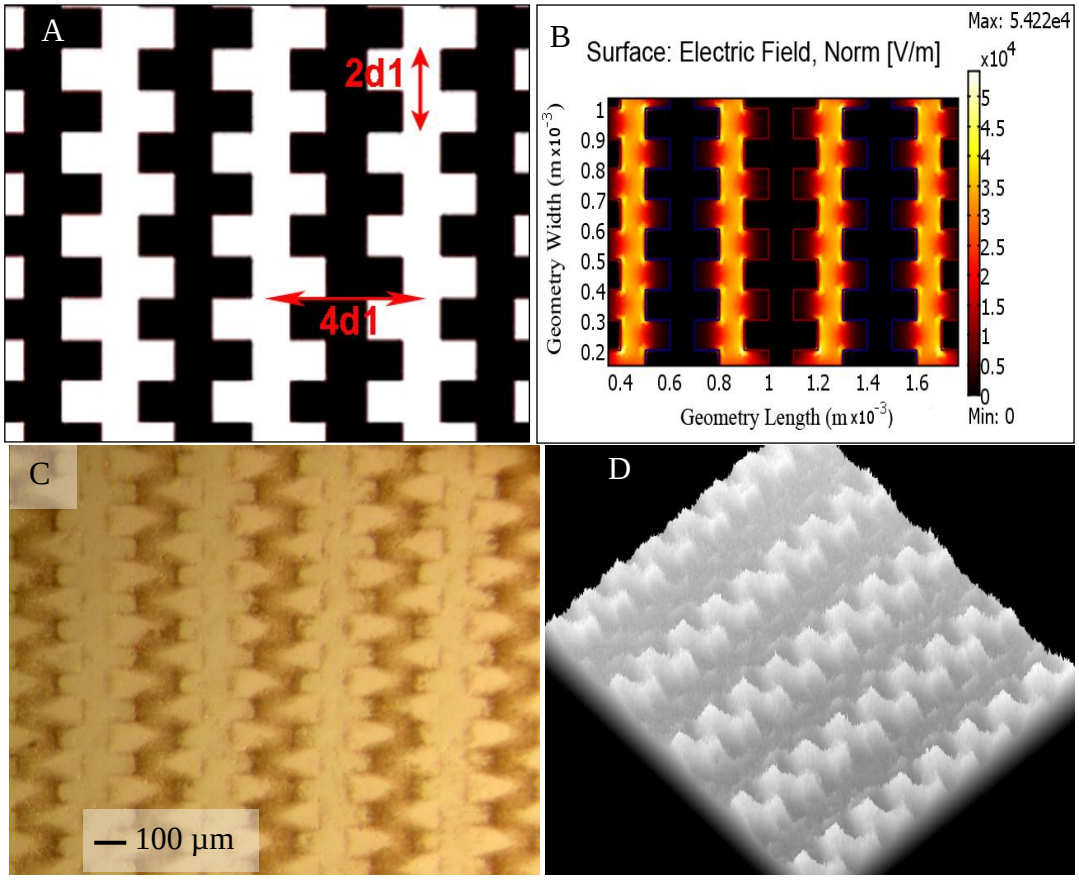

Figure 5.4-4. Aggregation of skin cells at standard interdigitated alternately castellated electrodes, forming "W" or zigzag pattern. A: Microelectrode design. B: Electric field simulation. C: Bright field image of the aggregates of skin cells formed using positive DEP. D: 3D representation of pixel intensity in the original image, mimicking the surface topography of the aggregates (d1=100 µm).

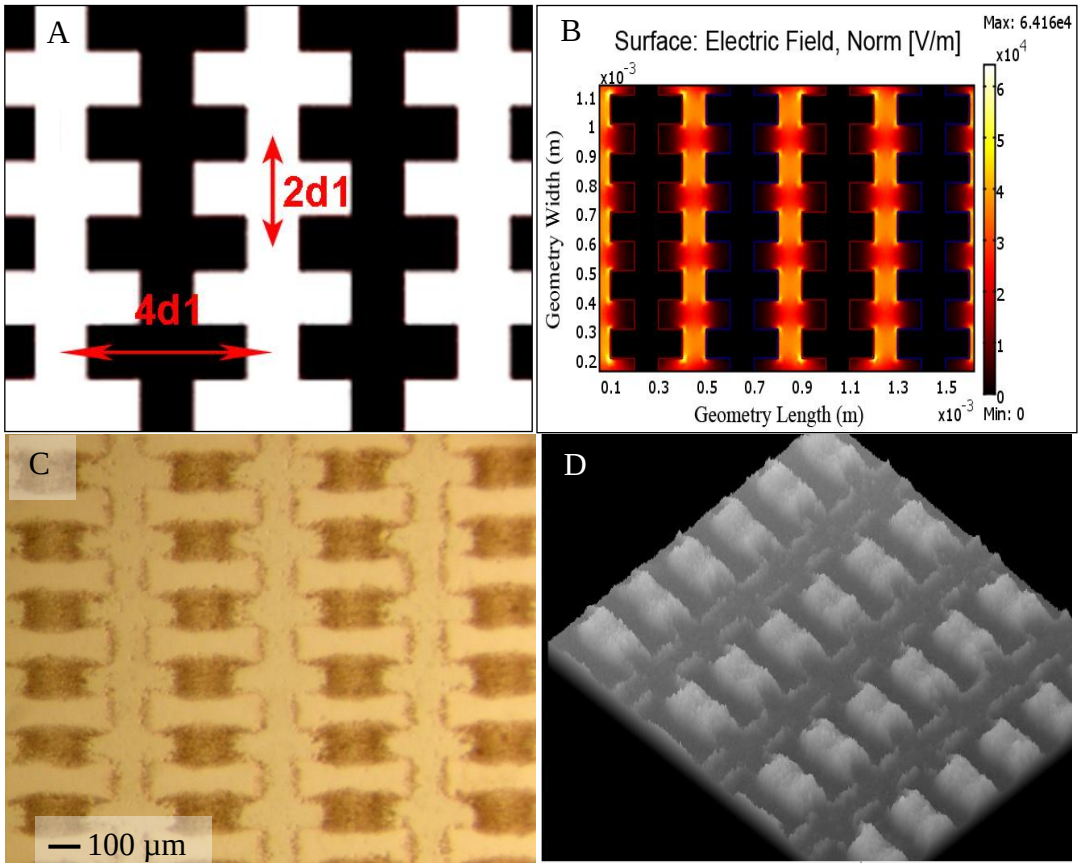

Figure 5.4-5. Aggregation of skin cells at standard interdigitated alternately castellated electrodes, forming rectangular pattern (4 x 2). A: Microelectrode design. B: Electric field simulation. C: Bright field image of the aggregates of skin cells formed using positive DEP. D: 3D representation of pixel intensity in the original image, mimicking the surface topography of the aggregates (d1=100 µm).

Comparison of the aggregates formed with the calculated electric field distribution shows that the location of the aggregates is very well described by the calculated electric field distribution. It can also be observed that not all cells are present in the high field regions between the castellations, but that cells also accumulate at other regions which have locally raised electric fields, for example at the electrode edges between the castellations of an individual electrode. Such an accumulation of cells outside the desired high field regions between the castellations has been observed previously (Gascoyne *et al.*, 1992; Wang *et al.*, 1993), and could be reduced if necessary by applying an insulating layer over the electrode arrays, only leaving the area between the castellations exposed.

Figure 5.4-6 and Figure 5.4-7, on the other hand, show examples of cell aggregates in line and hexagonal patterns. Unlike the previous patterns, such patterns have strong biological relevance, as line and hexagonal patterns are observed during the

development of placodes in chicken skin (Murray, 1989; Jiang *et al.*, 1999; Jiang *et al.*, 2004). The line pattern of cell aggregates is commonly found at a very early developmental stage of embryonic skin tissue in chicken prior to the formation of hexagonal pattern from a line pattern above the neural tube.

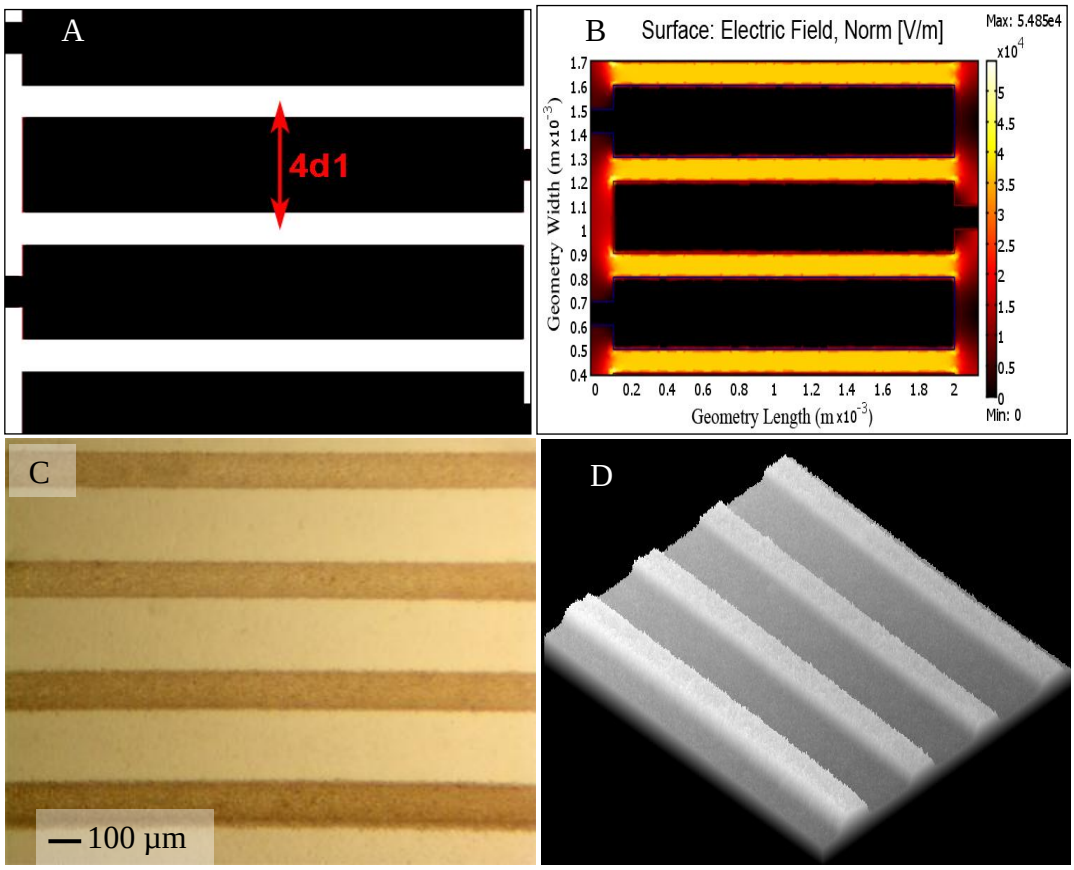

Figure 5.4-6. Aggregation of skin cells at standard interdigitated alternately castellated electrodes, forming line pattern. A: Microelectrode design. B: Electric field simulation. C: Bright field image of the aggregates of skin cells formed using positive DEP. D: 3D representation of pixel intensity in the original image, mimicking the surface topography of the aggregates (d1=100 µm).

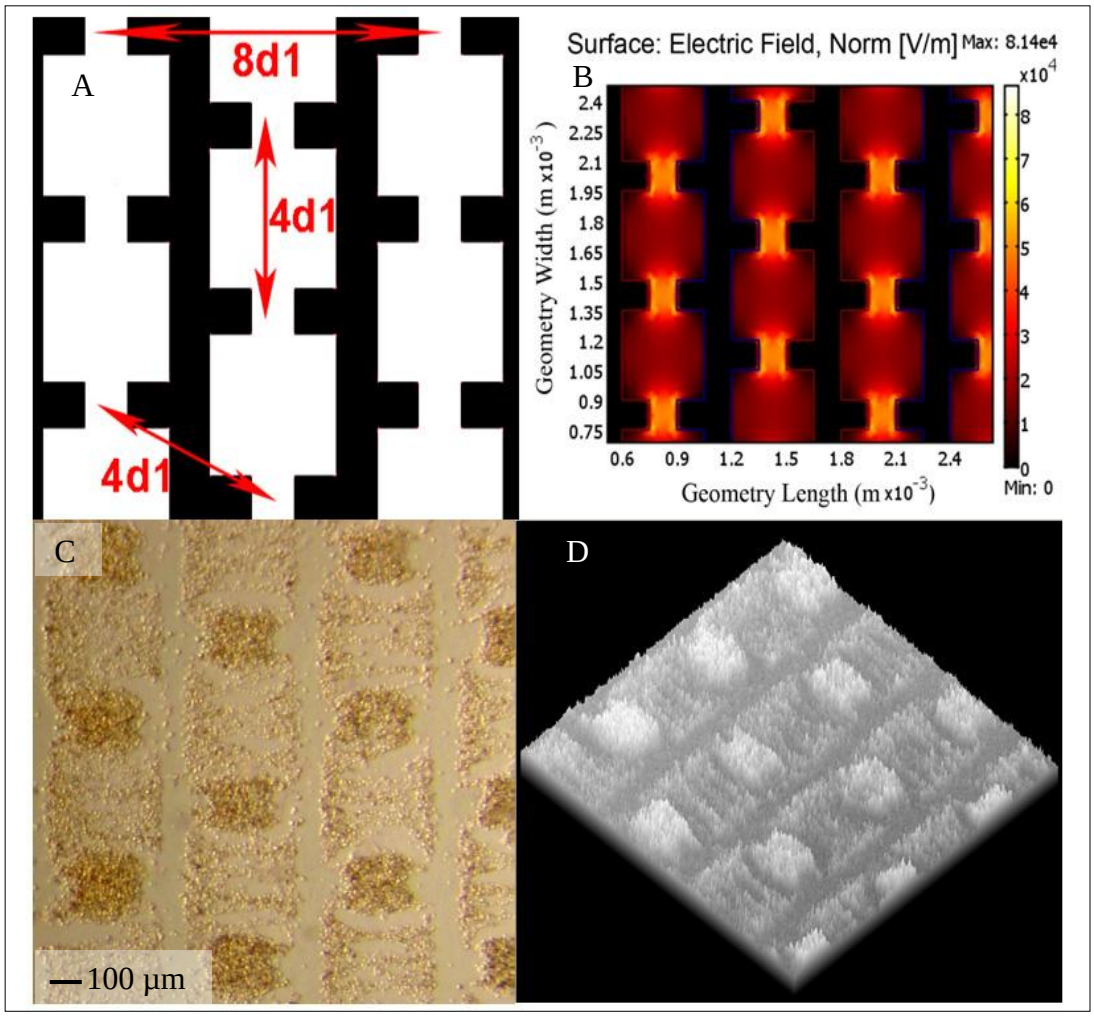

Figure 5.4-7. Aggregation of skin cells at interdigitated electrodes with a characteristic size (d1) of 100 µm forming a hexagonal pattern. A: Microelectrode design. B: Electric field simulation. C: Image of 3D aggregate pattern of skin cells formed using positive DEP. D: 3D representation of pixel intensity in the original image, mimicking the relative surface topography of the aggregate pattern.

5.4.4 Effect of 50% increase in dimensional size

Figure 5.4-8 and Figure 5.4-9 show electrode designs with a 50% increase in the electrode characteristic size. Increasing the distance between electrode edges reduces the electric field strength, which subsequently decreases the capture potential of the cell aggregates and results in a more saddle-shaped form of aggregates. This is in line with previous work conducted by Sebastian *et al.* (Sebastian *et al.*, 2007b). The effect is more clearly seen from the 3D representation of the DEP image. The electrode design or the pattern itself has no direct effect on the final shape of the cell aggregates.

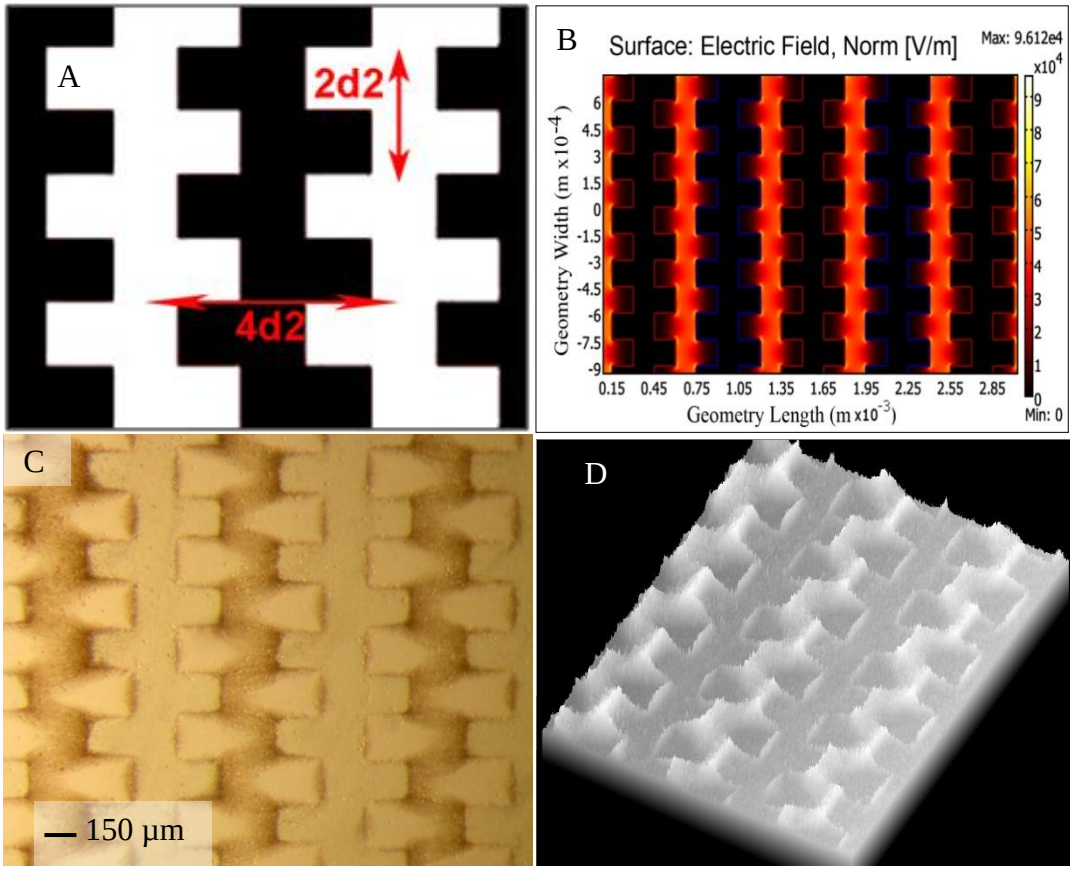

Figure 5.4-8. Chicken embryonic skin cells in 'W' patterns. A. Microelectrode designs of 'W' pattern with characteristic size 150 µm (d2). B. Electric field simulation. C. Bright-field image of the skin cell aggregates formed by positive dielectrophoresis. D. 3D visualisation of the cell aggregates based on pixel intensity.

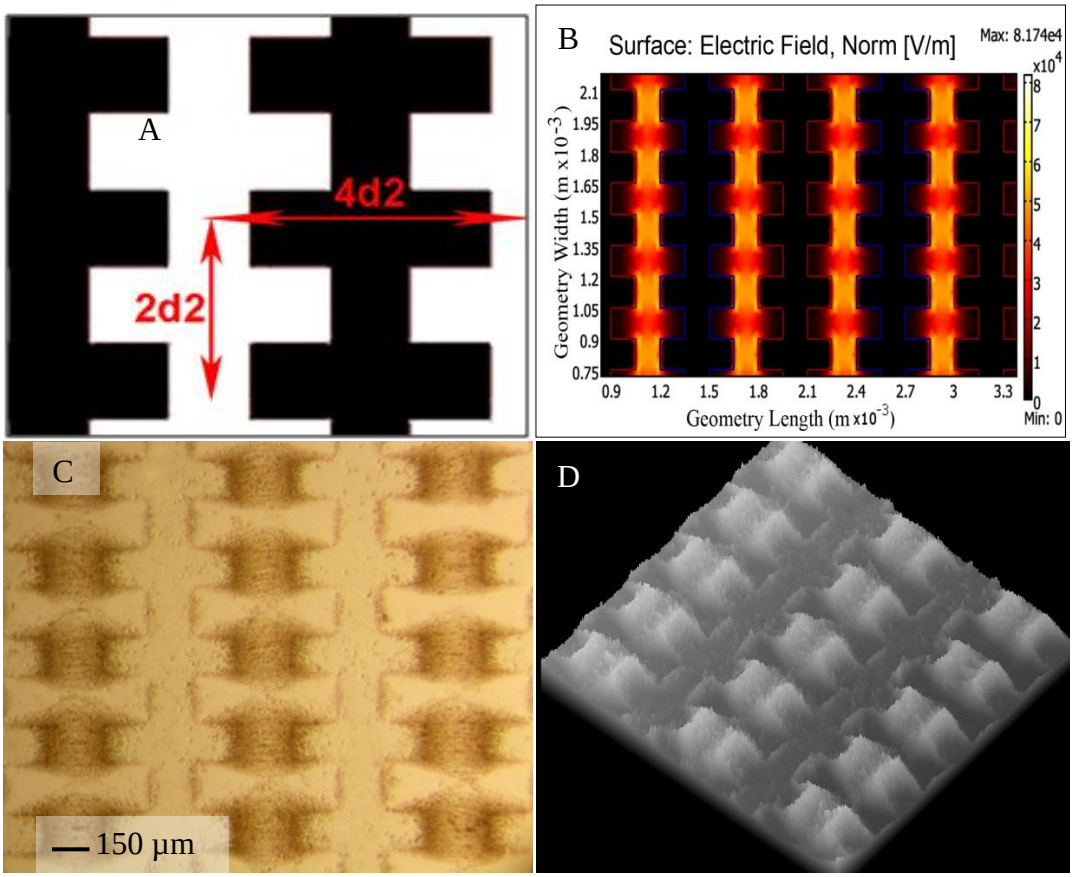

Figure 5.4-9. Chicken embryonic skin cells in square (4x2) patterns. A. Microelectrode designs of square (4x2) pattern with characteristic size 150 µm (d2). B. Electric field simulation. C. Bright-field image of the skin cell aggregates formed by positive dielectrophoresis. D. 3D visualisation of the cell aggregates based on pixel intensity.

5.4.5 Variation of the inter-aggregate distance

The distance between aggregates is an important biological parameter as it determines the distance between any appendages (e.g. hairs, feathers) that may grow out of the placodes. Experiments in which it was attempted to vary the inter-aggregate distance whilst keeping the aggregate size constant were performed with an interdigitated castellated design which produced aggregates in a regular square pattern. Although less biologically relevant than the hexagonal pattern, this design makes it easier to perform analyses on individual aggregates. Figure 5.4-10 to Figure 5.4-12 show that it is indeed possible to make aggregates of approximately the same size with different inter-aggregate distances. In this experiment, the distance between the aggregates was modified to 3x, 5x and 7x the electrode characteristic size. Transfer of the same principles to hexagonal patterns should be straightforward.

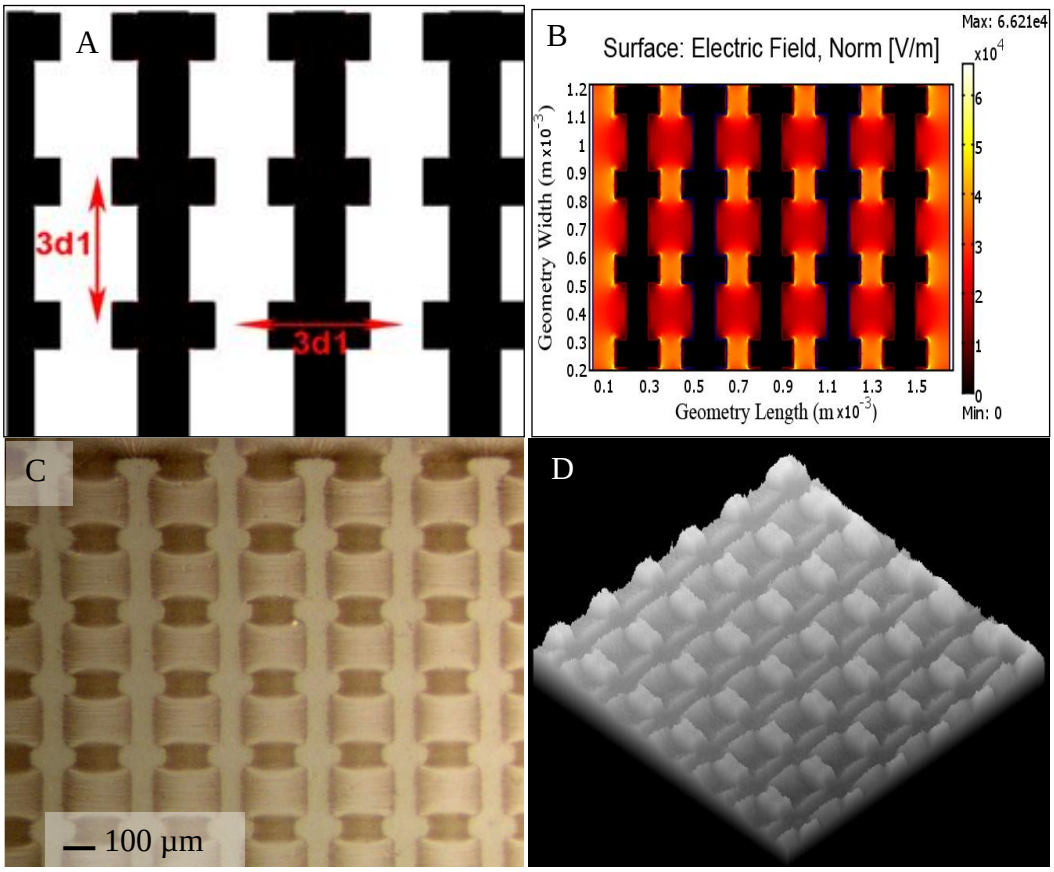

Figure 5.4-10. Aggregation of skin cells at interdigitated oppositely castellated electrodes with a characteristic size d1=100 µm, forming a square pattern of aggregates at a distance of 3x the characteristic size d1. A: Microelectrode design. B: Electric field simulation of a microelectrode with a characteristic size of 100 µm. C: Image of 3D aggregate pattern of skin cells by positive DEP. D: 3D representation of pixel intensity in the original image, mimicking the surface topography of the aggregate.

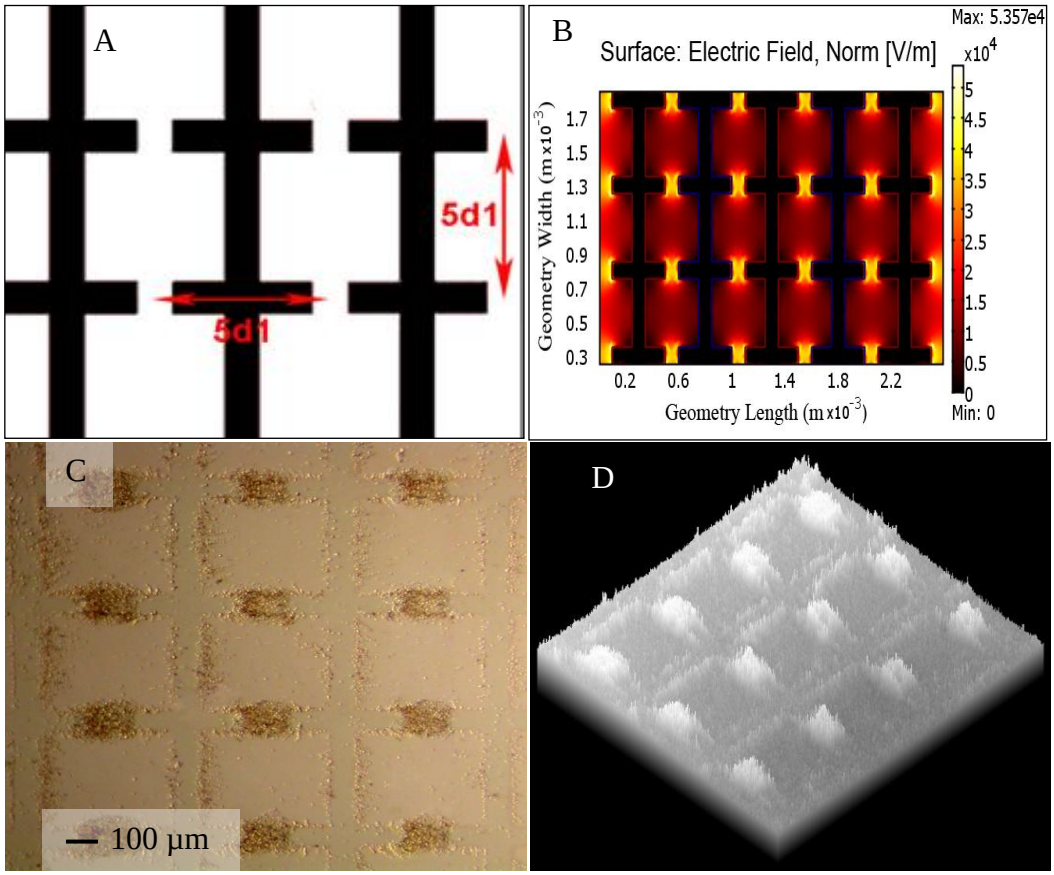

Figure 5.4-11. Aggregation of skin cells at interdigitated oppositely castellated electrodes with a characteristic size d1=100 µm, forming a square pattern of aggregates at a distance of 5x the characteristic size d1. A: Microelectrode design. B: Electric field simulation of a microelectrode with a characteristic size of 100 µm. C: Image of 3D aggregate pattern of skin cells by positive DEP. D: 3D representation of pixel intensity in the original image, mimicking the surface topography of the aggregate.

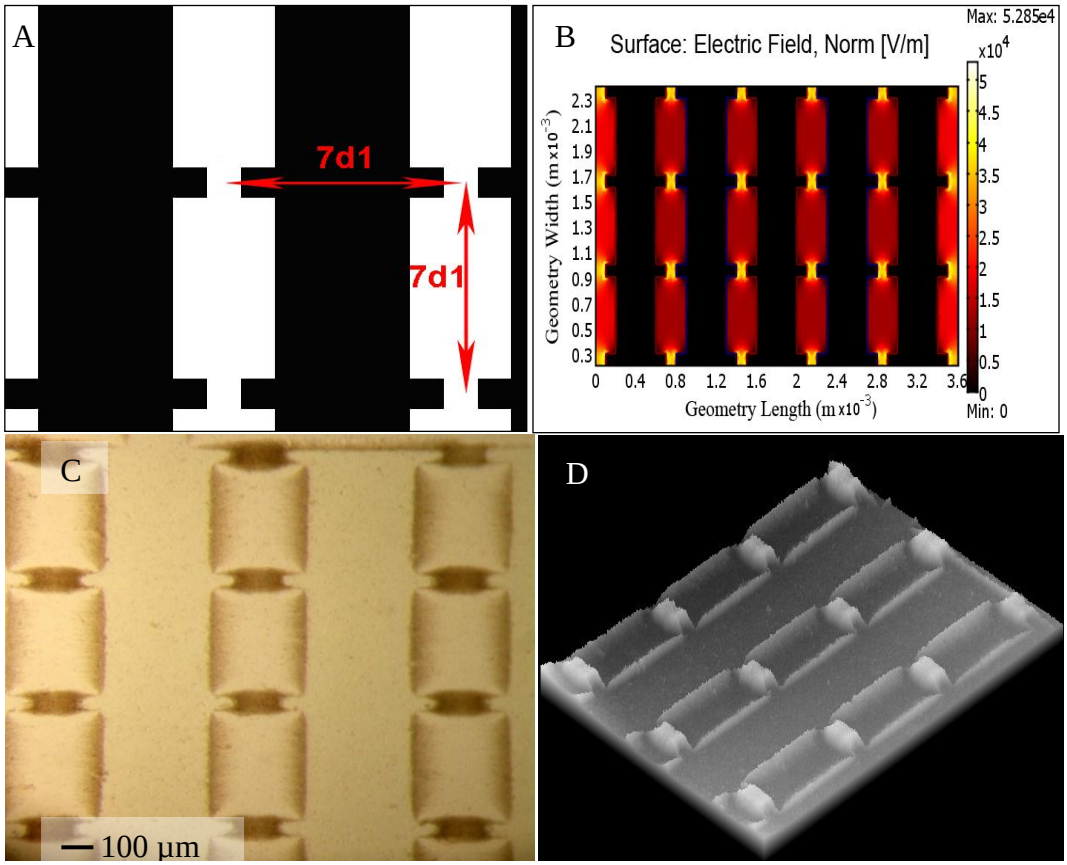

Figure 5.4-12. Aggregation of skin cells at interdigitated oppositely castellated electrodes with a characteristic size d1=100 µm, forming a square pattern of aggregates at a distance of 7× the characteristic size d1. A: Microelectrode design. B: Electric field simulation of a microelectrode with a characteristic size of 100 µm. C: Image of 3D aggregate pattern of skin cells by positive DEP. D: 3D representation of pixel intensity in the original image, mimicking the surface topography of the aggregate.

5.4.6 Variation of the inter-aggregate distance with 50% increase in aggregate size

Figure 5.4-13 and Figure 5.4-15 show the effects of changing the inter-aggregate distance with 50% increase in electrode characteristic size. As mentioned previously, increasing the distance between electrode edges reduces the electric field strength, which subsequently decreases the capture potential to the cell aggregates and results in a more saddle-shaped form of aggregates, assuming all other variables such as liquid flow rates and cell concentration in the liquid medium remain the same. This is in line with the previous work carried out by Sebastian *et al.* (Sebastian *et al.*, 2007b). The effect is more clearly seen in the 3D representation of the DEP image. The inter-aggregate distance itself has no direct effect on the final shape of the cell aggregates.

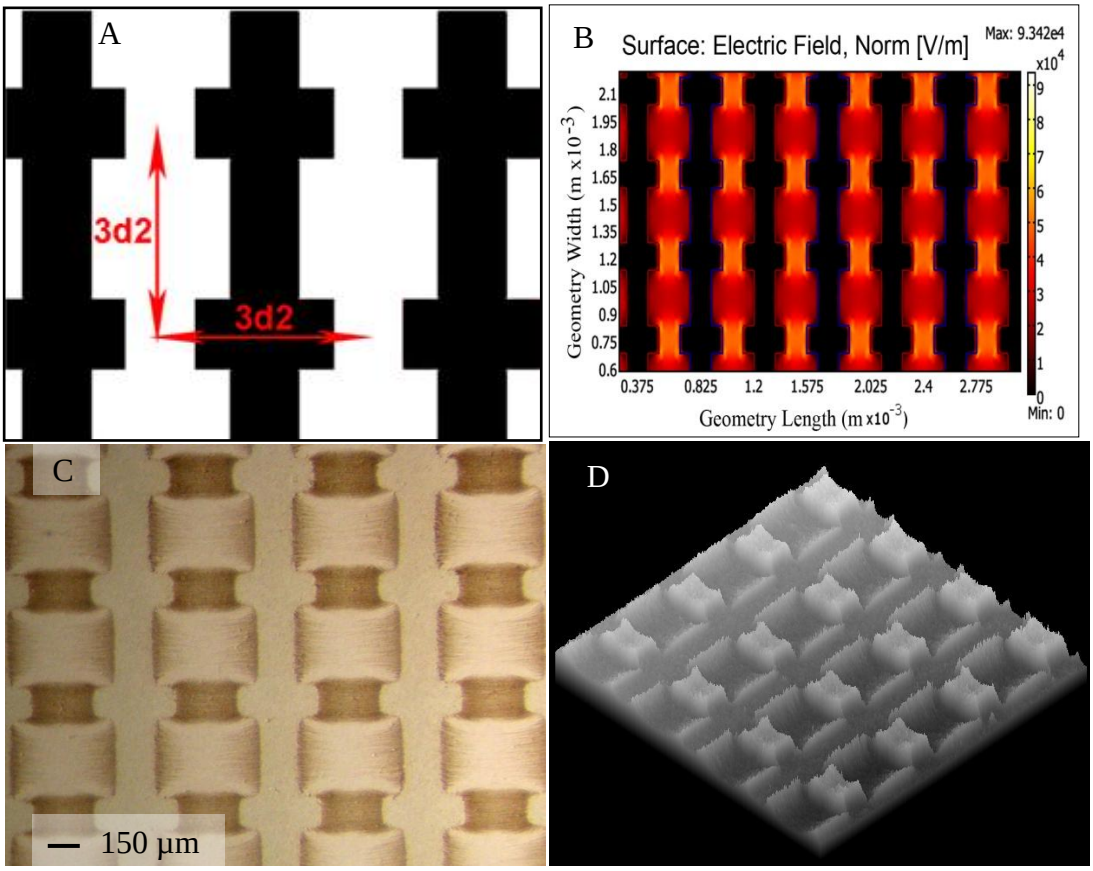

Figure 5.4-13. Aggregation of skin cells at interdigitated oppositely castellated electrodes with a characteristic size d2=150 µm, forming a square pattern of aggregates at a distance of 3x the characteristic size d2. A. Microelectrode designs of square (3x3) pattern with characteristic size 150 µm (d2). B. Electric field simulation with 150 µm characteristic size. C. The resulting 3D aggregates of skin cells by positive dielectrophoresis. D. 3D visualisation of the cell aggregates based on pixel intensity.

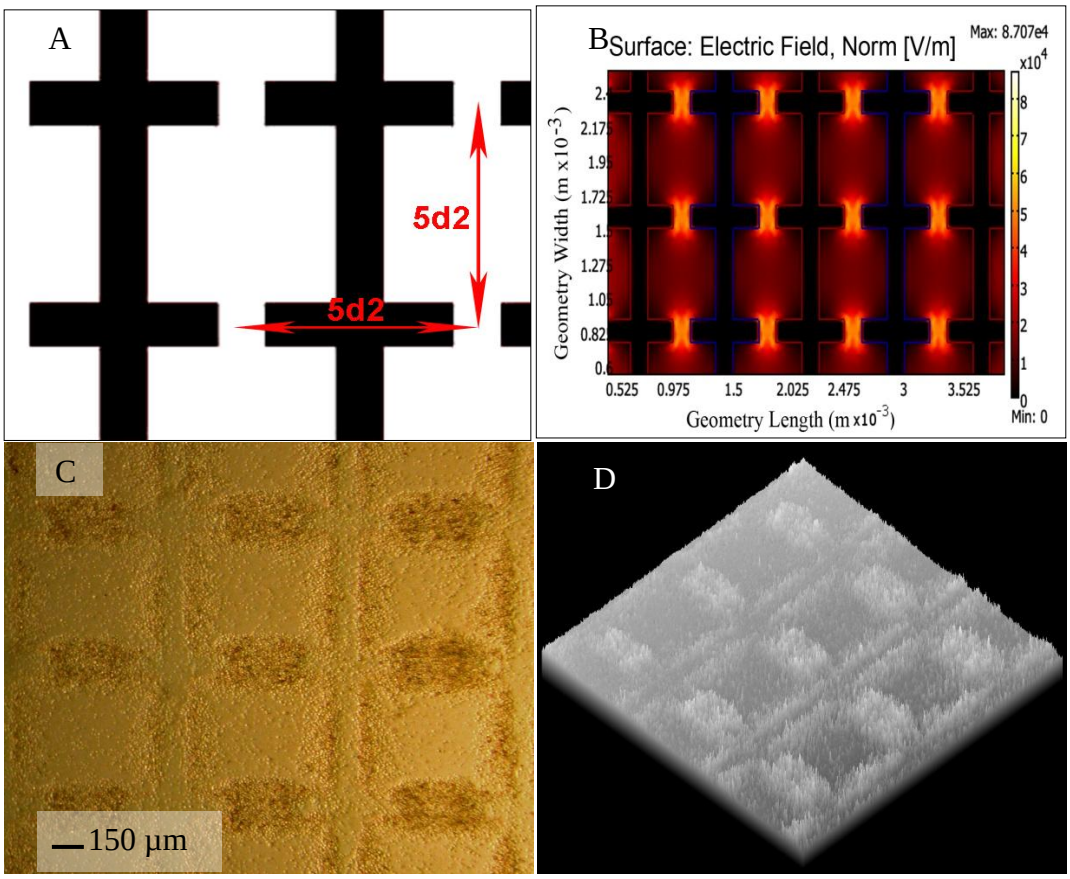

Figure 5.4-14. Aggregation of skin cells at interdigitated oppositely castellated electrodes with a characteristic size d2=150 µm, forming a square pattern of aggregates at a distance of 5x the characteristic size d2. A. Microelectrode designs of square (5x5) pattern with characteristic size 150 µm (d2). B. Electric field simulation with 150 µm characteristic size. C. The resulting 3D aggregates of skin cells by positive dielectrophoresis. D. 3D visualisation of the cell aggregates based on pixel intensity.

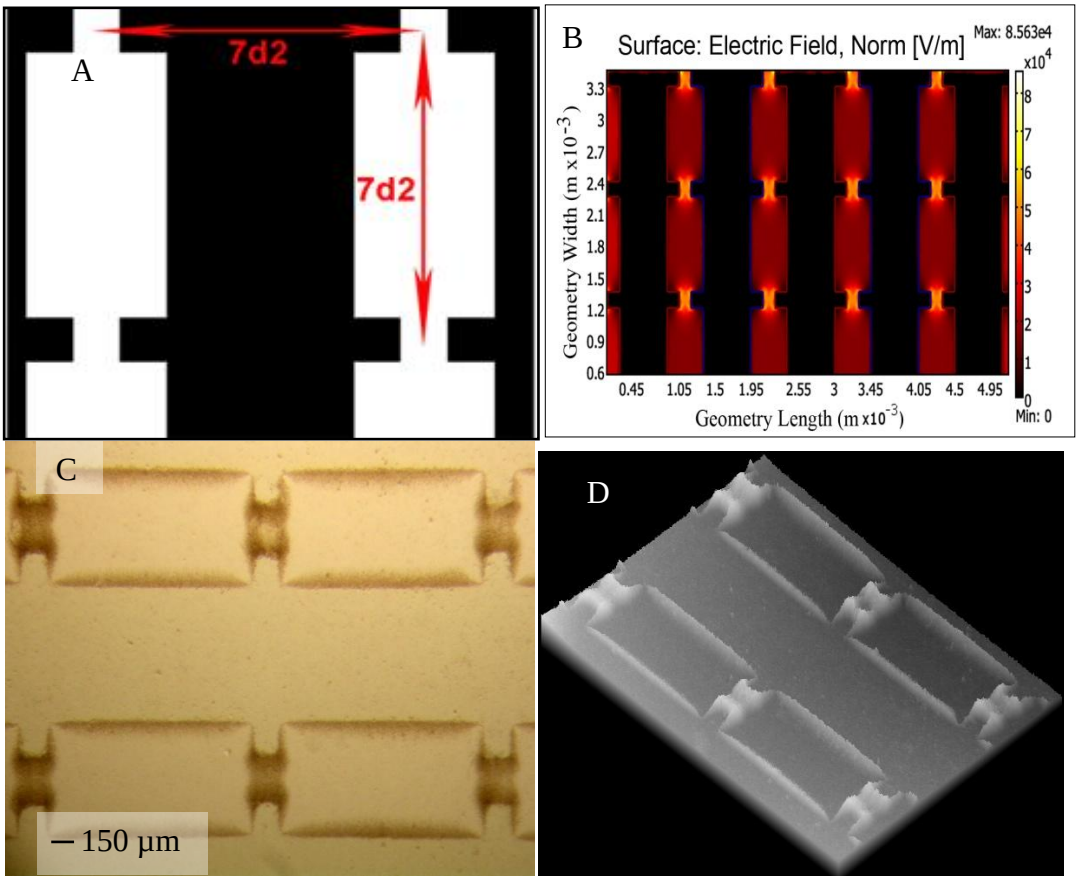

Figure 5.4-15. Aggregation of skin cells at interdigitated oppositely castellated electrodes with a characteristic size d2=150 µm, forming a square pattern of aggregates at a distance of 7x the characteristic size d2. A. Microelectrode designs with a square (7x7) pattern with a characteristic size of 150 µm (d2). B. Electric field simulation with 150 µm characteristic size. C. The resulting 3D aggregates of skin cells formed by positive dielectrophoresis. D. 3D visualisation of the cell aggregates based on pixel intensity.

5.4.7 The effects of electrode bar width and castellation dimension

The electrodes can be described as interdigitated parallel electrodes with castellations. Figure 5.4-16 to Figure 5.4-19 show the effect of changing the size of the "fingers" (this can also be seen as changing the size of the connections between castellations; widening the connection has the effect of shortening the length of the castellations), for different electrode sizes. The images show that when the connecting bars are less (and the length of the castellations longer) the accumulations of cell at the electrode edges is more pronounced, whilst a more even cell distribution is obtained when the connecting bar is wider. Figure 5.4-16 to Figure 5.4-19 show cell accumulation at interdigitated electrodes with rectangular castellations in a square pattern, investigating the effect of changing the electrode connection bar-width and castellation dimension (or the distance between the tips of the castellations) has on aggregate formation. This is further

simulated by the shape and intensity of 2D high field regions between each castellations.

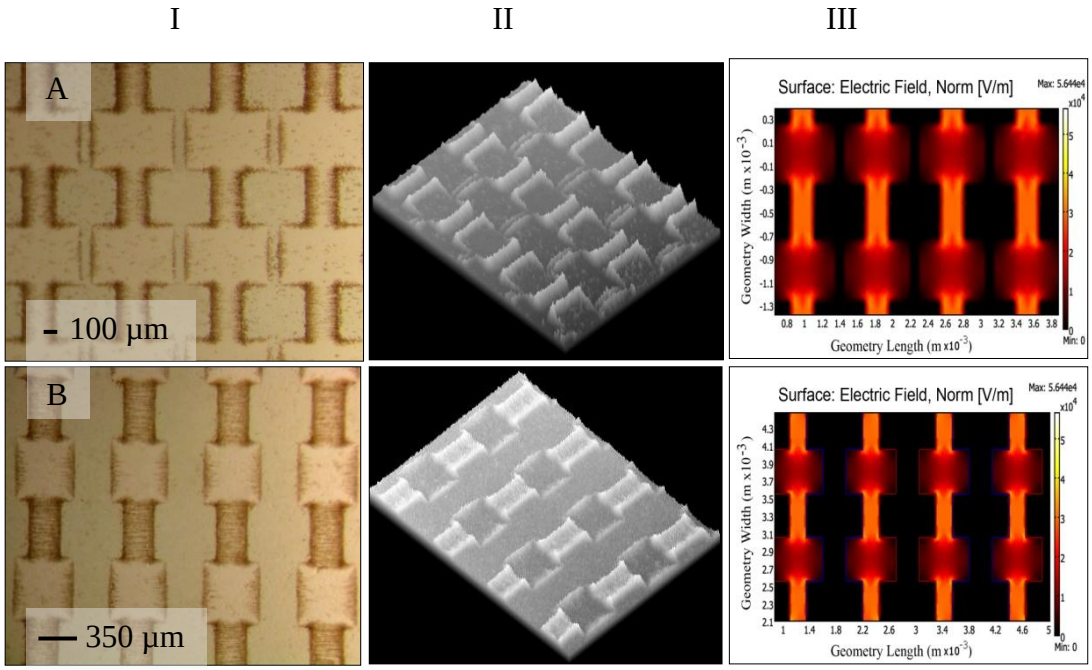

Figure 5.4-16. The effects of electrode bar width and castellation dimension on the shape and distribution of cell density in the aggregates. Bar width shown are: A. 100 µm and B. 350 µm. Column: I. Aggregation of skin cells at interdigitated oppositely castellated electrodes with castellation dimension of 500 x 250 µm. II. 3D visualisation of the cell aggregates, based on pixel intensity. III. Electric field simulation.

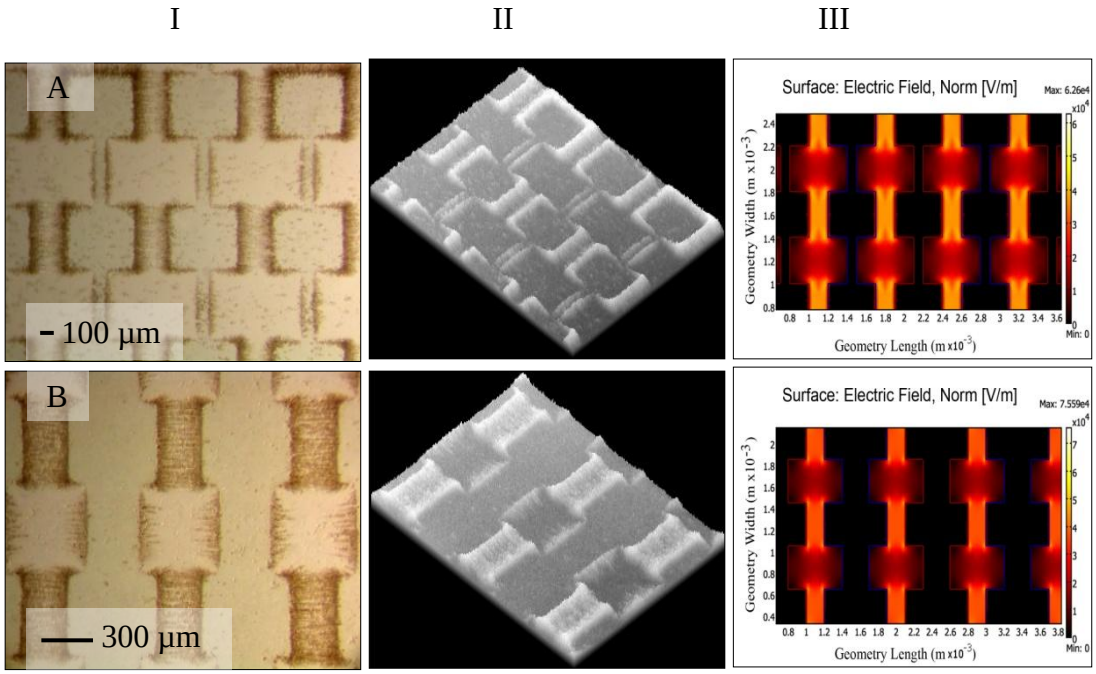

Figure 5.4-17. The effects of electrode bar width and castellation dimension on the shape and distribution of cell density in the aggregates. Bar width shown are: A. 100 µm and B. 300 µm. Column: I. Aggregation of skin cells at interdigitated oppositely castellated electrodes with castellation dimension of 400 x 200 µm. II. 3D visualisation of the cell aggregates, based on pixel intensity. III. Electric field simulation.

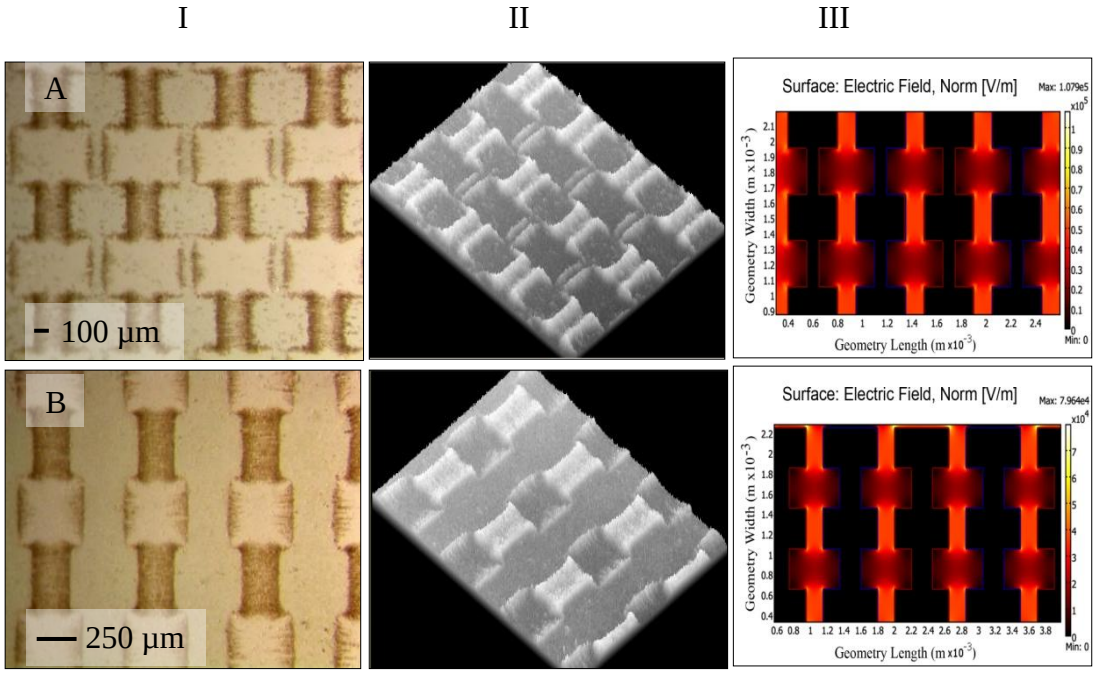

Figure 5.4-18. The effects of electrode bar width and castellation dimension on the shape and distribution of cell density in the aggregates. Bar width shown are: A. 100 µm and B. 250 µm. Column: I. Aggregation of skin cells at interdigitated oppositely castellated electrodes with castellation dimension of 300 x 150 µm. II. 3D visualisation of the cell aggregates, based on pixel intensity. III. Electric field simulation.

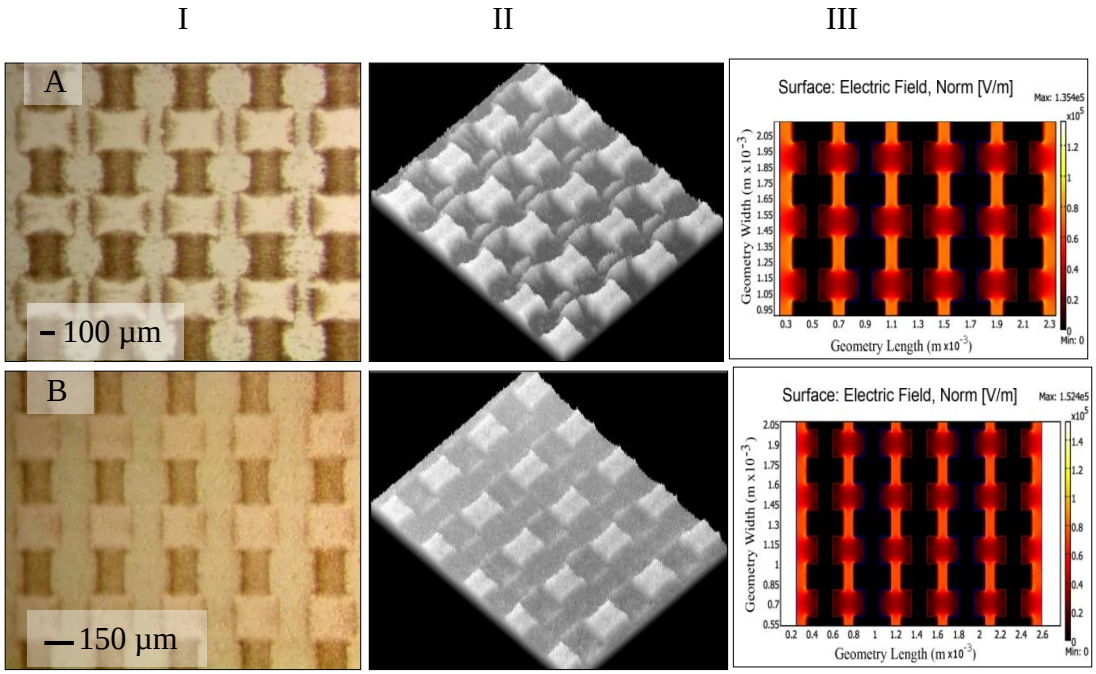

Figure 5.4-19. The effects of electrode bar width and castellation dimension on the shape and distribution of cell density in the aggregates. Bar width shown are: A. 100 µm and B. 150 µm. Column: I. Aggregation of skin cells at interdigitated oppositely castellated electrodes with castellation dimension of 200 x 100 µm. II. 3D visualisation of the cell aggregates, based on pixel intensity. III. Electric field simulation.

5.4.8 The effects of reducing the distance between the tips of the castellations

Figure 5.4-20 shows the effect of reducing the distance between the tips of the castellations, whilst keeping everything else constant (including the width of the castellations). Reducing the distance between the tips of the castellations does not only change the shape of the aggregates from long to narrow. When the distance is large the aggregates tend to be less wide in the middle; when the distance is short, the high electric field region extends further from the middle, widening the aggregate (as shown in column II of 3D image analysis of each sample). This is further simulated by the shape and intensity of 2D high field regions between each castellations. Figure 5.4-20 shows cell accumulation at interdigitated electrodes with rectangular castellations in a hexagonal pattern, investigating the effect of the distance between the tips of the castellations has on aggregate formation.

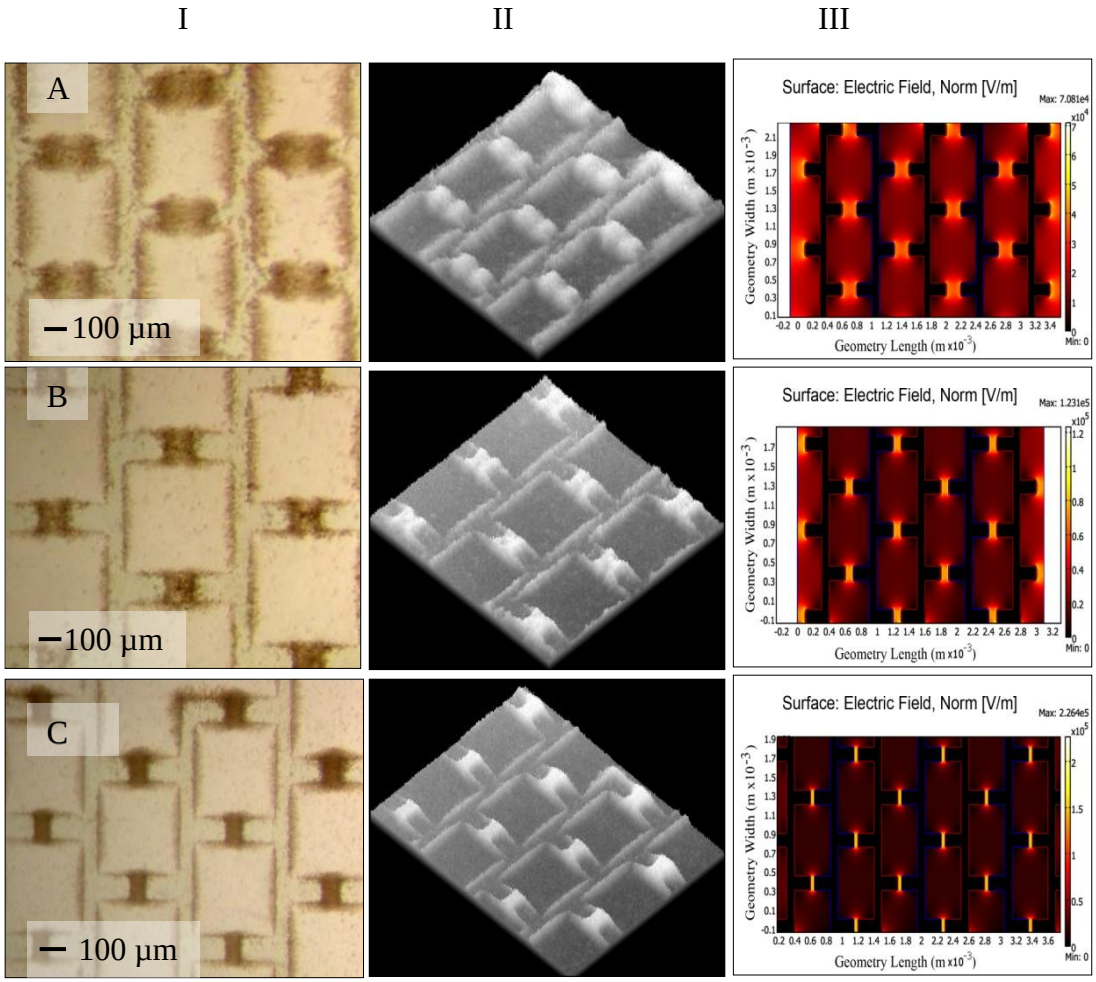

Figure 5.4-20. The effects of reducing the distance between the tips of the castellations (from 200 µm to 50 µm), on the shape and distribution of cell density in the aggregates. Column: I. Aggregation of skin cells at interdigitated oppositely castellated electrodes with castellation dimensions of (A) 150 x 200 µm, (B) 150 x 100 µm and (C) 150 x 50 µm. II. 3D visualisation of the cell aggregates, based on pixel intensity. III. Electric field simulation.

5.4.9 The effects of increasing the distance between the tips of the castellations

Figure 5.4-21 shows the effects of increasing the distance between the tips of the castellations, whilst proportionally increasing the width of the castellations as well as the bar width from 25 µm (part A) to a maximum of 100 µm (part B-D).

Increasing the distance between the tips of the castellations changes the size of the aggregates until the aggregate finally splits into two smaller-size aggregates, each attached to the electrode edges. The splitting also leaves behind a very thin layer of cells between the castellations. This effect started to occur when the distance between castellation is around 400 µm (at 20 V_{pk-pk}). The thin layer of cells can also clearly be

seen in the quasi-3D images of the samples (Column II). When the distance between the tips of castellation is large the aggregates tend to be less wide in the middle; when the distance is short the high electric field region extends further from the middle, widening the aggregate. Figure 5.4-21 shows cell accumulation at interdigitated electrodes with rectangular castellations in a hexagonal pattern, demonstrating the effect of increasing the distance between the tips of the castellations on aggregate formation.

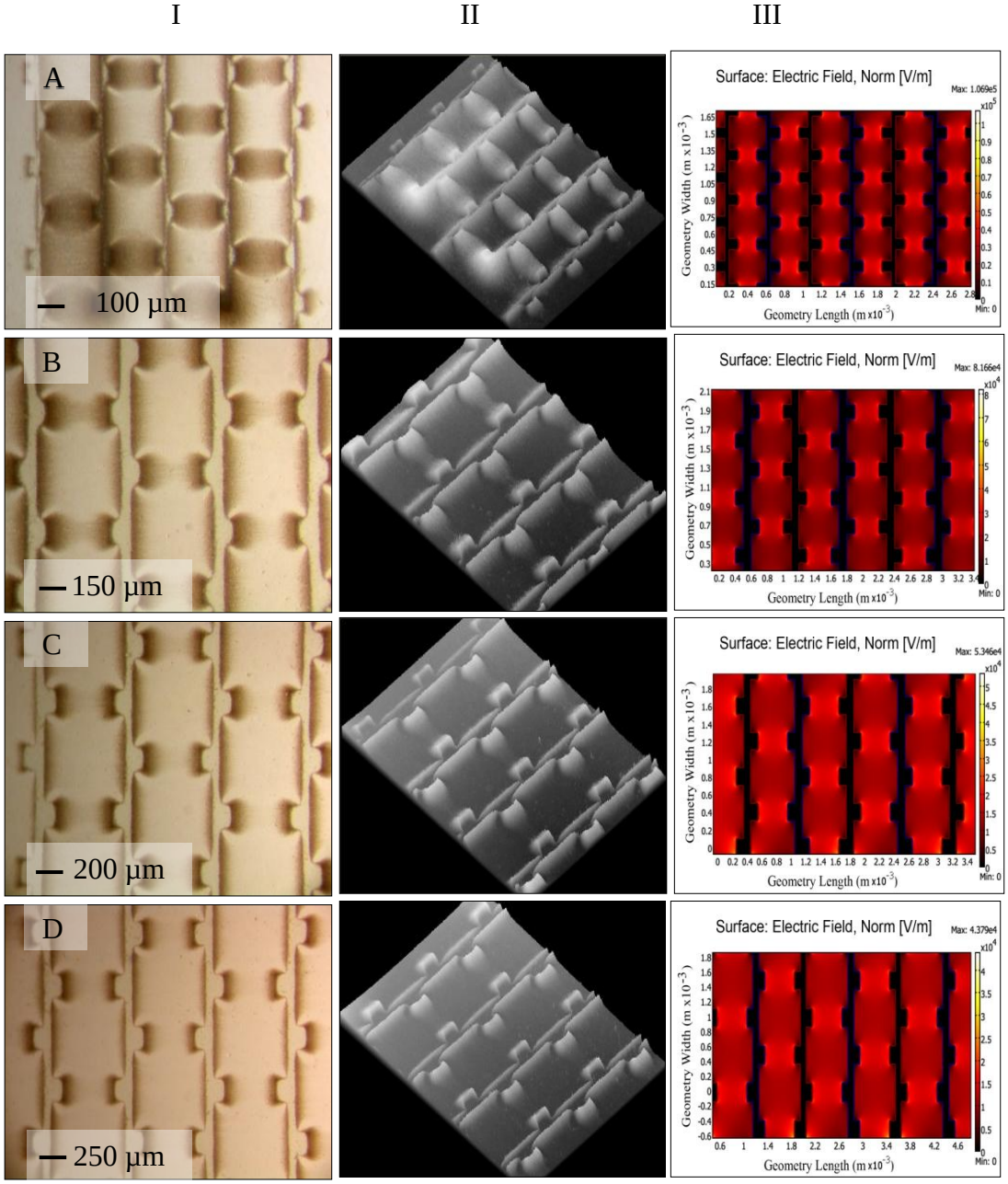

Figure 5.4-21. The effects of increasing the distance between the tips of the castellations (from 200 µm to 500 µm), on the shape and distribution of cell density in the aggregates. Column: I. Accumulation of skin cells at interdigitated oppositely castellated electrodes with castellation dimensions of (A) 100 x 200 µm, (B) 150 x 300 µm, (C) 200 x 400 µm and (D) 250 x 500 µm, in hexagonal pattern. II. 3D visualisation of the cell aggregates, based on pixel intensity. III. Electric field simulation.

5.4.10 The effects of reducing the width of the castellations

Figure 5.4-22 shows the effects of reducing the width of the castellations, whilst keeping everything else (including the distance between the tips of the castellations) constant. Interestingly, reducing the width of the castellations to 50 x 100 µm has a pronounced effect on the length of the aggregates. The narrower the electrode, the more the cells tend to cover the castellations. Figure 5.4-22 shows cell accumulation at interdigitated electrodes with rectangular castellations in a hexagonal pattern, investigating the effect of reducing the width of the castellations on aggregate formation. The overall shape of aggregates does not change when a castellation dimension of 100 x 100 µm was changed to 300 x 100 µm (or more) along the width of castellation as shown in the 3D image analysis of the sample (Column II) and is further simulated by the 2D modeling of electric field regions between castellations.

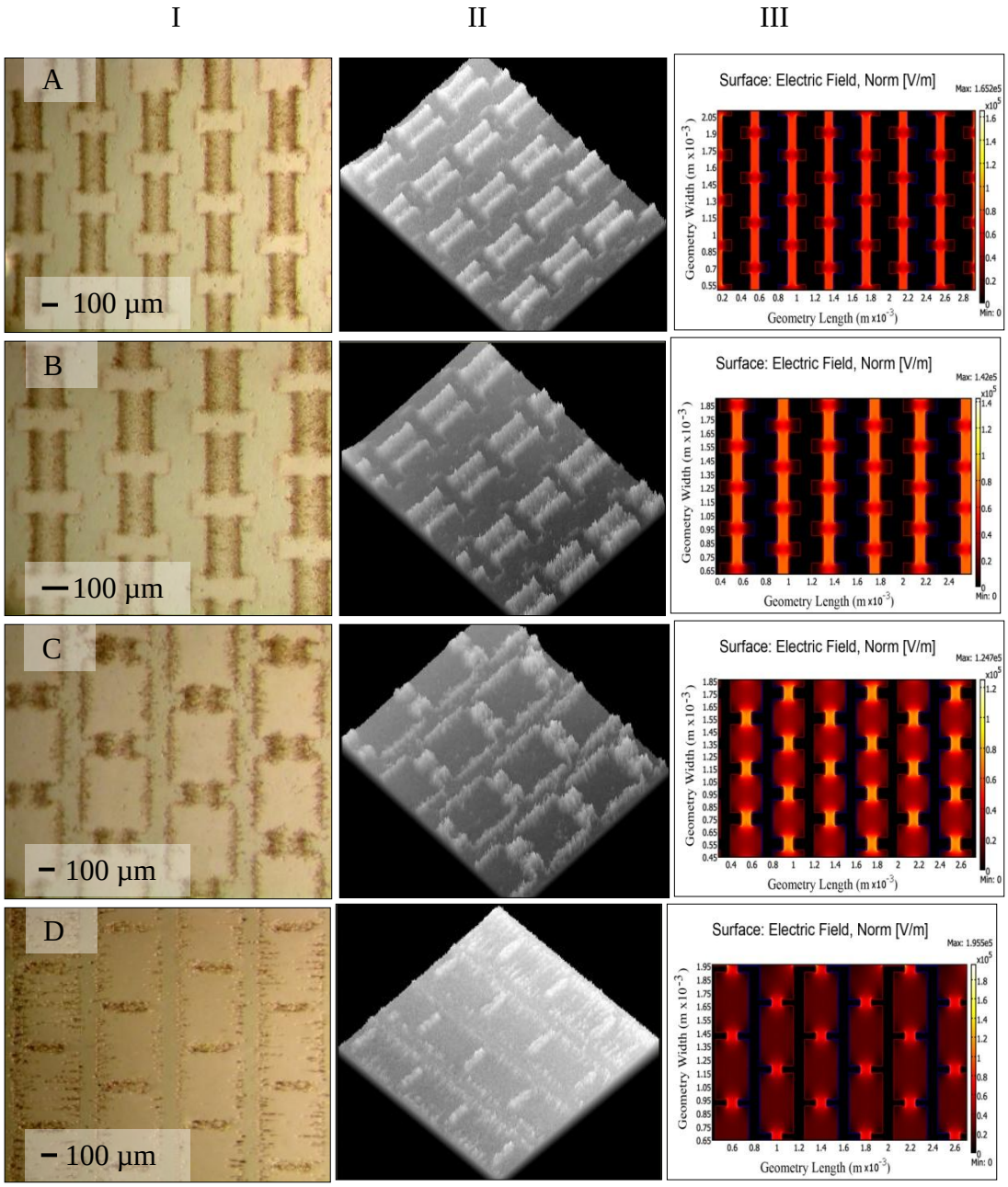

Figure 5.4-22. The effect of reducing the width of the castellations (from 300 µm to 50 µm), on the shape and distribution of cell density in the aggregates. Column: I. Aggregation of skin cells at interdigitated oppositely castellated electrodes with castellation dimensions of (A) 300 x 100 µm, (B) 200 x 100 µm, (C) 100 x 100 µm, and (D) 50 x 100 µm. II. 3D visualisation of the cell aggregates, based on pixel intensity. III. Electric field simulation.

5.4.11 The effects of changing the shape of the castellation tips

Many of the aggregates in the previous figures had cells preferentially accumulating at the edges of the castellations. Figure 5.4-23 shows the effects of changing the shape of the castellation tips. The shape chosen was aimed at producing aggregations at right angles to the electrode edges.

The figure shows that changing the shape of the castellations edge can profoundly change the aggregation pattern, and that the required pattern could be produced. Figure 5.4-23 also shows that large differences exist in the cell pattern at different scales. At small scales significant numbers of cells are present in the middle of the aggregate pairs, whilst at larger scales cells are absent. If a convex, rather than a concave shape had been used, one would have expected the cell accumulation to have predominantly in the middle of the aggregates as shown in the electric field simulation data shown in Figure 5.4-24.

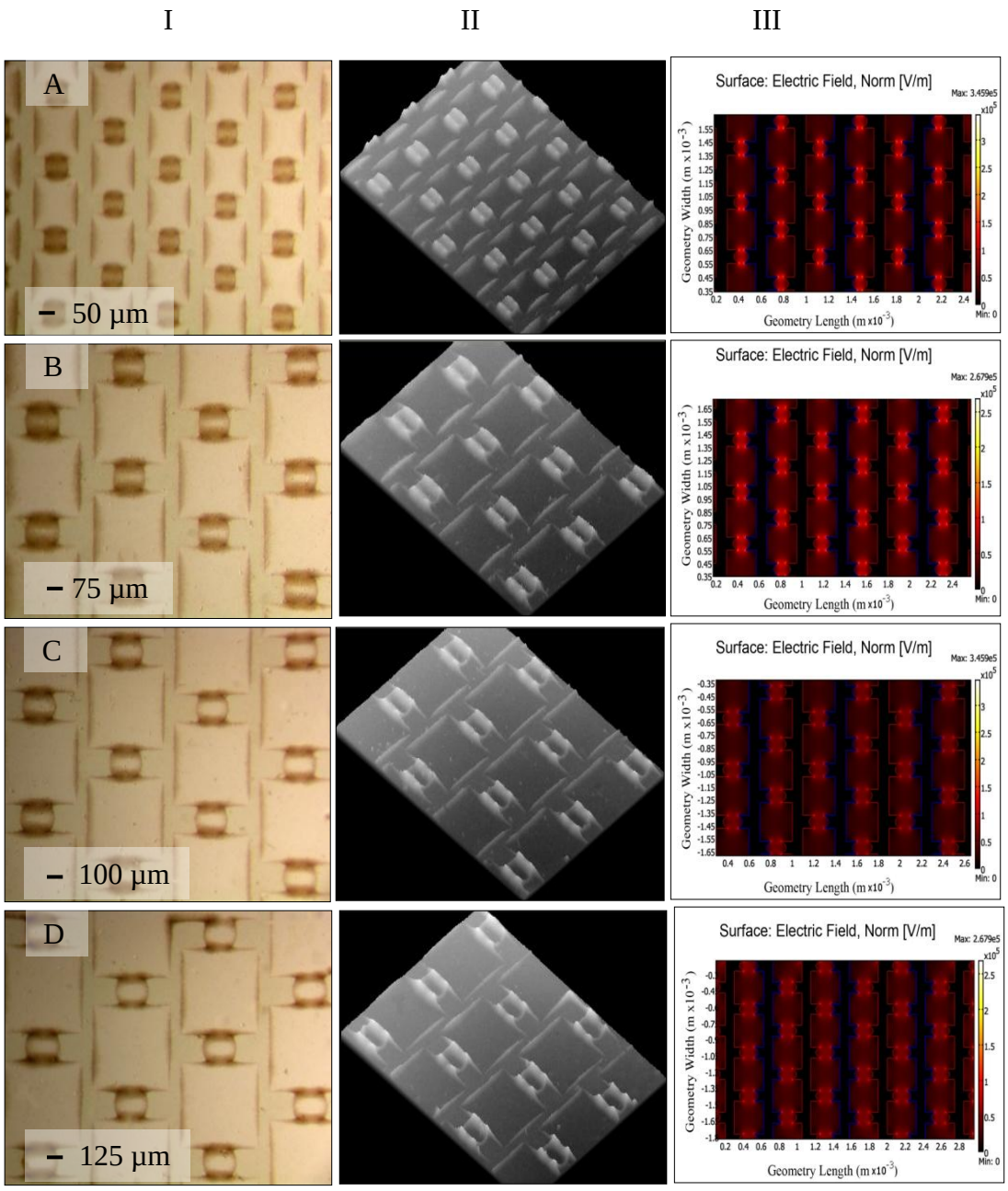

Figure 5.4-23. Cell accumulation at castellations with a rounded edge and concave-shape tips in a hexagonal pattern. Column: I. Aggregation of skin cells at interdigitated

oppositely castellated electrodes with castellation dimensions of (A) 10 x 50 µm, (B) 10 x 75 µm, (C) 10 x 100, and (D) 10 x 125 µm. II. 3D visualisation of the cell aggregates, based on pixel intensity. III. Electric field simulation.

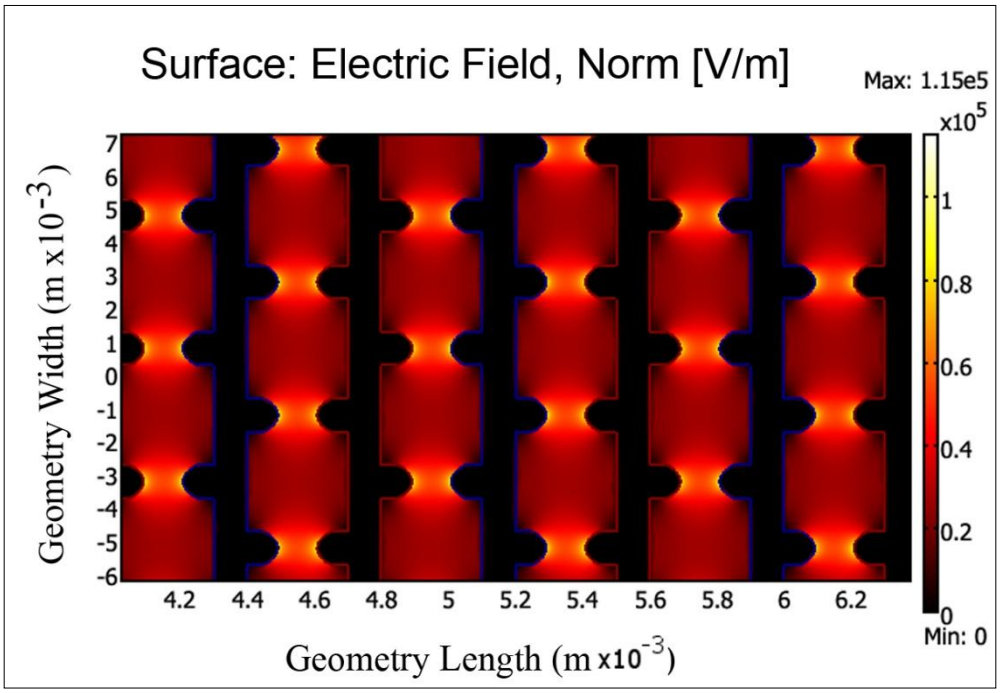

Figure 5.4-24. Electric field simulation of castellated electrode with rounded (convex) edges.

5.4.12 The effects of (increasing or decreasing) the electrode characteristic size.

Figure 5.4-25 and Figure 5.4-26 show the effects of changing the electrode characteristic size in the range of 50 to 300 µm. As shown previously (Markx *et al.*, 1997; Morgan *et al.*, 2001; Sebastian *et al.*, 2007b), when the characteristic size of the electrode increases, the capture volume around the electrodes at first increases as the region of high field strength becomes larger, but then declines as the electric field strength itself becomes less as the electrode distance increases but the applied voltage remains constant. A change in the shape of the aggregates can also be seen, with a more rounded aggregate being formed at small electrode sizes as shown in Figure 5.4-25 A, B, and C followed by their respective 3D images shown in Figure 5.4-26 A, B, and C. More saddle-shaped aggregates with cells accumulating along the electrode edges at higher electrode sizes are shown in Figure 5.4-25 D, E, and F followed by 3D representation of the images respectively in Figure 5.4-26 D, E, and F. The difference can clearly be seen from the corresponding 3D (relative intensity) view of the cell aggregates image.

Image analysis was performed on these aggregates. The results of image analysis of the cell aggregates shown in Figure 5.4-25 are given in Chapter 6). The isolation of distinct features (i.e. the aggregates) and 2D geometrical measurement utilized a simple programming steps using the user-specified multi regions masking technique in LabVIEW Vision Developmental Module (National Instruments, Austin, Texas – USA), in order to give numerical measurements such as aggregate's 2D area, perimeter, elongation and circularity factor, as well as its horizontal orientation and hydraulic radius.

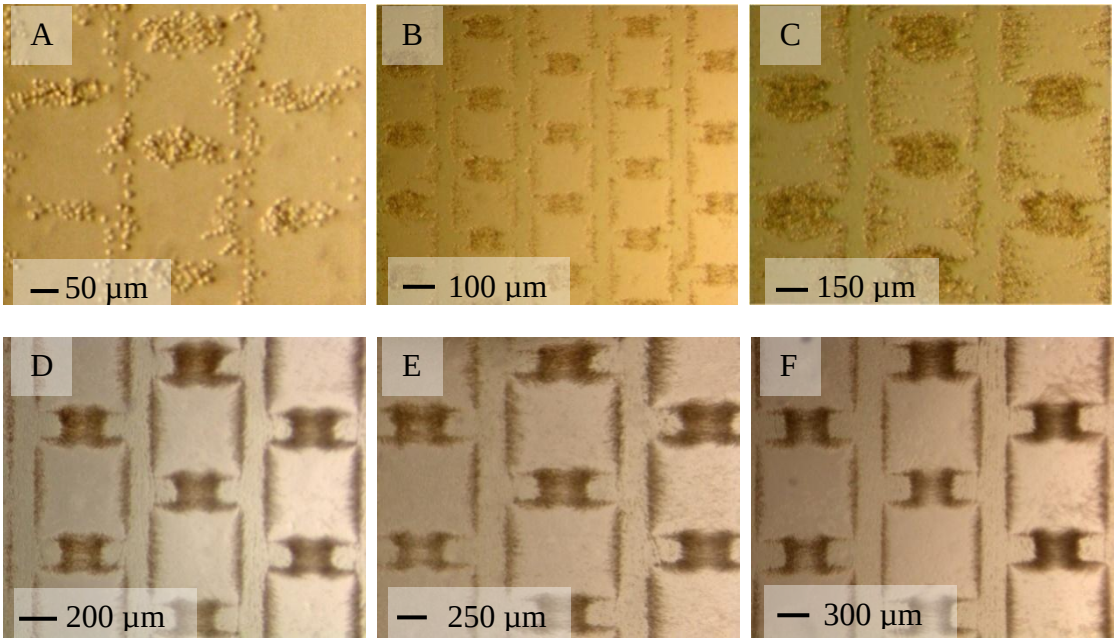

Figure 5.4-25. The effect of increasing electrode characteristic size from (A) 50 µm to (F) 300 µm with 50 µm step size, showing the bright field image of skin cell aggregates, formed using positive DEP.

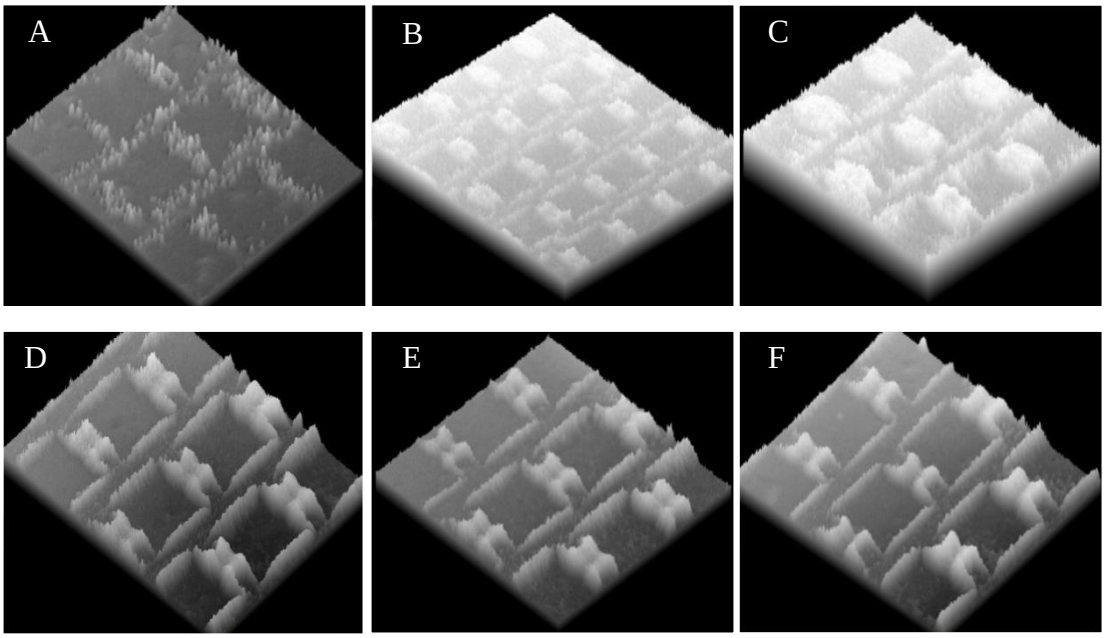

Figure 5.4-26. The effect of increasing electrode characteristic size from (A) 50 µm to (F) 300 µm with 50 µm step size. The image shows the relative surface topography of the aggregate pattern in 3D as well as cell aggregates density distribution based on pixel intensity in the original images (Figure 5.4-25) respectively.

5.5 The Effect of Dielectrophoresis on Cell Viability

A basic requirement in tissue-engineering is the ability to maintain high cell viability and physiological activity after cell or tissue manipulation and patterning. Major drawbacks associated with using DEP to manipulate mammalian cells derive from working with high electric field strengths that may cause cell damage (Tanase *et al.*, 2005), and the use of low conductivity DEP buffer instead of growth media which may affect normal cell physiology if used for extended periods of time.

5.5.1 The effect of AC electric fields

In our system, the trapping of embryonic skin cells involves the transient exposure of the cells to radio-frequency AC electric fields generated using planar microelectrodes with (non-growth medium) iso-osmotic buffer solution for a minimum of 15 – 30 minutes. The suspension of cells in 300 mM sorbitol and their exposure to the electric field however, puts stresses on the cells. To determine the effect of these stresses on the cell viability, cells were exposed to DEP and harvested from microelectrode arrays by removing the electric field after a certain interval of time. Cell viability was determined

as a function of time using TrypanBlue™ Live/Death cell assay immediately. Control cells were suspended in iso-osmotic 300 mM sorbitol solution without DEP exposure. Sample processing was done immediately to minimize other effects that may contribute to cell death. As shown in Figure 5.5-1, some but limited decline in cell viability occurred. Cell viability was maintained to around 85% during 30 minutes exposure to electric field (10 $V_{pk\text{-}pk}$ and 1 MHz frequency), whilst in the control cells, the viability declined to around 95%. Therefore, exposure to electric field accounts for around 10% loss in cell population under the conditions of the experiment and type of cells being used. There are however, other factors that may cause a decline in cell viability that remained to be elucidated. This includes changes of pH as a result of metabolic activity or mechanical handling such as centrifugation, that may cause cellular injury. It is also important to note that cell viability tests immediately post DEP may not reflect the proliferative capability of the cells after dielectrophoresis.

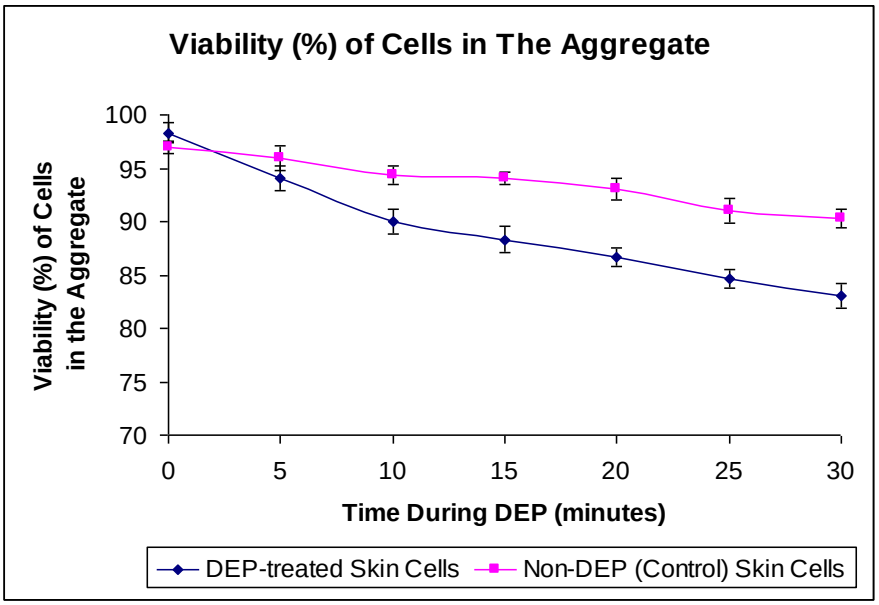

Figure 5.5-1. Analysis of viability of the cells in the aggregates. The viability of chicken embryonic skin cells during electric field exposure (1 MHz, 10 $V_{pk\text{-}pk}$) at the 100 µm microelectrode regions, using TrypanBlue LIVE/DEATH Assay. Control cells are chicken skin cells suspended in 300 mM sorbitol (without DEP). Error bars depict standard errors of sample size (n) of 3.

5.6 Immobilization of Cell Aggregates

To show that cells in the aggregate remain viable and physiologically active, the DEP-immobilized cell aggregate was further immobilized using fibrin gel, and allowed to grow for a few days under a controlled environment in an incubating chamber (37ºC

and 5% CO_2) and continuous supply of growth medium (RPMI). Initially, cells were isolated from chicken embryonic skin tissue, and aggregates were made of the cells using electrodes of the interdigitated castellated design in a hexagonal pattern. The electrodes had a dimensional size of 150 x 300 μm. After the cells had collected, the electric field was maintained for a further 10 minutes to force the cells to adhere to each other, as described by Sebastian et al. (2007a). Following this, a 9:1 v/v mixture of a fibrinogen (10 mg ml^{-1} in RPMI 1640 medium) and thrombin solution (10 units ml^{-1} in a 4 μM $CaCl_2$ solution) was put into the chamber to immobilize the cells in a fibrin gel, forming a skin-like material with placode-like aggregates.

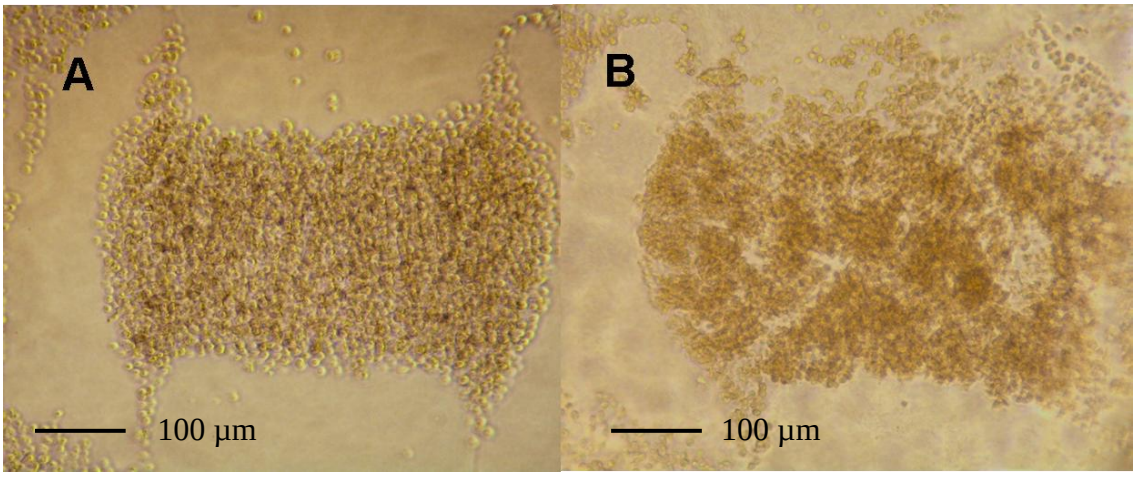

Figure 5.6-1. Investigation of cell behaviour in the aggregates after the formation of the artificial embryonic chicken skin. Aggregates were formed from a cell suspension obtained from embryonic chicken skin and contained both epidermal and dermal cells. A: aggregate formed at interdigitated oppositely castellated electrode 300 μm (1 MHz, 10 V_{pk-pk}) immediately after its formation; B: same aggregate after 24 hours. Further condensation of the cells within the aggregate can be seen to have occurred randomly across the aggregate.

Some limited loss of cells from the aggregates occurred. Incubation of the artificial skin in RPMI 1640 growth medium for up to 3 days showed limited expansion of the aggregates in the first day, followed by the local compaction of some of the cells into denser aggregates. A typical example is shown in Figure 5.6-1. Compaction of cells into dense aggregates is also observed in natural skin during placode and follicle formation.

5.7 Conclusions

In this study we have investigated the ability of dielectrophoresis to create arrays of cell aggregates in defined patterns. Although the use of negative dielectrophoresis for the

formation of cell aggregates is also possible (Pethig *et al.*, 1992), we have used positive dielectrophoresis because the trapping forces are higher. Another major advantage is also that the electric field used strongly forces the cells within the aggregates in direct contact with each other, encouraging exchange of signals between cells by direct cell-cell contact. In addition, the more natural distribution of cells mimicking the actual 3D structures of placode *in vivo*) encourages the formation of more natural distributions of oxygen, nutrients, diffusible cytokines and other factors in the artificial tissues. As explained earlier, cells on the surface of the 3D structure get more access to oxygen from the environment than the cells on the inside of the aggregate.

We have shown that positive dielectrophoresis can be used to produce artificial tissues with aggregates of cells in patterns similar to that during development in chicken embryonic skin. It was also shown that variations of the pattern could be made in which the aggregate size, the pattern itself and the distance between the aggregates were varied. The patterns were shown to be highly predictable and reproducible. Some loss of cells from the aggregates occurred during the immobilization step, and further optimization of this step is needed. Further incubation has shown that cells remain active after the formation of the aggregates, and resume many of the activities seen *in vivo*, including compaction into more dense aggregates.

The method developed could be used to elucidate the mechanisms in which follicle patterns are produced during development. Although this work has concentrated in chicken embryonic skin, we believe that the approach could also work with other systems. Since the aggregates within the artificial tissues will be 3-dimensional it is expected that they will more closely mimic the natural distributions of cells than standard 2-D cultures, and more closely reproduce the tissue microenvironment that determines the cell phenotypes during development (Schmeichel *et al.*, 1998; Khademhosseini *et al.*, 2006b; Lund *et al.*, 2009).

To be most useful the pattern formation process has to be usable for any type of cells, and highly predictable and reproducible. Dielectrophoresis is a physical rather than a biological effect. As all intact, viable cells have an intact, low conducting lipid membrane surrounding an aqueous high-conductivity cytoplasm (Pethig and Kell, 1987), all cells will display a Maxwell-Wagner type polarization around 1 MHz which

will result in positive dielectrophoresis when cells are immersed in a low-conductivity medium. Patterning with dielectrophoresis is therefore possible with any cell type.

CHAPTER 6

Isolation and Measurement of Distinct Features of Arrays of Cell Aggregates Using The User-Specified Multi Region Masking Technique

6.1 Abstract

The use of dielectrophoresis for the construction of artificial skin tissue with skin cells in follicle-like 3D cell aggregates in well-defined patterns is demonstrated. To analyze the patterns produced and to study their development after their formation, a Virtual Instrument (VI) system was developed using the LabVIEW IMAQ Vision Development Module. A series of programming functions (algorithms) was used to isolate the features on the image (in our case; the patterned aggregates) and separate them from all other unwanted regions on the image. The image was subsequently converted into a binary version, covering only the desired microarray regions which could then be analyzed by computer for automatic object measurements. The analysis utilized a simple and easy-to-use user-specified multi-region masking technique, which allows one to concentrate the analysis on the desired regions specified in the mask. This simplified the algorithms for the analysis of images of cell arrays having similar geometrical properties. By having a collection of scripts containing masks of different patterns, it was possible to quickly and efficiently develop sets of custom virtual instruments for the offline or online analysis of images of cell arrays in the database.

6.2 Introduction

During embryonic development of skin tissue in chicken feather bud primordia are formed in regular hexagonal patterns. Patterning starts at a line above the neural tube, which subsequently breaks up into individual placodes. Formation of placodes then spreads from this line in a cascade over the whole skin, forming a hexagonal array of feather buds. The exact details of the mechanisms by which this pattern is formed are still unknown, but are thought to involve the condensation of cells into aggregates (placodes) whose position is determined by a reaction-diffusion mechanism of activator and inhibitor molecules distributing themselves at differential rate across the skin (Mou *et al.*, 2006).

The creation of artificial skin with cell aggregates of known size and shape spaced in well defined and regular patterns could help with elucidating the mechanisms by which

the regular arrays of feather bud primordia are formed. In this study the use of dielectrophoresis (DEP), the induced movement of particles in non-uniform electric fields (Markx, 2008) was explored for the formation of cell aggregates of controlled size and shape in well-defined patterns.

After the formation of the aggregates, it is often necessary to analyze the patterns produced simultaneously (rather than on an individual cell aggregate basis) and to study their development after their formation. To aid in this we have developed a LabVIEW-based Virtual Instrument (VI) system to effectively and simultaneously analyze images of microarrays of cell aggregates using IMAQ Vision Development Module, which we will describe here.

6.3 Materials and Methods

Electrode designs were made using Protel Design Explorer 99. Electric field calculations were made using COMSOL Multiphysics. Microelectrodes were made from ITO-covered glass slides using standard photolithography. A simple microfluidic chamber was created above the microelectrode array using glass slides and a silicone spacer Figure 6.3-1. Chicken embryonic skin cells were isolated by enzymatic tissue digestion from the dorsal part of an 8-day old white leghorn chicken embryo. The dissociated skin cells were suspended in Dulbecco medium (DMEM) prior to DEP experiments. When needed, the cells were centrifuged and washed several times before transferring to low conductivity iso-osmotic sorbitol solution (300 mM, $\sigma = 6.1 \times 10^{-4}$ S m^{-1}). The cells were introduced into the DEP chamber (approximate height = 560 μm) at a constant flow rate of around 40 μL. min^{-1} using a peristaltic pump.

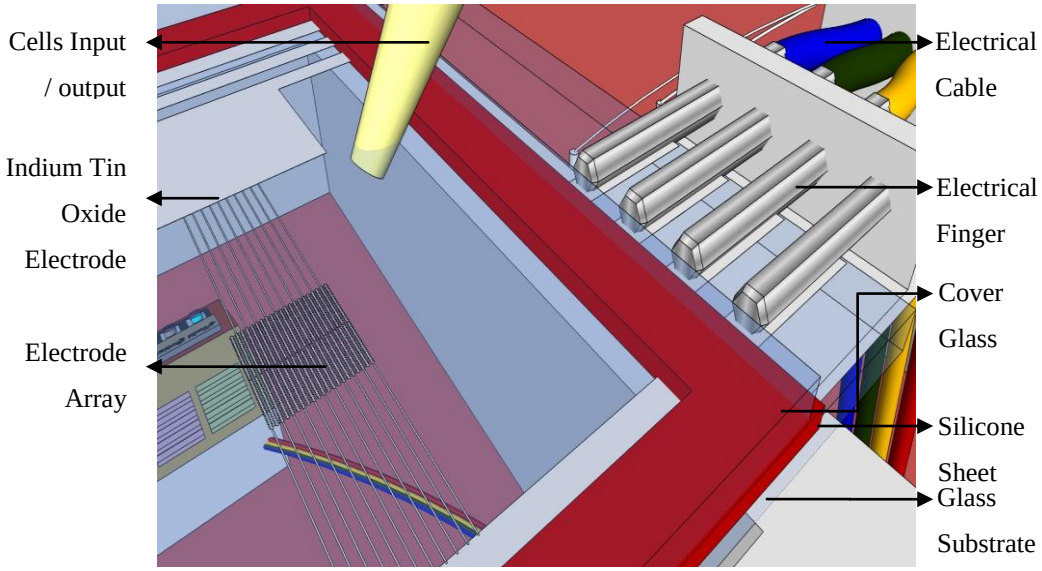

Figure 6.3-1. Dielectrophoresis chamber for the formation of well defined biodielectric patterns.

Construction of the biodielectric patterns involved the application of a high frequency (1 MHz, 10 $V_{pk\text{-}pk}$) AC signal using TG120 Thurlby-Thandar frequency generator, to the microelectrodes to create non-uniform electric fields and use dielectrophoresis to force the cells together. This was followed by the immobilization of the cells in a 50% Puramatrix gel in order to create a skin-like material and enable the long-term incubation of the immobilized cells. Images were taken of the aggregates using a wide field stereo microscope from Celsi and a NIKON Coolpix E4500 digital camera. Image analysis was performed with LabVIEW IMAQ Vision.

6.4 Results and Discussion

6.4.1 Formation of various well-defined biodielectric patterns

As shown previously (Sebastian *et al.*, 2007b), the shape of cell aggregates between a set of castellated electrodes can be predicted using standard finite element analysis package such as COMSOL Multiphysics. The shape of the cell aggregates could be expected to follow the pattern of the high electric field strength regions between castellations.

Electric field patterns formed between electrodes of different shapes are shown in Figure 6.4-1. Images of the actual aggregates of skin cells formed and their associated pseudo-3D representations based on the distribution of the pixel intensities are shown in

Figure 6.4-2 and Figure 6.4-3 respectively. Although the shape of the cell aggregation followed the predicted pattern based on electric field calculations well, it was also affected by factors such as the liquid flow rate and the concentration of cells entering the chamber, as well as the electrode geometry, frequency and potential difference between the castellations.

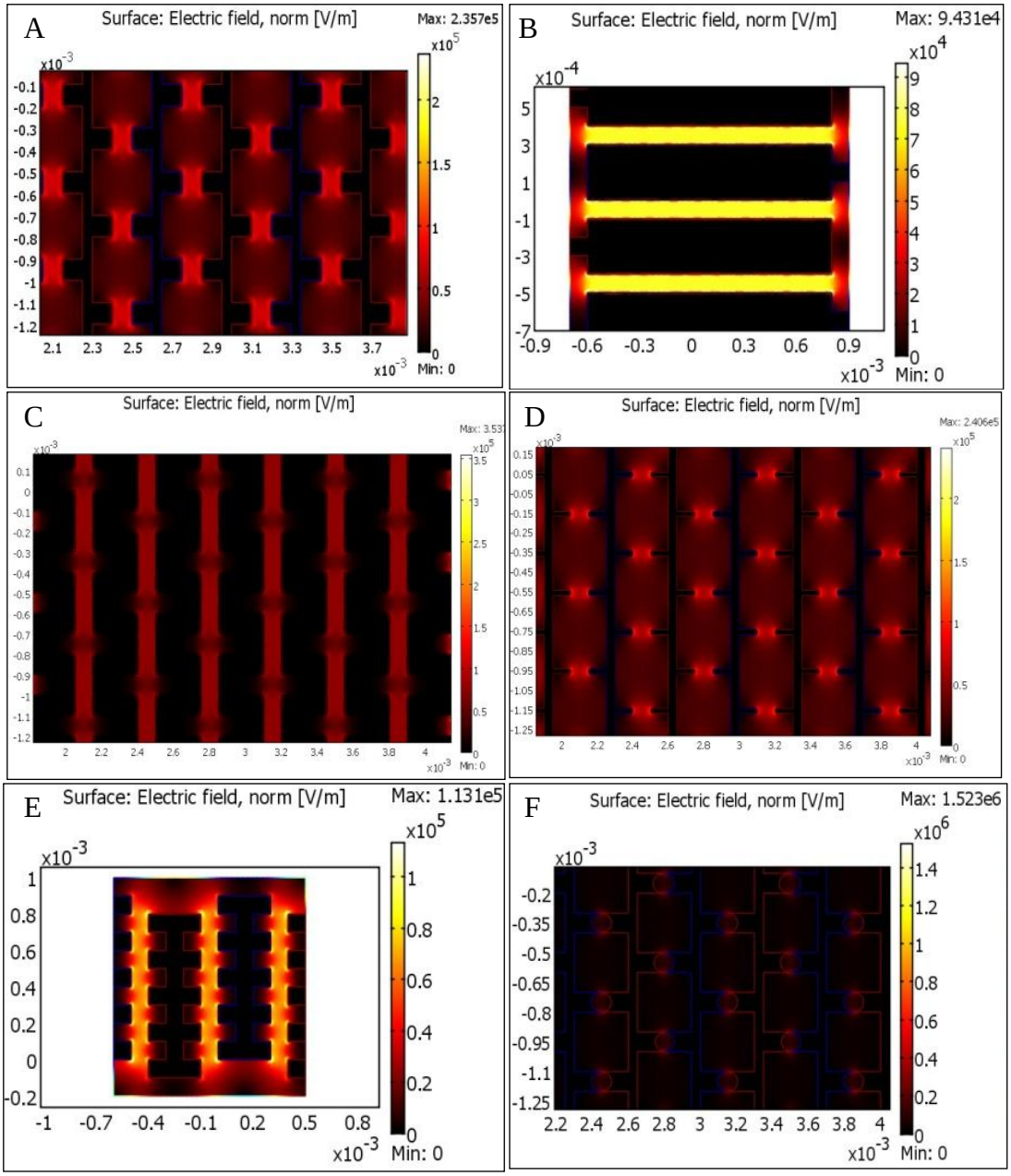

Figure 6.4-1. Modelling of electric field calculation between sets of interdigitated electrodes with various design patterns (in meter unit). A. Small Hexagon. B. Line Pattern. C. Large Hexagon. D. Elongated Hexagon. E. 'W' Pattern. F. Round Edge with Hexagonal Pattern.

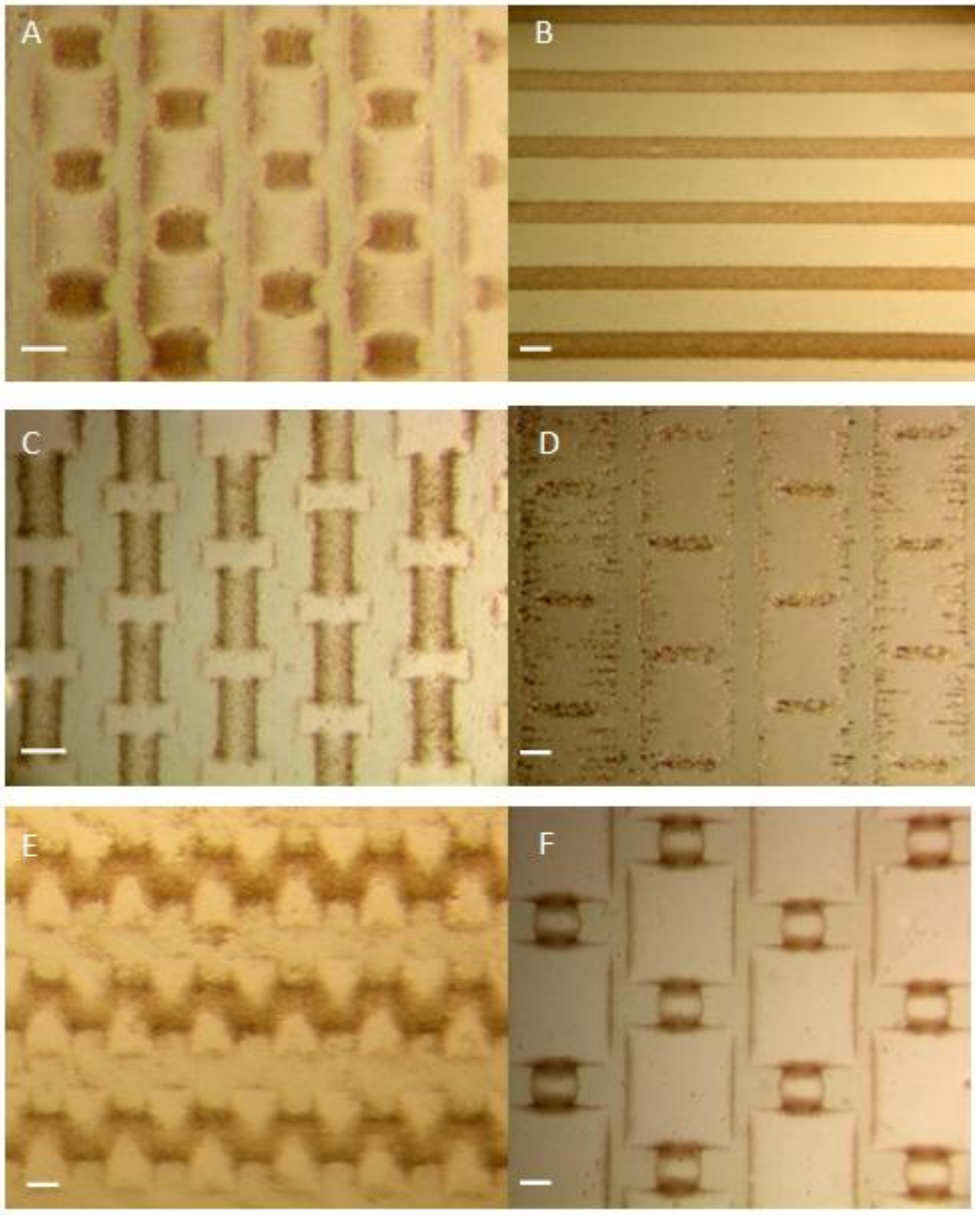

Figure 6.4-2. Images of embryonic skin cell aggregates formed with DEP in various patterns. A. Small Hexagon. B. Line Pattern. C. Large Hexagon. D. Elongated Hexagon. E. 'W' Pattern. F. Round Edge with Hexagonal Pattern. Scale bar is 100 µm.

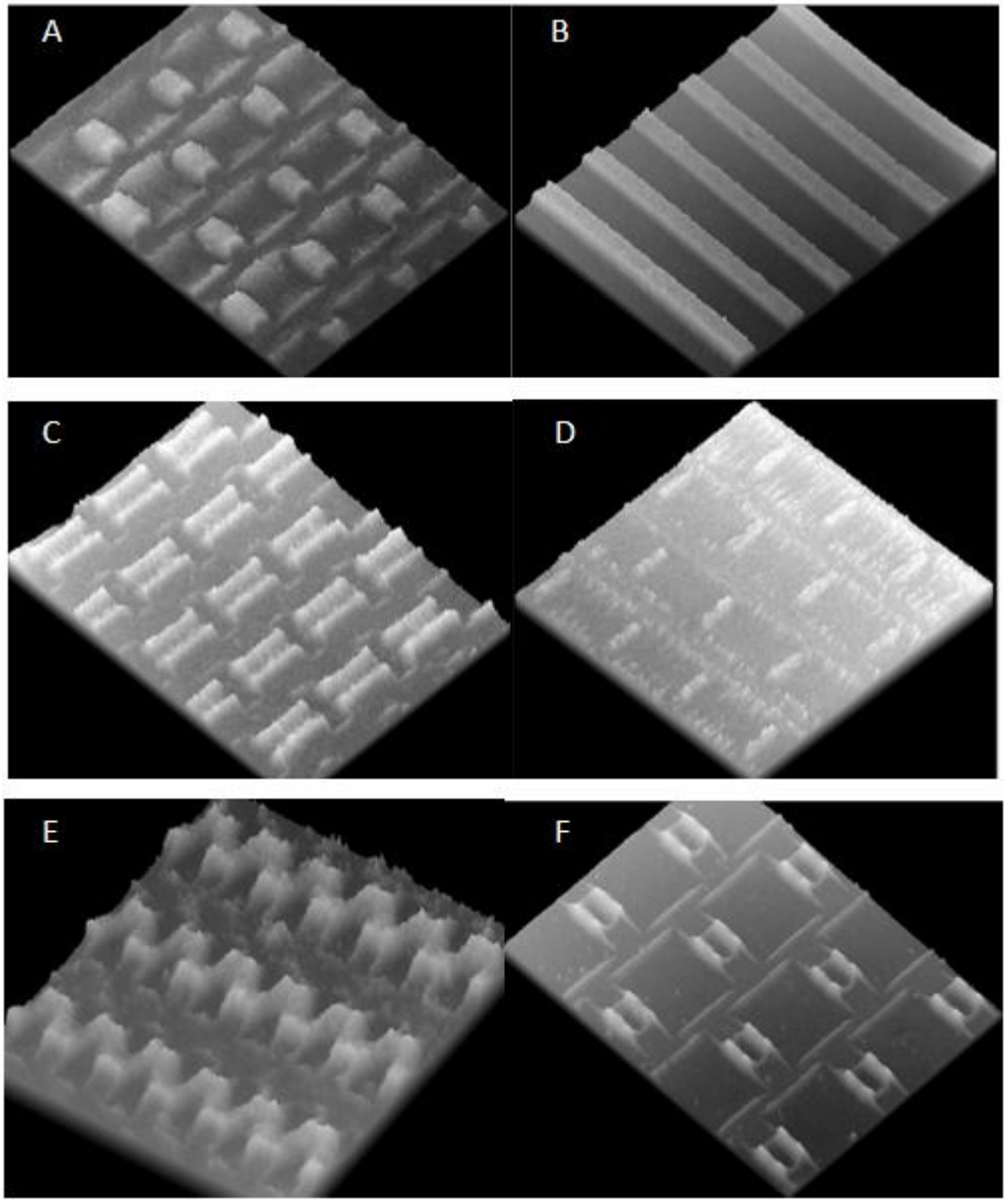

Figure 6.4-3. Pseudo-3D representation of the cell aggregates from Figure 6.4-2, based on pixel intensity. A. Small Hexagon. B. Line Pattern. C. Large Hexagon. D. Elongated Hexagon. E. 'W' Pattern. F. Round Edge with Hexagonal Pattern.

6.4.2 Analyzing the images using user-specified multi regions masking technique

Analysis of the images of cell aggregates could provide information about - amongst others - the quality of the aggregates, the aggregation process itself, and the development of the aggregates after their formation. To achieve this, it is necessary to take a series of graphical programming steps to convert the original image to binary version showing only the regions of interest (in our case, cell aggregates in the regions specified by the castellations), based on a certain threshold value. To achieve the desired binary version covering only the aggregate regions (Regions of Interest), a

series of graphical programming (algorithms) must be applied to the image. In some cases this often involves numerous algorithms. The use of user-specified multi-regions masking technique simplifies this problem as illustrated in Figure 6.4-4. Once the correct (representative) binary version of the particles is achieved, subsequent analysis is relatively straight forward.

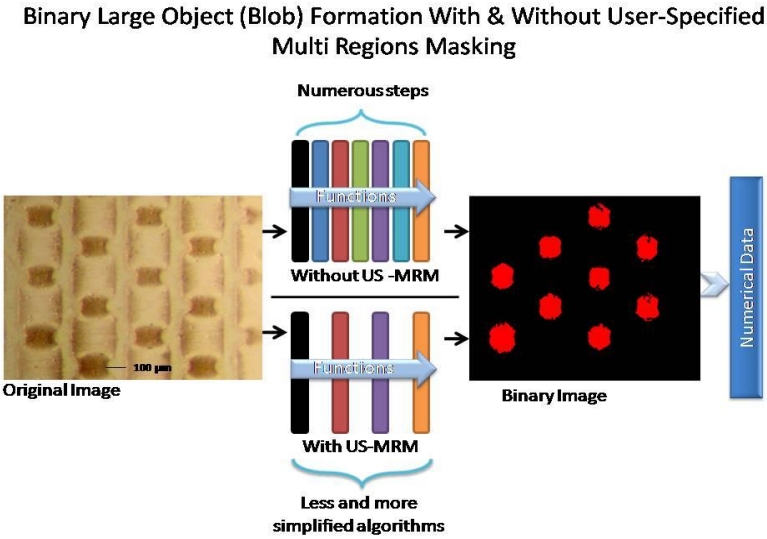

Figure 6.4-4. Diagram illustrating differences in graphical programming steps from original image to the formation of binary version of the image.

A series of graphical programming functions (algorithms) was tested and optimized in order to develop Virtual Instruments (VIs) which are capable of analyzing images of arrays of aggregates in a database by simply changing the set parameter values according to the unique conditions of the individual images (e.g. light intensity, and edge sharpness). Due to the complex processes that occur during DEP pattern formation and the large number of potential sources of interference (such as unbound cells, contaminating cell debris or other particles), the isolation and measurements of distinct features (immobilized cell aggregates) in the image was complicated. This can be clearly seen in Figure 6.4-2 , where cells can be seen to aggregate in areas outside the main areas of interest as local high electric field regions also occur outside the main areas (Wang *et al.*, 1993). The ROI isolation problems were minimized by using the user-specified multi-regions masking technique prior to binarizing the image for subsequent automatic particle measurements. A similar masking approach was previously used by Gascoyne for measuring aggregate formation with dielectrophoresis (Gascoyne *et al.*, 1992). However, their interest was mainly in the speed of the particles

forming the aggregates, whilst our interest is mainly in the final shape, size and position of the aggregates.

It was found that the best method of specifically (but simultaneously) isolating only the cell aggregates for further analysis involved applying a set of user-specified multi-region masks prior to thresholding the images based on other parameter values. Thus, image analysis using LabVIEW IMAQ Vision mainly involved the following major group of functions (National-Instrument, 2008;February 2007;July, 2007):

- **Image Acquisition** (Algorithm used: *Image open*). This step could be performed online / real-time using various types of image acquisition (National-Instrument, 2008) hardware or offline (from large collection of images previously saved in a database). In this work only the offline method of image analysis was used.

- **Pre-Processing**. This step is where multi-regions masking technique was applied (Algorithm used: *Image Masking*). A series of maskings was applied on the displayed image using the various masking tools available in the package (circular / oval, square, polygon, annulus, rotated rectangle, or freehand region tool). This was achieved by holding the Ctrl button (in PC) during multi-regions masking. The mask covered or filtered out the majority of the unwanted regions in the image, leaving only the regions of interest for further analysis (Figure 6.4-7). Other algorithms that could be used in this pre-processing step are Calibration (to give real-life metric measurements instead of pixel measurements), and Plane Extraction (to give a grayscale version of the original full color image).

- **Thresholding**. This step isolated the pixels of interest in the previously unmasked areas (to be a set value = 1) and set the remaining pixels as background pixels (set value = 0) thereby creating a binary image. A locally adaptive thresholding method (*Niblack*) was used which categorized a pixel as part of a particle or the background based on the intensity statistics of its neighboring pixels. This method was particularly good when the original images exhibited non-uniform lighting effect during acquisition.

- **Filtering**. Because thresholding is a subjective process, the resulting binary

image may still contain unwanted information, such as small residual noise particles. Use of the Multi-regions masking technique cut out the majority of these noises. The remaining filtering algorithms used were therefore *Remove small objects* and *Remove border objects* (i.e. the mask itself). Other optional algorithms that were sometimes needed fell under binary morphology modification functions. These included *Fill holes*, *Close objects*, and *Dilate / Erode objects*. The final binary images form the closest possible representative shapes of the actual biodielectric patterns (Figure 6.4-7).

- **Measurement**. IMAQ Vision Particle Analysis could be used to calculate all (up to 49) requested measurements in pixel or metric values. Measurements used here included object *perimeter*, *area*, *hydraulic radius*, *elongation factor* and *Heywood Circularity factor* (Table 6.4-1 and Table 6.4-2).

The final step was generation of custom LabVIEW VIs, based on selected algorithms above. The block diagram of the VI is shown in Figure 6.4-5 and Figure 6.4-6. This was used to simultaneously analyze 2D biodielectric pattern and subsequent processing into binary-type image for numerical measurements (National-Instrument, February 2007). However, adjustment of the threshold value was often required for a more representative binary version of the original image.

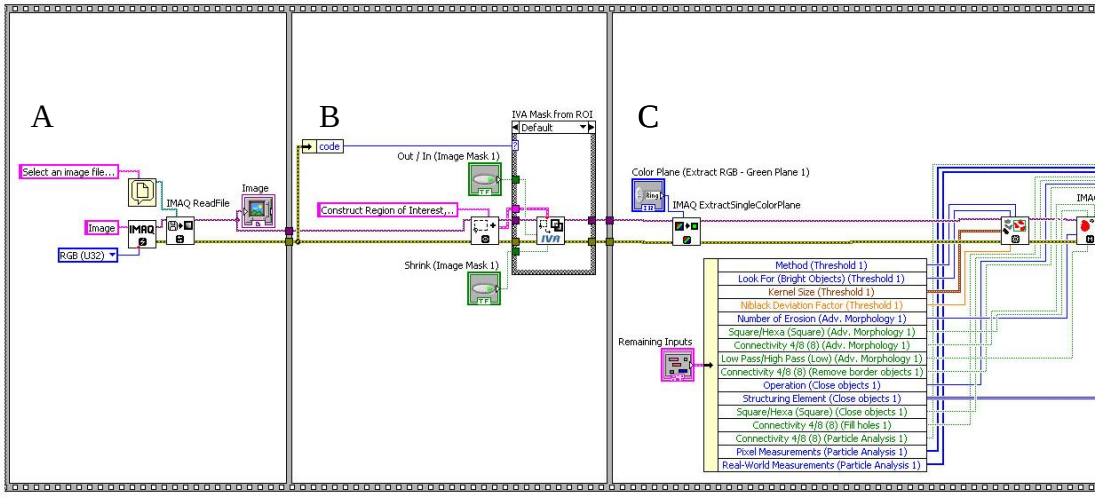

Figure 6.4-5. Snapshot of custom-built block diagram (Part I) of the VI showing graphical algorithms used for biodielectric image processing using a user-specified multi- regions masking technique. The codes inside the flat sequence structure are used for: (A) Selecting an image file from the database, (B) Constructing user-specified multi-regions mask, (C) Image processing (continued to Figure 6.4-6).

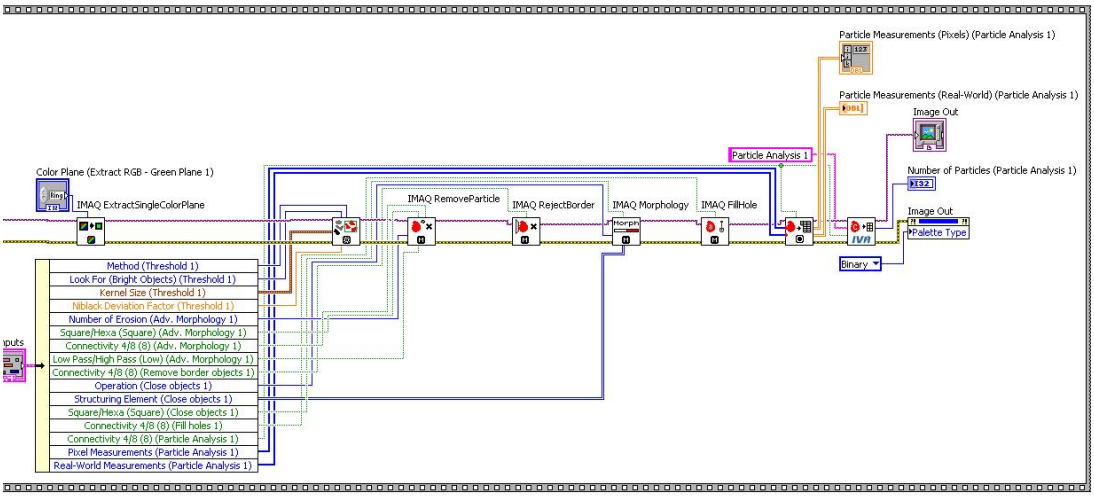

Figure 6.4-6. Snapshot of custom-built block diagram (Part I) of the VI showing graphical algorithms used for biodielectric image processing using a user-specified multi- regions masking technique. The codes inside the flat sequence structure are used for image processing to produce a binary version of the image for 2D numerical measurements.

The calculations performed were relatively fast. All steps taken to analyze all objects simultaneously in each image (including isolation and measurement processes) could be implemented efficiently with a total time less than 0.5 seconds, on a 2 GHz Pentium 4 processor.

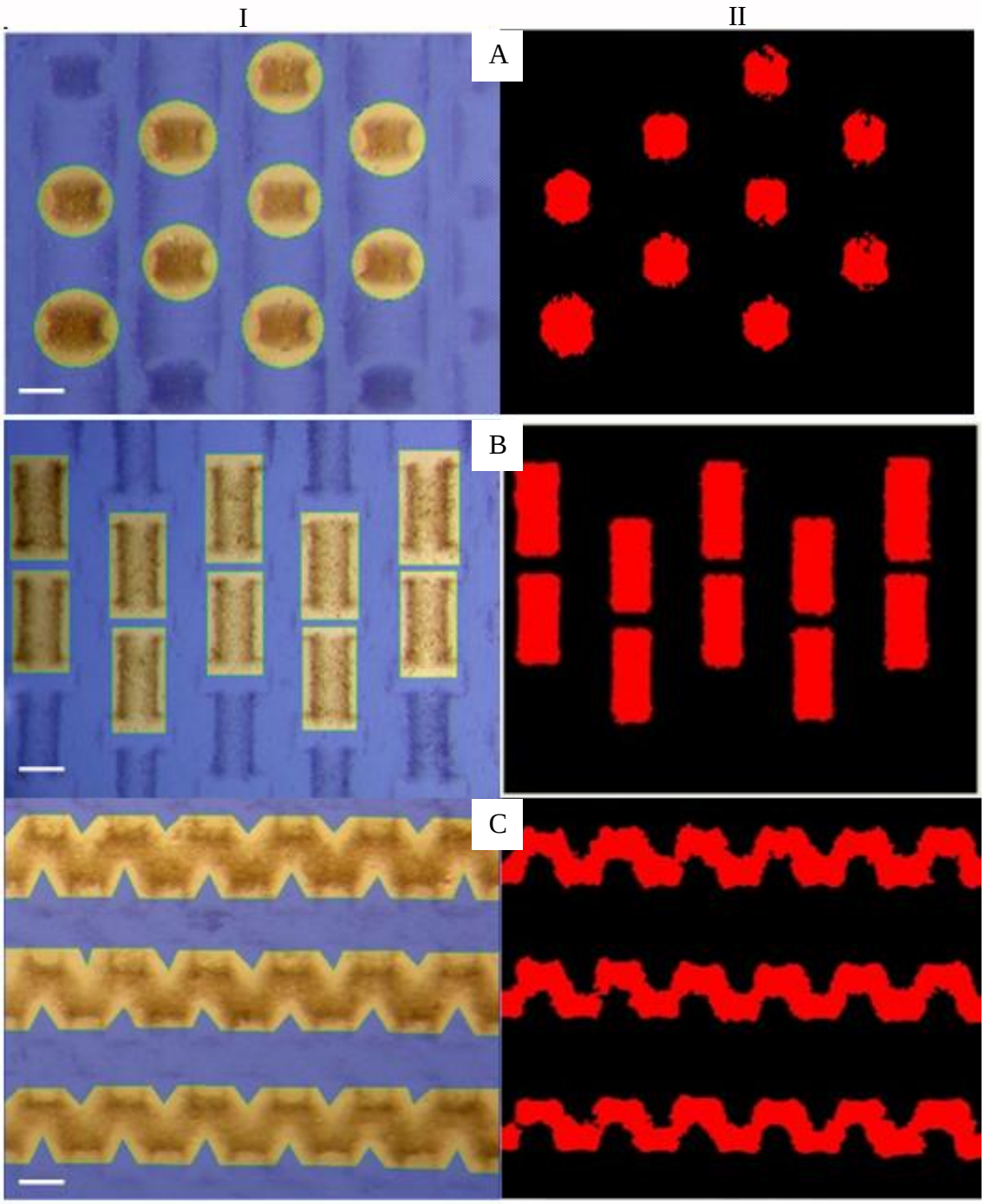

Figure 6.4-7. Conversion of user-specified masked images (I) to binary large objects (II), a group of contiguous pixels that have the same intensity value (i.e. 1) and shown in red colour. The user-specified multi regions mask is shown in transparent blue colour. A. Small Hexagon. B. Large Hexagon. C. 'W' Pattern. Scale bar is for 100 µm.

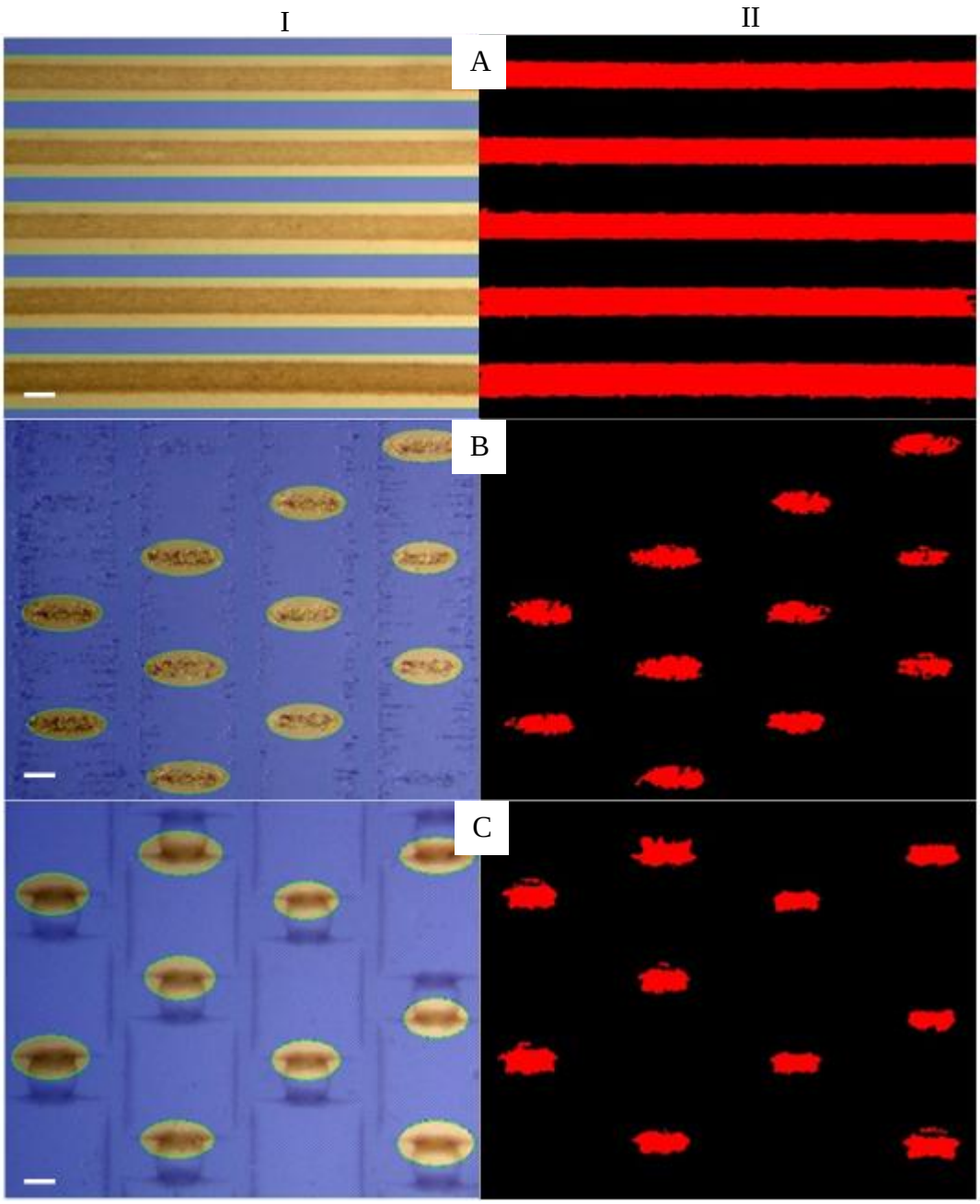

Figure 6.4-8. Conversion of user-specified masked images (I) to binary large objects (II), a group of contiguous pixels that have the same intensity value (i.e. 1) and shown in red colour. The user-specified multi regions mask is shown in transparent blue colour. A. Line Pattern. B. Elongated cell aggregates in hexagonal pattern. C. Round Edge with Hexagonal Pattern. Scale bar is for 100 µm.

6.4.3 Results of the image analysis

The analysis of the images using the user-specified multi-regions masking technique is shown in Figure 6.4-7 and Figure 6.4-8. A summary of the results of the numerical analysis using the technique described here is given in Table 6.4-1 and Table 6.4-2.

Table 6.4-1 shows that the masking technique can be used to generate data from images

of cell aggregates formed at a variety of electrode shapes. Table 6.4-2 shows a comparison of the distances and angles between cell aggregates and compares them with the expected values based on the specifications of the actual photo mask design. The analysis shows a very good agreement between the two sets of data.

Table 6.4-1. Summary of 2D geometric measurements / analysis of aggregates on various electrode designs. All electrodes had a characteristic size of 100 µm. Values given are the mean and standard error of mean.

Electrode Designs	Mask Type	Perimeter (µm)	Elongation Factor	Circularity Factor	Area (μm^2)	Hydraulic Radius(µm)
Small Hexagon	Circular	490.8 ± 12.3	1.67 ± 0.04	1.24 ± 0.03	12510.8 ± 227.8	25.5 ± 0.4
Line Pattern	Square	4772.2 ± 101.2	10.53 ± 0.51	2.72 ± 0.08	247428.7 ± 14917.6	51.9 ± 2.8
Large Hexagon	Square	1119.1 ± 10.3	2.43 ± 0.03	1.38 ± 0.02	52590.7 ± 970.2	47.0 ± 1.1
Elongated	Oval	328.5 ± 11.7	3.21 ± 0.10	1.30 ±0.03	5087.9 ± 343.9	15.5 ± 0.6
'W' Pattern	Polygon	9320.1 ± 587.9	N/A	N/A	223079.2 ± 7683.2	N/A
Round Edge	Oval	298.9 ± 28.6	3.38 ± 0.21	1.70 ±0.09	4899.2 ± 187.6	16.4 ± 1.0

N/A = Not Available

According to the National Instrument™ (NI) LabVIEW Vision Development Module user guide, the term Elongation Factor is the ratio of Maximum Feret Diameter with the equivalent rectangle short side. The higher the elongation value, the more elongated the object is. Heywood Circularity factor is on the other hand, defined as the perimeter of the object divided by circumference of a circle with the same area. The closer the value is to 1, the more circular the object. The Hydraulic Radius is defined as the ratio of the area and the perimeter of the object. The Hydraulic Radius appears most commonly in various empirical formulas for determining the flow velocity of a liquid that gives the same (wetted) perimeter in a channel. In this case however, the author used the term to describe the overall 2D shape (or foot print) of the resulting cell aggregate pattern (i.e. according to the definition of the term by the LabVIEW Vision™ image analysis module). Elongation and Circularity factor gives a measure of how elongated and circular an object is, respectively.

Table 6.4-2. Summary of measured distances and angles between cell aggregates formed at different electrode designs and the expected value based on the electrode design. All electrodes had a characteristic size of 100 µm. Values given are the mean and standard error of mean.

Electrode Designs	Vertical Distances (µm)	Exp. Value (µm)	Horizontal Distances (µm)	Exp. Value (µm)	3-Points Angle 1 (º)	Exp. Value (º)	3-Points Angle 2 (º)	Exp. Value (º)
Small Hexagon	393.2 ± 1.2	400	442.7 ± 1.3*	450*	115.2 ± 1.1	116.4	124.8 ± 2.3	127.3
Line Pattern	402.0 ± 5.0	400	N/A	N/A	180.1 ± 1.1	180	N/A	N/A
Large Hexagon	397.8 ± 3.6	400	803.5 ± 5.8	800	119.1 ± 2.7	120	122.5 ± 5.1	120
Elongated	401.7 ± 2.8	400	799.5 ± 3.9	800	121.9 ± 4.1	120	119.7 ± 4.8	120
'W' Pattern	403.6 ± 6.6	400	N/A	N/A	181.4 ± 3.7	180	N/A	N/A
Round Edge	398.4 ± 2.9	400	807.1 ± 5.9	800	120.8 ± 1.9	120	121.3 ± 2.9	120

*Diagonal data shown. Exp. = Expected Value. N/A = Not Available

It should be noted that the multi regions masking technique is invariant to the scale, shape and rotation of the features as the users can specify the region just outside the features of interest. The technique is therefore highly useful in the sense that a single mask design can correctly isolate other features (from other images in the database) within the unmasked area with only a few threshold level adjustments, depending on the variation in illumination level and camera viewpoint during acquisition.

Successful isolation of features is often a key and fundamental aspect of many problems in computer vision and image analysis. The multi regions masking technique described here is particularly useful due to its reusability with only a few threshold level adjustments. Furthermore, statistical analysis can be performed on the data to determine whether the changes are significant or not.

6.5 Image Analysis of Cell Aggregates with Increasing Characteristic Size

Chapter 5 demonstrated the construction of arrays of embryonic skin cell aggregates in well defined patterns. In order to check the accuracy of the 2D geometrical pattern formation (in relation with the mask design) and to obtain information about the reliability of the pattern formation process as well as the size and shape of the aggregates, image analysis was used to analyze the cell patterns created of the chicken

embryonic cells. Image analysis was only performed on the aggregates formed in the high field regions between electrode castellations.

Using the same technique described earlier, one can generate a set of numerical measurements in order to assess the effect of certain modifications, such as an increasing electrode characteristic size, on the shape of cell aggregate (quantified by elongation and circularity factor), area and perimeter, as well as the (initial) horizontal orientation of the aggregate in a two-dimensional system.

The change in the size of the aggregates (perimeter and area) at an increasing electrode characteristic size can be seen in Figure 6.5-1 and Figure 6.5-2 respectively, and is summarized in Table 6.5-1. Already shown previously in Figure 5.4-25 were the corresponding pictures of the aggregates. Within the range of microelectrode characteristic sizes used (50 – 300 µm), the cell aggregate perimeters and their corresponding hydraulic radii seem to develop proportionally with increasing electrode size (Figure 6.5-1 and Figure 6.5-3). The area, however, develops at a more quadratic rate (Figure 6.5-2). We do not have data for aggregates formed at electrodes with characteristic sizes higher than 300 µm. However, in Figure 5.4-21 it can be seen that when using electrodes of 300 µm characteristic size, the cell density in the middle of the aggregate becomes very low. It can therefore be expected that, if the electrode size is increased further, the aggregate will split into two smaller size aggregates, each attached to the edges of the castellations. As has previously been observed with carbon nano tubes (Chung *et al.*, 2004), the interaction between two neighboring electrodes will become negligible if the distance between the electrodes becomes large. The aggregate patterns will then remain unchanged and the final curve will be a sigmoidal one.

Table 6.5-1. Summary of 2D geometry image analysis of skin cells with increasing aggregate size (with the hexagonal pattern only, as shown in Figure 5.4-25).

Size (µm)	Mean Value (± Standard Error)					
	Perimeter (µm)	Elongation Factor	Circularity Factor	Area (μm^2)	Hydraulic Radius (µm)	Horizontal Orientation (^{o})
50	310.2± 17.5	2.20±0.09	1.54±0.04	3254.5± 241.1	10.4±0.4	0.63±1.28
100	546.0±25.8	2.02±0.08	1.47±0.05	10954.9±496.6	20.2±0.7	2.81±2.05
150	870.5± 25.9	1.89±0.06	1.59±0.02	23965.7± 1277	27.4±0.7	-2.49±4.07
200	1119.1±29.1	1.82±0.02	1.45±0.06	42906.6± 3811.8	38.2±3.2	-2.70±2.47
250	1343.7±34.4	2.00±0.04	1.54±0.07	69413.7± 2817	52.0±2.6	-0.59±0.81
300	1658.7±30.4	1.99±0.02	1.49±0.06	100927.7± 5071.5	61.1±3.4	-0.83±0.72

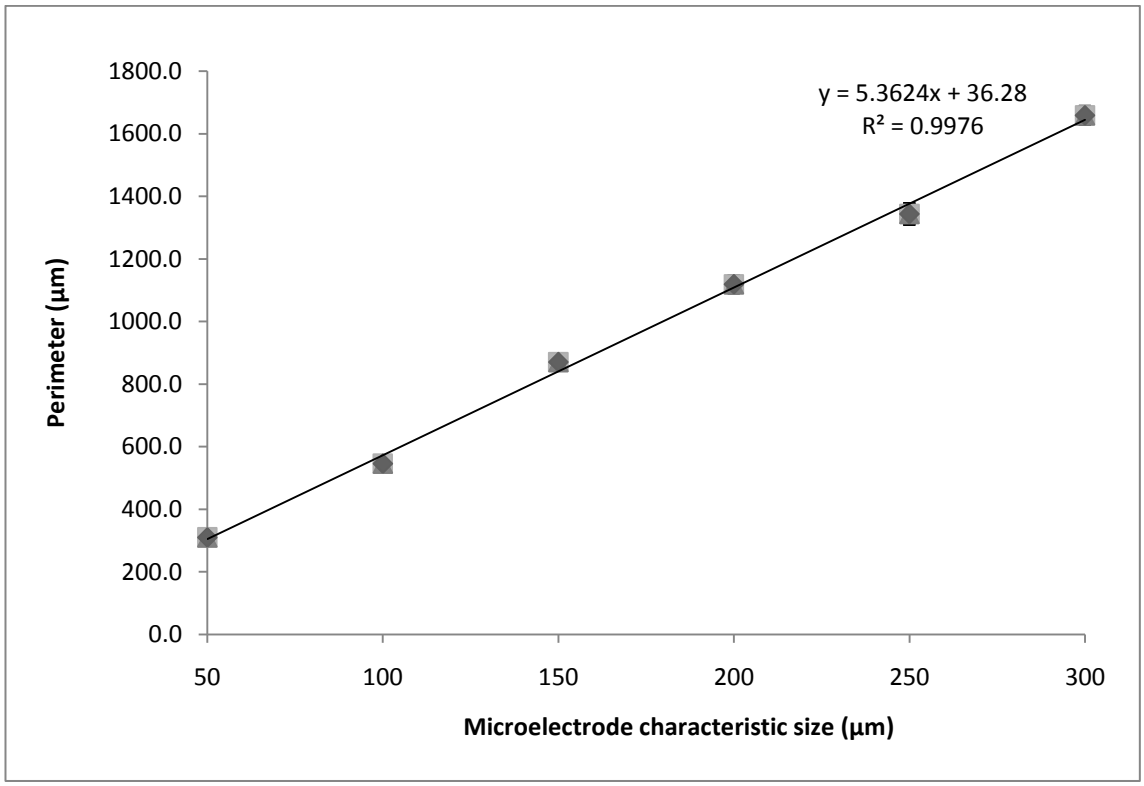

Figure 6.5-1. Analysis of the change in the perimeter of cell aggregates with increasing electrode characteristic size. Error bars depict standard errors of three (3) sample size (n).

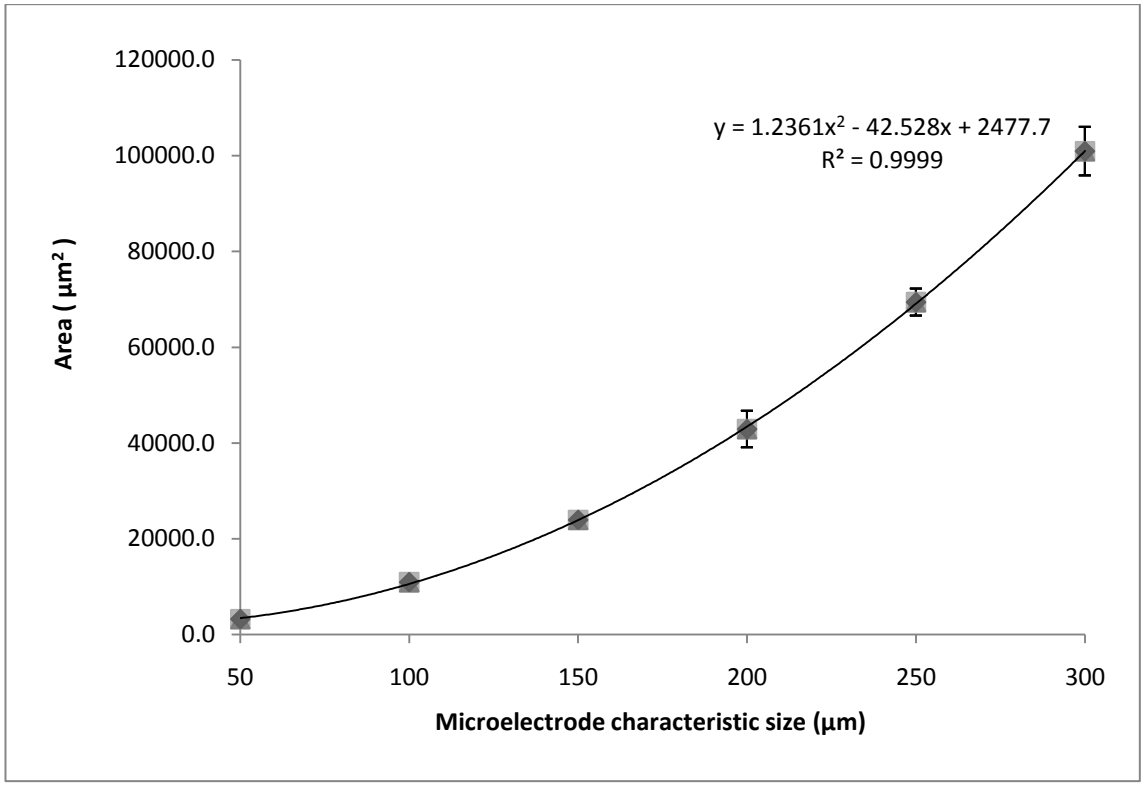

Figure 6.5-2. Analysis of the change in the area of cell aggregates with increasing electrode characteristic size. Error bars depict standard errors of three (3) sample size (n).

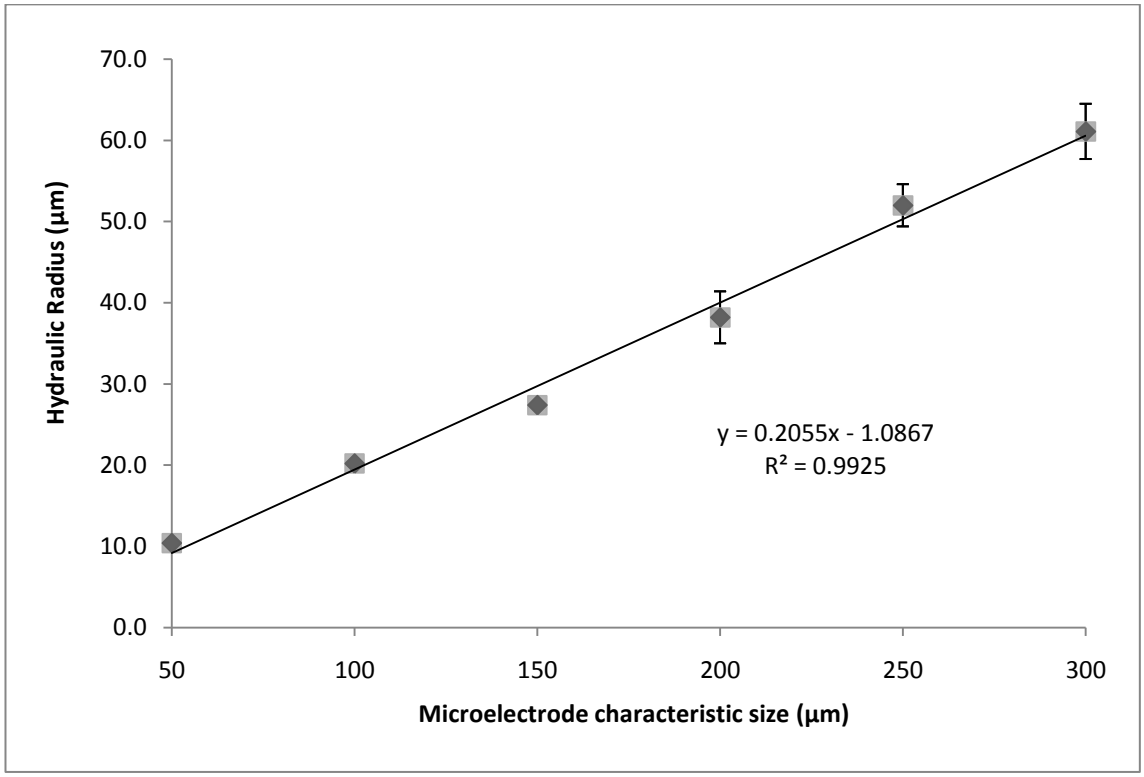

Figure 6.5-3 Analysis of the change in the hydraulic radius of cell aggregates with increasing electrode characteristic size. Error bars depict standard errors of three (3) sample size (n).

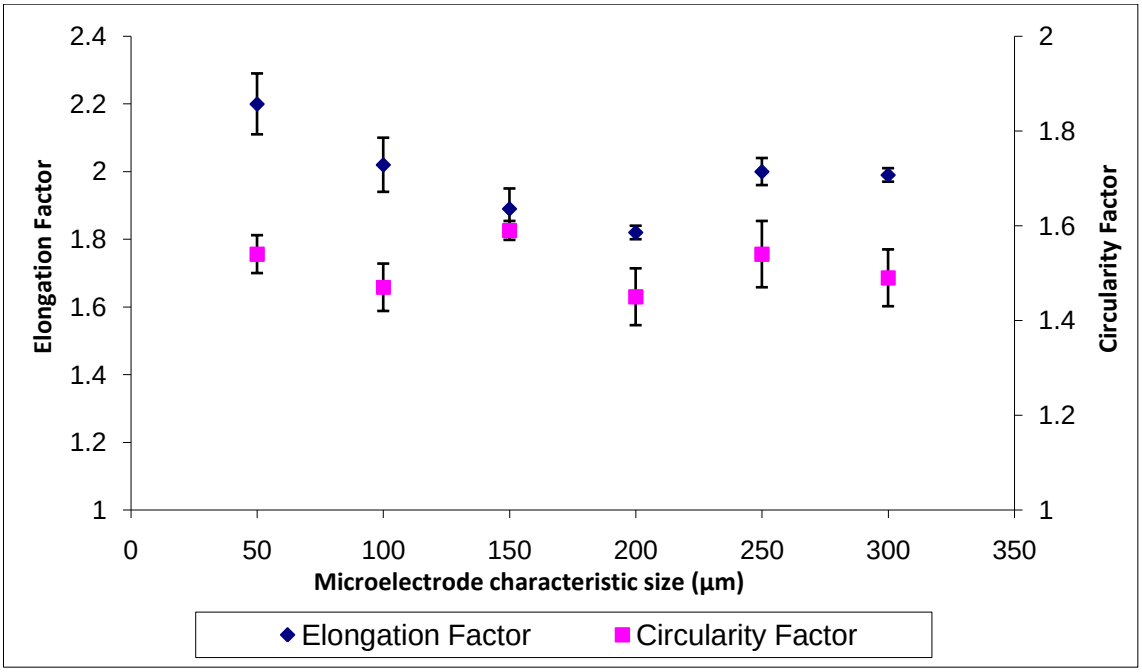

Figure 6.5-4 Analysis of the change in the geometry of cell aggregates with increasing electrode characteristic size, showing the variation in the elongation and circularity factors. Error bars depict standard errors of three (3) sample size (n).

The results of image analysis show that the aggregates tend to be more elongated (i.e. have a higher elongation factor) at smaller electrode sizes (50 µm or less) and at a higher electrode sizes (250 – 300 µm). Between these two range of values, the aggregates have a smaller elongation factor (Figure 6.5-4). As described in Figure 6.5-5, the circularity factor of the aggregates never reach a perfect circle (with Circularity Factor of 1). The values of circularity factor of aggregates fluctuate between 1.4 – 1.6.

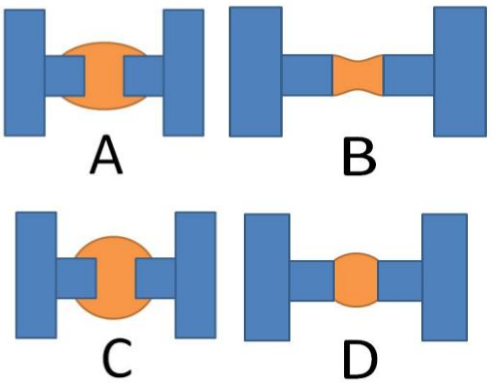

Figure 6.5-5. Illustration explaining changes in elongation and circularity factors of cell aggregates with electrode characteristic size in the regions of: A. < 50 µm, B. 250 – 300 µm, C. 50 – 150 µm, and D. 150 – 200 µm. Both geometries A and B result in higher elongation factors due to extension of cell aggregates to the regions closer to the main castellation bar (A) or higher physical distance (B). Both C and D electrode geometries result in circularity factors that never reach a perfect circle, as similarly shown in (A) and (B).

The fluctuation in roundness (circularity factor) is not only affected by electrode geometry, but also by other factors such liquid flow rates entering the chamber and cell concentrations.

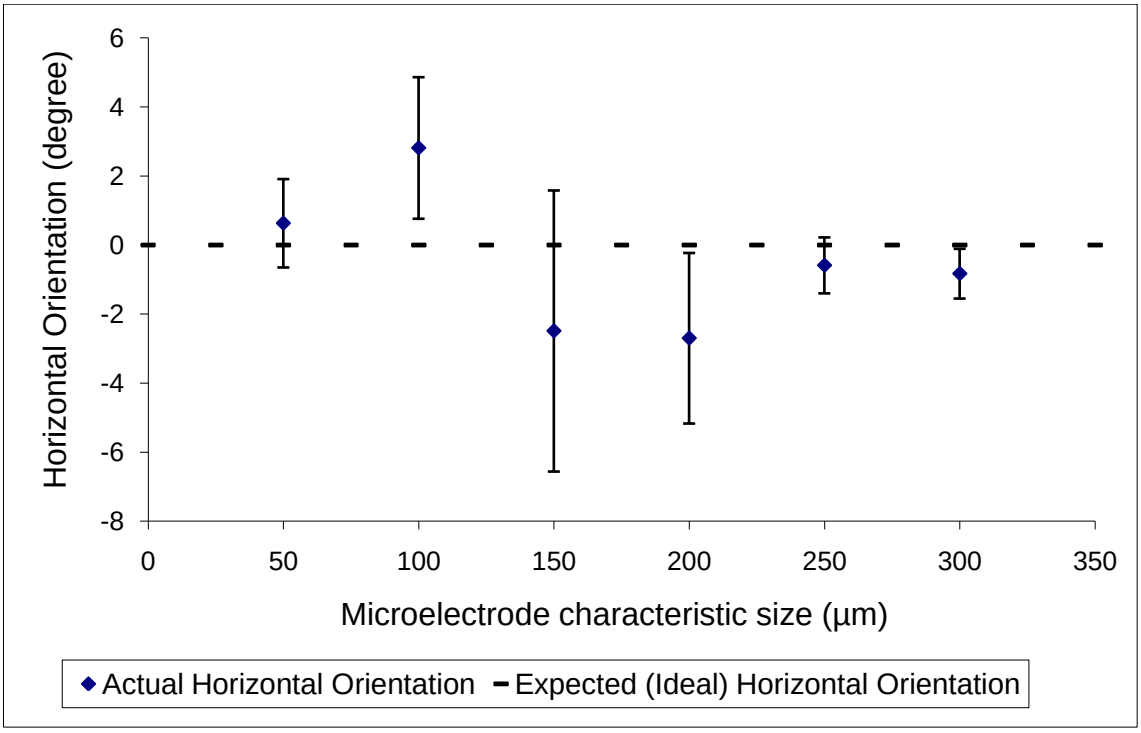

Figure 6.5-6 Analysis of cell aggregates 2D geometry with increasing electrode characteristic size, showing variation in horizontal orientation. Error bars depict standard errors.

The orientation of the resulting cell aggregates relative to the horizontal line (0°) is shown in Figure 6.5-6. As can be seen, the aggregates formed are only slightly (0° - 4°) oriented away from the horizontal line, and the direction can either be clockwise (negative values) or counter-clockwise (positive values).

6.6 Conclusions

It has been shown that dielectrophoresis can be used to create arrays of cell aggregates in well-defined patterns. By controlling the design of the microelectrode geometry it is possible to manipulate the 2D and 3D geometry of the resulting cell aggregates. The relative 3D distribution of the cells in the aggregates is given as a pseudo 3D images using LabVIEW Vision Development module. This includes their spacing (distance and angle between the aggregates), their size and shape as well as cell density distribution.

Control of the timing of the introduction of different cells entering the chamber (e.g. dermal cells followed by epidermal cells on top) allows one to form multi-layers (Sebastian *et al.*, 2007a), making it possible to use the system as a tool for the study of the interactions between cells (Markx *et al.*, 2009).

It has also been shown that the Multi Regions Masking technique greatly simplifies sets of graphical programming (functions) used in image analysis. It allows users to focus directly on the region of interest (ROI) and perform various numerical measurements only on the desired regions (objects). LabVIEW IMAQ Vision Assistant facilitates the development of custom Virtual Instruments for subsequent batch image processing with only a few (minor) threshold level adjustments. The custom VI development is particularly useful if combined with a permanent imaging setup (giving minimum variation in illumination level between acquisition batches). The results of image analysis performed here and the geometry of electrode design used have shown excellent agreement in terms of expected distance, angle and orientation of the desired features.

There are many directions for further research such as the addition of recognition features of biodielectric patterns, based on either shape alone or shape in combination with a distinctive color. This includes algorithm development aimed at individually learning the repeating structure (individual cell aggregate) which will then be used to recognize and subsequently analyze other objects within the same group or categories. Some of these developments may combine or utilize shape recognition techniques with edge-based features (Mikolajczyk *et al.*, 2003).

CHAPTER 7

Towards Engineering Embryonic Skin With Artificial Follicle Precursor Patterns

7.1 Abstract

Regular arrays of cell aggregates can be produced from chicken skin embryonic cells suspended in low conductivity iso-osmotic medium by attracting them by dielectrophoresis using 1 MHz non-uniform AC electric fields to defined locations between microelectrodes. Different placode arrangements, shapes and sizes can be created by changing the electrode design. Immobilization of the cells in hydrogels after patterning gives an artificial skin with placode-like structures. When the artificial skin is incubated in growth medium progressive condensation of the cells in the aggregates can be observed, initially forming micro aggregates which merge into larger aggregates. This condensation process is very complex, and is influenced by pearl chain formation during assembly. In small round aggregates of approximately 50 µm size a single condensate was formed, in larger aggregates many aggregates were formed which were in the main randomly distributed. In long and narrow aggregates there was some evidence for the formation of regular patterns; however, it is unclear whether these regular patterns were a consequence of a biological patterning mechanism such as occurs during a Turing-type reaction diffusion patterning process or Rayleigh-type instabilities during the aggregation process

7.2 Introduction

Some of the best examples of periodic patterns generated during development are those of the feather and hair follicles in avian and mammalian skin. The importance of cell-cell interactions in this tissue has long been appreciated, being supported by innumerable embryonic tissue grafting experiments (Sengel, 1990; Dhouailly *et al.*, 2004). The avian and mammalian embryo is initially covered with a simple epithelial sheet in which each cell has a choice of two fates: they can opt to become follicles, or else they become skin proper (Figure 7.2-1 part A). In just 2 days (in mouse and chicken) these naïve cells choose between the two options, resolving themselves into a pattern of equally spaced follicles, with the cells between the follicles becoming skin (see Figure 7.2-1 part B). Throughout this process interactions between the epithelium (the epidermis) and underlying mesenchyme (the dermis) are required (Sengel, 1990;

Lin *et al.*, 2006b). Neither tissue attempts to make a follicle when maintained in isolation (Jiang *et al.*, 1999). The first morphological indication of follicle formation is the condensation of epithelial and mesenchymal cells to form a placode. Whether this focal increase in cell density is wholly an outcome of prior chemical signaling, or whether it has an instructive effect on follicle development, is unknown.

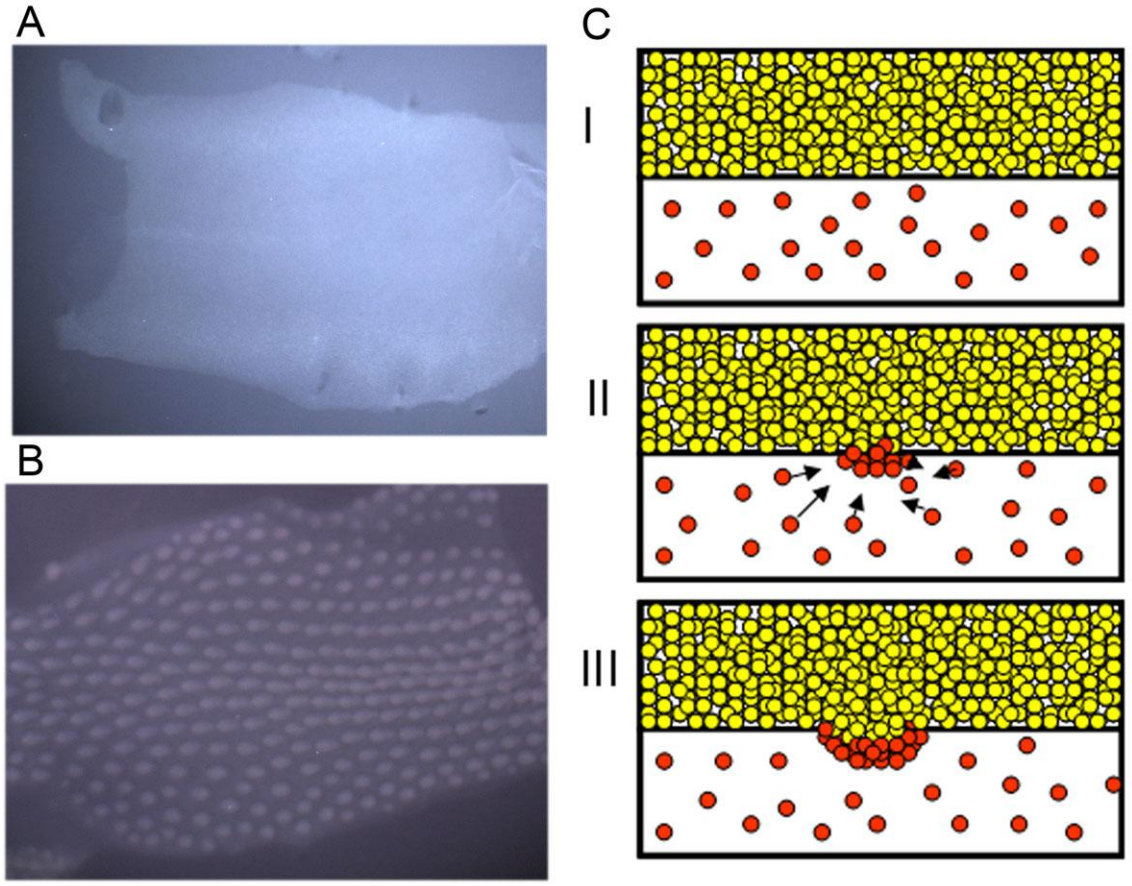

Figure 7.2-1. Bud formation in embryonic chicken skin. A. Embryonic chicken skin at day 6, before the formation of feather buds. B: Embryonic chicken skin at day 8. Fully developed feather buds in regular arrays can be observed. C: Outline of phenomena that can be observed during bud formation: I: epidermis and dermis up to day 6 do not shown any sign of bud formation; II: bud formation starts by the migration of dermal cells to form placodes; at this stage cell commitment is still reversible; III: formation of stable dermal condensates (images courtesy of Ankita Singal).

Various Reaction-Diffusion models have been used to explain the formation of hair follicle and feather primordia (Harris *et al.*, 1984; Baker *et al.*, 2009), and have shown that the initial conditions and the way pattern formation is initiated can strongly affect the pattern formed. This is exemplified in Figure 7.2-2, which shows the results of the mathematical modeling of follicle formation in mouse and chicken. The biochemical mechanisms involved in hair formation in mouse and feather formation in chicken are

very similar. Figure 7.2-2 part A shows the results starting with a random distribution of cells, resulting in the spontaneous formation of follicles in an irregular pattern similar to that of hair follicles in mouse (or human) skin. Figure 7.2-2 part B on the other hand shows the results of modeling of chicken feather follicle formation as wave, in which follicle formation starts at a center line (above the neural tube for the feathers forming on the back of a chicken embryo), and then travels outward, giving rise to a regular hexagonal array of follicles (Baker *et al.*, 2009).

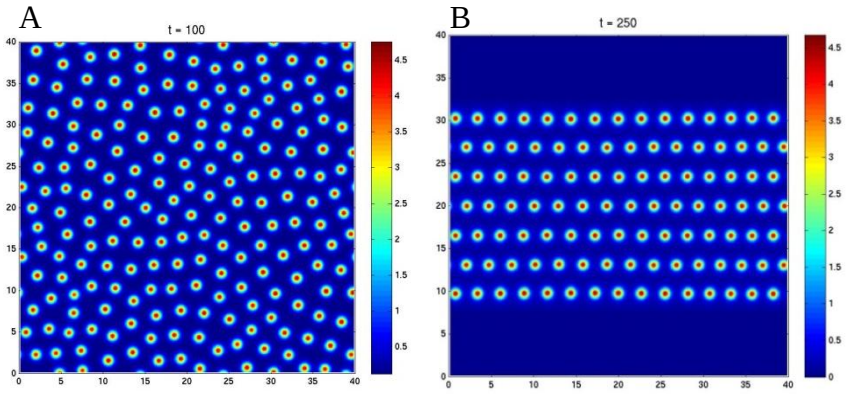

Figure 7.2-2. Modelling of follicle pattern formation based on a Turing-type reaction-diffusion system. A: random arrangements of aggregates are formed when aggregates formation can be initiated anywhere on a surface; B: a regular hexagonal array is formed when aggregate formation is initiated at a line in the centre, and travels as a wave through the tissue (images courtesy of Ankita Singal and Kevin Painter).

The initial regular pattern above the neural tube in chicken may be formed by a reaction-diffusion by confining the pattern to a long narrow strip of skin (Figure 7.2-3).

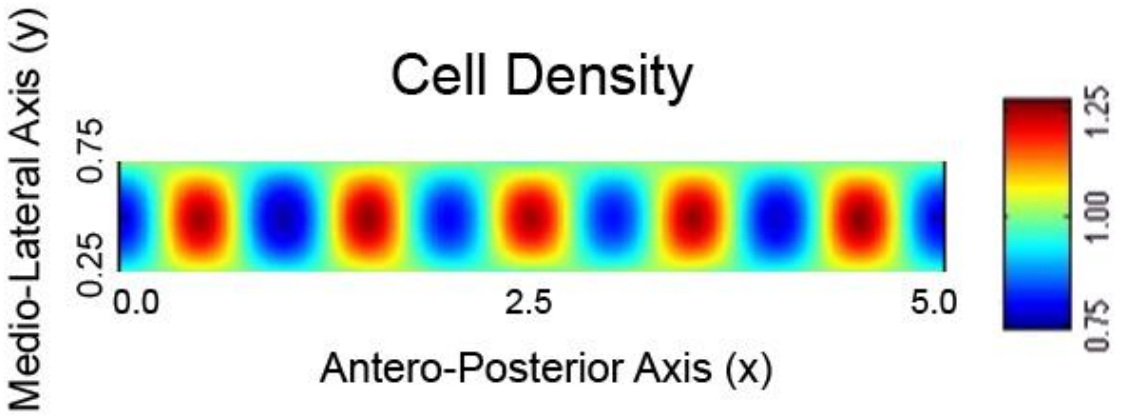

Figure 7.2-3. Simulation of pattern formation during skin follicle formation in a long narrow strip of skin. The simulation is based on a model from Lin *et al*. (2009), in which the pattern is proposed to be due to inhibition of p-ERK. Confining pattern formation to a long narrow strip leads to spatial oscillations occurring, resulting in spots

of high and low cell density. The periodic cell density distribution leads to regular patterns of follicle primordia during mesenchymal condensation stages as are found along the neural tube.

The quantities involved in the models, such as cell density, forces and chemical gradients, are both controllable and measurable. It should therefore be possible to obtain experimental values for parameters in the models, which should enable one to experimentally validate the models. However, as the formation of hair and feather primordia occur at early stages during embryogenesis, the scales involved are at the microscopic level. In order to have full control over all factors that control follicle formation at the microscopic level, a microfabrication/tissue engineering approach (Khademhosseini *et al.*, 2006b), in which artificial skin is created and full control over the initial distribution of cells and other components is obtained, seems most suitable.

This chapter will describe attempts of producing artificial skin with well-defined local skin properties, concentrating on the production of artificial skin with locally defined cell densities followed by studying their immediate (short-term) response or behavior as a result of being newly reconstructed in 3D shape using dielectrophoresis. Previously, alteration of cell density in a homogeneous manner across the entire skin field has been shown to influence the feather patterning process (Jiang *et al.*, 1998). Here, the aim was to build on these observations by engineering heterogeneous cell densities in assembled skin, essential if we are to understand the impact of this phenomenon on development. The method chosen for the creation of such local changes in cell density was dielectrophoresis - the induced movement of particles in non-uniform (AC) electric field (Pohl, 1978; Jones, 1995; Hughes, 2003). The method involved the attraction of cells to (or repulsion from) high field regions created by the application of high frequency AC electric signals to microelectrode arrays. Dielectrophoresis is a versatile technique that is increasingly used in cell manipulation, separation, characterisation and other applications (Pethig and Markx, 1997); applications of dielectrophoresis in tissue engineering, including the formation of stem cell microniches (Markx, 2008; Markx *et al.*, 2009), have been reviewed recently (Markx, 2008).

7.3 Materials and Methods

7.3.1 Isolation of cells

Dorsal chicken embryonic skin was obtained by dissecting 8-day old white leghorn chicken embryos (E8). GFP+ chicken embryos were also used in a cell tracking experiment in combination with cells from non-GFP (or GFP-) embryos. The GFP+ embryos were from a kind contribution of Dr. Denis J. Headon (Roslin Institute, Edinburgh – UK). Skin cells (a mixture of epidermal and dermal cells) were obtained by dissociating the dorsal skin tissue using 0.5% (v/v) trypsin / EDTA solution for 60 minutes, inside an incubator set at 37ºC and 5% CO_2, followed by enzymatically breaking the tissue into individual cell component. Both epithelium and mesenchyme cells were pooled into a single eppendorf tube. To ensure individual cells were obtained, they were gently and repeatedly drawn through a pipette with decreasing bore size or a fine syringe needle. At 1 MHz the maximum DEP force is exerted at very low medium conductivity; for this reason the cells were suspended into 300 mM sorbitol by repeated centrifugation and decanting of the supernatant. The final cell concentration used was approximately $3.75x10^6$ cells mL^{-1}. Cells from freshly dissected tissue were used in each DEP experiment. All tools used in the experiment, including the ones used for dissecting the tissue, were sterilized by autoclaving. Buffer solution was passed through a 0.45 μm filter for sterilization.

In some experiments, separation between epidermal and dermal tissue was done using a fine needle prior to enzymatic digestion. The epidermal and dermal cells were then treated separately.

7.3.2 Microelectrode fabrication, electric field simulation and construction of DEP chamber

Microelectrodes of the different interdigitated designs with or without castellations were drawn using Protel Design Explorer 99 and a photo mask (made of an acetate film) was printed by J.D Photo Tools, Oldham – UK. Following this, the microelectrodes of the required design were made using photolithography from ITO covered microscope slides (Delta Technologies, USA) as described previously (Flores-Rodriguez and Markx,

2006). Electric field distribution was calculated using COMSOL Multiphysics 3.4 as described previously (Sebastian *et al.*, 2007b). A chamber was created above the electrodes of height 400 μm, width 20 mm and length 25 mm using a microscope slide cover slip and an insulating tape as a spacer, leaving the sides open to allow cell suspension, suspending medium and other fluids to be pumped into the chamber using a Rainier low-pulse low flow peristaltic pump. All glass slides electrodes were autoclaved prior to experiments and cleaned using 70% alcohol after each experiment.

7.3.3 Formation of cell aggregates using dielectrophoresis

Following the introduction of cells suspended in 300 mM sorbitol solution, a 1 MHz 20 $V_{pk\text{-}pk}$ (electrodes with 100-300 μm characteristic size) or 10 $V_{pk\text{-}pk}$ (50 μm characteristic size) sinusoidal signal was applied to the microelectrodes using a Thurlby-Thandar TG120 signal generator in order to attract cells to high field regions between the electrodes using positive dielectrophoresis. Fresh 300 mM sorbitol was continuously pumped into the chamber at a rate of 40 μL min^{-1} to keep the medium conductivity low and the positive DEP force high. The aggregates obtained their full height in approximately 20 minutes. After their formation, the electric field was maintained for a further 10 minutes; this forced the cells to adhere to each other, and stabilized the aggregate (Sebastian *et al.*, 2007a).

7.3.4 Immobilization of the cell aggregates pattern for developmental studies

To form a skin-like material following cell aggregate pattern formation by DEP, liquid-phase PuraMatrix™ peptide hydrogel precursor was introduced into the chamber at 50% concentration in 300 mM sorbitol and 5 μL. $minute^{-1}$ flow rate using a peristaltic pump. To solidify the gel DMEM medium (containing ionic compounds) was added at both ends of the open-ended chamber.

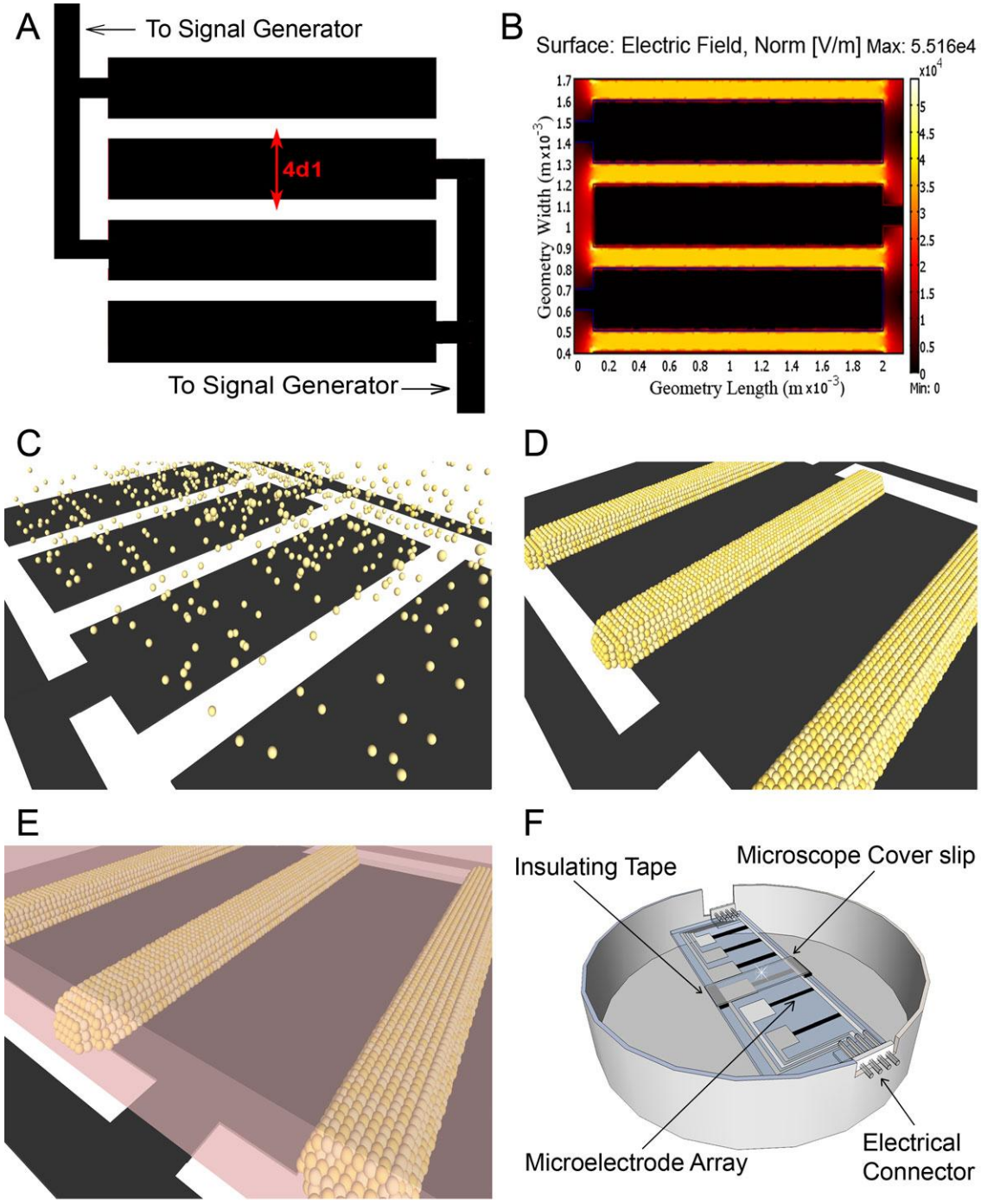

Figure 7.3-1. Outline of the method used to create artificial skin using dielectrophoresis. A: Microelectrode is designed. B: Electric field distribution is calculated. C: Cell suspension is introduced into the chamber. D: Under the conditions chosen (1 MHz, low conductivity medium) the cells are attracted by the DEP force to the high field regions between the electrodes and form aggregates whose position, size and shape were determined by the electric field pattern. E: Hydrogel is introduced to immobilize the cells in an artificial skin-like material and F: Chamber is placed in a Petri dish for culture.

Excess hydrogel solution must fully replace the low conductivity (sorbitol) buffer inside the chamber in order to ensure gel formation as artificial extracellular matrix as shown

in Figure 7.3-1. The liquid medium in which the aggregates were formed (in a 300 mM sorbitol solution) was replaced by a 50% PuraMatrix™ solution. Once the solution had gelled the artificial skin was incubated at 37ºC, 5% CO_2 air, and a fresh continuous flow of DMEM growth medium at 40 µl. minute^{-1} flow rate was supplied to the artificial skin. The behavior of the cells in the aggregates was observed by microscopy.

For long-term study of the cell aggregates, the slide with the artificial skin under a cover slip was placed in a petri dish as shown in Figure 7.3-1 part F. To supply the necessary nutrients a constant flow of fresh DMEM medium (40 µL. min^{-1}) was supplied to one side of the artificial skin, and allowed to flow over the slide. The slide was slightly inclined to aid in this process. The whole setup was placed inside an incubator at 37ºC and 5% CO_2, and removed regularly to observe the cells microscopically.

7.4 Results

7.4.1 Formation of aggregates with dielectrophoresis

Dielectrophoresis can be used to form cell aggregates in well-defined patterns at the high electric field regions in a microelectrode array (Pethig and Markx, 1997; Sebastian *et al.*, 2007b; Yusvana *et al.*, 2009). The electric field calculations based on a certain design of electrode castellation (as shown in Figure 7.4-1) indicate that patterns of high field regions could be created similar to that found in chicken skin, as well artificial patterns that are not normally found in chicken (Figure 7.4-2).

The first set of experiments demonstrate that it was possible to replicate placode patterns observed in real skin, as well as artificial patterns. Figure 7.4-2 part A shows that the dielectrophoretic methods can be used to create linear aggregations of cells, similar to the one observed in the first stages of feather development near the neural tube. Figure 7.4-2 part B shows that placode-like aggregates in a hexagonal pattern can be artificially created using dielectrophoresis, at a scale similar to that found in embryonic chicken skin at the later stages. Figure 7.4-2 part C to F shows that it is possible to make changes in a given pattern, including changes in the aggregate size, shape and the distance between the aggregates simply by changing electrode design accordingly. The effect of using various geometries of electrode design on the resulting

size, shape and pattern of the aggregate has been described previously (Chapter 5 and 6) as well as works done by other researchers (Sebastian *et al.*, 2007b).

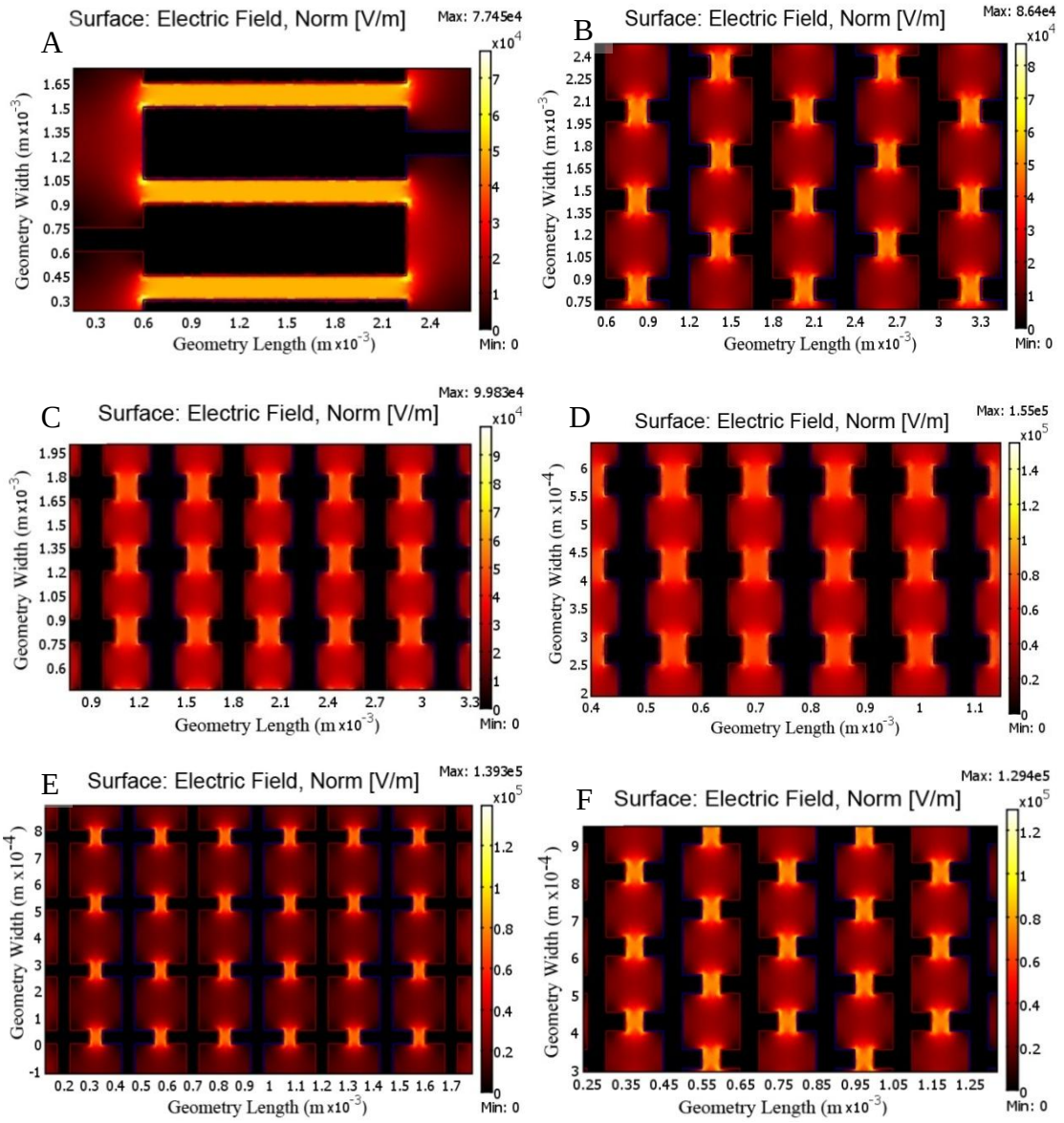

Figure 7.4-1. Electric field calculations in a variety of microelectrode structures. A: Line pattern with characteristic size (d) of 150 µm; B: Hexagonal pattern with characteristic size (d) of 150 µm. C: Square pattern with characteristic size (d) of 150 µm; the distance between high field regions is 3d; D: Square pattern with a characteristic size (d) of 50 µm; the distance between high field regions is 3d; E: Square pattern with a characteristic size (d) of 50 µm; the distance between high field regions is 5d; F: Hexagonal pattern with characteristic size of 50 µm.

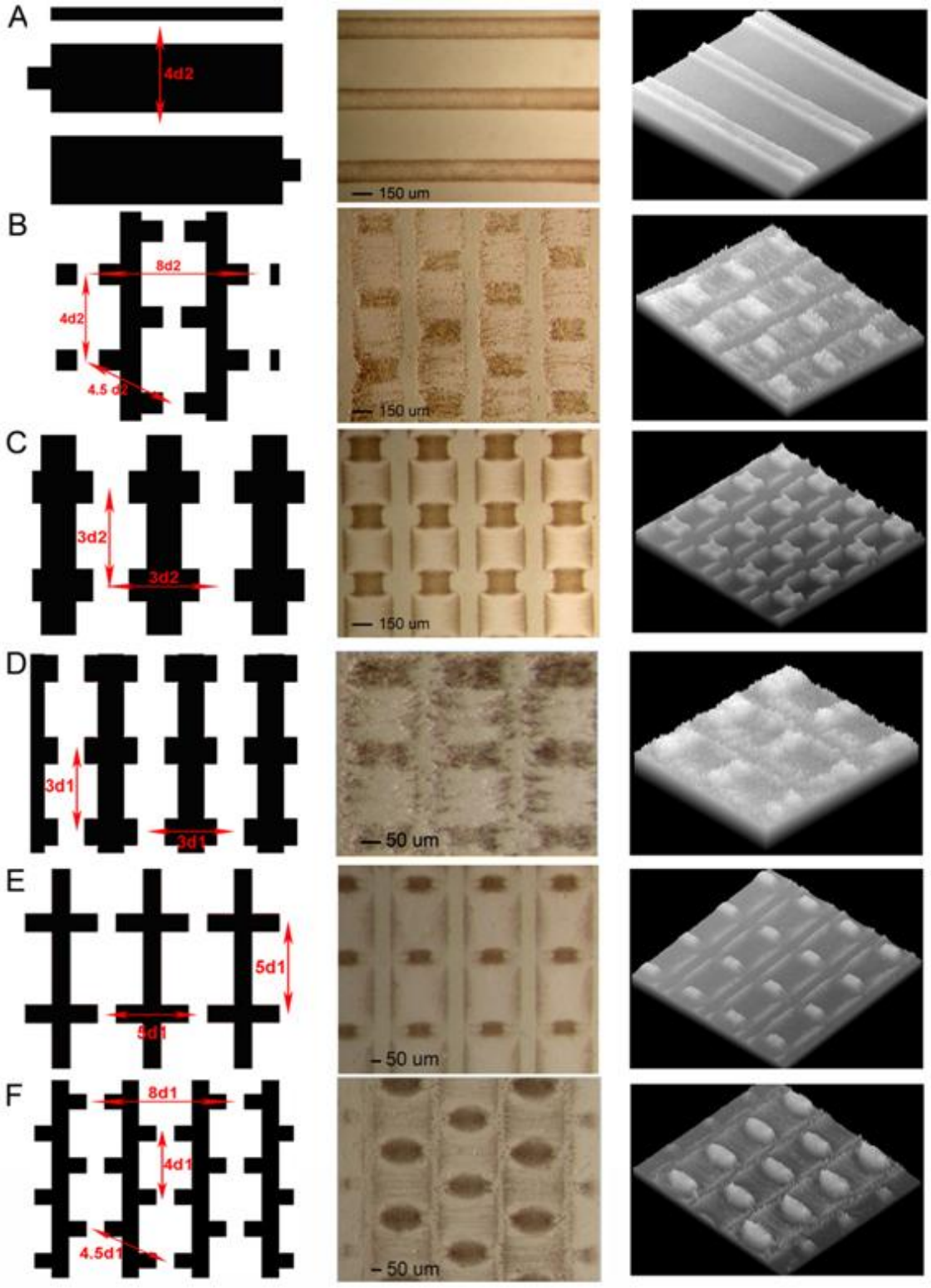

Figure 7.4-2. Aggregates of embryonic chicken skin cells formed by attracting suspended cells to high electric field regions between interdigitated microelectrodes. On the left column, the electrode design is shown. On the middle, a bright field image of the aggregates formed. On the right, 3D representation of the cell aggregates pattern, based on pixel intensity of the image. A: Parallel lines, d2 = 150 µm. B: Hexagonal arrangement, d2 = 150 µm. C: Square pattern, d2 = 150 µm; the aggregate distance is 3 x aggregate size d2; D: square pattern, characteristic size d1 = 50 µm; the aggregate distance is 3 x d1. E: square pattern, characteristic size d1 = 50 µm; the aggregate distance is 5x aggregate size d1. F: Hexagonal arrangement, d1 = 50 µm.

7.4.2 Cell aggregate formation without dielectrophoresis

Control experiments were done to investigate whether skin cells have the ability to self-aggregate (and move) *in vitro*. Chicken embryonic skin tissue was previously trypsinized for 1 hour (0.5% v/v) to dissociate the tissue into individual cells. The cells were then washed and centrifuged several times to remove the trypsin, and resuspended in DMEM. Skin cells were allowed to settle overnight in medium (DMEM) contained in plastic container for about 10 hours at 37°C and 5% CO_2.

Figure 7.4-3 shows the result of control experiments in which a suspension of embryonic chicken skin cells in DMEM was placed in a plastic well at low and high cell densities, which shows that after incubation overnight many of the cells had formed condensates at random locations. It is clear from this experiment that simple mixtures of epidermal and dermal embryonic cells actively associate *in vitro*, forming cell condensates. Initial cell population density appears to play a role in determining the number of cell condensates formed after certain period of time. At relatively low initial cell concentration (Figure 7.4-3 C), the number of cell condensates is less than at relatively higher initial cell concentrations.

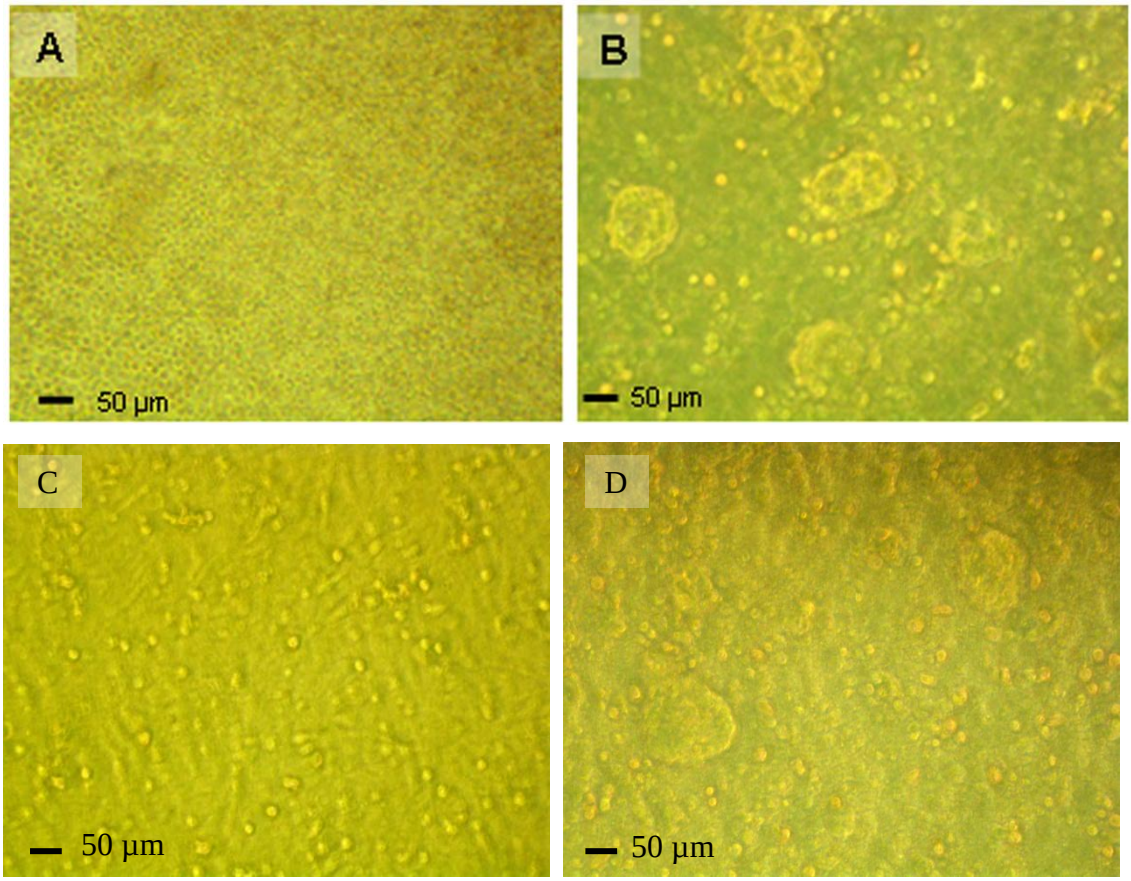

Figure 7.4-3. Aggregation of chicken skin cells in suspension. A. Initial conditions. B. After 10 hours incubation. Condensates have been formed randomly. C. Low density suspension at start. D. After incubation for 10 hours. Less condensates were formed.

7.4.3 Behavior of cells in small aggregates in a hexagonal pattern

Having shown that artificial patterns of embryonic skin cells of different designs can be created, and also that a mixture of dissociated dermal and epidermal embryonic stem cells are able to form cell condensates, it was decided to investigate the effects of domain size and shape on the *in vitro* cell condensation.

In the first set of experiments, the effect of aggregate size on the condensation process was investigated. Figure 7.4-4 and Figure 7.4-5 show cell behavior in small aggregates in a hexagonal pattern after having been immobilized in PuraMatrix™ hydrogel and incubated at 37ºC, 5% CO_2 air, and a continuous flow of DMEM growth medium. In the first 12 hours a slight expansion of the cell aggregates occurs. At the same time the cells start to condense into tighter aggregates. Typically, only one condensate was formed in each aggregate near the centre. Condensate formation in the smaller-size aggregates was typically simultaneous, although at the start there is some tendency for the condensation

process to occur at the edges of the artificial tissue, presumably because of the higher concentrations of nutrients and oxygen there. There was no evidence of interaction between aggregates.

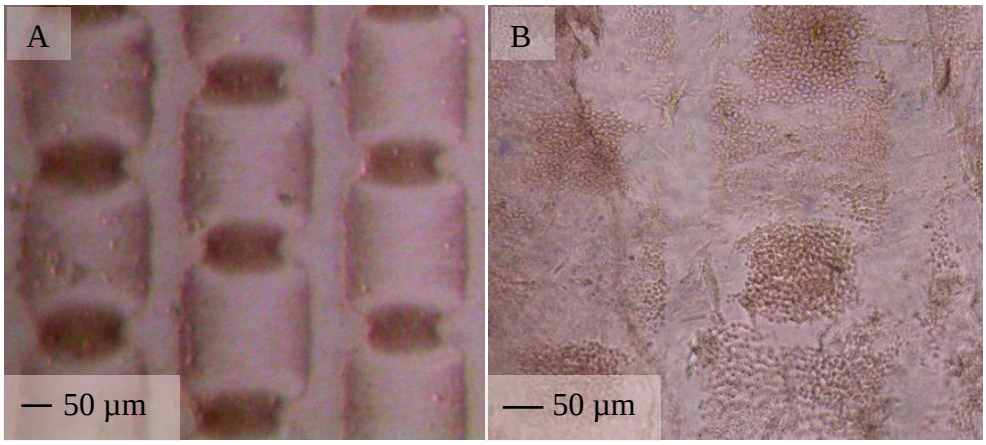

Figure 7.4-4. A. Aggregates of embryonic skin cell in aggregates in a hexagonal pattern formed by DEP using interdigitated oppositely castellated microelectrode with a characteristic size 50 µm. A. Immediately after immobilisation in PuraMatrix peptide hydrogel (viewed under wide field stereo microscope). B. Aggregates after 12 hours (viewed under higher magnification microscopy)

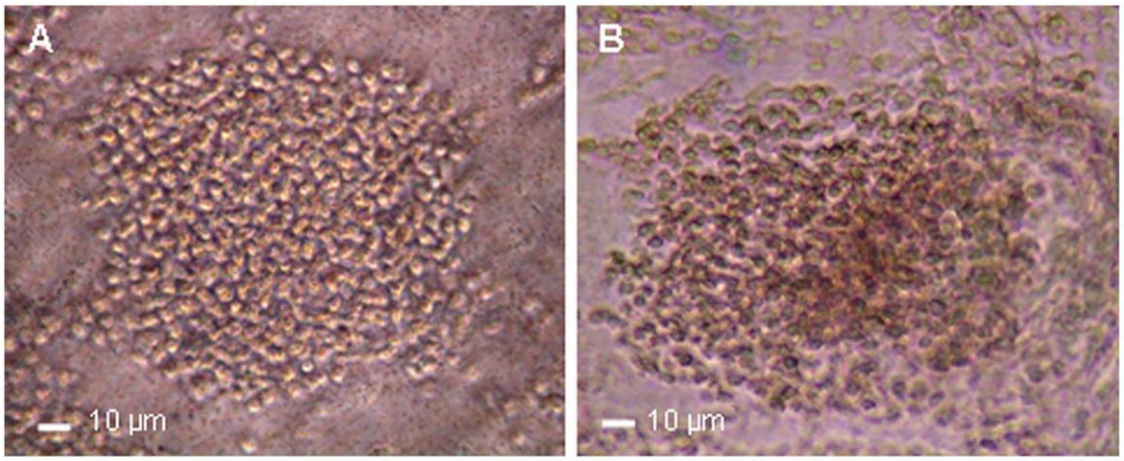

Figure 7.4-5. Close-up views of small aggregates of dorsal embryonic chicken skin cells. Aggregates were formed by DEP using interdigitated oppositely castellated microelectrodes with a characteristic size of 50 µm. Cells were immobilised in a 50% PuraMatrix peptide hydrogel. A: Close-up of single aggregate at the start. B: Formation of a (single) condensate can be observed after 18 hours of incubation.

7.4.4 Behavior of cells in large aggregates in a hexagonal pattern

Figure 7.4-6 shows cell behavior in large aggregates formed with DEP. These large aggregates were also arranged in a hexagonal pattern. It can be seen that the larger

aggregates give rise to multiple cell condensates. Condensate formation in the large aggregates was predominantly random, although at the start there is some tendency for the condensation process to start in parallel lines between the castellations. Cells tend to form "pearl-chains" during the dielectrophoretic assembly process due to the mutual attraction between the dipoles induced in the cells in the electric field. It is therefore possible that the lines observed are a consequence of pearl chain formation during the DEP assembly process.

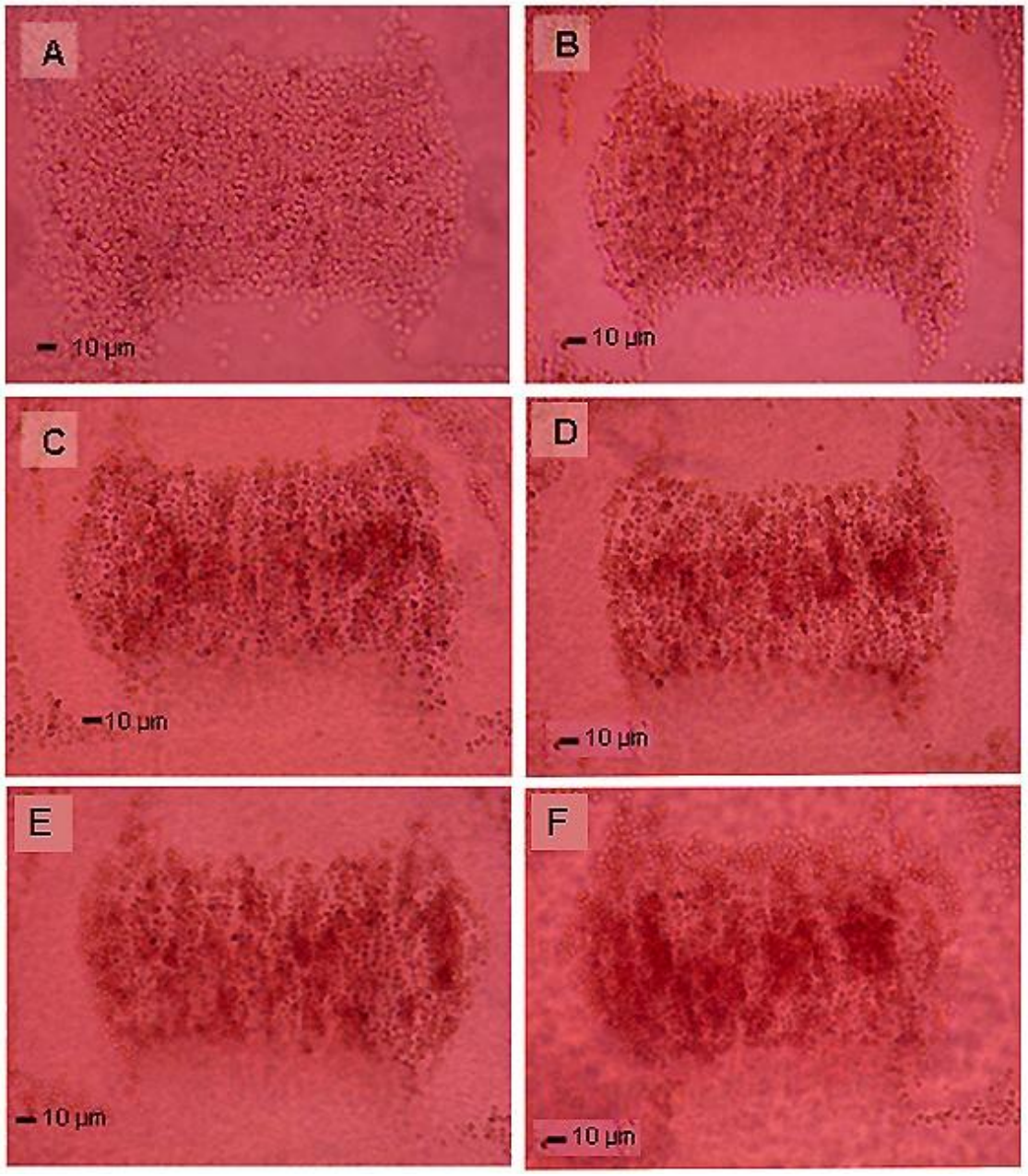

Figure 7.4-6. Development of large aggregates of dorsal embryonic chicken skin cells. Aggregates were formed by DEP in a hexagonal pattern using interdigitated oppositely castellated microelectrodes. The castellations are oriented vertically in the images shown and gave an aggregate with a nominal size of 150 x 300 µm. Cells were

immobilised in a 50% PuraMatrix peptide hydrogel. A: Initial conditions; B: Cell aggregate after 3 hours; C: After 12 hours; D: After 15 hours. E. After 18 hours and F. After 21 hours.

In the end, however, the cell condensates appear to be randomly spread across the aggregates. Aggregates in the hexagonal pattern are separated physically from each other, and there was no evidence of any interaction between aggregates. Other images of large cell aggregates after 21 hours resulting from this experiment are shown in Figure 7.4-7.

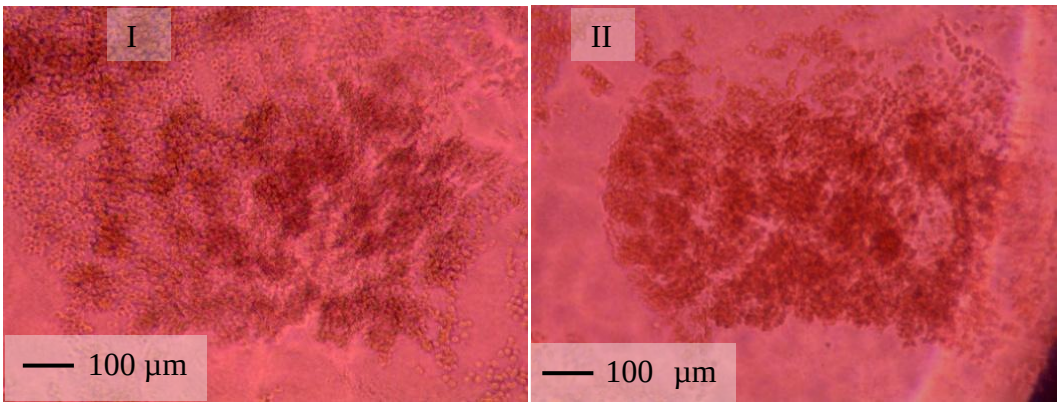

Figure 7.4-7. Large aggregates after 21 hours

7.4.5 Behavior of cells aggregated in a line pattern

Figure 7.4-8 shows an aggregate containing a mixture of dermal and epidermal cells, arranged in a line pattern. The aggregates were formed by dielectrophoresis between parallel interdigitated electrodes with no castellations, producing a line pattern similar to that in chicken embryonic skin at the earliest stages of feather placode formation. Figure 7.4-9 shows a time line view.

Aggregates maintain their DEP-assigned line pattern under the support of PuraMatrix™ peptide hydrogel. After the formation of the aggregates, a slight expansion of the line could be observed initially. Simultaneously the cells started to adhere to each other within the line. This effect was more pronounced at the electrode edges, where the cells would preferentially have accumulated as the electric field strength there is strongest, but occurred throughout the line. The aggregation then proceeded to give rise to cell condensates, with tightly packed cells. The shape and size of the condensates varied (Figure 7.4-8); but included dots and irregular lines (Figure 7.4-8 part E and

F).Condensates grew and became denser in time (see for example Figure 7.4-11 and Figure 7.4-12), indicating cell growth and division.

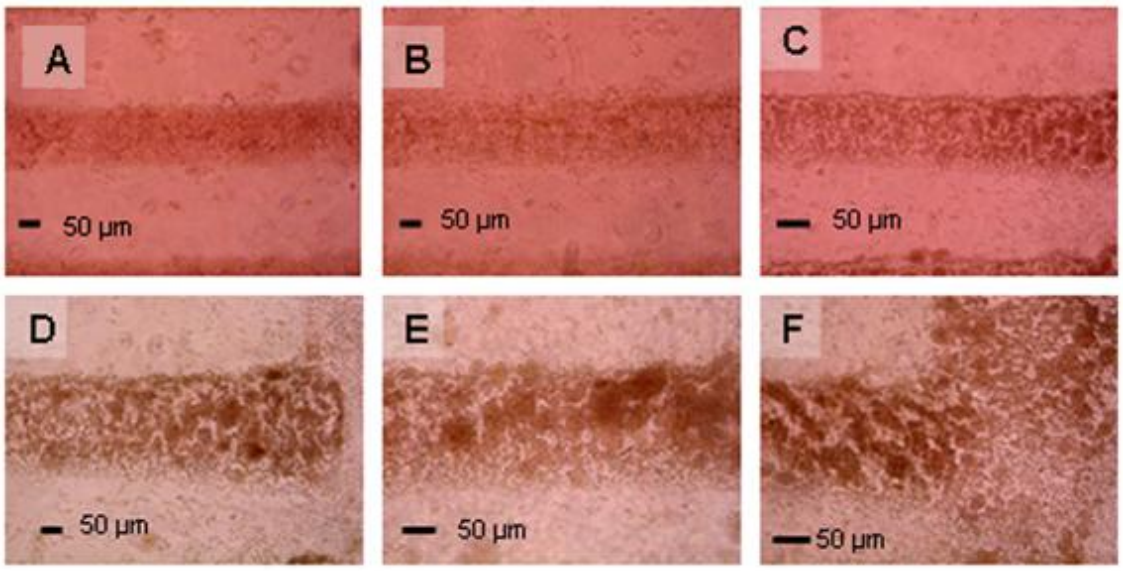

Figure 7.4-8. Behaviour of chicken embryonic skin cells after having been arranged in line pattern by dielectrophoresis; the cells were embedded in a 50% PuraMatrix™ gel. A: After 3 hours; B: After 6 hours; C: After 18 hours; D: After 21 hours; E: After 25 hours; F: After 25 hours; different area shown. Observed behaviour includes expansion of the aggregate (0-6 hours), formation of small condensates (0-18) hours followed by the formation of larger cell condensates (18 hours and later).

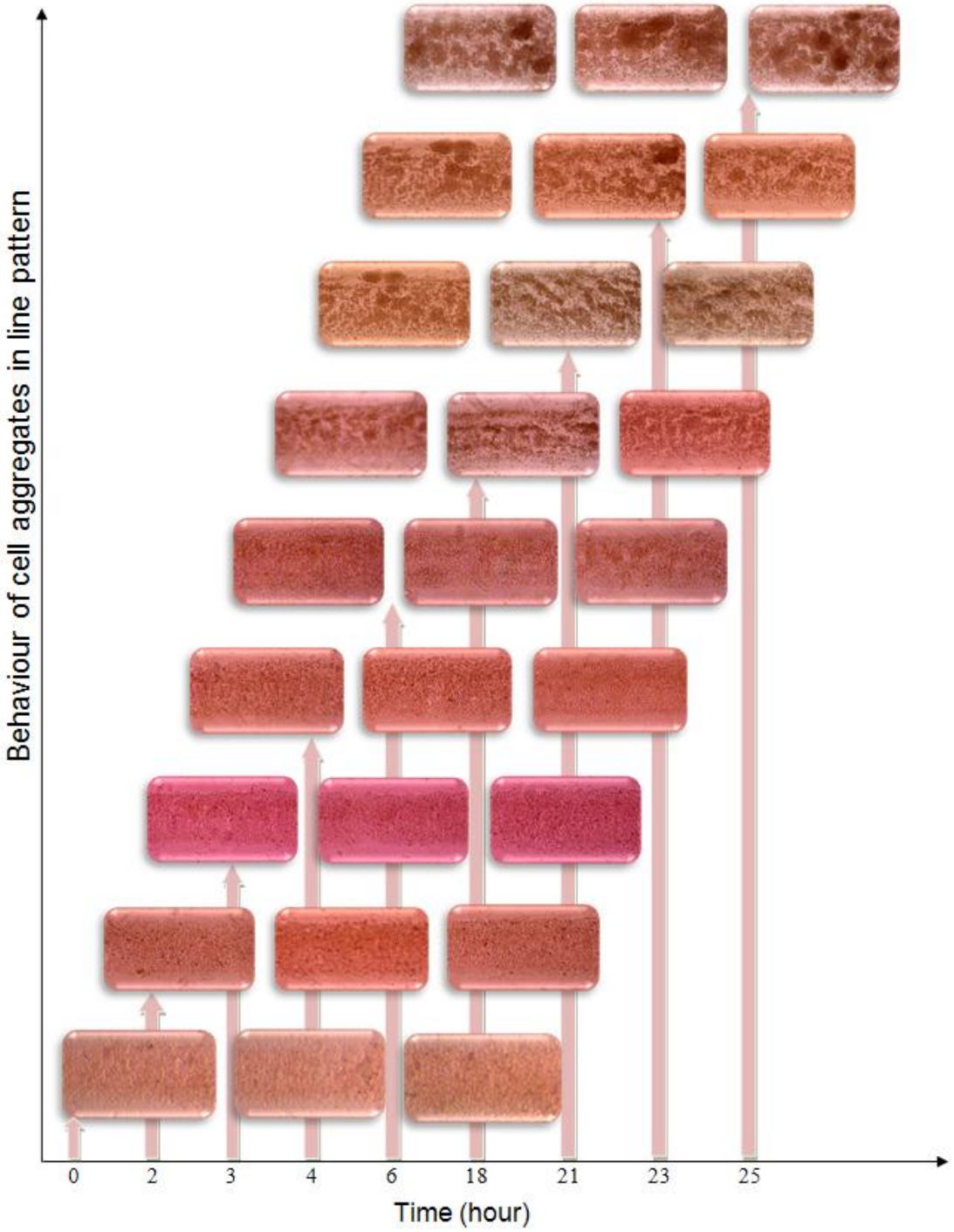

Figure 7.4-9. Time-line view of chicken embryonic skin cells after having been arranged in line pattern by dielectrophoresis; the cells were embedded in a 50% PuraMatrix™ gel.

Figure 7.4-10 to Figure 7.4-12 show close-up of the cells in a line pattern 10, 24 and 36 hours after their formation. It can clearly be seen that the cells initially form micro aggregates. Some of the micro aggregates then grow by acquisition of cells from other aggregates. This process, and the increase in cell number by cell division leads to the formation of large cell condensates.

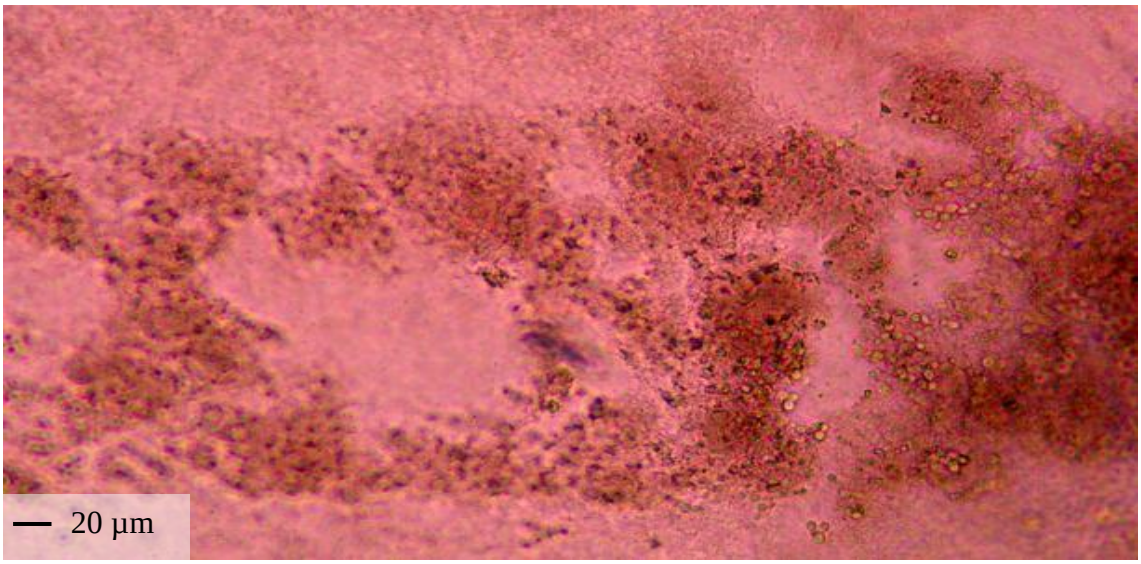

Figure 7.4-10. Condensates of chicken embryonic skin cell around 10 hours post DEP and gel immobilization. The cells are a mixture of epidermal and dermal cells. The aggregate was initially constructed in a line pattern of 150 by 1000 µm.

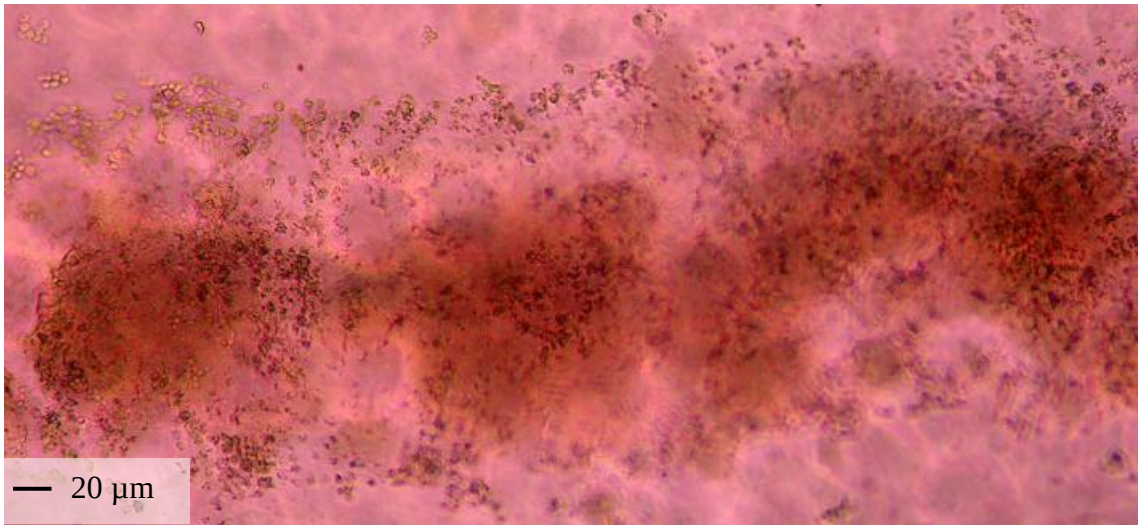

Figure 7.4-11. Condensates of chicken embryonic skin cell around 24 hours post DEP and gel immobilization. The cells are a mixture of epidermal and dermal cells. The aggregate was initially constructed in a line pattern of 150 by 1000 µm.

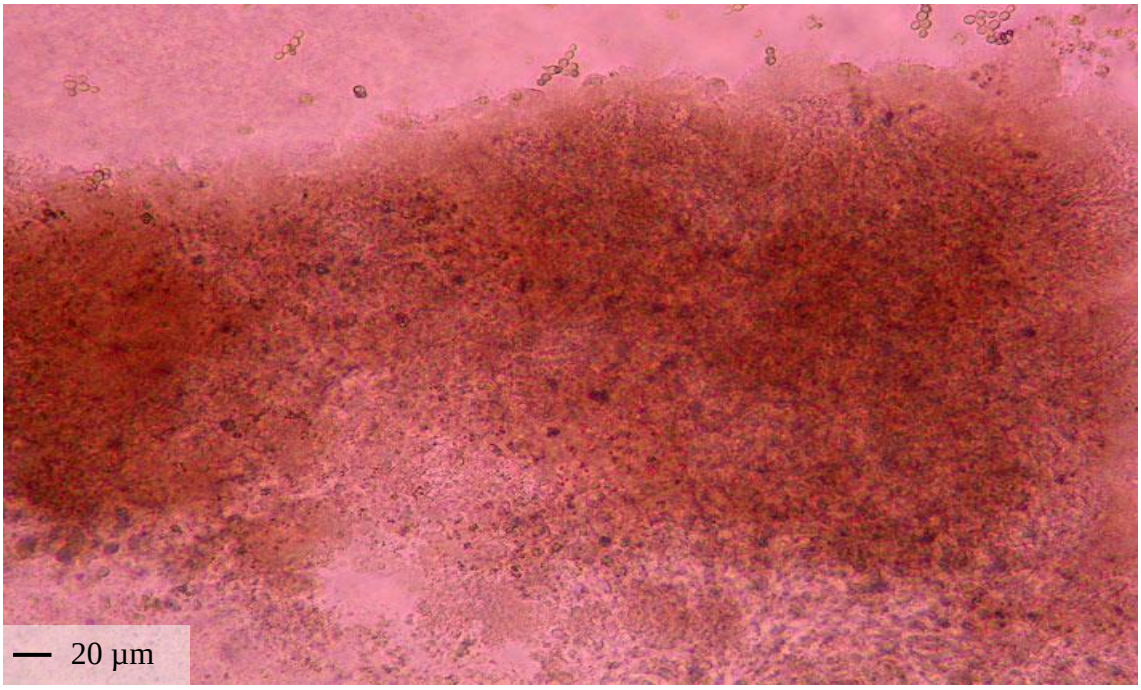

Figure 7.4-12. Condensates of chicken embryonic skin cell around 36 hours post DEP and gel immobilization. The cells are a mixture of epidermal and dermal cells. The aggregate was initially constructed in a line pattern of 150 by 1000 µm.

Oxygen and nutrient availability appears to play a critical role in the development of the aggregate after their formation. The sites of the most active condensate formation occurred at the end of the DEP chamber where fresh nutrients (DMEM) entered the chamber and the aggregates had more direct access to oxygen (Figure 7.4-13). Cells at the other end of the chamber began to form condensates later, and remained more sparse.

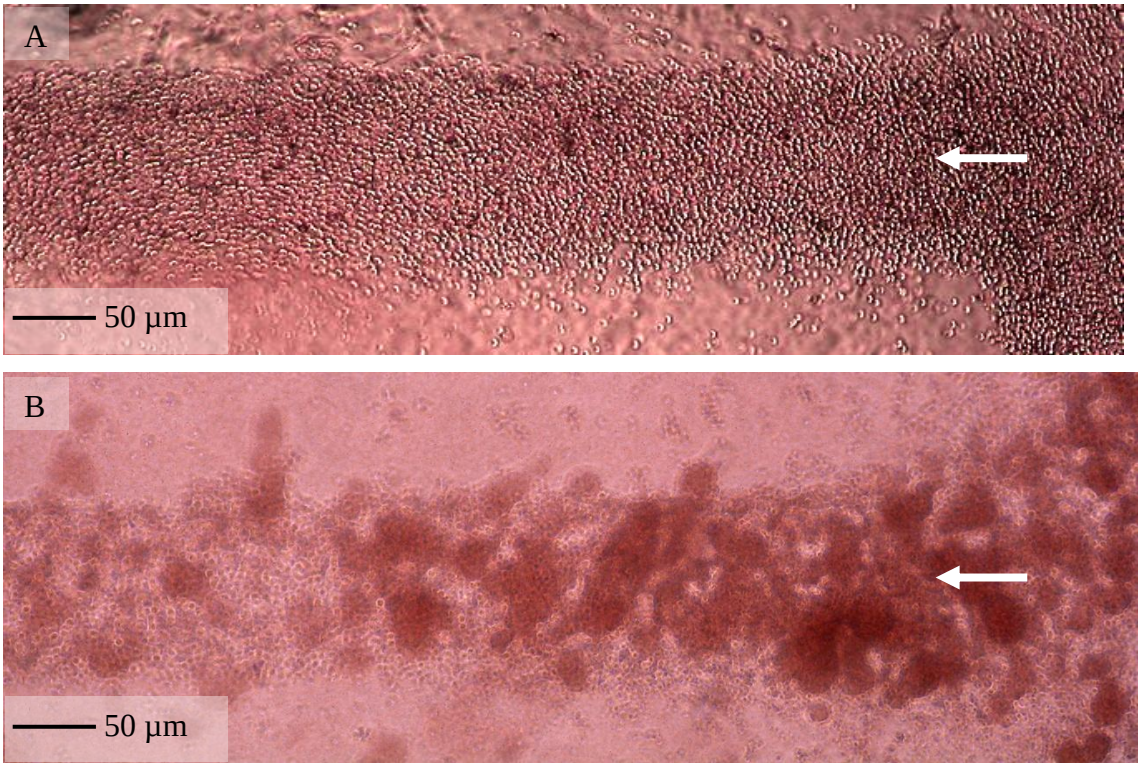

Figure 7.4-13. Formation of cell condensates in a linear aggregates. The distance between the parallel interdigitated electrodes was 150 µm. In the diagram above nutrients and oxygen entered the chamber from the right hand side (see arrow).Condensate formation occurred preferentially at the ends where nutrients and oxygen were more abundant. A. Initial conditions. B. After 21 hours.

7.4.6 Comparison of the behavior of dermal and epidermal cells

To further understand the developmental processes that occur *in vivo* more closely, it was attempted to separate the dermal and epidermal tissues. Dissection of the embryonic skin in the lab was difficult to achieve without some epidermis still adhering to epidermis and *vice versa*. All samples obtained therefore contained predominantly cells of one type, with some cells of the other type admixed.

Figure 7.4-14 shows the result of an aggregation experiment performed with a sample containing mainly dermal cells (i.e. epidermal cells were likely to be present in only very small amounts). The aggregates (with a size of approximately 150 x 300 µm) were constructed using dielectrophoresis in hexagonal pattern. After 21 hours of incubation in PuraMatrix hydrogel and a continuous flow of fresh medium (containing oxygen and nutrients) at 37ºC and 5% CO_2, some limited condensation can be seen. Less condensates were formed than in previous experiments in which whole skins were used, and the condensates that were formed were mainly micro aggregates containing 5-10

cells.

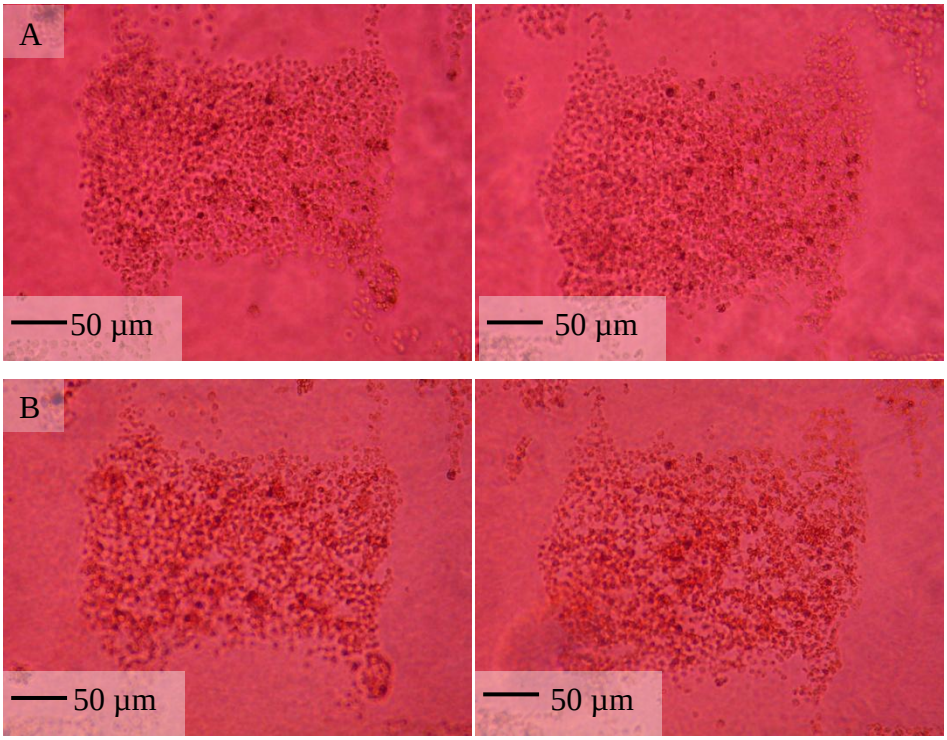

Figure 7.4-14. Cell aggregates containing predominantly dermal cells constructed using DEP in a hexagonal pattern. Aggregate dimension is approximately 150 x 300 µm. A. Aggregates immediately after their formation. B. After 21 hours of incubation in hydrogel.

In the next experiment large aggregates were constructed from a sample containing predominantly epidermal cells. A small amount of dermal cells was present, in approximately a 1:10 ratio of dermal cells to epidermal cells. The results (shown in Figure 7.4-15) show that the epidermal cells condense into large condensates that are randomly distributed over the aggregates.

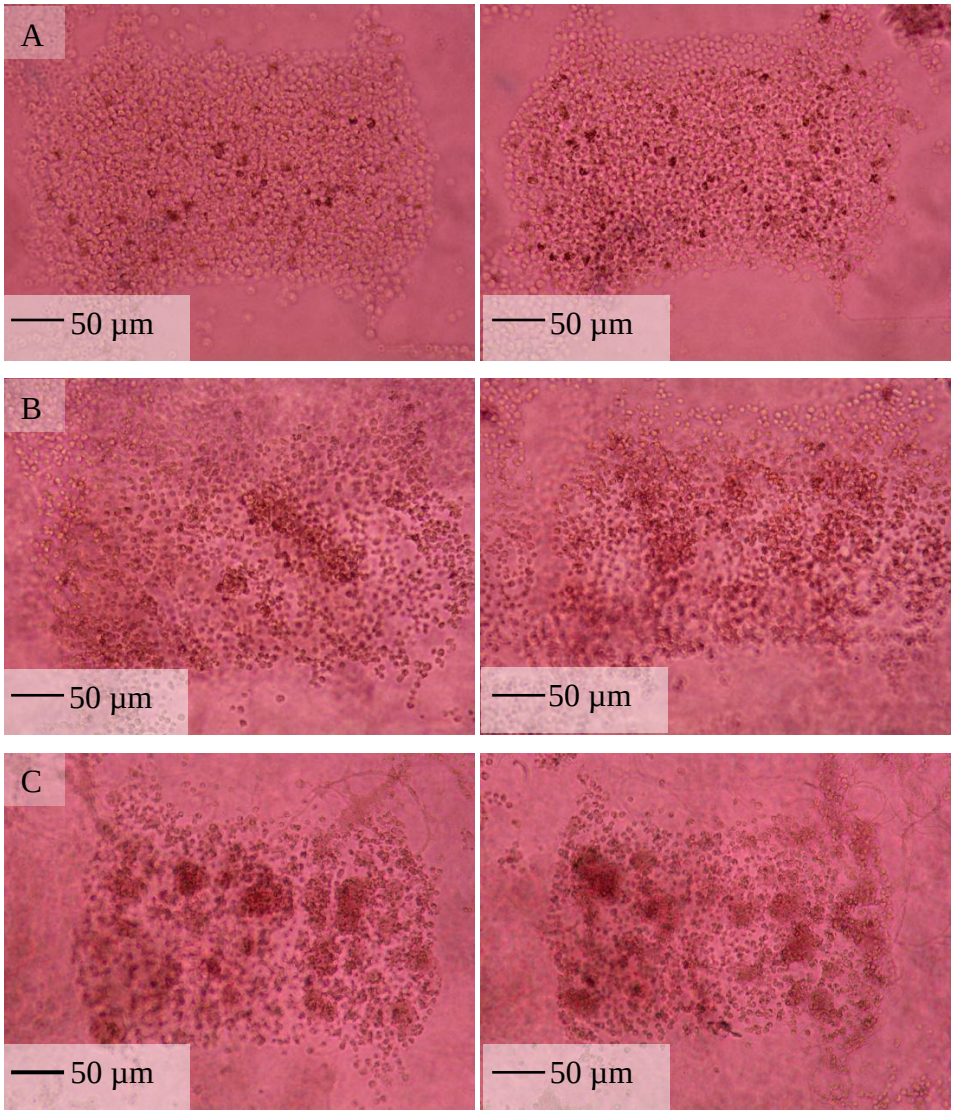

Figure 7.4-15. Cell behaviour in large aggregates containing predominantly epidermal cells. The aggregates were constructed using DEP in a hexagonal pattern. Aggregate dimension is approximately 150 x 300 µm. A. Aggregates immediately after their formation. B. After 6 hours of incubation. C. After 18 hours.

In the next experiment (Figure 7.4-16), aggregates were formed from a mixture of dermal cells and epithelium cells in a line pattern. The ratio of dermal cells to epidermal cells was approximately 10:1. Aggregates were constructed in a line pattern (as opposed to the previously shown hexagonal pattern of large cell aggregates). Each aggregate in the line pattern has a dimension of approximately 150 x 1000 µm. After 18 hours of incubation large condensates can be seen to have formed. This suggests that the presence of epidermal cells (even in a relatively small amount) may enhance the condensation process.

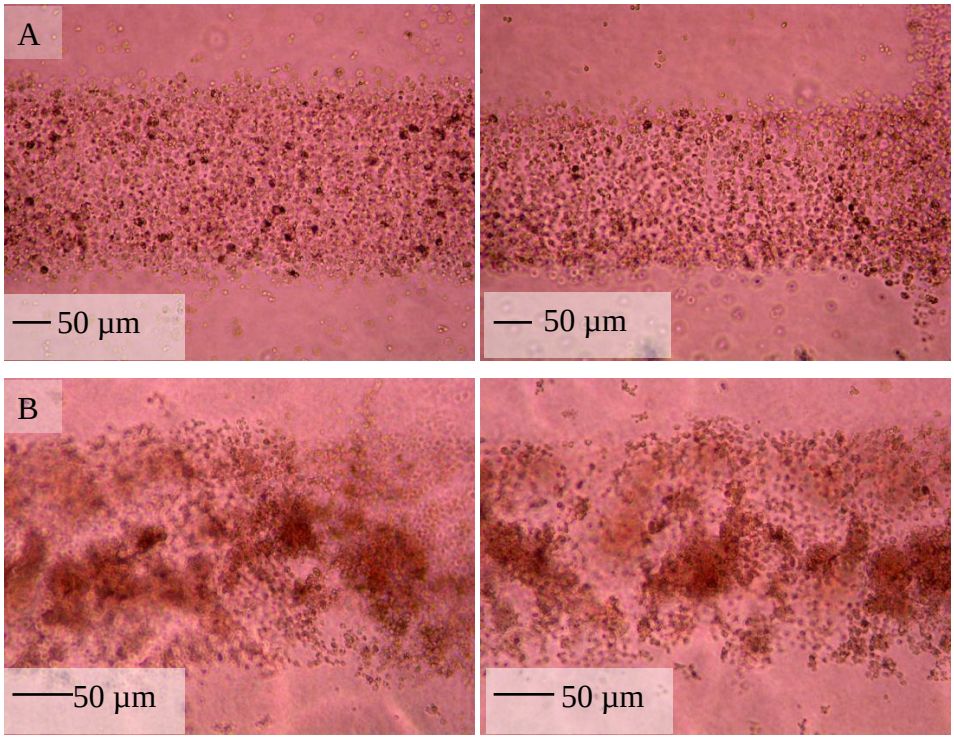

Figure 7.4-16. Cell behaviour in aggregates containing dermal cells and epidermal cells in the ratio 10:1. The aggregates were constructed using DEP in a line pattern. The aggregate dimension was approximately 150 x 1000 µm across. A. Initial conditions. B. After 18 hours of incubation in hydrogel.

In the next set of experiment (Figure 7.4-17), line aggregates were made of a sample containing mainly epidermal cells to check that it was not the aggregate shape that caused the dermal and epidermal cells to aggregate in the previous experiment (Figure 7.4-15). Although the experiment was stopped after only 9 hours, condensation of the cells can already be seen, indicating that it was not aggregate shape, but the interaction between dermal and epidermal cells.

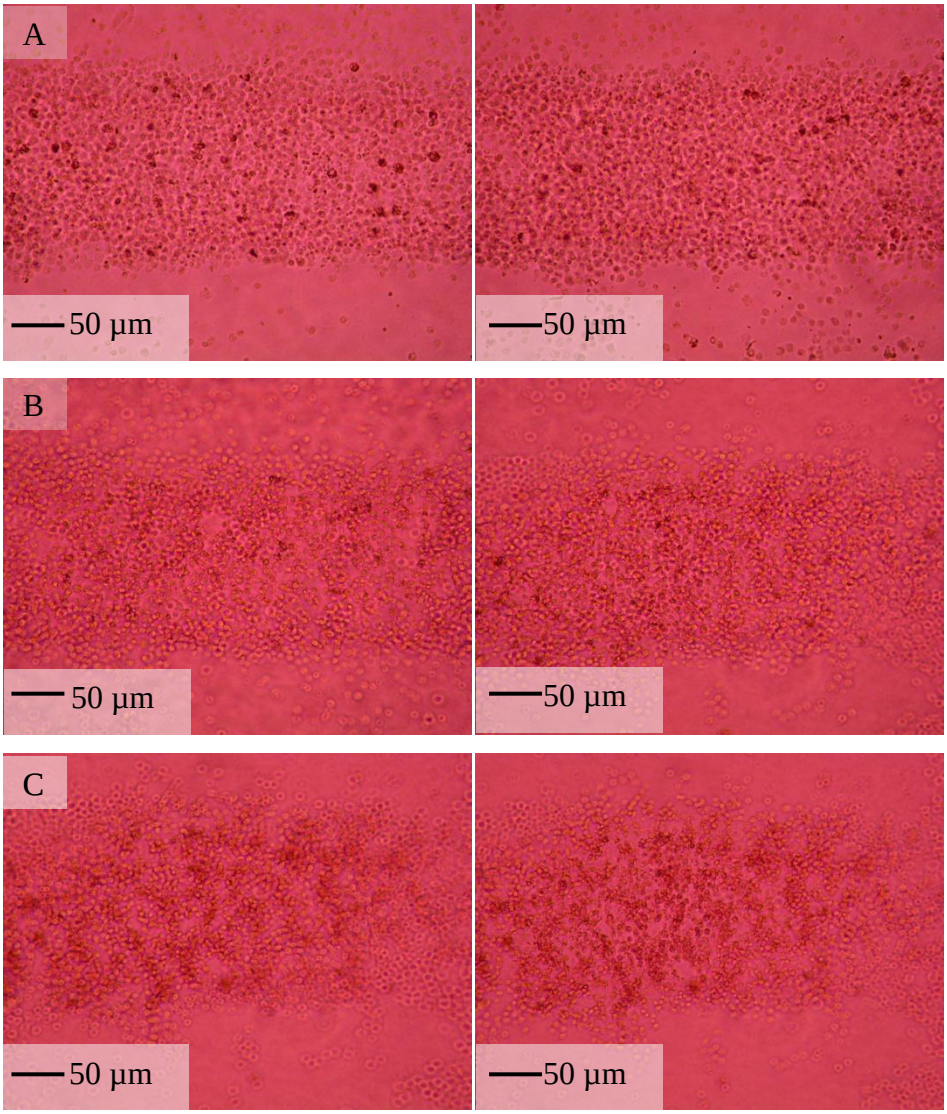

Figure 7.4-17. Cell aggregates containing predominantly epidermal cells, constructed using DEP in a line pattern. Aggregate dimension is approximately 150 x 1000 µm. A. Aggregates at start. B. After 6 hours of incubation in a hydrogel. C. After 9 hours incubation.

7.4.7 Cell tracking experiment using Green Fluorescence Protein (GFP+) skin cells

To further confirm the difference in behavior between dermal or epidermal cells, dermal and epidermal cells were separately isolated from GFP+ and GFP- embryos. GFP+ cells fluoresce green, GFP- cells do not fluoresce. In the first set of experiment, GFP+ dermal cells were mixed with GFP- epidermal cells before constructing an aggregate pattern. After 6 and 12 hours, aggregation of dermal cells was limited, and only a few dermal cells can be seen have started to form small micro aggregates (Figure 7.4-18).

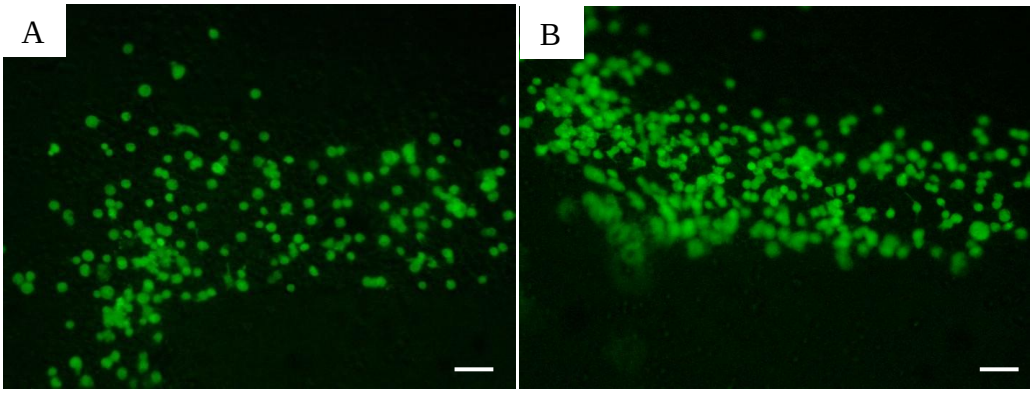

Figure 7.4-18. Cell tracking experiment using GFP+ and GFP- skin cells constructed using dielectrophoresis in a line pattern. GFP+ dermal cells were mixed with approximately equal amount of GFP- epidermal cells. The movement of dermal cells to form micro aggregates was tracked: A. After 6 hours. B. After 12 hours post DEP and gel immobilization of the aggregate. Scale bar = 20 μm.

In the second set of experiments, line aggregates were constructed from a mixture of epidermal and dermal GFP+ skin cells and GFP- skin cells (there were insufficient cells left to do epidermal and dermal cells separately). The results of the second set of experiment are shown in Figure 7.4-19 and demonstrate the formation of larger cell condensates. This again indicates the epidermal cells play a dominant role in condensate formation.

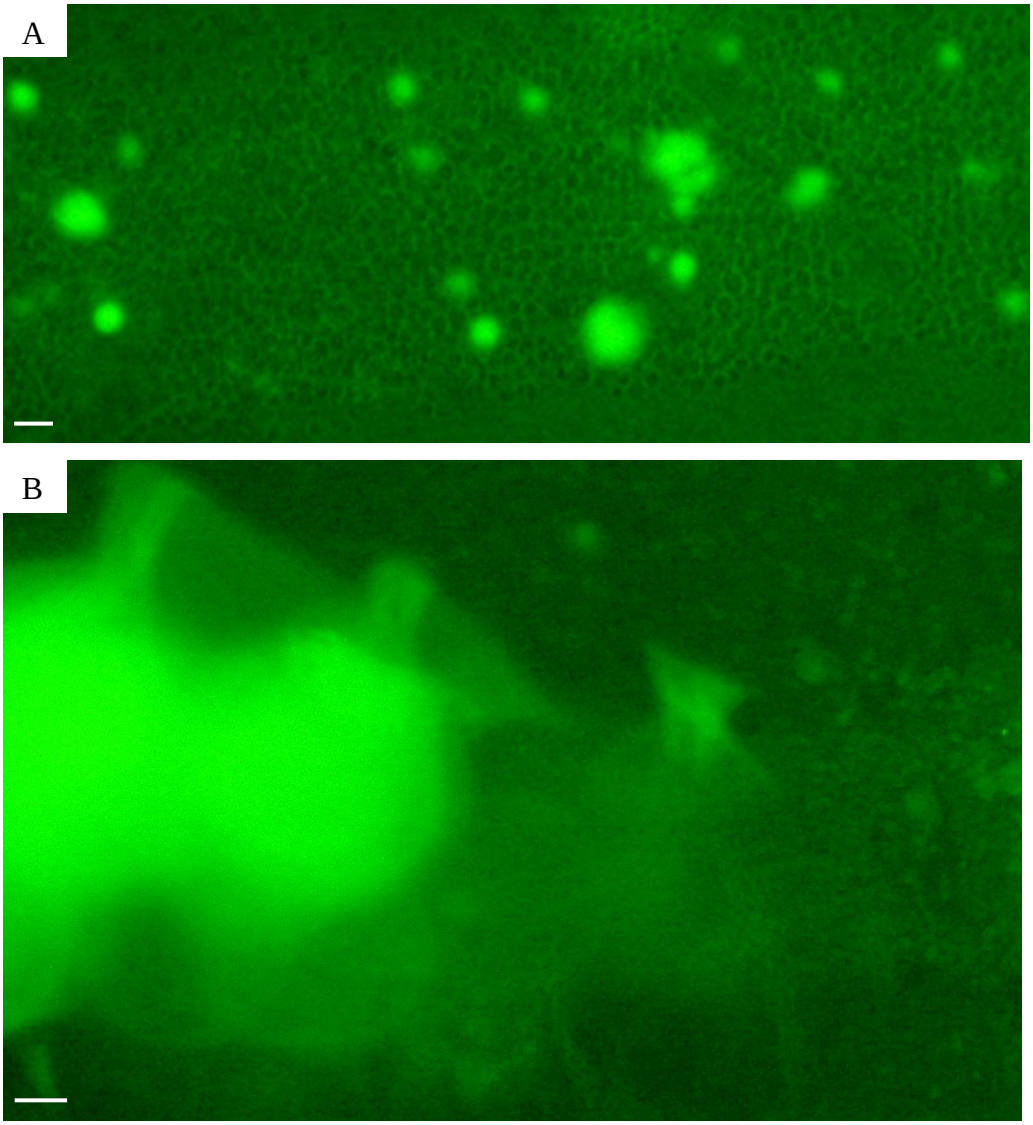

Figure 7.4-19. Cell tracking experiment using a mixture of GFP+ skin cells (containing both dermal and epidermal cells) and GFP- skin cells (containing both dermal and epidermal cells) in a line pattern, showing the formation of micro aggregates (Panel A, after 6 hours) followed by the formation of larger and cell condensates (Panel B, after 24 hours.). Scale bar = 20 µm.

7.5 Discussion

All of the works conducted in this research project were based on observation of short-term response of chicken embryonic skin cell aggregates constructed using dielectrophoresis on a chip (or *in vitro*) rather than *in vivo* studies. The question therefore has to be asked whether the findings from the *in vitro* studies are relevant the phenomena that are observed *in vivo*.

In actual chicken embryonic skin tissue, the development of placodes starts on E6, the

time when dermal cells condense in the form of line pattern above the neural tube. This line-shape aggregate then subsequently 'breaks up' in a wave-like fashion, forming individual placodes in a hexagonal pattern. The initial signal for pattern formation comes from the (intact) epidermis.

In our studies we used a mixture of epidermal and dermal cells from skin isolated from embryos of E8. E6 embryos contain much less skin, and many more embryos would have been needed. E8 cells have already been assigned follicular and interfollicular fates. Isolation of the cells from the embryonic skin tissue may bring the cells back to a more naïve state, but further investigations would be needed to explore this. It is interesting to note that after dissection and dissociation of the embryonic skin tissue to individual cell component, skin cells do not lose their intrinsic adhesion properties, typical characteristic of primary cell line, suggesting that the genes that code for these characteristics are constitutively expressed.

In their *in vitro* studies with intact epidermal skin and dermal cell suspensions, Jiang *et al*. (1999) found that the initial dermal cell density played a very important role in determining the subsequent development of the aggregates. The group showed that at low dermal cell density (around 1 x 10^6 cells / mL suspension) feather bud formation was limited and was randomly distributed within a fixed domain size. A hexagonal pattern could be achieved *in vitro* if the number of (mesenchymal) cells available was higher than a certain threshold value. As the initial cell concentration was increased, the number of feather bud primordia increased whilst the size of each bud remained relatively constant. The group found that the size of feather bud primordia was in the range of 200 – 300 μm in diameter. In our research project, the initial size range was around 20 - 50 μm (see example Figure 7.4-10). On further cell condensation the size increased to about 150 μm in diameter (as shown in Figure 7.4-11 and Figure 7.4-12), but at no stage were condensates formed with a size over 200 micron. It may therefore be necessary to do further experiments with aggregates much larger than 200 micron in size.

The initial DEP-constructed aggregates appear to 'break up' into smaller (micro) aggregates. The formation of unstable micro aggregate formation is well known as one of the events that occurs during feather morphogenesis (Lin *et al.*, 2006a), mainly after

the conversion of a non-competent tract field in the apteric region to a more competent tract field.

It is likely that the presence of adhesion molecules (NCAM) on the cell surface drives the cell aggregation process that leads to cell condensate formation (Jiang *et al.*, 1999). Each cell has a certain intrinsic adhesive property based on its composition of adhesion molecules or growth factor receptors (Lin *et al.*, 2006a). NCAM adhesion molecules are expressed at a basal level in the dense dermis prior to dermal condensation formation (Jiang *et al.*, 1999). In addition, FGFs super families (1, 2 and 4) are involved in feather pattern formation (Song *et al.*, 1996; Widelitz *et al.*, 1996; Mandler and Neubuser, 2004) and can induce many smaller feather buds from embryonic chicken skin explant cultures (Widelitz *et al.*, 1996) as well as induce the formation of dermal condensations (Song *et al.*, 2004).

Intact epidermal skin would have been needed to create a regular hexagonal array of placodes. Although in many *in vivo* studies follicles are predominantly epidermal structures, classical tissue recombination experiments have indicated that the underlying dermis defines their location during development (Sengel, 1990). The mesenchyme also determines the number, size, and structural identity of the appendage while the epithelium determines the orientation and competence state (Chuong *et al.*, 1996). The observed behavior, i.e. the formation of a single condensate in small aggregates, and a random distribution of condensates in large aggregates is commensurate to what would be expected if one started with a random distribution of cells.

Unlike the large aggregates, in long and narrow linear aggregates the initial conditions can be expected to lead to the formation of a regular periodic pattern even when a mixture of cells is used. In fact with the linear pattern it should be possible to determine from the regularity of the pattern whether the pattern is the result of an underlying chemical pattern involving a reaction-diffusion system with Activator and Inhibitor molecules or a similar mechano(chemical) model, or a stochastic process. A Turing-type reaction-diffusion system or similar should lead to the formation of a stable structure with regular periodic (alternating) regions of high and low cell density distribution. If the pattern is the result of a stochastic process a more random pattern of condensates should be formed within the line. There is currently insufficient data to

determine which type of pattern is formed here.

In the on-chip studies, cell proliferation may be restricted by the supply and distribution of fresh nutrients and oxygen (Figure 7.4-13) entering into the chamber. Cell proliferation does not seem to play a major role in initial stages of the condensation process, but is clearly a contributing factor to the growth of cell condensates in the later stages. *In vivo*, mesenchymal cells accumulate in the developing dermis through random cell proliferation (Noveen *et al.*, 1995).

7.6 Conclusions

This chapter has shown the construction of artificial skin with artificial placode-like aggregates using dielectrophoresis as a first step towards the creation of artificial skin with artificial hair of feather follicles. The relative position and distance between the aggregates as well as size and shape of the aggregates can be controlled by the changing the electrode design. The cells in the aggregates remain viable and show behavior similar to that in embryonic skin, including the formation of cell condensates.

Combining the results of our experiments to explore the properties of embryonic skin cells when constructed using DEP in a fixed and pre-determined domain size, we could envision the following short-term behavior of embryonic skin cells within the artificial environment: After dissociation of skin tissue into individual cells, the cells maintain their intrinsic adhesive properties. Dermal cells are less adhesive than epidermal cells. Random movement of cells and adhesion of the cells to each other leads initially to the formation of micro aggregate(s) within the DEP-constructed cell aggregates consisting of a few cells; the initial aggregation process is influenced by pearl-chain formation that occurs during the dielectrophoretic assembly of the aggregates. The aggregates formed are unstable, and some aggregates grow at the expense of others and become more condensed. Also cell division occurs. This leads to the formation of condensates of various sizes within the aggregates. The distribution of the condensates across the initial aggregate appears to be random. However, as the cell condensates become bigger in time by cell division and acquisition, and the area around them becomes more depleted of cells, they may eventually resolve themselves into a pattern.

CHAPTER 8

Conclusions, Potential Applications and Future Directions

8.1 Conclusions

It has been shown that dielectrophoresis can be used to create arrays of cell aggregates in well-defined patterns. By controlling the design of the microelectrode geometry it is possible to manipulate the 2D and 3D geometry of the resulting cell aggregates. This control includes their spacing (distance and angle between the aggregates), their size and shape as well as cell density distribution. Control of the timing of the introduction of different cells entering the chamber (e.g. dermal cells followed by epidermal cells on top) allows one to form distinct multi-layer micro niches within a controlled microenvironment (Sebastian *et al*., 2007a), making it possible to use the system as a tool for the study of the interactions between cells and their microenvironment (Markx *et al*., 2009).

There were a number of distinct stages in the bioengineering of artificial skin tissue. The first step was the design and modeling of the electrodes, during which calculations of the electric field strength between electrodes were performed using a finite element analysis tool and the 2D models were developed for the prediction of the shapes and patterns to be formed. The most promising designs were chosen and the CAD drawings of various microelectrode geometry were made using Protel™ Design Explorer for subsequent development of photomask used during microfabrication (photo lithography). In the next stage, the actual microfabrication of electrode array in the clean room laboratory was performed, followed by the construction of a chamber enclosure system. The next step was the formation of artificial skin tissue with defined patterns of 3D cell aggregates from a cell suspension.

Directing cells into a desired shape or pattern by dielectrophoretic force provides an

alternative method to achieve artificial cellular micro architecture for tissue engineering purposes and allow researchers to study the basic property of cell-cell interaction. The DEP-based method of cell patterning has several advantages, including a minimal need for cell pre-treatment. In addition, DEP-based cell manipulations allow one to work on a relatively large scale and in-parallel, whilst still obtaining a relatively high spatial resolution. The simplicity of the equipment and the ease of its combination with other techniques are additional benefits.

Although negative dielectrophoresis can also be used for the formation of cell aggregates, we have used positive dielectrophoresis because the trapping forces are higher. Another major advantage is also that the electric field used more strongly forces the cells within the aggregates to be in direct contact with each other, encouraging exchange of signals between cells by direct cell-cell contact. In addition, the more natural distribution of cells encourages the formation of more natural distributions of oxygen, nutrients, diffusible cytokines and other factors in the artificial tissues.

The construction of artificial skin with artificial placode-like aggregates using dielectrophoresis acts as a first step towards the creation of artificial skin with artificial hair of feather follicles. The cells in the aggregates are viable and show behavior similar to that in embryonic skin, including the formation of micro aggregates which subsequently merge and expand to form dense cell condensates. Epidermal cells appear to be more strongly involved in micro aggregate and condensate formation then dermal cells. The distribution of condensates in the aggregates is predominantly random, though some line formation has been observed. It is not clear whether this line formation is caused by the dielectrophoretic assembly process/ a random aggregation process associated with cell-cell adhesion, or an actual developmental process. Domain size does have an influence on the condensation process, with small aggregates forming only one condensate near the middle, and larger aggregates several condensates of follicle precursors. No interactions were observed between aggregates in a pattern.

8.2 Potential Applications

To be most useful the pattern formation process has to be usable for any type of cells, and be highly predictable and reproducible. Dielectrophoresis is a physical rather than a biological effect. As all intact, viable cells have an intact, low conducting lipid

membrane surrounding an aqueous high-conductivity cytoplasm (Pethig and Kell, 1987), all cells will display a Maxwell-Wagner type polarization around 1 MHz which will result in positive dielectrophoresis when cells are immersed in a low-conductivity medium. Patterning with dielectrophoresis is therefore possible with any cell type. Although this work has concentrated in chicken embryonic skin, the approach however could also work with other systems. Since the aggregates within the artificial tissues will be 3-dimensional, it is expected that they will more closely mimick the natural distributions of cells than standard 2-D cultures, and more closely reproduce the tissue microenvironment that determines the cell phenotypes during development (Khademhosseini *et al.*, 2006a).

The system developed can be used to test models of skin formation, and in particular feather and hair formation during skin development. Many of these models are based on reaction-diffusion systems, in which the spacing between placode regions is regulated by the distribution of Activator and Inhibitors molecules (Mou *et al.*, 2006; Sick *et al.*, 2006). However, other forces are known to be involved (Harris *et al.*, 1984; Chuong *et al.*, 1991). Imposition of artificial cell arrangements and the study of the subsequent rearrangement of the cells after its formation should give information about the validity of these models. Conversely, the *in vitro* system also allows the administration of proteins or pharmacological compounds, either homogeneously or focally, and the measurement of endogenous rates of signal production, allowing one to investigate the relationship between chemical signaling and cell densities in the formation of patterns in detail. Finally, tissue-engineered skin is already used therapeutically. However, it lacks hair follicles and other appendages such as sebaceous and sweat glands. The method developed could also be adapted to engineer more natural skin substitutes for grafting purposes.

In order to aid in the analysis of the patterns produced and to study their development after their formation, a Virtual Instrument (VI) system was developed to analyze the resulting microarray of cell aggregates using the LabVIEW with IMAQ Vision Development Module. The VI developed could be used for any other application such as single cell analysis requiring measurements of geometrical features. A series of programming functions (algorithms) such as thresholding, were used to isolate the distinct features on the image (i.e. the patterned biodielectric cell aggregates) and separate them from all other unwanted regions on the image (such as electrode

components, interfollicular regions, unbound cells aggregate, contaminants, etc).

The simple and easy to use User-Specified Multi-Regions Masking (MRM) technique allowed us to concentrate the analysis only on the desired regions specified in the mask, making it a very versatile technique for object analysis. This simplified the algorithms for the analysis of any microarray images having similar geometrical properties. By having a collection of scripts (containing masks of different patterns), it was possible to quickly and efficiently develop sets of custom virtual instruments for the offline (or online) analysis of any microarray images in the database and automatically generate sets of numerical measurements (such as an individual aggregate's area, radius, circumference, orientation, elongation and circularity factor, distances and angles between several aggregates, etc).

8.3 Future Directions

Rapid progress in the development of technology required to control spatial arrangement of cells to the micro scales have resulted in advances in the tissue engineering field. Scientists have now used all physical phenomena available such as electrical, mechanical, optical, and chemical to create 2D and 3D arrangements of cells. Two fundamental directions for the future would probably be to increase the throughput, the ability to control and to make things more user- friendly. This will increase the usage of the technology and make it more widely accepted.

Aggregate formation and analysis to date has only been done with a small number of electrode characteristic size and shapes. A larger range of electrode sizes should be explored, in particular in the lower range (i.e. smaller than 50 μm) and in the upper range (i.e. around 200 – 300 μm), and particularly in a line pattern. Also it should be attempted to establish 3D structures of different designs (by manufacturing new micro electrodes), improve the understanding of 3D pattern formation and optimizing the overall process control and precision of 3D pattern formation.

Experiments that still need to be done include better separation of dermal and epidermal cells using enzymes such as dispase (to separate between dermal and epidermal tissue), collagenase (to isolate individual cells from dermal tissue) and trypsin (to isolate individual cells from epidermal tissue). This could be followed by further studies of the

role of the different cell types in embryonic skin development. Pattern formation with individual epidermal and dermal cells and intact whole skin and intact epidermis and individual dermal cells should be compared.

Future directions of research should also focus on, but not be limited to, more fully investigating the roles of cell adhesion in pattern formation. Changes in cell adhesive properties could be studied by either studying gene or protein expression, or by directly measuring the adhesive forces between cells or cells and substrates.

Experiments need to be done in which the behavior of embryonic skin cells is observed over an extended duration of time post DEP and immobilization in a gel. Acquisition of video data is probably the most convincing way to present evidence and certainly the easiest way to understand processes particularly in response to certain treatment in real time. As long as suitable controls over particular experiments have been provided, conclusions can be drawn with less or no ambiguity and a high level of confidence. The drawbacks of using video data files lie in the massive file size required for collecting data for a particular experiment, as opposed to relatively manageable size of image data. Combining the two techniques should increase the accuracy of experimental results and strengthen the interpretation of the data analysis.

There are many other directions for further research in image analysis, in which the algorithm development includes addition of recognition features of biodielectric patterns, based on either shape or in combination with their distinctive color. This includes algorithm development which is aimed at learning the repeating structure (of individual cell aggregates) which will then be used to recognize and subsequently analyze other objects within the same group or categories. Some of these developments may combine or utilize the shape recognition technique with edge-based features (Mikolajczyk et al., 2003).

Answers to these questions and overcoming the obstacles require interdisciplinary efforts from biologists, engineers, and other scientific disciplines.

APPENDIX A

Technical Notes on Fabrication and Testing of Microelectrodes for Cell Patterning

A.1 Abstract

The microfabrication process is comprised of sample preparation, spin coating, UV exposure, soft- and hard-baking as well as feature development. Both positive- and negative- tone photoresist materials (Shipley S1813 and SU8-50 respectively) were used in the fabrication. Characterization of the electrode surfaces serves as a means of assessing the quality of microfabrication technique, the steps involved and reproducibility of the devices used in the experiments and to optimize parameters such as resist spin rates. The vertical scanning white-light interferometry technique was used to obtain spectral data representing the surface topography of the resist layer at user-defined regions at a certain distance from a centre point (radial distance point). The data revealed that the photoresist surfaces were devoid of major process-related physical disruptions such as holes and cracks. In some cases however, minor defects on the edges and spikes on the SU8 surfaces were present. SU8 layers with a height of around 200 µm (obtained at a spin rate of 1000 rpm) had an uneven height profile. Higher spin rates (around 2000 rpm) resulted in a more even height profile.

A.2 Introduction

Microelectrodes are some of the most important components of lab-on-a-chip devices (Monaghan *et al.*, 2007; Mushfique *et al.*, 2008; Blanco-Gomez *et al.*, 2009). In microfluidic-based chemical and bioanalytical operations non-reactive metal materials such as gold, platinum and indium tin oxide are often preferred for the construction of microelectrodes as their use ensures that any interactions with buffers (chemicals) or biomolecules in the system are minimized due to their chemical inertness. Thin films (around 90 nm) of indium tin oxide offer additional benefits in that the resulting conductive layer is optically transparent.

The microelectrodes are commonly fabricated by a process called photolithography. Photoresist coating is a critical step in photolithography. Photoresist is a photosensitive material that temporarily coats the wafer and is used to transfer the image of the chip design on the mask to the wafer surface. Thin coats of photoresist are usually put down on a surface using a technique called spin coating. Although advanced photoresist

coating techniques such as meniscus coating (Britten, 1983) exist for odd shaped substrates, none have the ease of implementation, equipment simplicity, and robustness that spin coating offers. The chemical composition of the photoresist solution, temperature, chamber humidity, spinning rate (expressed in rotation per minute - rpm), spinning duration and acceleration rate all affect the thickness and quality of the photoresist film. Trial and error is often used to find the most suitable combination of process parameters. However, this approach is sometime time-consuming and may result in failure to obtain the best process condition. Many industries have employed the Taguchi method using statistical methods to improve the quality of manufactured products and process performance (Taguchi, 1990; Ross, 1996). This method is powerful and effective in helping manufacturers to design their products and processes as well as to solve troublesome quality problems.

2D or 3D optical profilers are often used to optimize the photoresist deposition and etching process and have become one of the most valuable tools for characterizing the surfaces of MEMS devices. These are advanced interference-based microscopy methods that, as the name implies, exploit the interference of two light beams to characterize topography of a surface.

In this analysis, vertical scanning white light interferometric (SWLI) microscopy technique has been used to generate the height profile of deposited photoresist. When white light is bounced off from a sample and combined with the same light coming off of a high-standard reflector surface (as a reference) interference signals are generated. An objective lens examines the surface directly. A high-speed camera connected to a computer reports the fringes as a result of interference at certain points in a vertical (z) direction during the scan. The software evaluates the fringes to accurately measure the height of, in our case, the deposited photoresist on every picture element (pixel) captured by the image sensor.

In this appendix it is described how some process parameters for microelectrode microfabrication were optimized so maximum photoresist uniformity could be achieved over rectangular-shaped substrates. The effects of the spinning rate on the resulting height of various types of photoresist are discussed. Scanning electron microscopy was used to visualize the finished product in 3D.

A.3 Methods for the Fabrication of Microelectrode Arrays

As described in the Chapter of Materials and Methods, photolithography processes generally can be subdivided into several main operations. These include sample preparation and cleaning of the substrate, spin-coating of the photoresist, alignment and exposure using UV mask aligner, and finally photoresist development and etching of the underlying metal (i.e. ITO) materials. The entire process was conducted in a clean room laboratory.

A.3.1 Sample preparation and cleaning

Initially, the wafers (microscope glass slide, 75 mm x 25 mm) were cleaned by means of ultra sonication in a solution of acetone, followed by isopropyl alcohol or methanol. This should remove major contaminants such finger print marks, grease, dirt and dusts which will affect the quality of microelectrode or MEMS devices in general. After the cleaning step, the wafer was blow-dried using compressed air or a nitrogen gun followed by thermal evaporation in the 90º oven. The heating makes sure that all H_2O molecules on the surface of the sample evaporate, which is particularly essential for substrates that oxidize quickly (such as silicon). The oxides on the surface then react with water molecules in the vicinity. During spin-coating with the photoresist, the resist solution deposits on top of the H_2O surface and does not bind properly to the actual sample, creating many problems in the downstream processes.

A.3.2 Spin coating

Spin-coating of the wafer was used to create a layer of a few micrometer thick of photoresist. The photoresist solution consists of three main components, a base material (resin), a photo active compound (PAC) and a solvent. The wafer was positioned on the centre of a spindle using a vacuumed chuck (Figure A.1. part A) that can hold the wafer during high-speed rotation.

Shipley S1813 is a photoresist that is commonly used for photolithography. The sensitizer in a positive photoresist such as Microposit Shipley S1813 is a dissolution inhibitor, which is cross-linked within the resin (Campbell, 2001). During exposure, the light energy dissociates the sensitizer and breaks down the cross-links, making the

exposed resin soluble in the subsequent development process. Shipley S1813 photoresist solution was filtered using a 0.22 micron sieve and applied onto the wafer surface using a syringe and spun at various maximum spin rates (2000 – 4500 rpm) with 500 rpm increments; each rate was applied for a constant duration of 30 seconds. Maximum acceleration was maintained at 500 rpm/second from an initial ramp at 1000 rpm to spread the resist evenly and minimize abrupt evaporation rate which can lead to the formation of a hard skin on the resist surface.

SU8-50 photoresist is typically used to create permanent structures such as micro channels with high aspect ratios. The sensitizer for a negative photoresist such as SU8-50 is an organic molecule containing a labile nitrogen group. Exposure to UV light liberates nitrogen gas, forming free radicals that help to cross-link the polymers during hard-baking and subsequently rendering it insoluble to development solution. The chain reaction of the cross-links results in the polymerization of the exposed areas, which subsequently leads to greater bonding strength and higher chemical resistance. SU8-50 was applied the same way as S1813, but only two speeds were used (1000 and 2000 rpm) for a constant duration of 30 seconds. Maximum acceleration was maintained at 300 rpm/second from an initial ramp at 500 rpm.

Afterwards, the sample was left at room temperature to evaporate the solvents in the photoresist for 20-30 minutes to improve uniformity of resist deposition.

A.3.3 Alignment and exposure

Prior to UV exposure, the sample coated with photoresist S1813 was soft-baked in a 90º C oven for 5 minutes. After this, the sample was exposed to ultraviolet (UV) light through a mask with the pattern of clear and dark areas, forming hexagonal, square and line patterns of different sizes. Photoresists from the positive Microposit S1800 series photoresist can be exposed with light sources in the spectral output range of 350 - 450 nm. The photoresists' properties have been optimized for exposure at 436 nm for 5 seconds. Negative SU-8 photoresist however, has been optimized for exposure at near UV (350-400nm) for 60 seconds. SU-8 is a practically clear (see-through) material and not responsive a UV wavelength above 400 nm, but has high actinic absorption below 350nm.

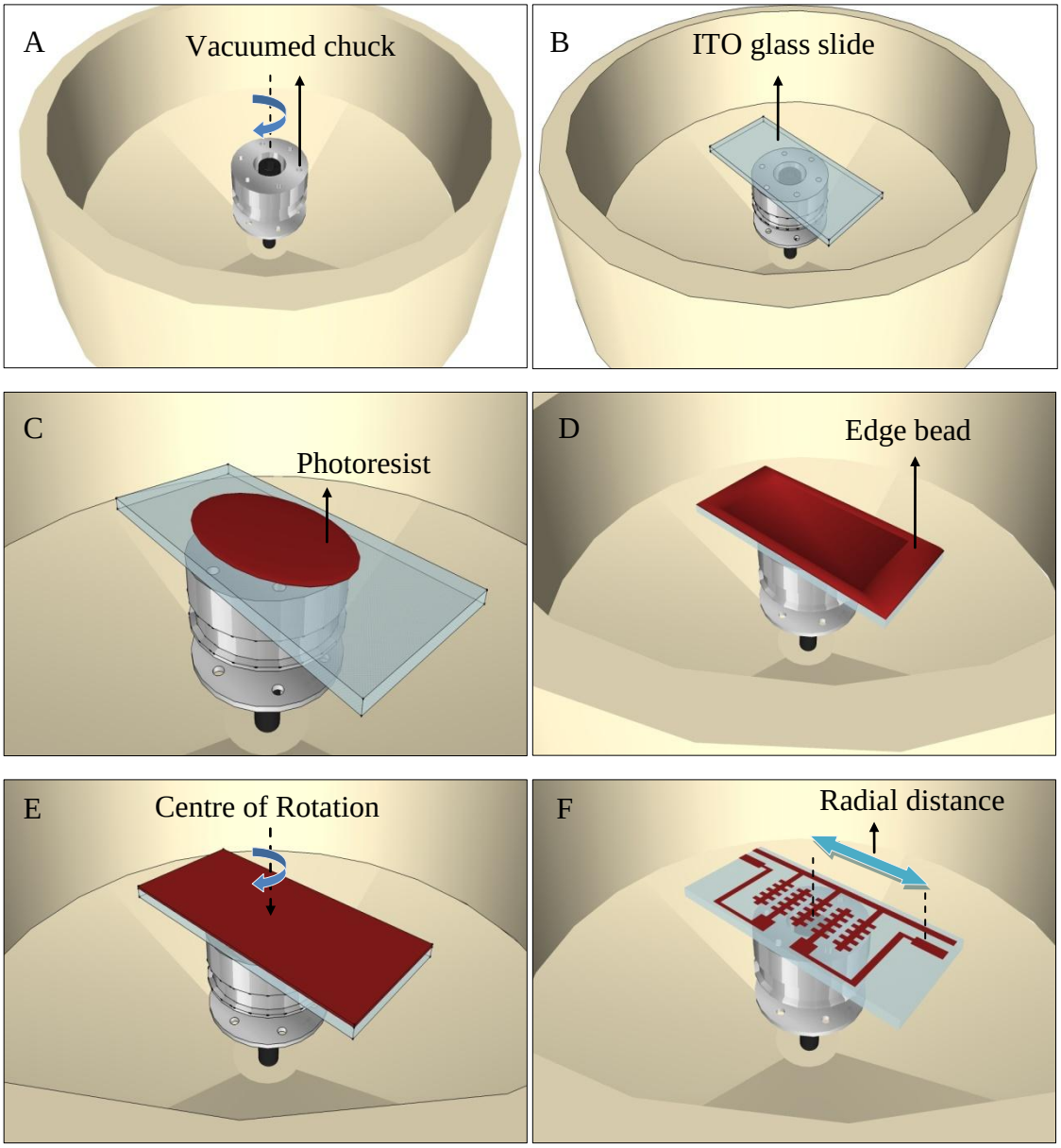

Figure A. 1. Spin coating processes and illustration of radial distance. A. Vacuumed chuck and direction of rotation. B. Balanced placement of ITO glass slide in the chuck. C. Deposition of photoresist on the sample. D. Formation of edge-bead in a rectangular sample. E. Flat photoresist surface after edge bead removal. F. Radial distance on developed photoresist sample.

A.3.4 Development and etching

Prior to development, the exposed negative SU-8 photoresist was post-baked for 5 minutes at 65ºC and another 5 minutes at 95ºC. Microposit S1813 photoresist is compatible with both Metal-lon-Free (MIF) and Metal-Ion-Bearing (MIB) developers. These developers were diluted with distilled water in 1:1 ratio. Development typically took less than 1 minute.

The exposed negative SU-8 photoresist was post-baked for 5 minutes at 65ºC and another 5 minutes at 95ºC prior to development using EC solvent (Ethyl-lactate Containing solvent) for 10 minutes followed by rinsing briefly with isopropyl alcohol (IPA). An absence of white precipitates was taken as an indication that development was complete. The sample was then rinsed with plenty of running water, which was subsequently dried with a compressed air or nitrogen gun.

The height profiles of both types of photoresist were recorded using vertical scanning white-light interferometry. The height data were measured from the centre of rotation, which was also the centre of the square wafer.

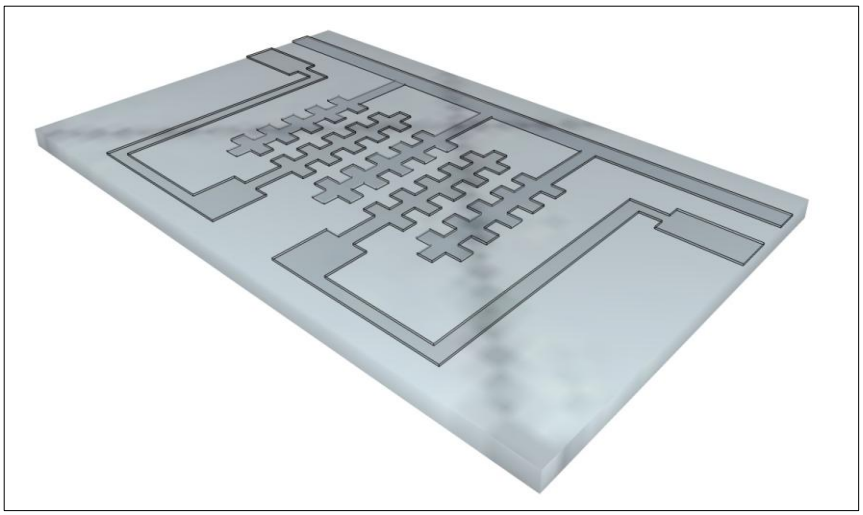

Figure A. 2. Illustration of a fully etched microelectrode array, after the protective photoresist layer has been removed by liquid solvent (such as acetone).

Once the substrate was fully developed, the underlying ITO layer was then etched away according to the pattern defined by the mask, using a solution consisting of 20% HCl, 5% HNO_3 (wet etching technique). This solution was mixed in an acid-resistant container (such as glass bottle) in a fume hood at room temperature. Typically, it took 20 – 30 minutes to completely etch an underlying patterned metal electrode as can be seen in Figure A.2, though there were variations which may be contributed to differences in the thickness of the ITO. As the etchant mixture is consumed by repeated etching, variation in the quality or concentration of the solution may affect the etch rate. After the etching completes, the substrate was washed with a 10% (w/v) sodium carbonate (basic solution) to neutralize any acid that may still be present on the coated surface. In the next step, the remaining photoresist layer was removed using acetone that was subsequently and immediately rinsed off with plenty of water, and finally the

slides were blow dried with compressed air or a nitrogen gun.

A.4 Results and Discussion

There are mainly four distinct processes that occur during spin coating. The first (deposition) step involves dispensing of an excess amount of resist fluid onto a stationary substrate. The fluid is deposited through a nozzle at the center of the substrate at an excessive amount to prevent coating discontinuities caused by the fluid front evaporating prior to reaching the edge of the rectangular sample. In the spin up process, the substrate is accelerated to the final spin speed (usually after an initial ramp speed). During the spin off stage, the excess solvent is spun off. The final evaporation stage occurs throughout the four processes, which is the primary means of thinning the resist layer.

In this section, the physical changes which occur in a resist layer after spin-coating, exposure and development are discussed, especially the effect of spin speed to the resulting film thickness. This section aims to assess and analyze the issues involved in spin coating rectangular-type substrates for photoresist thickness and photoresist uniformity.

A.4.1 The effect of spin-coating speed to the thickness profile of S1813

In general, the chemistry of the exposed photoresist changes by the photochemical reactions occurring under the clear areas of the mask through which the UV light penetrates. Certain groups of photo active compounds (known as sensitizer) in the photoresist solution act with a high photo activity. The compounds are able to control and modify the photochemical reactions of the photoresist during the UV exposure depending on the chemical properties.

Samples of resist heights were randomly taken at points with a known distance from the centre of rotation. Figure A.3 and Figure A.4 plot and compare the surface thickness profile of S1813 photoresist using 2D and 3D representations at various spin rates and various distances from the central point of rotation (i.e. the radial distance).

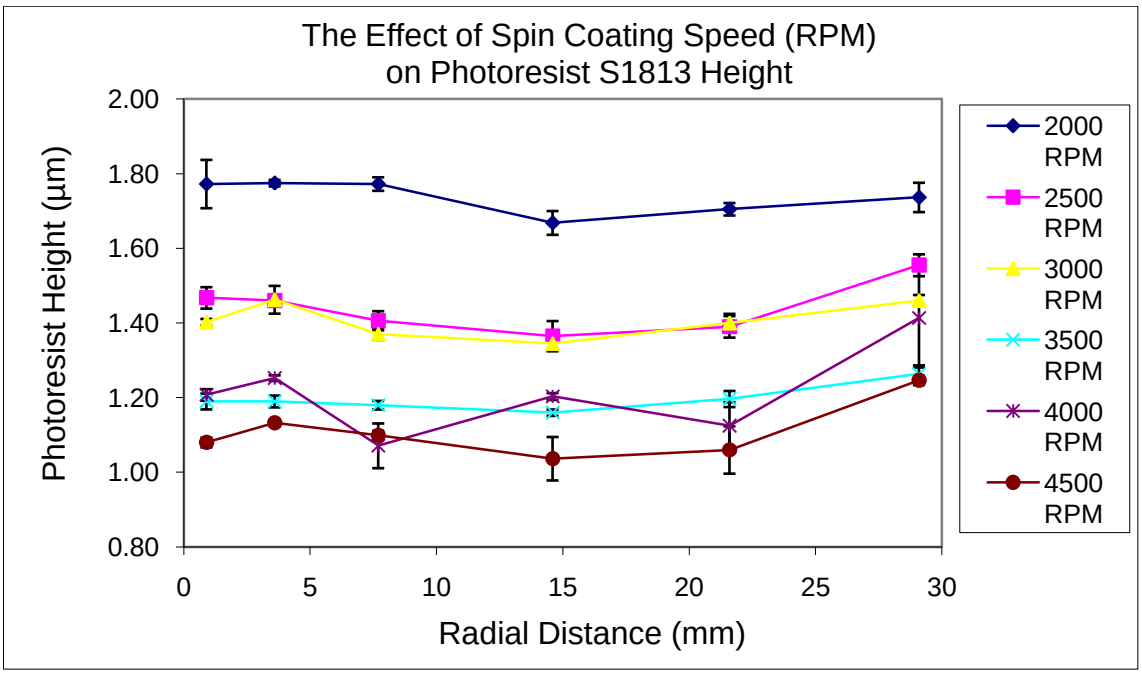

Figure A. 3. The effect of spin coating speed (in rotation per minute, rpm) on the thickness of deposited photoresist layer Microposit Shipley S1813 (assessed after development step) at points from the centre of rotation (the radial distance). Error bars show standard errors of 3 sample size (n).

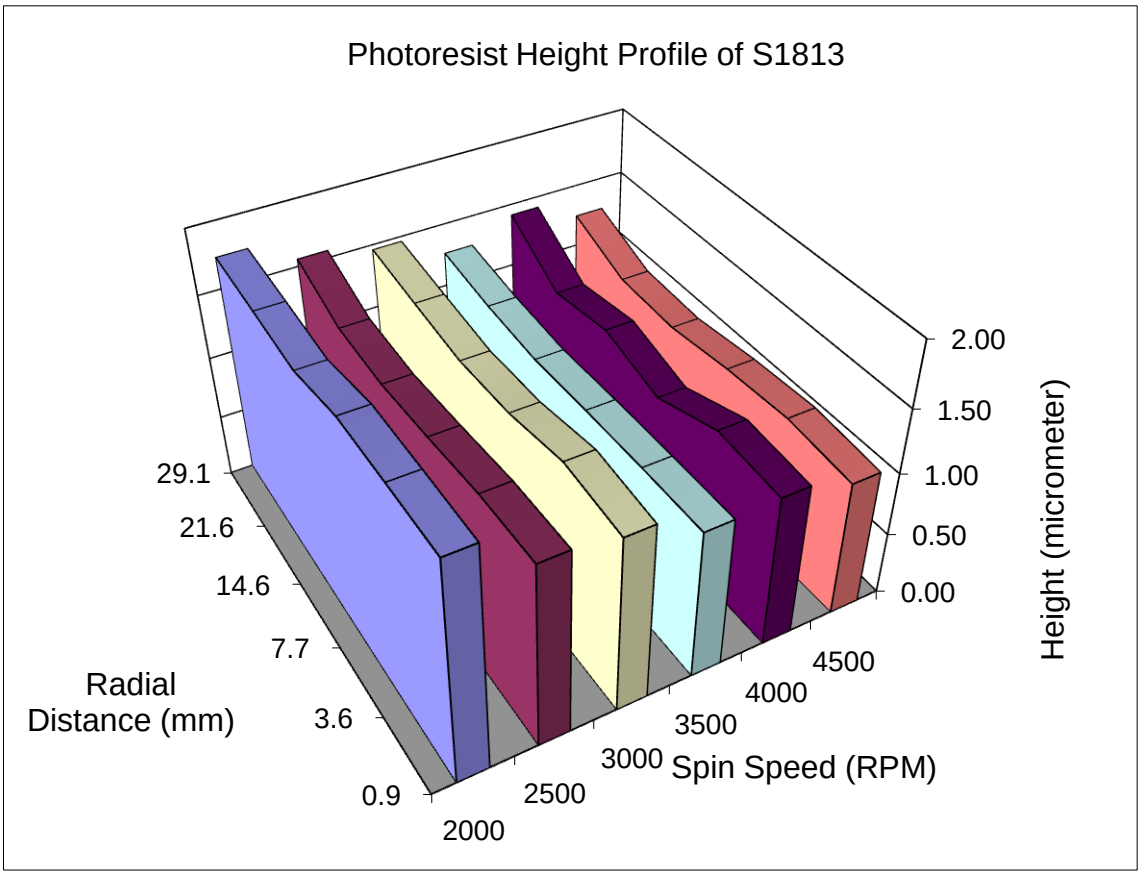

Figure A. 4. Three-D representation of S1813 deposition showing the effect of spin coating speed (in rotation per minute, rpm) on the thickness of deposited photoresist layer at points from the centre of rotation (the radial distance).

As expected, the higher the spin rate of the sample, the lower the thickness of the resulting photoresist height. Spinning S1813 photoresist between 2000 – 3500 rpm for 30 seconds gives rise to a relatively uniform thickness along the longest side of the rectangular sample. Spinning at higher spin rates gave a greater variation in the resulting heights of the photoresist. The variation was in the range of 0.1 to 0.3 of a micrometer. For microstructure development, this variation could be important, especially in metal lift-off processes where a clear cut between exposed and non-exposed regions is required after spin-coating, exposure, development and metal deposition.

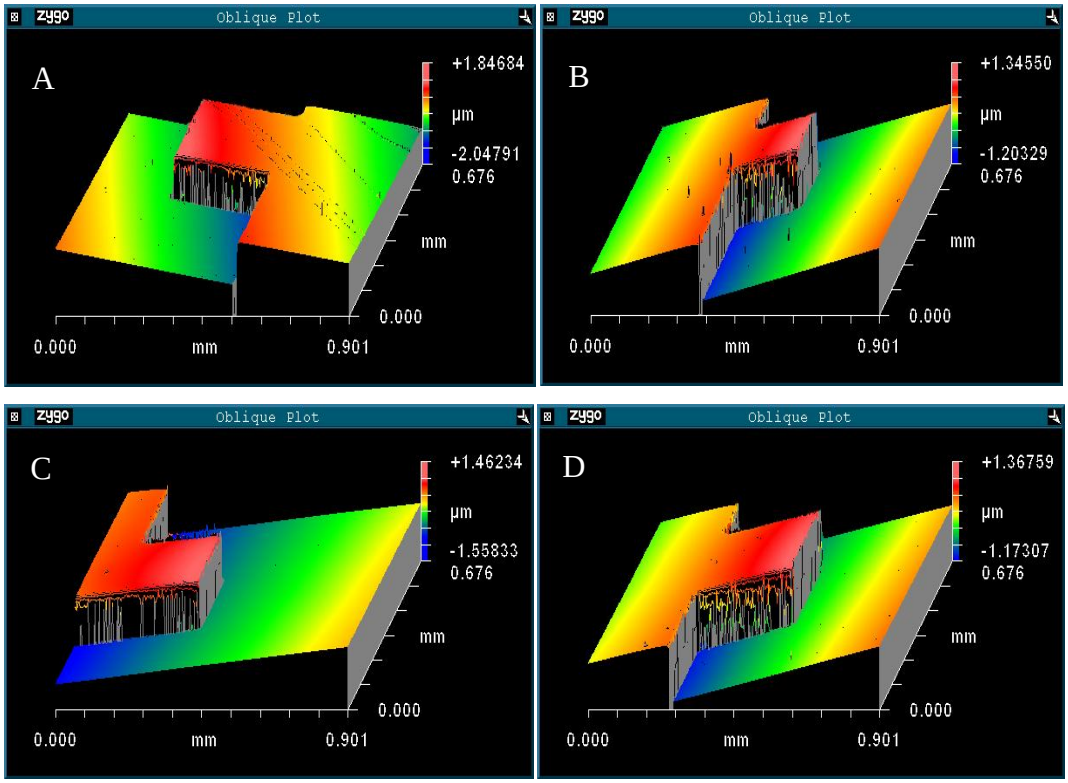

Figure A. 5. Typical height profiles (oblique plot) of positive photoresist S1813 spun at 2500 rpm, at radial distance of: (A) 29.1 mm; 1.56 (±0.07) µm (B), 7.7 mm; 1.41 (±0.05) µm (C) 14.6 mm; 1.37 (±0.10) µm (D) 21.6 mm; 1.39 (±0.07) µm.

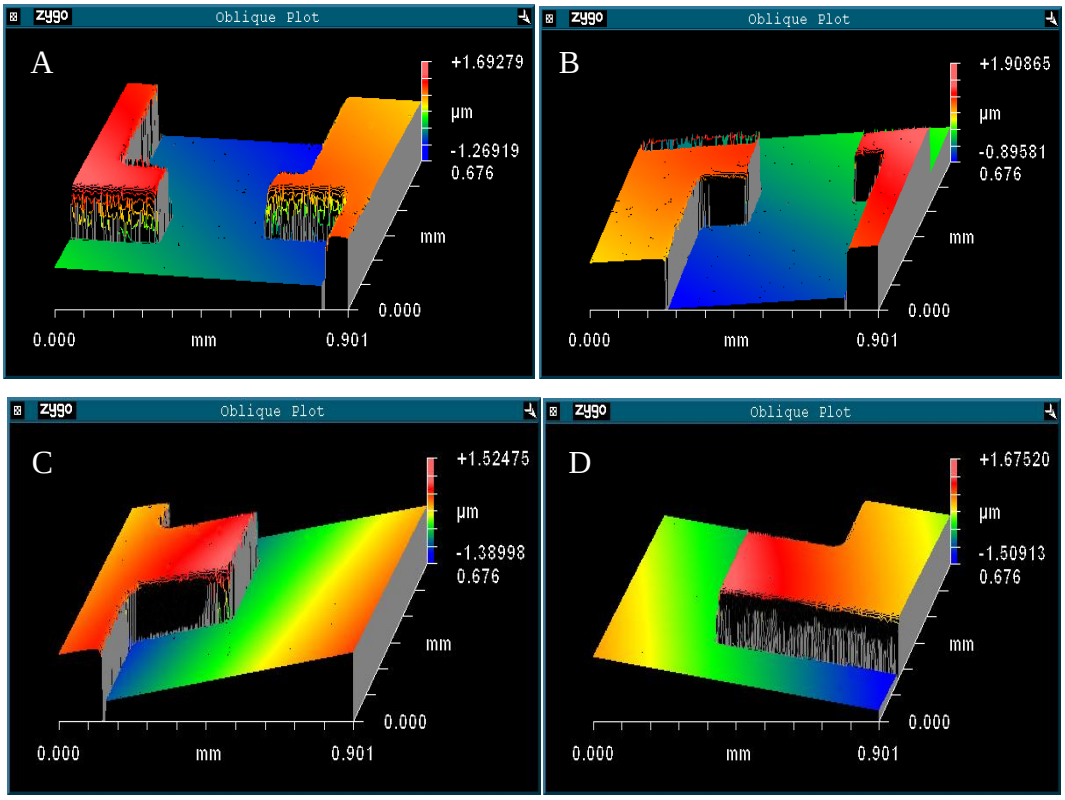

Figure A. 6. Typical height profiles (oblique plot) of positive photoresist S1813 spun at 3000 rpm, at radial distance of: (A) 3.6 mm; 1.46 (±0.07) µm (B), 7.7 mm; 1.37 (±0.04) µm (C) 21.6 mm; 1.40 (±0.06) µm (D) 29.1 mm; 1.46 (±0.04) µm

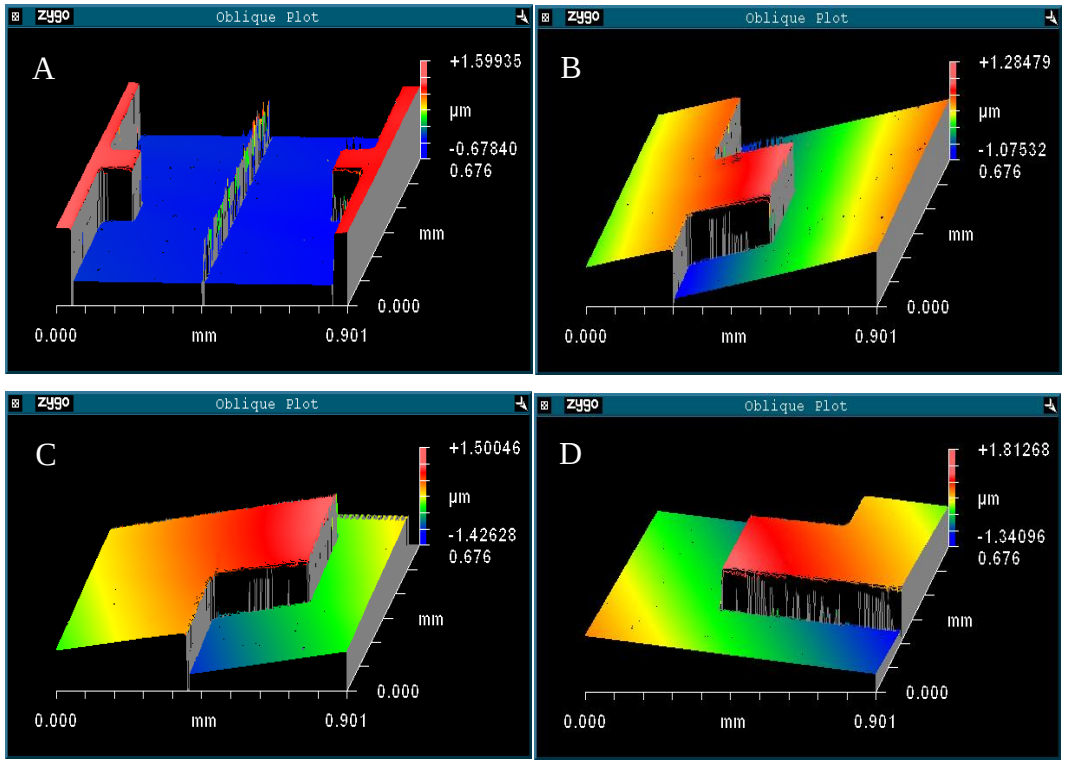

Figure A. 7. Typical height profiles (oblique plot) of positive photoresist S1813 spun at 3500 rpm, at radial distance of: (A) 0.9 mm; 1.19 (±0.04) µm (B), 14.6 mm; 1.16 (±0.02) µm (C) 21.6 mm; 1.20 (±0.05) µm (D) 29.1 mm; 1.26 (±0.06) µm

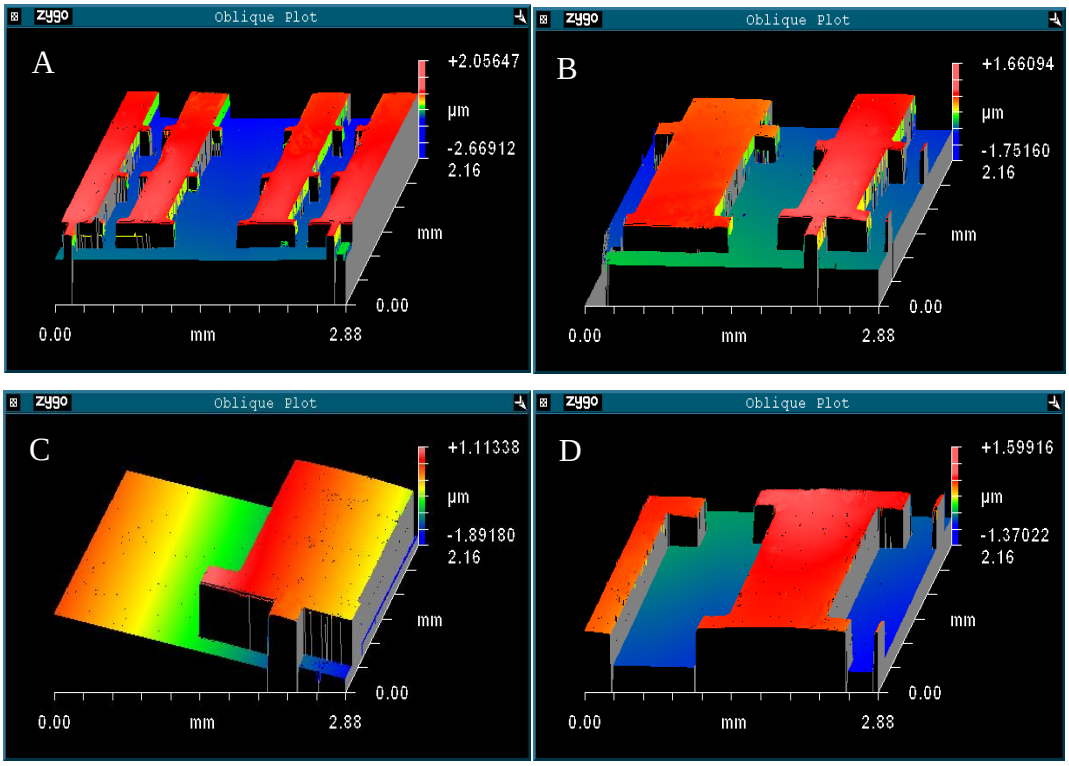

Figure A. 8. Typical height profiles (oblique plot) of positive photoresist S1813 spun at 4000 rpm, at radial distance of: (A) 0.9 mm; 1.21 (±0.03) µm (B), 7.7 mm; 1.07 (±0.17) µm (C) 29.1 mm; 1.41 (±0.13) µm (D) 21.6 mm; 1.13 (±0.06) µm.

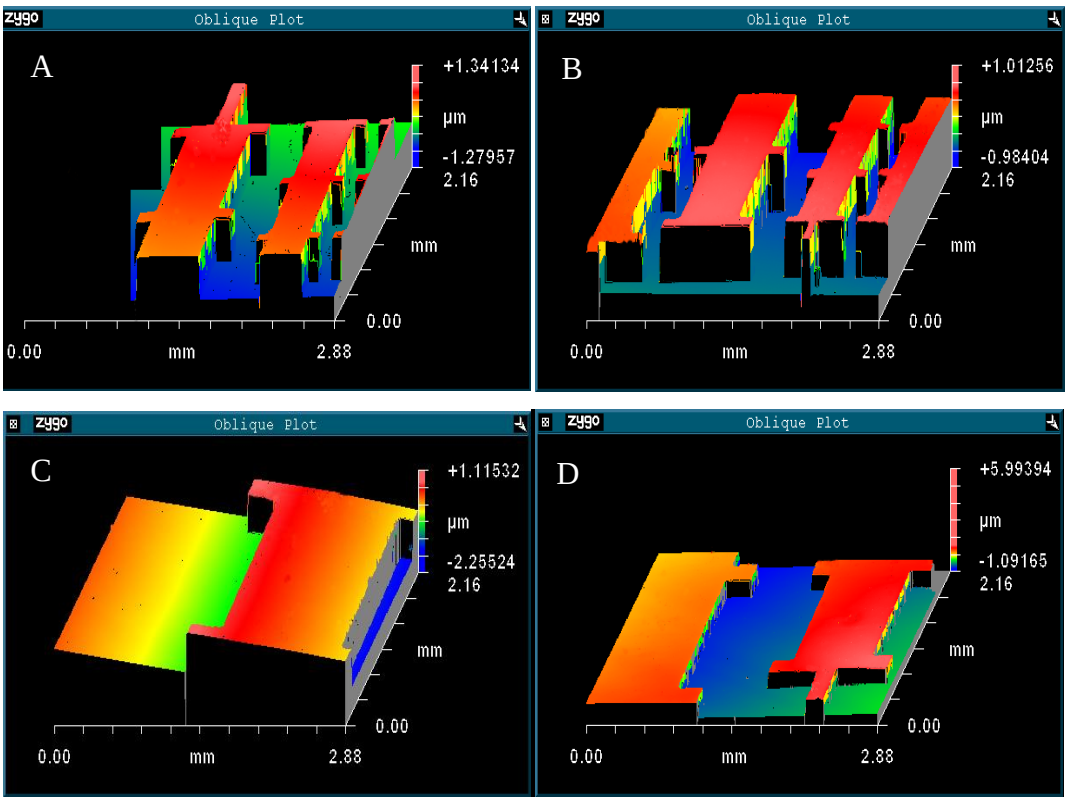

Figure A. 9. Typical height profiles (oblique plot) of positive photoresist S1813 spun at 4500 rpm, at radial distance of: (A) 7.7 mm; 1.10 (±0.01) µm (B), 3.6 mm; 1.13 (±0.01) µm (C) 29.1 mm; 1.25 (±0.01) µm (D) 14.6 mm; 1.04 (±0.06) µm.

The thickest S1813 photoresist layer (1.8 µm) was achieved when spinning S1813 at 2000 rpm for 30 seconds. Varying the duration of the spinning by ± 10% did not affect the heights significantly (data not shown). All height measurements were therefore done after spinning samples for 30 seconds. The thinnest photoresist layer (1.1 µm) was achieved when spinning the resist at 4500 rpm. As mentioned, the height variations along the radial distance were stronger at higher spinning rates (4000 – 4500 rpm) than at lower spinning rates (2000 – 3500).

Figure A.5 to Figure A.9 show some of the surface characteristics of the deposited photoresist, mainly on the edge regions. Some of these plots indicate that the samples were slightly tilted on the surface of microscope stage when measurement by vertical scanning white-light interferometry was done, giving rise to rainbow-color oblique plots.

Some minor spikes or lines could be observed based on the spectral image of the sample (as can be seen in Figure A.5 part A and B), but cracks or any major defects such as holes were generally absent. A larger view of the sample image under lower magnification (Figure A.8 and Figure A.9 part A and B) confirmed this finding further. The quality of the S1813 photoresist was considered sufficient for further processing such as metal lift-off and etching of the underlying metal layer.

A.4.2 The effect of spin-coating speed to the thickness profile of SU8-50

Figure A.10 and Figure A.11 plot and compare the surface thickness profiles of negative-tone SU8-50 photoresist, using 2D and 3D representations at two main spin rates (1000 and 2000 rpm), with various distances from the central point of rotation (i.e. the radial distance).

Analysis of the graphs indicate a similar pattern as with S1813 i.e. that the higher the spin rate of the sample, the lower the thickness of the resulting photoresist heights due to greater centrifugal force acting on the surface. Spinning SU8-50 photoresist on a rectangular sample at 2000 rpm for 30 seconds gave a relatively uniform thickness along the longest side of the rectangular sample. Spinning a rectangular sample at a lower spin rate (1000 rpm) gave rise to the formation of edge effects, the size of which

depended on the spin rates (i.e. the lower the spin rate the greater the size of the edge beads). The difference between the centre area and the edge area of the rectangular sample (as shown in Figure A.10 and Figure A.11) was in the range of 10 to 20 micrometer. For microstructure development, this variation in surface height is generally undesirable, especially if a later step involves UV exposure as full contact between pattern mask and the entire area of photoresist surface is then required. In order to achieve this, a completely flat surface is required. The uneven surface characteristic of SU8-50 spun at 1000 rpm or less also discourages its application for fabricating micro channels. A thinner (and relatively more flat) photoresist layer of around 68 µm was achieved when spinning the resist at 2000 rpm or more.

Figure A.12 and Figure A.13 show some of the surface characteristics of the deposited SU8-50 photoresist and edge regions where sample heights have been measured. In general, the process parameters of UV exposure and development have been optimized and resulting in vertical (sharp) edges of resist layer on the wafer. Some of these plots indicate that the samples were slightly tilted on the surface of microscope stage when measurement by vertical scanning white-light interferometry was done, hence giving rise to rainbow-color oblique plots.

Some very minor cracks of lines were present based on the spectral image of the sample (as shown in Figure A.12 part C and F), but any major defects such as holes were generally absent. The presence of such physical disruptions indicate that one or more process parameters need further optimization. This may include the use of a longer evaporation time between spin coating and soft-baking.

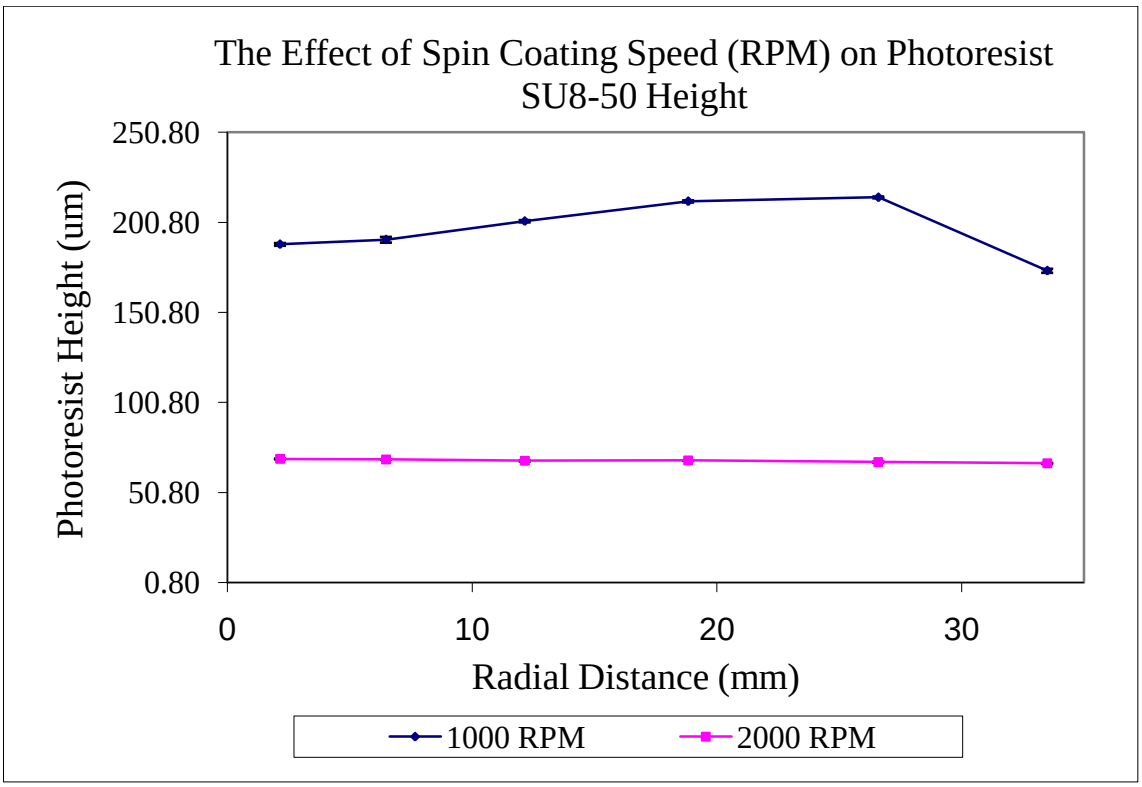

Figure A. 10. The effect of spin coating speed (in rotation per minute, rpm) on the thickness of deposited photoresist layer SU8-50 (assessed after development step) at points from the centre of rotation (the radial distance). Error bars show standard errors of each data points

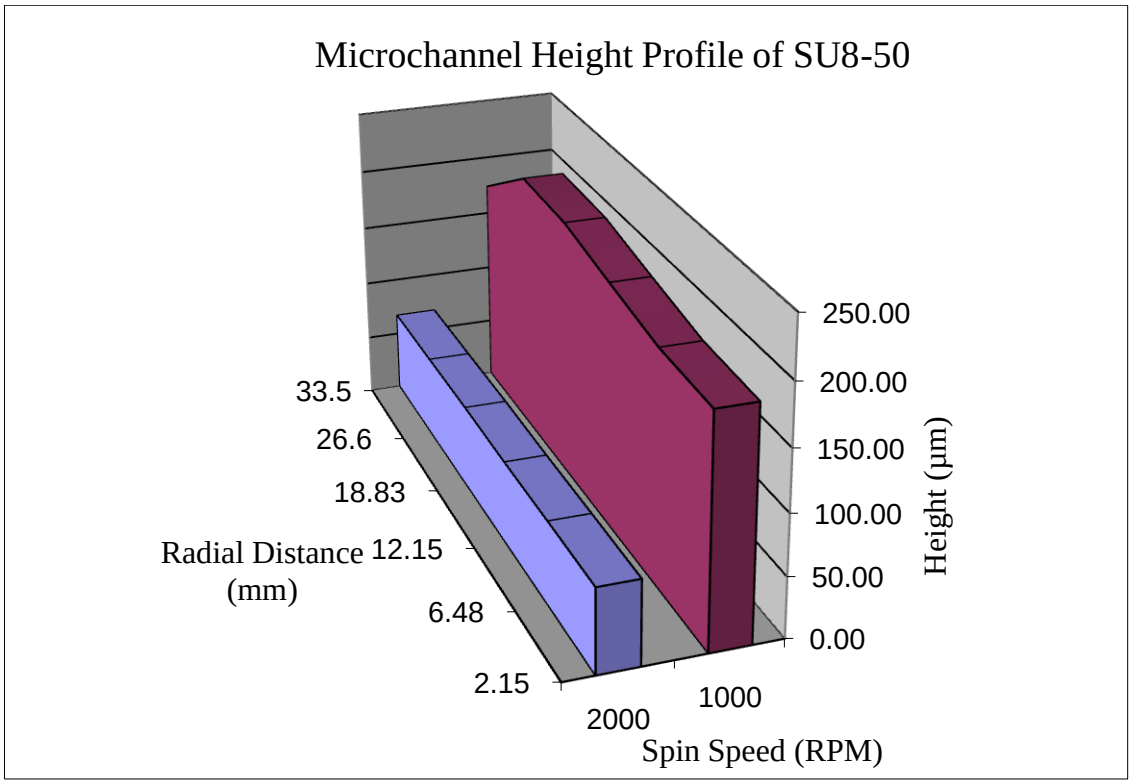

Figure A. 11. 3D representation of SU8-50 deposition showing the effect of spin coating speed (in rotation per minute, rpm) on the thickness of deposited photoresist layer at points from the centre of rotation (the radial distance).

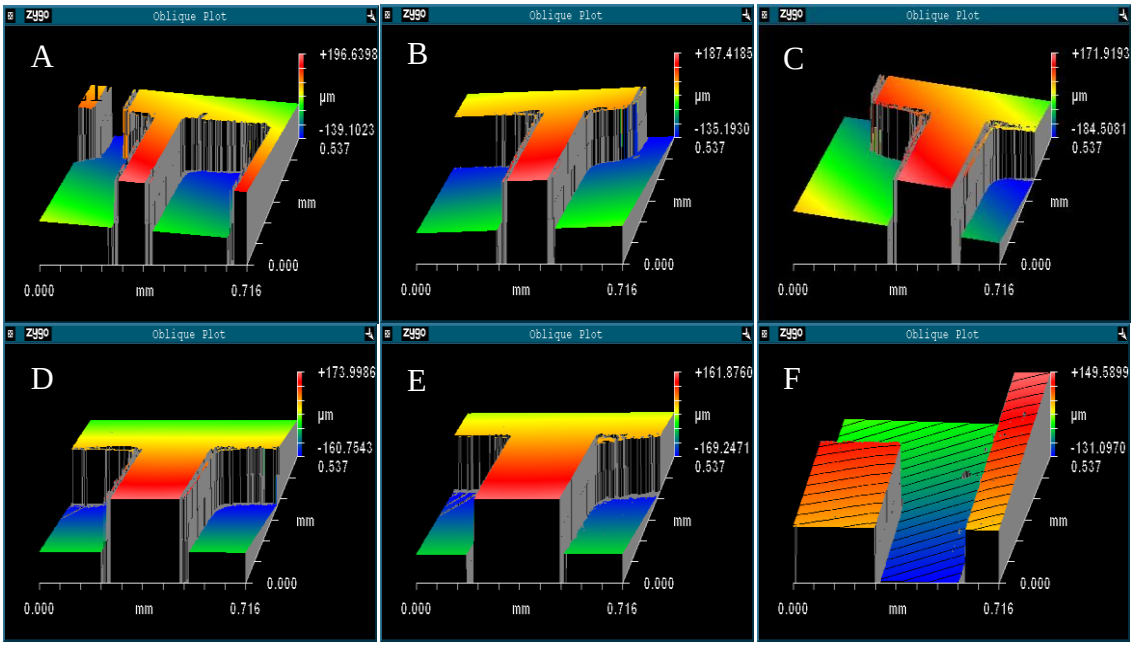

Figure A. 12. Typical height profile (oblique plot) of negative photoresist SU8-50, when spun at 1000 rpm, at a radial distance of (A) 2.2 mm; 188.7 (± 0.7) µm, (B) 6.5 mm; 191.2 (± 1.6) µm, (C) 12.2 mm; 201.5 (± 0.6) µm, (D) 18.8 mm; 212.5 (± 0.6) µm (E) 26.6 mm; 214.7 (± 0.5) µm and (F) 33.5 mm; 174.0 (± 1.1) µm, as measured using white-light interferometry technique.

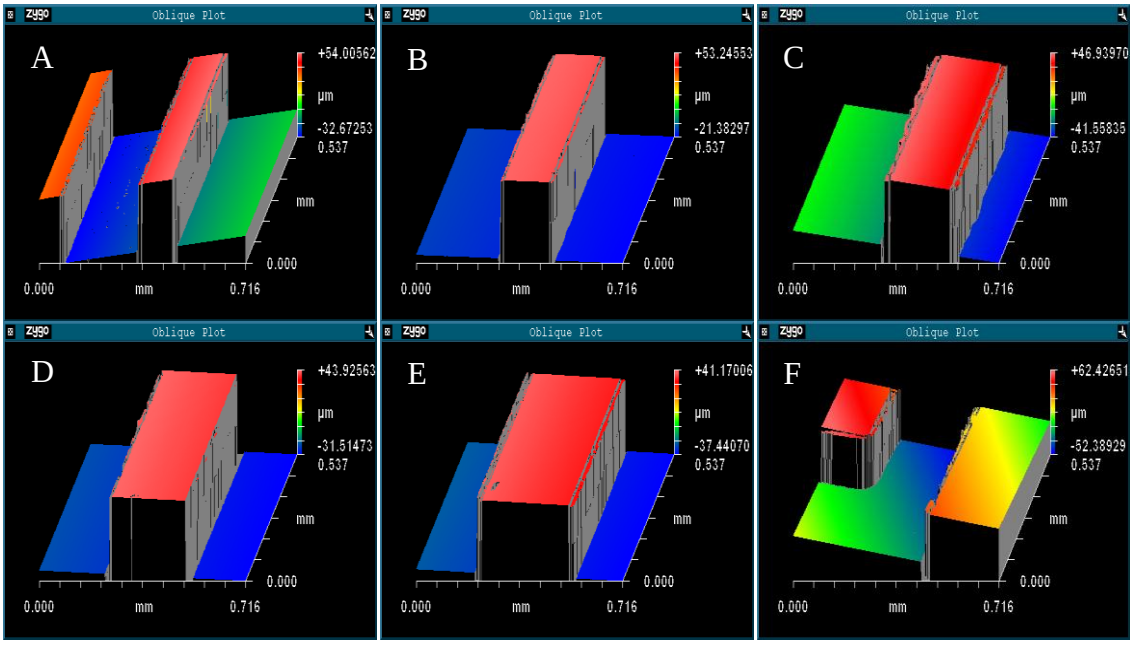

Figure A. 13. Typical height profile (oblique plot) of negative photoresist SU8-50, when spun at 2000 rpm at radial distance of (A) 2.2 mm; 69.5 (± 0.1) µm, (B) 6.5 mm; 69.2 (± 0.1) µm, (C) 12.2 mm; 68.5 (± 0.3) µm, (D) 18.8 mm; 68.7 (± 0.1) µm, (E) 26.6 mm; 67.8 (± 0.3) µm and (F) 33.5 mm; 67.0 (± 0.2) µm, as measured using white-light interferometry technique.

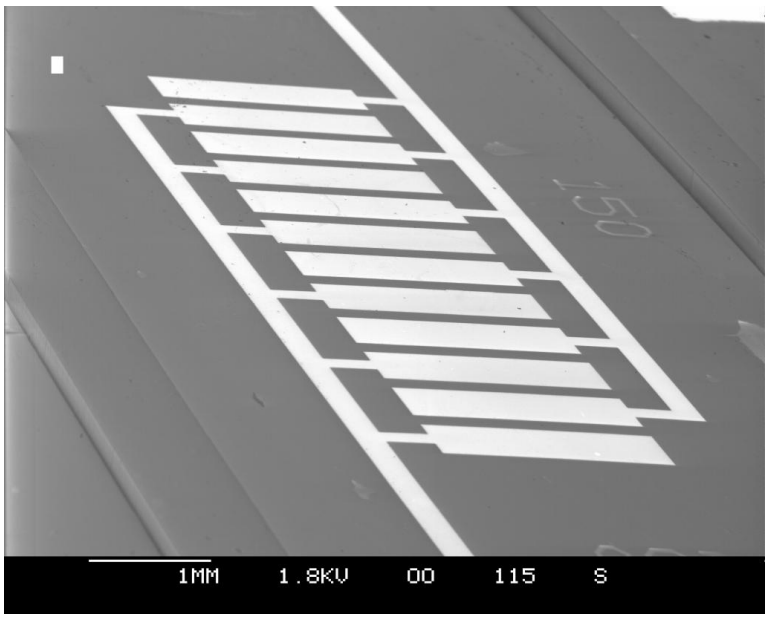

Figure A. 14. Scanning electron microscope (SEM) image of microchannel made of SU8-50, containing ITO microelectrodes with horizontal line pattern (150 µm feature size).

A.4.3 Pattern formation on the fabricated electrodes using dielectrophoresis

All micro electrodes were subjected to the same signal frequency of 1 MHz and 20 $V_{pk\text{-}pk}$, and cells were introduced. As can be seen from Figure A.15, cells of *Saccharomyces cerevisiae*, suspended in low conductivity medium, aligned themselves according to areas of strong electric field produced as a result of non-uniform AC electric field. The quality of the microelectrodes seems to be acceptable.

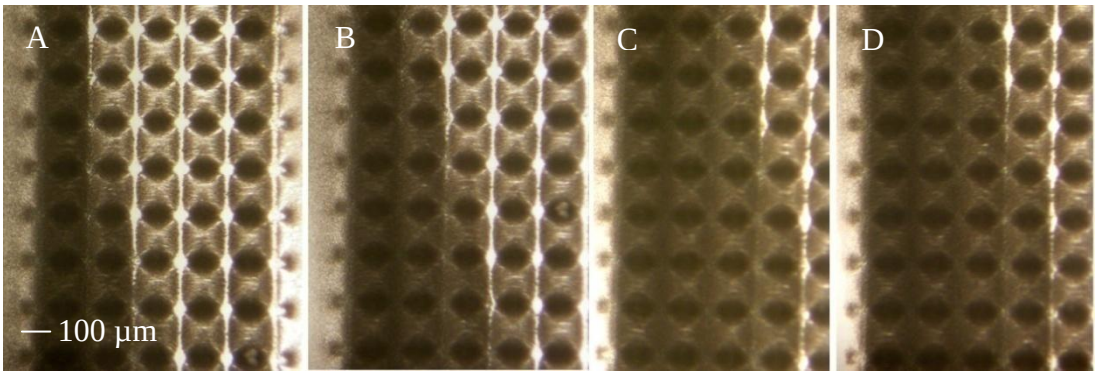

Figure A. 15. Formation of tissue-like 3D structure of aggregated (packed) yeast cells under non-uniform (AC) electric field of dielectrophoresis for A.10, B.20, C.30, D.40 minutes. The dark rounded shapes are the cell aggregates. The white bar regions, visible mainly in Panel A and B show the main bars of the microelectrodes. These regions were covered in time as more and more yeast cells were trapped, forming tissue-like materials.

A.5 Conclusions

It was shown that optimal process parameters for electrode microfabrication could be obtained with the help of spectral data produced by the white light vertical-scanning interferometry technique. The resulting interferograms show the 3D surface topography.

S1813 was shown to be a suitable photoresist for microelectrode formation from ITO using photolithography. SU8, however, did not give a smooth and flat surface at the desired height (around 200 μm). This is because SU8 photoresist must be spun at a very low spin rates (1000 rpm) to achieve a photoresist height of 200 micron, which gives edge bead effects. An uneven surface could potentially cause leaks. The dielectrophoresis device used in the experiments requires a highly sealed chamber, and the use of other more flexible materials such as polydimethyl siloxane (PDMS), silicone rubber or thin teflon sheet should be explored.

APPENDIX B

Image Gallery From the Scientific Image Competition

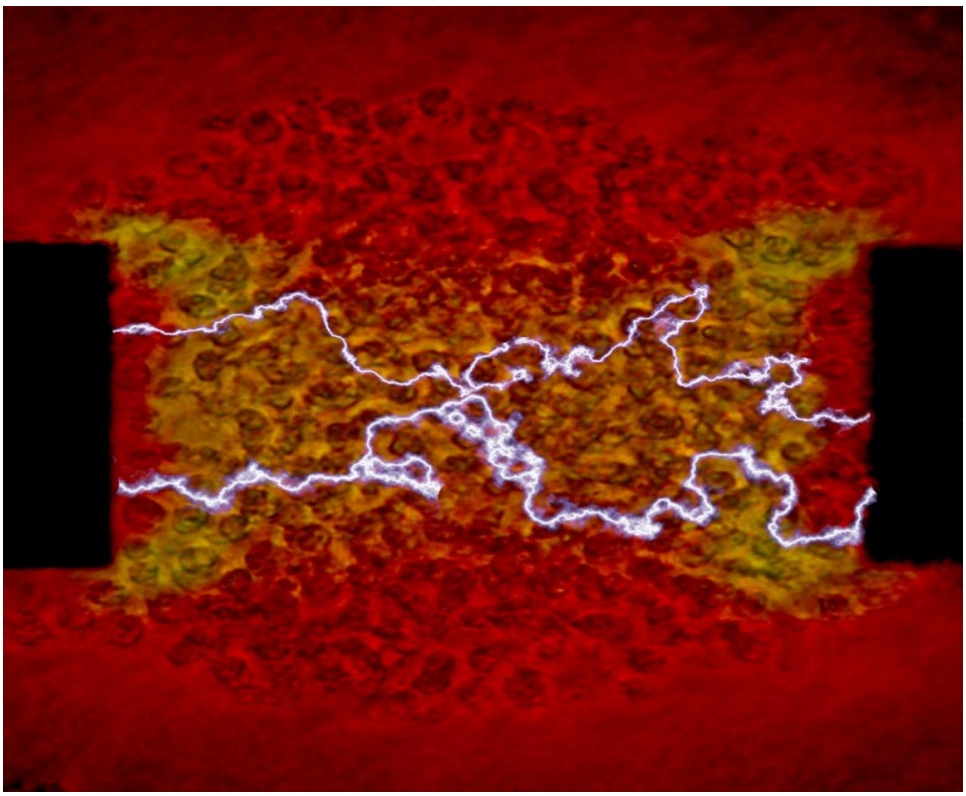

Image 1. Cell aggregation (*2nd Price in EPS Technical Photo Competition 2009*). Microscopic view of a single cell aggregate (of skin cells) between electrode castellations.

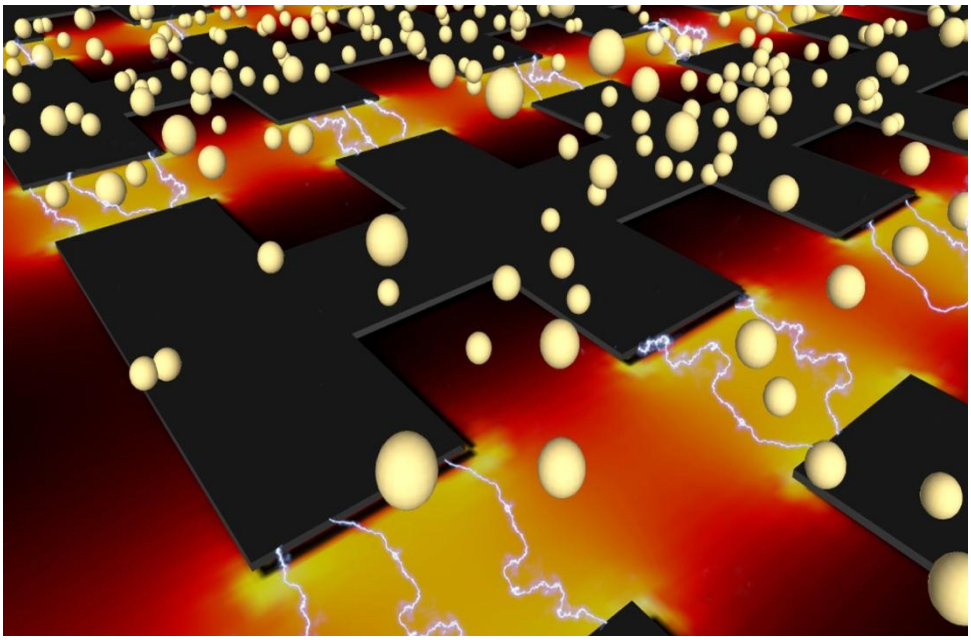

Image 2. Dielectrophoresis in 3D (*Runner Up in EPS Technical Photo Competition 2009*). Stylized image showing cells accumulating at electrode edges where the electric field strength is the highest.

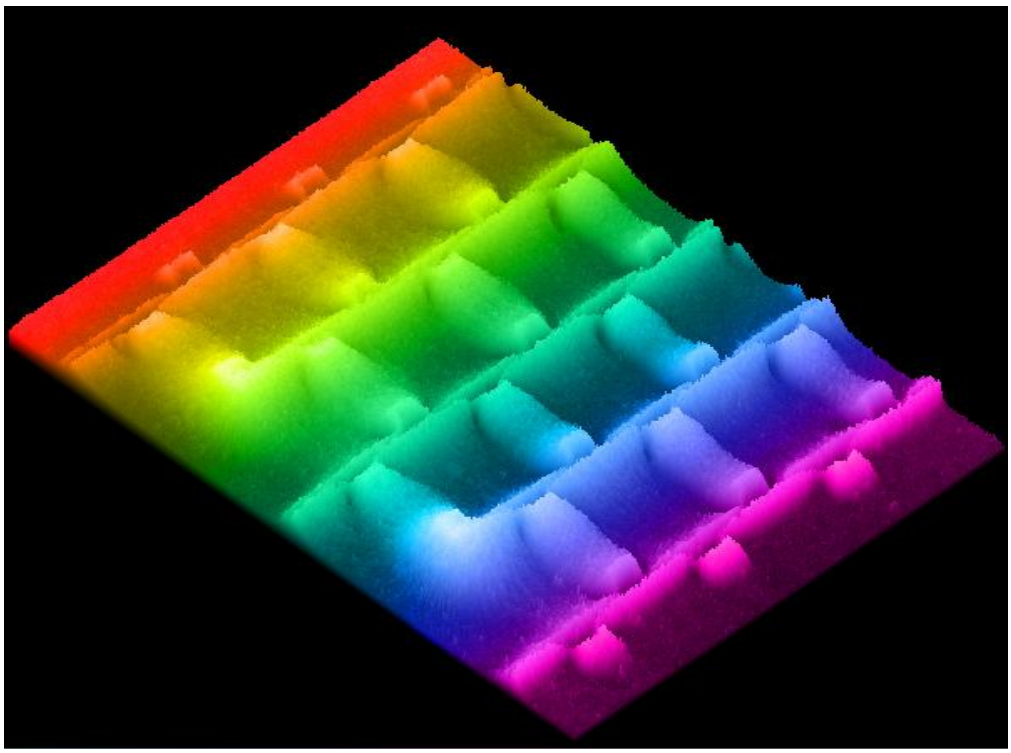

Image 3. 3D density plots (*Runner Up in EPS Technical Photo Competition 2009*). Image analysis of the various cell patterns made using dielectrophoresis can be used to obtain information about the cell aggregation process and further development. The images presented are 3D density plots. Rainbow colors are for artistical purposes.

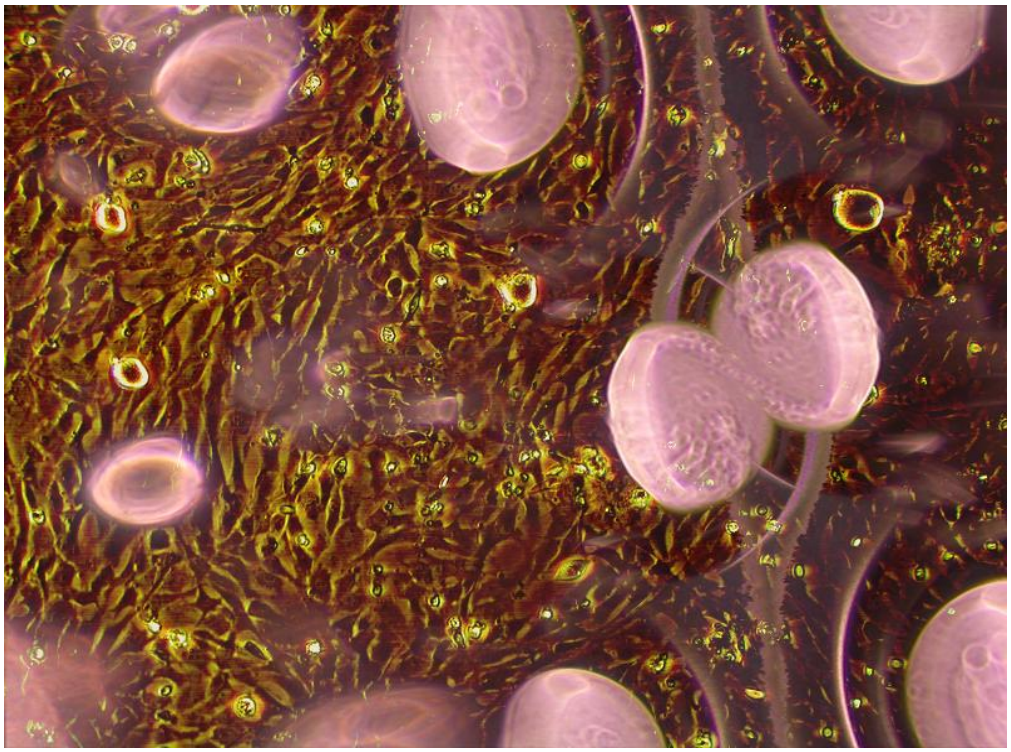

Image 4. Fibroblast cells (*Runner Up in EPS Technical Photo Competition 2010*). Fibroblast-type morphology of embryonic skin cells. The pink structures are colored artifact for presentational purposes only.

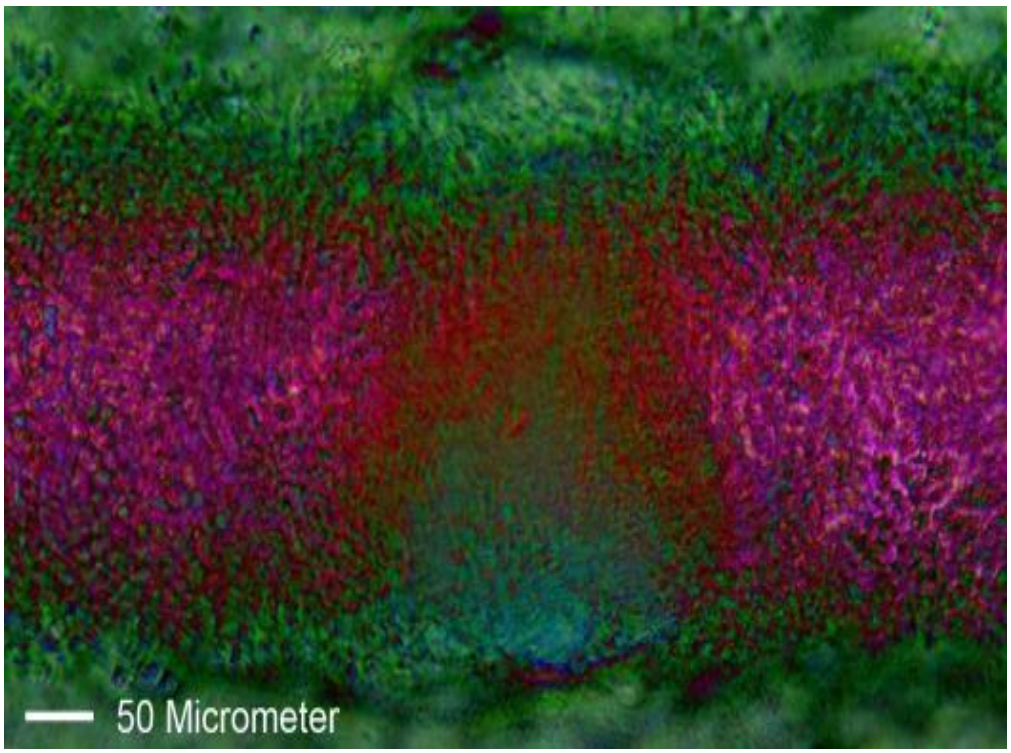

Image 5. Line Aggregates (*Runner Up in EPS Technical Photo Competition 2010*). Embryonic skin cells (dermal and epidermal) confined in specific areas in a well-defined geometrical pattern (Parallel Lines), of a known size and shape between microelectrodes that can be used for the study of developmental processes in skin.

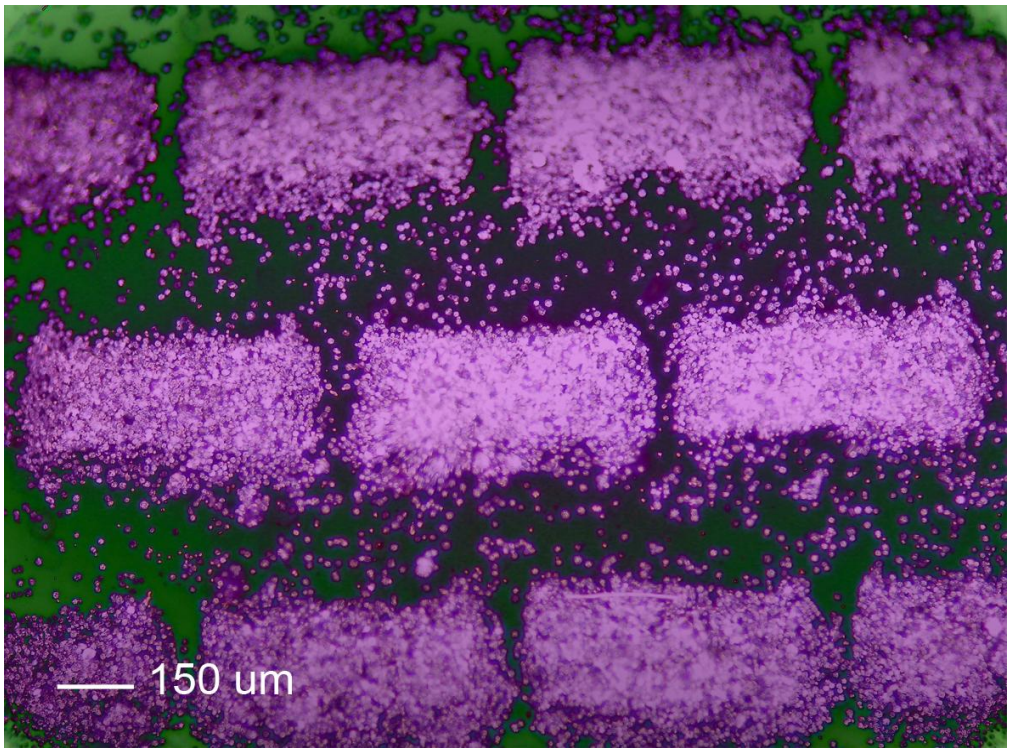

Image 6.Embryonic Skin Cell ((*Runner Up in EPS Technical Photo Competition 2010*). Embryonic skin cells (dermal and epidermal) confined in specific areas in a well-defined geometrical pattern (hexagonal), of a known size and shape between microelectrodes that can be used for the study of developmental processes in skin.

References

Abidin, Z. Z., L. Downes and G. H. Markx (2007). "*Large scale dielectrophoretic construction of biofilms using textile technology*." Biotechnol. Bioeng. **96**: 1222-1225.

Abreu, J. G., N. I. Ketpura, B. Reversade and E. M. D. Robertis (2002). "*Connective-tissue growth factor (CTGF) modulates cell signalling by BMP and TGF-beta*." Nat. Cell Biol., **4**: 599–604.

Ainslie, K. M., G. Sharma, M. A. Dyer, C. A. Grimes and M. V. Pishko (2005). "*Attenuation of protein adsorption on static and oscillating magnetostrictive nanowires*." Nano Lett. **5**(9): 1852–6.

Akam, M. (1989). "*Drosophila development: making stripes inelegantly*." Nature, **341**: 282 - 283.

Alberts, B. (2001). *Molecular Biology of the Cell*. New York, Garland Science.

Albrecht, D. R., R. L. Sah and S. N. Bhatia (2004). "*Geometric and material determinants of patterning efficiency by dielectrophoresis*." Biophys. J. **87**: 2131-2147.

Albrecht, D. R., V. L. Tsang, R. L. Sah and S. N. Bhatia (2005). "*Photo- and electropatterning of hydrogel-encapsulated living cell arrays.*" Lab Chip **5**: 111-118.

Albrecht, D. R., G. H. Underhill, A. Mendelson and S. N. Bhatia (2007). "*Multiphase electropatterning of cells and biomaterials.*" Lab Chip **7**: 702-709.

Albrecht, D. R., G. H. Underhill, T. B. Wassermann, R. L. Sah and S. N. Bhatia (2006). "*Probing the role of multicellular organization in three-dimensional microenvironments.*" Nature Methods **3**: 369-375.

Alp, B., J. S. Andrews, V. P. Mason, R. Wolowacz and G. H. Markx (2003). "*Building structured biomaterials using AC electrokinetics*." IEEE Eng. Med. Biol. **22**(6): 91-97.

Alp, B., G. M. Stephens and G. H. Markx (2002). "*Formation of artificial, structured microbial consortia (ASMC) by dielectrophoresis*." Enzyme Microb. Technol. **31**: 35-43.

Andl, T., K. Ahn, A. Kairo, E. Y. Chu, L. Wine-Lee, S. T. R. Eddy, N. J. Croft, J. A. Cebra-Thomas, D. Metzger and P. C. hambon (2004). "*Epithelial Bmpr1a regulates differentiation and proliferation in postnatal hair follicles and is essential for tooth development*." Development **131**: 2257 – 2268.

Andl, T., S. T. Reddy, T. Gaddapara and S. E. Millar (2002). "*WNT signals are required for the initiation of hair follicle development.*" Dev. Cell **2**: 643–653.

Andrews, J. S., V. P. Mason, I. P. Thompson, G. M. Stephens and G. H. Markx (2006). "*Construction of artificially structured microbial consortia (ASMC) using dielectrophoresis: Examining bacterial interactions via metabolic intermediates within environmental biofilms*." J. Microb. Methods **64**: 96-106.

Archer, S., T. T. Li, A. T. Evans, S. T. Britland and H. Morgan (1999). "*Cell reactions to dielectrophoretic manipulation.*" Biochem. Biophys. Res. Comm. **257**: 687-698.

Armstrong, N. J., K. J. Painter and J. A. Sherratt (2006). "*A continuum approach to modelling cell-cell adhesion.*" J. Theor. Biol. **243**: 98 - 113.

Arnold, W. M. (2008). "*Particle Patterning Using Fluidics and Electric Fields*." IEEE Trans. Diel. Electr. Insul. **15**(1): 144-151.

Arnold, W. M. and N. R. Franich (2006). "*Cell isolation and growth in electric-field defined micro-wells*." Curr. Appl. Phys. **6**: 371–374.

Asokan, S. B., L. Jawerth, R. L. Carroll, R. E. Cheney, S. Washburn and R. Superfine (2003). "*Two-dimensional manipulation and orientation of actin-myosin systems with dielectrophoresis*." Nano. Lett. **3**: 431–437.

Atit, R., R. A. Conlon and L. Niswander (2003). "*EGF signaling patterns the feather array by promoting the interbud fate*." Dev. Cell, **4**: 231 - 240.

Auger, F. A., R. Pouliot, N. Tremblay, R. Guignard, P. Noe, J. Juhasz, L. Germain and L. Goulet (2000). "*Multi-step production of bioengineered skin substitutes: sequential modulation of culture conditions*." In Vitro Cell Dev. Biol.- Animal **36**: 96-103.

Baker, R. E., S. Schnell and P. K. Maini (2009). "*Waves and patterning in developmental biology: vertebrate segmentation and feather bud formation as case studies*." Int. J. Dev. Biol. **53**: 783-94.

Balemans, W. and W. V. Hul (2002). "*Extracellular regulation of BMP signaling in vertebrates: a cocktail of modulators.*" Dev. Biol., **250**: 231–250.

Birkbeck, A. L., R. A. Flynn, M. Ozkan, D. Q. Song, M. Gross and S. C. Esener (2003). "*VCSEL Arrays as micromanipulators in chip-based biosystems*." Biomed. Microdev. **5**: 47-54.

Blanco-Gomez, G., A. Glidle, L. M. Flendrig and J. M. Cooper (2009). "*Integration of Low-Power Microfluidic Pumps with Biosensors within a Laboratory-on-a-Chip Device*." Anal. Chem. **81**: 1365-1370.

Botchkarev, V. A., N. V. Botchkareva, W. Roth, M. Nakamura, L. H. Chen, W. Herzog, G. Lindner, J. A. McMahon, C. Peters, R. Lauster, A. P. McMahon and R. Paus (1999). "*Noggin is a mesenchymally derived stimulator of hairfollicle induction*." Nat. Cell Biol. **1**: 158 – 164.

Bouyer, D., F. Geier, F. Kragler, A. Schnittger, M. Pesch, K. Wester, R. Balkunde, J. Timmer, C. Fleck and M. Hülskamp (2008). "*Two-Dimensional Patterning by a*

Trapping/ Depletion Mechanism: The Role of TTG1 and GL3 in Arabidopsis Trichome Formation." PLoS Biology **6**: 1166 - 1177.

Britten, J. A. (1983). "*A simple theory for the entrained film thickness during meniscus coating*." Chem. Eng. Comm. **120**(1): 59 - 71.

Campbell, S. A. (2001). *The Science and Engineering of Microelectronic Fabrication*. New York, Oxford University Press.

Castellanos, A., A. Ramos, A. Gonzalez, N. G. Green and H. Morgan (2003). "*Electrohydrodynamics and dielectrophoresis in microsystems: scaling laws*." J. Phys. D: Appl. Phys **36**: 2584–2597.

Chang, C. H., M. Yu, P. Wu, T. X. Jiang, H. S. Yu, R. B. Widelitz and C. M. Chuong (2004). "*Sculpting skin appendages out of epidermal layers via temporally and spatially regulated apoptotic events*." J. Invest. Dermatol. **122**: 1348-1355.

Chen, E. A., Z. Neeman and F. T. Lee (2006). "*Thermal protection with 5% dextrose solution blanket during radiofrequency ablation*." Cardio. Intervent. Radiology **29**(6): 1093-1096.

Cho, M. R., H. S. Thatte, R. C. Lee and D. E. Golan (1996). "*Reorganization of microfilament structure induced by ac electric fields*." FASEB J. **10**: 1552-1558.

Chung, J., K. Lee, J. Lee and R. Ruoff (2004). "*Toward large-scale integration of carbon nanotubes*." Langmuir **20**: 3011-3017.

Chuong, C. M., H. M. Chen, T. X. Jiang and C. J (1991). "*Adhesion molecules in skin development: morphogenesis of feather and hair*." Ann. N. Y. Acad. Sci. **642**: 263-80.

Chuong, C. M. and G. M. Edelman (1985a). "*Expression of cell adhesion molecules in embryonic induction. II. Morphogenesis of adult feathers*." J. Cell Biol. **101**: 1027–1043.

Chuong, C. M. and G. M. Edelman (1985b). "*Expression of cell-adhesion molecules in embryonic induction. I. Morphogenesis of nestling feathers*." J. Cell Biol. **101**: 1009-1026.

Chuong, C. M., R. B. Widelitz, S. Ting-Berreth and T. X. Jiang (1996). "*Early events during avian skin appendage regeneration: dependence on epithelial-mesenchymal interaction and order of molecular reappearance*." J. Invest. Dermatol. **107**: 639-646.

Coakley, W. T., D. Bazou, J. Morgan, G. A. Foster, C. W. Archer, K. Powell, K. A. J. Borthwick, C. Twomey and J. Bishop (2004). "*Cell–cell contact and membrane spreading in an ultrasound trap*." Colloids and Surfaces B: Biointerfaces **34**(4): 221-230.

Cooper, M. K., J. A. Porter, K. E. Young and P. A. Beachy (1998). "*Teratogen-mediated inhibition of target tissue response to Shh signaling*." Science **280**: 1603–1607.

Crampin, E. J., E. A. Gaffney and P. K. Maini. (1999). "*Reaction and diffusion on growing domains: Scenarios for robust pattern formation.*" Bull. Math. Biol., **61**: 1093 – 1120.

Cui, Y., R. Hackenmiller and L. Berg (2001). "*The activity and signaling range of mature BMP-4 is regulated by sequential cleavage at two sites within the prodomain of the precursor*." Genes Dev. **15**(21): 2797-802.

Cummings, E. B. (2003). "*Streaming dielectrophoresis for continuousflow microfluidic devices*." IEEE Eng. Med. Biol. Mag. **22**: 75–84.

Curtis, J. E., B. A. Koss and D. G. Grier (2002). "*Dynamic holographic optical tweezers*." Opt. Comm. **207**: 169.

Dahmane, N., J. Lee, P. Robins, P. Heller and A. R. i. A. . (1997). "*Activation of the transcription factor Gli1 and the Sonic hedgehog signalling pathway in skin tumours*." Nature **389**: 876 – 881.

DasGupta, R. and E. Fuchs (1999). "*Multiple roles for activated LEF/TCF transcription complexes during hair follicle development and differentiation*." Development **126**: 4557– 4568.

Desai, J. P., A. Pillarisetti and A. D. Brooks (2007). "*Engineering approaches to biomanipulation*." Ann. Rev. Biomed. Eng. **9**: 35-53.

Dhouailly, D., I. Olivera-Martinez, I. Fliniaux, S. Missier, J. P. Viallet and J. Thelu (2004). "*Skin field formation: morphogenetic events*." Int. J. Dev. Biol. **48**: 85-91.

Dillon, R., P. K. Maini and H. G. Othmer (1994). "*Pattern formation in generalised Turing systems. I. Steady state patterns in systems with mixed boundary conditions.*" J. Math. Biol. **32**: 345–393.

Djuzenova, C., U. Zimmermann, H. Frank and V. Sukhorukov (1996). "*Effect of medium conductivity and composition on the uptake of propidium iodide into electropermeabilized myeloma cells*." Biochim. Biophys. Acta **1284**: 143-152.

Docoslis, A. and P. Alexandridis (2002). "*One-, two-, and three-dimensional organization of colloidal particles using non-uniform alternating current electric field*." Electrophoresis **23**: 2174 - 2183.

Docoslis, A., N. Kalogerakis and L. A. Behie (1999). "*Dielectrophoretic forces can be safely used to retain viable cells in perfusion cultures of animal cells*." Cytotechnology **30**: 133-142.

Doljanski, F. (2004). "*The sculpturing role of fibroblast-like cells in morphogenesis*." Persp. Biol. Med. **47**: 339 - 356.

Dulos, E., J. Boissonade, J. J. Perraud, B. Rudovics and P. De Kepper (1996). "*Chemical morphogenesis: turing patterns in an experimental chemical system.*" Acta Biotheor. **44**: 249-261.

Eaton, S. (2006). "*Release and trafficking of lipid-linked morphogens.*" Curr. Opin. Genet. Dev., **16**: 17–22.

Edahiro, J., K. Sumaru, Y. Tada, K. Ohi, T. Takagi and M. Kameda (2005). "*In situ control of cell adhesion using photoresponsive culture surface*." Biomacromolecules **6**(2): 970–4.

Fallman, E. and O. Axner (1997). "*Design for fully steerable dual-trap optical tweezers*." Appl. Opt. **36**(10): 2107.

Flores-Rodriguez, N. and G. H. Markx (2004). "*Improved levitation and trapping of particles by negative dielectrophoresis by the addition of amphoteric molecules*." J. Phys. D: Appl. Phys. **37**: 353-361.

Flores-Rodriguez, N. and G. H. Markx (2006). "*Flow-through devices for the AC electrokinetic construction of microstructured materials*." J. Micromech. Microeng. **16**: 349-355.

Flynn, R. A., A. L. Birkbeck, M. Gross, M. Ozkan, B. Shao, M. M. Wang and S. C. Esener (2002). "*Parallel transport of biological cells using individually addressable VCSEL arrays as optical tweezers*." Sens. Act. **87**: 239.

Fuchs, E. (2007). "*Scratching the surface of skin development*." Nature **445**: 834 – 842.

Fuchs, J. R., B. A. Nasseri and J. P. Vacanti (2001). "*Tissue Engineering: A 21st Century Solution to Surgical Reconstruction*." Ann. Thorac. Surg. **72**: 577-591.

Fuhr, G., W. M. Arnold, R. Hagedom, T. Muller, W. Benecke, B. Wagner and U. Zimmermann (1992a). "*Levitation, holding, and rotation of cells within traps made by high-frequency fields*." Biochimica et Biophysica Acta **1108**: 215-223.

Fuhr, G., R. Hagedorn, T. Muller, W. Benecke and B. Wagner (1992b). "*Microfabricated electrohydrodynamic (EHD) pumps for liquids of higher conductivity*." J. Microelectromech. Syst **1**: 141–146.

Gascoyne, P., Y. Huang, R. Pethig, J. Vykoukal and F. F. Becker (1992). "*Dielectrophoretic separation of mammalian cells studied by computerized image analysis*." Measurement Science & Technology **3**: 439-445.

Gascoyne, P. and J. Vykoukal (2002). "*Particle separation by dielectrophoresis*." Electrophoresis **23**: 1973-1983.

Gascoyne, P. and J. Vykoukal (2004). "*Dielectrophoresis-based sample handling in general-purpose programmable diagnostic instruments*." Proc. IEEE **92**: 22 - 42.

Gat, U., R. DasGupta, L. Degenstein and E. Fuchs (1998). "*De Novo hair follicle morphogenesis and hair tumors in mice expressing a truncated betacatenin in skin*." Cell **95**: 605 – 614.

Gaugiran, S., S. Gétin and J. M. Fedeli (2005). "*Optical manipulation of microparticles and cells on silicon nitride waveguides*." Optical Society of America **13**(18).

Gherardini, L., C. Cousins, J. Hawkes, J. Spengler, S. Radel, H. Lawler, B. Devcic-Kuhar and M. Groschl (2005). "*A new immobilisation method to arrange particles in a gel matrix by ultrasound standing waves*." Ultrasound in Medicine and Biology **31**: 261-272.

Gierer, A. and H. Meinhardt (1972). "*A theory of biological pattern formation.*" Kybernetik. **12**: 30-39.

Gilbert, S. F. (2006). *Developmental Biology.*, Sinauer Associates, Sunderland,.

Gonzalez, A., A. Ramos, N. G. Green, A. Castellanos and H. Morgan (2000). "*Fluid flow induced by non-uniform AC electric fields in electrolytes on microelectrodes II: A linear double-layer analysis*." Phys. Rev. E **61**: 4019–4028.

Gray, D. S., J. L. Tan, J. Voldman and C. S. Chen (2004). "*Dielectrophoretic registration of living cells to a microelectrode array.*" Biosens. Bioelectron. **19**: 1765-1774.

Green, N. G., H. Morgan and J. J. Milner (1997). "*Manipulation and trapping of sub-micron bioparticles using dielectrophoresis*." J. Biochem. Biophys. Methods **35**: 89-102.

Green, N. G., A. Ramos, A. Gonzalez, H. Morgan and A. Castellanos (2000). "*Fluid flow induced by non-uniform AC electric fields in electrolytes on microelectrodes I: experimental measurements*." Phys. Rev. E **61**: 4011–4018.

Green, N. G., A. Ramos, H. Morgan and A. Castellanos (1999). "*Sub-micrometre AC electrokinetics: particle dynamics under the influence of dielectrophoresis and electrohydrodynamics*." Inst. Phys. Conf. Ser. **163**: 89-92.

Harding, K., T. Hoey, R. Warrior and M. Levine (1989). "*Autoregulatory and gap gene response elements of the even-skipped promoter of Drosophila.*" EMBO J., **8**: 1205–1212.

Hardy, M. H. (1992). "*The secret life of the hair follicle*." Trends. Genet. **8**: 55-61.

Harris, A. K., D. Stopak and P. Warner (1984). "*Generation of spatially periodic patterns by a mechanical instability: a mechanical alternative to the Turing model.*" J. Embryol. Exp. Morphol. **80**: 1-20.

Harris, M. P., J. F. Fallon and R. O. Prum (2002). "*Shh-Bmp2 signaling module and the evolutionary origin and diversification of feathers*." J. Exp. Zool. **294**: 160-176.

Harris, M. P., S. Williamson, J. F. Fallon, H. Meinhardt and R. O. Prum (2005). "*Molecular evidence for an activator-inhibitormechanism in development of embryonic feather branching.*" Proc. Natl. Acad. Sci. U.S.A., **102**: 11734–11739.

Headon, D. J. and K. J. Painter (2009). "*Stippling the skin: generation of anatomical periodicity by reaction-diffusion mechanisms*." Math. Model. Nat. Phenom. **4**:

83 - 102.

Heida, T., W. L. C. Rutten and E. Marani (2001a). "*Dielectrophoretic trapping of dissociated fetal cortical rat neurons*." IEEE Trans. Biomed. Eng. **48**: 921-930.

Heida, T., P. Vulto, W. L. Rutten and E. Marani (2001b). "*Viability of dielectrophoretically trapped neural cortical cells in culture.*" J. Neurosci. Methods. **110**: 37-44.

Ho, C. T., R. Z. Lin, W. Y. Chang, H. Y. Chang and C. H. Liu (2006). "*Rapid heterogeneous liver-cell on-chip patterning via the enhanced field-induced dielectrophoresis trap*." Lab. Chip. **6**: 724-734.

Hofmann, F., H. Ohnimus, C. Scheller and W. Strupp (1999). "*Electric field pulses can induce apoptosis*." J. Membr. Biol. **169**: 103-109.

Holzel, R., N. Calander, Z. Chiragwandi, M. Willander and F. F. Bier (2005). "*Trapping single molecules by dielectrophoresis*." Phys. Rev. Lett. **95**: 128102.1–128102.4.

Horch, R., A. Munster and B. Achauer (2001). *Cultured human keratinocytes and tissue engineered skin substitutes*. Germany, Thieme.

Huang, Y. and R. Pethig (1991). "*Electrode design for negative dielectrophoresis*." Meas. Sci. Technol. **2**: 1142-1146.

Huelsken, J. and W. Birchmeier (2001). "*New aspects of Wnt signaling pathways in higher vertebrates*." Curr. Opin. Genet. Dev. **11**: 547 – 553.

Hughes, M. P. (2002). "*Strategies for dielectrophoretic separation in laboratory-on-a-chip systems*." Electrophoresis **23**: 2569-2582.

Hughes, M. P. (2003). *Nanoelectromechanics in Engineering and Biology,* CRC Press.

Hughes, M. P., H. Morgan, F. J. Rixon, J. P. H. Burt and R. Pethig (1998). "*Manipulation of herpes simplex virus type 1 by dielectrophoresis*." Biochim. Biophys. Acta. **1425**: 119–126.

Hultström, J., O. Manneberg, K. Dopf, H. M. Hertz, H. Brismar and M. Wiklund (2007). "*Proliferation and viability of adherent cells manipulated by standing-wave ultrasound in a microfluidic chip*." Ultrasound in Medicine & Biology **33**(1): 145-151.

Hyun, J., W. K. Lee, N. Nath, A. Chilkoti and S. Zauscher (2004). "*Capture and release of proteins on the nanoscale by stimuli-responsive elastin-like polypeptide ‘‘switches’’*." J. Am. Chem. Soc. **126**(23): 7330–5.

Jacques, S. L. and D. J. McAuliffe (1991). "*The melanosome — threshold temperature for explosive vaporization and internal absorption-coefficient during pulsed laser irradiation*." Photochem. Photobiol. **53**: 769-775.

Jamora, C., R. DasGupta, P. Kocieniewski and E. Fuchs (2003). "*Links between signal transduction, transcription and adhesion in epithelial bud development*." Nature

422: 317 – 322.

Jiang, T. X., H. S. Jung, R. B. Widelitz and C. M. Chuong (1998). "*Self organization is the initial event in periodic feather patterning: roles of signalling molecules and adhesion molecules*." Development **126**: 4997-5009.

Jiang, T. X., H. S. Jung, R. B. Widelitz and C. M. Chuong (1999). "*Self-organization of periodic patterns by dissociated feather mesenchymal cells and the regulation of size, number and spacing of primordia*." Development **126**: 4997-5009.

Jiang, T. X., R. B. Widelitz, W. M. Shen, P. Will, D. Y. Wu, C. M. Lin, H. S. Jung and C. M. Chuong (2004). "*Integument pattern formation involves genetic and epigenetic controls: feather arrays simulated by digital hormone models.*" Int. J. Dev. Biol. **48**(2-3): 117-135.

Jiang, X. Y., R. Ferrigno, M. Mrksich and G. M. Whitesides (2003). "*Electrochemical desorption of self-assembled monolayers noninvasively releases patterned cells from geometrical confinements.*" J. Am. Chem. Soc. **125**: 2366-2367.

Jinjie, S., A. Daniel, M. Xiaole, S. L. Chin, L. Aitan and J. H. Tony (2009). "*Acoustic tweezers: patterning cells and microparticles using standing surface acoustic waves (SSAW)†*." Lab Chip **9**(2890–2895).

Jones, T. B. (1995). *Electromechanics of particles*. Cambridge, Cambridge University Press.

Jung, H. S., P. H. Francis-West, R. B. Widelitz, T. X. Jiang, S. Ting-Berreth, C. Tickle, L. Wolpert and C. M. Chuong (1998). "*Local inhibitory action of BMPs and their relationships with activators in feather formation: implications for periodic patterning.*" Dev. Biol. **196**: 11–23.

Kaji, H., M. Kanada, D. Oyamatsu, T. Matsue and Nishizawa (2004a). "*Microelectrochemical approach to induce local cell adhesion and growth on substrates*." Langmuir **20**: 16-19.

Kaji, H., K. Tsukidate, M. Hashimoto, T. Matsue and M. Nishizawa (2005). "*Patterning the surface cytophobicity of an albuminphysisorbed substrate by electrochemical means.*" Langmuir **21**: 6966-6969.

Kaji, H., K. Tsukidate, T. Matsue and Nishizawa (2004b). "*In situ control of cellular growth and migration on substrates using microelectrodes*." J. Am. Chem. Soc. **126**: 15026-15027.

Kashiwagi, M., T. Kuroki and N. Huh (1997). "*Specific inhibition of hair follicle formation by epidermal growth factor in an organ culture of developing mouse skin.*" Dev. Biol., **189**: 22–32.

Kato, M. and M. Mrksich (2004). "*Rewiring cell adhesion*." J. Am. Chem. Soc. **126**: 6504-6505.

Keller, E. F. and L. A. Segel. (1970). "*Initiation of slime mold aggregation viewed as an instability.*" J.Theor. Biol., **26**: 399–415.

Khademhosseini, A., G. Eng, J. Yeh, J. Fukuda, J. Blumling, R. Langer and J. A. Burdick (2006a). "*Micromolding of photocrosslinkable hyaluronic acid for cell encapsulation and entrapment*." J. Biomed. Mater. Res. A **79**(3): 522-532.

Khademhosseini, A., R. Langer, J. Borenstein and J. P. Vacanti (2006b). "*Microscale technologies for tissue engineering and biology*." Proc. Natl. Acad. Sci. USA **103**: 2480-2487.

Kobielak, K., H. A. Pasolli, L. Alonso, L. Polak and E. Fuchs (2003). "*Defining BMP functions in the hair follicle by conditional ablation of BMP receptor IA*." J. Cell Biol. **163**: 609 – 623.

Kopan, R. and D. L. Turner (1996). "*The Notch pathway: democracy and aristocracy in the selection of cell fate.*" Curr. Opin. Neurobiol. **6**: 594-601.

Kwok, C. S., P. D. Mourad, L. A. Crum and B. D. Ratner (2001). "*Self-assembled molecular structures as ultrasonically-responsive barrier membranes for pulsatile drug delivery*." J. Biomed. Mater. Res. **57**(2): 151–64.

Langer, R. and J. P. Vacanti (1993). "*Tissue engineering*." Science **260**: 920-926.

Lanza, R. P., R. Langer and J. Vacanti (2000). *Principles of tissue engineering*. New York, Academic Publishing.

Lapizco-Encinas, B. H., R. V. Davalos, B. A. Simmons, E. B. Cummings and Y. Fintschenko (2005). "*An insulator-based (electrodeless) dielectrophoretic concentrator for microbes in water*." J. Microbiol. Methods **62**.

Lapizco-Encinas, B. H., B. A. Simmons, E. B. Cummings and Y. Fintschenko (2004a). "*Dielectrophoretic concentration and separation of live and dead bacteria in an array of insulators.*" Anal. Chem. **76**: 1571–1579.

Lapizco-Encinas, B. H., B. A. Simmons, E. B. Cummings and Y. Fintschenko (2004b). "*Insulator-based dielectrophoresis for the selective concentration and separation of live bacteria in water*." Electrophoresis **25**: 1695–1704.

Laurell, T., F. Petersson and A. Nilsson (2007). "*Chip integrated strategies for acoustic separation and manipulation of cells and particles*." Chem. Soc. Rev. **36**: 492-506.

Laurikkala, J., M. Mikkola, T. Mustonen, T. Aberg, P. Koppinen, J. Pispa, P. Nieminen, J. Galceran, R. Grosschedl and I. Thesleff (2001). "*TNF signaling via the ligand-receptor pair ectodysplasin and edar controls the function of epithelial signaling centers and is regulated by Wnt and activin during tooth organogenesis*." Dev. Biol. **229**: 443 – 455.

Laurikkala, J., J. Pispa, H. S. Jung, P. Nieminen, M. Mikkola, X. Wang, U. Saarialho-Kere, J. Galceran, R. Grosschedl and I. Thesleff. (2002). "*Regulation of hair follicle development by the TNF signal ectodysplasin and its receptor Edar.*" Development, **129**: 2541–2553.

Lee, J. H., B. J. Jeong and H. B. Lee (1997). "*Plasma protein adsorption and platelet adhesion onto comb-like PEO gradient surfaces*." J. Biomed. Mater. Res. A **34**(1): 105–14.

Lemmo, A. V., D. J. Rose and T. C. Tisone (2005). "*Inkjet printing of viable mammalian cells*." Biomaterials **26**: 93–99.

Levy, V., C. Lindon, Y. Zheng, B. D. Harfe and B. A. Morgan (2007). "*Epidermal stem cells arise from the hair follicle after wounding*." FASEB J. **21**: 1358 – 1366.

Lin, C. M., T. X. Jiang, R. B. Widelitz and C. M. Chuong (2006a). "*Molecular signaling in feather morphogenesis*." Curr. Opinion Cell Biol. **18**: 730–741.

Lin, J. T. Y. and J. T. W. Yeow (2007). "*Enhancing dielectrophoresis effect through novel electrode geometry*." Biomed. Microdev. **9**(6): 823-831.

Lin, R. Z., L. F. Chou, C. C. Chien and H. Y. Chang (2006b). "*Dynamic analysis of hepatoma spheroid formation: roles of E-cadherin and beta1-integrin*." Cell Tissue Res. **324**: 411-422.

Lisa, G., M. C. Caroline, J. J. H, S. Johannes, R. Stefan, L. Helen, D. K. Branka, G. Martin, C. Terence and A. J. M (2005). "*A New Immobilisation Method to Arrange Particles in a Gel Matrix by Ultrasound Standing Waves*." Ultrasound in Medicine and Biology **31**(2): 261–272.

Litvinov, R. I., H. Shuman, J. S. Bennett and J. W. Weisel (2002). "*Binding strength and activation state of single fibrinogen-integrin pairs on living cells*." Proc. Natl Acad. Sci. USA **99**: 7426–7431.

Lund, A., B. Yener, J. Stegemann and G. Plopper (2009). "*The natural and engineered 3D microenvironment as a regulatory cue during stem cell fate determination*." Tissue Engineering: Part B **15**: 371-380.

MacArthur, B. D. and R. O. C. Oreffo (2005). "*Bridging the gap*." Nature **433**: 19.

Mandler, M. and A. Neubuser (2004). "*FGF signaling is required for initiation of feather placode development.*" Development **131**: 3333–3343.

Markx, G. H. (2008). "*The use of electric fields in tissue engineering*." Organogenesis **4**: 11-17.

Markx, G. H., J. S. Andrews and V. P. Mason (2004). "*Towards microbial tissue engineering?*" Trends Biotechnol. **22**(8): 417-422.

Markx, G. H. and A. M. Buckle (2005). *Tissue engineering: AC electrokinetics*. Encyclopedia of Biomaterials and Biomedical Engineering. New York, Taylor & Francis.

Markx, G. H., L. Carney, M. Littlefair, A. Sebastian and A. M. Buckle (2009). "*Recreating the hematon: microfabrication of artificial haematopoietic stem cell microniches in vitro using dielectrophoresis*." Biomed. Microdev. **11**: 143-150.

Markx, G. H. and C. L. Davey (1999). "*The dielectric properties of biological cells at radio-frequencies: applications in biotechnology*." Enzyme Microb. Technol. **25**: 161-171.

Markx, G. H., Y. Huang, X. F. Zhou and R. Pethig (1994a). "*Dielectrophoretic characterisation and separation of micro-organisms*." Microbiology **140**: 585-591.

Markx, G. H., J. Rousselet and R. Pethig (1997). "*Dielectrophoretic levitation of latex beads, with reference to Field Flow Fractionation*." J. Phys. D: Appl. Phys. **30**: 2470-2477.

Markx, G. H., M. S. Talary and R. Pethig (1994b). "*Separation of viable and non-viable yeast using dielectrophoresis*." J. Biotechnol. **32**: 29-37.

Mason, V. P., G. H. Markx, I. P. Thompson, J. S. Andrews and M. Manefield (2005). "*Colonial architecture in mixed species assemblages affects AHL mediated gene expression*." FEMS Microbiology Letters. **244**: 121-127.

Matsue, T., N. Matsumoto and I. Uchida (1997). "*Rapid micropatterning of living cells by repulsive dielectrophoretic force*." Electrochim. Acta **42**: 3251-3256.

McArthur, S. L., K. M. McLean, P. Kingshott, H. A. W. St John, R. C. Chatelier and H. J. Griesser (2000). "*Effect of polysaccharide structure on protein adsorption*." Colloids Surf. B Biointerfaces **17**(1): 37–48.

McCabe, K. and M. Bronner-Fraser (2009). "*Molecular and tissue interactions governing induction of cranial ectodermal placodes*." Dev. Biol. **332**: 189-195.

Mehrishi, J. N. and J. Bauer (2002). "*Electrophoresis of cells and the biological relevance of surface charge*." Electrophoresis **23**: 1984-1994.

Meinhardt, H. (2004). "*Models for positional signalling with application to the dorsoventral patterning of insects and segregation into different cell types.*" Development, **107**: 169–180.

Menachery, A. and R. Pethig (2005). "*Controlling cell destruction using dielectrophoretic forces*." IEE Proc. Nanobiotechnol. **152**: 145-149.

Mikolajczyk, K., A. Zisserman and C. Schmid (2003). "*Shape recognition with edge-based features*." Proceeding of the British Machine Vision Conference, Norwich U.K.

Millar, S. E. (2002). "*Molecular mechanisms regulating hair follicles development*." Dev. Biol. **118**: 216-225.

Mironov, V. (2003). "*Organ printing: computer-aided jet-based 3D tissue engineering.*" Trends Biotechnol. **21**: 157-161.

Mittal, N., A. Rosenthal and J. Voldman (2007). "*N DEP microwells for single-cell patterning in physiological media.*" Lab Chip **7**: 1146-1153.

Monaghan, P. B., K. M. McCarney, A. Ricketts, R. E. Littleford, F. Docherty, W. E. Smith, D. Graham and J. M. Cooper (2007). "*Bead-based DNA diagnostic assay for chlamydia using nanoparticle-mediated surface-enhanced resonance Raman scattering detection within a lab-on-a-chip format*." Anal. Chem. **79**(7): 2844-2849.

Mooney, J. R. and B. N. Nagorcka (1985). "*Spatial patterns produced by a reaction-diffusion system in primary hair follicles.*" J. Theor. Biol. **115**: 299–317.

Morgan, B. A. and D. M. Fekete (1996). "*Manipulating gene expressionwith replication-competent retroviruses*." Methods Cell Biol. **51**: 185–218.

Morgan, B. A., R. W. Orkin, S. Noramly and A. Perez (1998). "*Stage-specifi c effects of sonic hedgehog expression in the epidermis*." Dev. Biol. **201**: 1 – 12.

Morgan, H. and N. G. Green (2003). *AC Electrokinetics: Colloids and Nanoparticles*, Herts: Research Studies Press.

Morgan, H., A. G. Izquierdo, D. Bakewell, N. G. Green and A. Ramos (2001). "*The dielectrophoretic and traveling wave forces generated by interdigitated electrode arrays: Analytical solution using Fourier series*." J. Phys.D: Appl. Phys. **34**: 1553-1561.

Mou, C., B. Jackson, P. Schneider, P. A. Overbeek and D. J. Headon (2006). "*Generation of the primary hair follicle pattern.*" Proc. Natl. Acad. Sci. USA. **103**: 9075-9080.

Murray, J. D. (1989). *Mathematical Biology*. Berlin, Springer Verlag.

Murray, J. D. (2003). "*On the mechanochemical theory of biological pattern formation with application to vasculogenesis.*" C R Biol. **326**(2): 239–252.

Murray, J. D., G. F. Oster and A. K. Harris (1983). "*A mechanical model for mesenchymal morphogenesis*." J. Math. Biol. **17**: 125-129.

Mushfique, H., J. Leach, R. D. Leonardo, M. J. Padgett and J. M. Cooper (2008). "*Optically driven Pump and Flow Sensors for Microfluidic Systems*." Proc. IMechE: J. Mech. Eng. Sci. **222**: 829-837.

Nagorcka, B. N. and J. R. Mooney (1982). "*The role of a reaction-diffusion system in the formation of hair fibres.*" J. Theor. Biol. **98**: 575-607.

Nagorcka, B. N. and J. R. Mooney (1985). "*The role of a reaction-diffusion system in the initiation of primary hair follicles.*" J. Theor. Biol., **114**: 243–272.

Nagy, A., M. Gertsenstein and K. Vintersten (2003). *Manipulating the Mouse Embryo: A Laboratory Manual*. New York, Cold Spring Harbor Laboratory Press.

Narhi, K., E. Jarvinen, W. Birchmeier, M. M. Taketo, M. L. Mikkola and I. Thesleff. (2008). "*Sustained epithelial beta-catenin activity induces precocious hair development but disrupts hair follicle down-growth and hair shaft formation.*" Development **135**: 1019–1028.

National-Instrument (2008). "*NI Image Acquisition Fundamentals*." National Instrument Manual.

National-Instrument (February 2007). "*NI Vision Assisstant Tutorial*." National Instrument Manual.

National-Instrument (July, 2007). "*NI Vision Concepts Manual*." National Instrument Manual.

Noramly, S., A. Freeman and B. A. Morgan. (1999). "*Beta-catenin signaling can initiate feather bud development.*" Development **126**: 3509–3521.

Noramly, S. and B. A. Morgan (1998). "*BMPs mediate lateral inhibition at successive stages in feather tract development.*" Development **125**: 3775–3787.

Noveen, A., T. X. Jiang, S. A. Ting-Berreth and C. M. Chuong (1995). "*Homeobox genes Msx-1 and Msx-2 are associated with induction and growth of skin appendages*." J. Invest. Dermatol. **104**: 711-719.

Nyborg, W. L. (2002). "*Safety of medical diagnostic ultrasound*." Seminars in ultrasound **23**: 377 - 386.

Okamoto, T., T. Suzuki and N. Yamamoto (2000). "*Microarray fabrication with covalent attachment of DNA using bubble jet technology*." Nat. Biotechnol. **18**(4): 438–441.

Oro, A. E. and K. Higgins (2003). "*Hair cycle regulation of Hedgehog signal reception*." Dev. Biol. **255**: 238 – 248.

Oro, A. E., K. M. Higgins, Z. Hu, J. M. Bonifas, E. H. E. Jr and M. P. Scott (1997). "*Basal cell carcinomas in mice overexpressing sonic hedgehog*." Science **276**: 817 – 821.

Oster, G. F., J. D. Murray and A. K. Harris (1983). "*Mechanical aspects of mesenchymal morphogenesis*." J. Embryo. Exp. Morphol. **78**: 83-125.

Oster, G. F., J. D. Murray and P. K. Maini (1985). "*A model for chondrogenic condensations in the developing limb: the role of extracellular matrix and cell tractions*." J. Embryol. Exp. Morphol. **89**: 93-112.

Ozkan, M., C. S. Ozkan, O. Kibar, M. M. Wang, S. Bhatia and S. C. Esener (2001). "*Heterogeneous integration through electrokinetic migration.*" IEEE Eng Med Biol **20**: 144-151.

Ozkan, M., T. Pisanic, J. Scheel, C. Barlow, S. Esener and S. N. Bhatia (2003). "*Electro-optical platform for the manipulation of life cells*." Langmuir **19**: 1532-1538.

Ozuna-Chaco´n, S., B. H. Lapizco-Encinas, M. Rito-Palomares, S. O. Martý´nez-Chapa and C. Reyes-Betanzo (2008). "*Performance characterization of an insulator-based dielectrophoretic microdevice*." Electrophoresis **29**: 3115–3122.

Panayiotou, M. and R. Freitag (2005). "*Influence of the synthesis conditions and ionic additives on the swelling behaviour of thermo-responsive polyalkylacrylamide hydrogels*." Polymer **46**(18): 6777–85.

Paus, R. and G. Cotsarelis (1999). "*The biology of hair follicles.*" N. Engl. J. Med. **341**: 491–497.

Pethig, R. (1996). "*Dielectrophoresis: Using Inhomogeneous AC Electrical Fields to Separate and Manipulate Cells*." Critical Reviews in Biotechnology **16**(4): 331-348.

Pethig, R., Y. Huang, X. B. Wang and J. P. H. Burt (1992). "*Positive and negative dielectrophoretic collection of colloidal particles using interdigitated castellated electrodes.*" J. Phys. D: Appl. Phys. **25**: 881-888.

Pethig, R. and D. Kell (1987). "*The passive electrical properties of biological systems: their significance in physiology, biophysics and biotechnology.*" Phys. Med. Biol. **32**: 933-970.

Pethig, R. and G. H. Markx (1997). "*Applications of dielectrophoresis in biotechnology*." Trends Biotechnol. **15**: 426-432.

Pirlo, R. K., D. M. D. Dean, D. R. Knapp and B. Z. Gao (2006). "*Cell deposition system based on laser guidance*." Biotechnol. J. **1**: 1007–1013.

Pohl, H. A. (1978). *Dielectrophoresis*. Cambridge, Cambridge University Press.

Price, J. A. R., J. P. H. Burt and R. Pethig (1988). "*Application of a new optical technique for measuring the dielectrophoretic behaviour of microorganisms*." Biochim. Biophys. Acta **964**: 221-230.

Pucihar, G., T. Kotnik, M. Kanduser and D. Miklavcic (2001). "*The influence of medium conductivity on electropermeabilization and survival of cells in vitro*." Bioelectrochemistry **54**: 107-115.

Pummila, M., I. Fliniaux, R. Jaatinen, M. J. James, J. Laurikkala, P. Schneider, I. Thesleff and M. L. Mikkola (2007). "*Ectodysplasin has a dual role in ectodermal organogenesis: inhibition of Bmp activity and induction of Shh expression*." Development **134**: 117 – 125.

Ramos, A., H. Morgan, N. G. Green and A. Castellanos (1998). "*AC Electrokinetics: A Review Of Forces in Microelectrode Structures*." J. Phys. D: Appl. Phys. **31**: 2338-2353.

Ramos, A., H. Morgan, N. G. Green and A. Castellanos (1999). "*AC electric-field induced fluid flow in microelectrodes*." J. Colloid Interface Sci. **217**: 420–422.

Reddy, S., T. Andl, A. Bagasra, M. M. Lu, D. J. Epstein, E. E. Morrisey and S. E. Millar (2001). "*Characterization of Wnt gene expression in developing and postnatal hair follicles and identifi cation of Wnt5a as a target of Sonic hedgehog in hair follicle morphogenesis*." Mech. Dev. **107**: 69 – 82.

Revzin, A., R. J. Russell, V. K. Yadavalli and W. G. Koh (2001). "*Fabrication of poly(ethylene glycol) hydrogel microstructures using photolithography*." Langmuir **17**: 5440-5447.

Reynolds, A. J. (1999). "*Trans-gender induction of hair follicles*." Nature **402**: 33-34.

Rhee, H., L. Polak and E. Fuchs (2006). "*Lhx2 maintains stem cell character in hair follicles.*" Science **312**(5782): 1946-1949.

Rintoul, G. L., L. A. Raymond and K. G. Baimbridge (2001). "*Calcium buffering and protection from excitotoxic cell death by exogenous calbindin-D28k in HEK 293 cells*." Cell Calcium **29**(4): 277-287.

Robert, W. A. J., J. Squier, T. Vestad, J. Oakey and D. W. M. Marr (2004). "*Optical trapping, manipulation, and sorting of cells and colloids in microfluidic systems with diode laser bars*." Optics Express **12**(19): 4390.

Roda, A., M. Guardigli, C. Russo, P. Pasini and M. Baraldini (2000). "*Protein microdeposition using a conventional ink-jet printer*." Biotechniques **28**(3): 492–496.

Rosenthal, A. and J. Voldman (2005). "*Dielectrophoretic traps for single-particle patterning.*" Biophys. J. **88**: 2193-2205.

Ross, P. J. (1996). *Taguchi Techniques for Quality Engineering*. New York, McGraw-Hill.

Roth, E. A., T. Xua, M. Dasa, C. Gregorya, J. J. Hickman and T. Boland (2004). "*Inkjet printing for high-throughput cell patterning*." Biomaterials **25**(17): 3707-3715.

Schmeichel, K., V. Weaver and M. Bisell (1998). "*Structural cues from the tissue microenvironment are essential determinants of the human mammary epithelial cell phenotype*." Journal of Mammary Gland Biology and Neoplasia **3**: 201-213.

Schmidt-Ullrich, R. and R. Paus (2005). "*Molecular principles of hair follicle induction and morphogenesis.*" Bioessays **27**: 247–261.

Sebastian, A., A. M. Buckle and G. H. Markx (2006). "*Formation of multilayer aggregates of mammalian cells by dielectrophoresis*." J. Micromech. Microeng. **16**: 1769-1777.

Sebastian, A., A. M. Buckle and G. H. Markx (2007a). "*Tissue engineering with electric fields: immobilisation of mammalian cells in multilayer aggregates using dielectrophoresis*." Biotechnol. Bioeng. **98**: 694-700.

Sebastian, A., A. G. Venkatesh and G. H. Markx (2007b). "*Tissue engineering with electric fields: Investigation of the shape of mammalian cell aggregates formed at interdigitated oppositely castellated electrodes*." Electrophoresis **28**: 3821-3828.

Sengel, P. (1975). *Feather pattern development. In Cell Patterning*. Ciba Foundation

Symposium, Amsterdam, Elsevier.

Sengel, P. (1976). *Morphogenesis of skin*. Cambridge, CUP.

Sengel, P. (1990). "*Pattern formation in skin development*." Int. J. Dev. Biol. **34**: 33-50.

Shi, J., X. Mao, D. Ahmed, A. Colletti and T. J. Huang (2008). "*Focusing microparticles in a microfluidic channel with standing surface acoustic waves (SSAW).*" Lab Chip. **8**(2): 221–223.

Sick, S., S. Reinker, J. Timmer and T. Schlake. (2006). "*WNT and DKK determine hair follicle spacing through a reaction-diffusion mechanism.*" Science **314**: 1447–1450.

Song, H., S. H. Lee and P. F. Goetinck (2004). "*FGF-2 signaling is sufficient to induce dermal condensations during feather development*." Developmental Dynamics **231**(4): 741-749.

Song, H., Y. Wang and P. F. Goetinck (1996). "*Fibroblast growth factor 2 can replace ectodermal signaling for feather development.*" Proc. Natl. Acad. Sci. USA **93**: 10246–10249.

Spengler, J. F. and W. T. Coakley (2003). "*Ultrasonic Trap To Monitor Morphology and Stability of Developing Microparticle Aggregates*." Langmuir **19**(9): 3635-3642.

Steinberg, M. S. and M. Takeichi (1994). "*Experimental specification of cell sorting, tissue spreading, and specific spatial patterning by quantitative differences in cadherin expression*." Proc. Natl. Acad. Sci. USA **91**: 206-209.

St-Jacques, B., H. R. Dassule, I. Karavanova, V. A. Botchkarev, J. Li, P. S. Danielian, J. A. McMahon, P. M. Lewis, R. Paus and A. P. McMahon (1998). "*Sonic hedgehog signaling is essential for hair development*." Curr. Biol. **8**: 1058 – 1068.

Sukhorukov, V. L., H. Mussauer and U. Zimmermann (1998). "*The effect of electrical deformation forces on the electropermeabilization of erythrocyte membranes in low- and high-conductivity media.*" J. Membrane Biol. **163**: 235-245.

Sung, K. E. and M. A. Burns (2006). "*Optimization of Dielectrophoretic DNA Stretching in Microfabricated Devices*." Anal. Chem. **78**: 2939–2947.

Sung, W. J. and Y. H. Bae (2003). "*A glucose oxidase electrode based on polypyrrole with polyanion/PEG/enzyme conjugate dopant*." Biosens. Bioelectron. **18**(10): 1231–9.

Suzuki, M., T. Yasukawa, H. Shiku and T. Matsue (2008). "*Negative dielectrophoretic patterning with different cell types*." Biosensors Bioelectron. **24**(4): 1043-1047.

Svoboda, K., P. P. Mitra and S. M. Block (1994). "*Fluctuation analysis of motor protein movement and single enzyme-kinetics*." Proc. Natl. Acad. Sci. USA **91**: 11782–11786.

Taguchi, G. (1990). "*Introduction to quality engineering*." Asian Productivity Organization, Japan.

Tan, W. and T. Desai (2004). "*Layer-by-layer microfluidics for biomimetic three-dimensional structures*." Biomaterials **25**: 1355-1364.

Tanase, M., E. J. Felton, D. S. Gray, A. Hultgren, C. S. Chen and D. H. Reich (2005). "*Assembly of multicellular constructs and microarrays of cells using magnetic nanowires*." Lab Chip **5**: 598-605.

Teleman, A. A., M. Strigini and S. M. Cohen (2001). "*Shaping morphogen gradients.*" Cell **105**: 559–562.

Toriello, N. M., E. S. Douglas and R. A. Mathies (2005). "*Microfluidic device for electric field-driven single-cell capture and activation*." Anal. Chem. **77**: 6935-6941.

Tsang, V. L. and S. N. Bhatia (2004). "*Three-dimensional tissue fabrication.*" Adv. Drug Delivery Rev. **56**: 1635-1647.

Turing, A. (1952). "*The chemical basis of morphogenesis*." Phil. Trans. B. **237**: 37-72.

Turk, G. (1991). "*Generating textures on arbitrary surfaces using reaction-diffusion.*" Comp. Graphics, **25**: 289–298.

Tzagoloff, A. (1982). *Mitochondria*. Amsterdam, Kluwer Academic.

Van Genderen, C., R. M. Okamura, I. Farinas, R. G. Quo, T. G. Parslow, L. Bruhn and R. G. . (1994). "*Development of several organs that require inductive epithelial-mesenchymal interactions is impaired in LEF-1 deficient mice*." Genes Dev. **8**: 2691 – 2703.

Vargas, L. H. M., A. C. S. Pia˜o, R. N. Domingos and E. C. Carmona (2004). "*Ultrasound effects on invertase from Aspergillus niger*." World Journal of Microbiology & Biotechnology **20**: 137–142.

Velev, O. D. and K. H. Bhatt (2006). "*On-chip micromanipulation and assembly of colloidal particles by electric fields.*" Soft Matter **2**: 738-750.

Verduzco-Luque, C. E., B. Alp, G. M. Stephens and G. H. Markx (2003). "*Construction of biofilms with defined internal architecture using dielectrophoresis and flocculation.*" Biotechnol. Bioeng. **83**: 39-44.

Vidal, V. P., M. C. Chaboissier, S. Lutzkendorf, G. Cotsarelis, P. Mill, C. C. Hui, N. Ortonne, J. P. Ortonne and A. Schedl (2005). "*Sox9 is essential for outer root sheath differentiation and the formation of the hair stem cell compartment*." Curr. Biol. **15**: 1340 – 1351.

Vincent, J. P. and J. Briscoe (2001). "*Morphogens*." Curr. Biol. **11**: R851–854.

Voldman, J. (2006). "*Electrical forces for microscale cell manipulation.*" Ann. Rev.

Biomed. Eng. **8**: 425-454.

Wang, M. M., E. Tu, D. E. Raymond, J. M. Yang, H. C. Zhang, N. Hagen, B. Dees, E. M. Mercer, A. H. Forster and I. Kariv (2005). "*Microfluidic sorting of mammalian cells by optical force switching*." Nat. Biotechnol. **23**: 83-87.

Wang, X., F. Becker and P. Gascoyne (1996). "*A theoretical method of electrical field analysis for dielectrophoretic electrode arrays using Green's theorem*." J. Phys. D: Appl. Phys. **29**: 1649-1660.

Wang, X., J. Yang and P. R. Gascoyne (1999). "*Role of peroxide in AC electrical field exposure effects on friend murine erythroleukemia cells during dielectrophoretic manipulations*." Biochim. Biophys. Acta **1426**: 53-68.

Wang, X. B., Y. Huang, J. P. H. Burt, G. H. Markx and R. Pethig (1993). "*Selective dielectrophoretic confinement of bioparticles in potential energy wells.*" J. Phys. D: Appl. Phys. **26**: 1278-1285.

Widelitz, R. B., T. X. Jiang, J. Lu and C. M. Chuong (2000). "*Beta-catenin in epithelial morphogenesis: conversion of part of avian foot scales into feather buds with a mutated beta-catenin.*" Dev. Biol., **219**: 98–114.

Widelitz, R. B., T.-X. Jiang, A. Noveen, C. W. Chen and C. M. Chuong (1996). "*FGF induces new feather buds from developing avian skin*." J. Invest. Dermatol. **107**: 797–803.

Wolpert, L. (1971). "*Positional information and pattern formation*." Curr. Top. Dev. Biol. **6**: 183-224.

Wolpert, L. (2006). *Principles of development.* Oxford, OUP.

Wu, P., L. Hou, M. Plikus, M. Hughes, J. Scehnet, S. Suksaweang, R. B. Widelitz, T. X. Jiang and C. M. Chuong (2004). "*Evo-devo of amniote integuments and appendages*." Int. J. Dev. Biol. **48**: 249-270.

Xu, T., J. Jin, C. Gregory, J. J. Hickman and T. Boland (2005). "*Inkjet printing of viable mammalian cells*." Biomaterials **26**: 93-99.

Yamaguchi, M., E. Yoshimoto and S. Kondo. (2007). "*Pattern regulation in the stripe of zebrafish suggests an underlying dynamic and autonomous mechanism.*" Proc. Natl. Acad. Sci. USA **104**: 4790–4793.

Yamamoto, T., O. Kurosawa, H. Kabata, N. Shimamoto and M. Washizu (2000). "*Molecular surgery of DNA based on electrostatic micromanipulation*." IEEE Trans. Ind. Appl. **36**: 1010–1017.

Yochelis, A., Y. Tintut, L. L. Demer and A. Garfinkel (2008). "*The formation of labyrinths, spots and stripe patterns in a biochemical approach to cardiovascular calcification*." New J. Phys. **10**(055002).

Yoshida, K. and H. Munakata (2007). "*Connective tissue growth factor binds to fibronectin through the type I repeat modules and enhances the affinity of*

fibronectin to fibrin." Biochim. Biophys. Acta, **1770**: 672–680.

Yosioka, K. and Y. Kawasima (1955). "*Acoustic radiation pressure on a compressible sphere*." Acustica **5**(167–173).

Yousaf, M. N., B. T. Houseman and M. Mrksich (2001). "*Using electroactive substrates to pattern the attachment of two different cell populations*." Proc. Natl. Acad. Sci. USA **98**: 5992-5996.

Yu, M., P. Wu, R. B. Widelitz and C. M. Chuong (2002). "*The morphogenesis of feathers*." Nature **420**: 308-312.

Yu, M., Z. Yue, P. Wu, D. Y. Wu, J. A. Mayer, M. Medina, R. B. Widelitz, T. X. Jiang and C. M. Chuong. (2004a). "*The biology of feather follicles.*" Int. J. Dev. Biol. **48**: 181–191.

Yu, Z., G. Xiang, L. Pan, L. Huang, Z. Yu, W. Xing and J. Cheng (2004b). "*Negative dielectrophoretic force assisted construction of ordered neuronal networks on cell positioning bioelectronic chips.*" Biomed. Microdev. **6**: 311-324.

Yusvana, R., D. J. Headon and G. H. Markx (2009). "*Isolation and measurement of the features of arrays of cell aggregates formed by dielectrophoresis using the user-specified Multi Regions Masking (MRM) technique*." J. Phys. Conf. Series. Dielectrics 2009: Measurement Analysis and Applications **183**.

Yusvana, R., D. J. Headon and G. H. Markx (2010). "*Creation of Arrays of Cell Aggregates in Defined Patterns for Developmental Biology Studies Using Dielectrophoresis*." Biotechnol. Bioeng. **105**(5): 945-954.

Zhang, J., X. C. He, W. G. Tong, T. Johnson, L. M. Wiedemann, Y. Mishina, J. Q. Feng and L. Li (2006). "*Bone morphogenetic protein signaling inhibits hair follicle anagen induction by restricting epithelial stem/progenitor cell activation and expansion*." Stem Cells **24**: 2826 – 2839.

Zhou , P., C. Byrne, J. Jacobs and E. Fuchs (1995). "*Lymphoid enhancer factor 1 directs hair follicle patterning and epithelial cell fate*." Genes Dev. **9**: 700 – 713.

Zhu, X., J. De Graaf, F. M. Winnik and D. Leckband (2004). "*Tuning the interfacial properties of grafted chains with a pH switch*." Langmuir **20**(4): 1459–65.